Promoted Co-CNT nano-catalyst for green diesel production using Fische r- Tropsch synthesis in a fixed bed reactor

A Thesis Submitted to the College of Graduate Studies and Research

in Partial Fulfillment of the Requirements

for the Degree of Doctor of Philosophy in the

Department of Chemical Engineering

University of Saskatchewan

Saskatoon, Saskatchewan

By

MARIANE TRÉPANIER

PERMISSION TO USE

In presenting this thesis in partial fulfillment of the requirements for a Ph.D degree from the University of Saskatchewan, I agree that the Libraries of this University may make it freely available for inspection. I further agree that permission for copying of this thesis in any manner, in whole or in part, for scholarly purposes may be granted by the professor or professors who supervised my thesis work or, in their absence, by the Head of Department or the Dean of the College of Engineering. It is understood that any copying or publication or use of this thesis or parts there of for financial gain should not be allowed without my written permission. It is also understood that due recognition should be given to me and to the University of Saskatchewan in any scholarly use which may be made of any material in my thesis.

Request for permission to copy or to make other uses of materials in this thesis in whole or part should be addressed to:

Head of Department of Chemical Engineering
University of Saskatchewan
57 Campus Drive
Saskatoo, Sk
S7N 5A9
Canada

ABSTRACT

This research project is part of a larger Canadian endeavour to evaluate feasibility of using new nanocatalyst formulations for Fischer-Tropsch synthesis (FTS) to convert fossil-derived or renewable gaseous fuels into green diesel. The green diesel is a clean fuel (with no aromatics and sulfur compounds) suitable for the commonly used transportation system. The catalyst investigated is cobalt metal supported on carbon nanotubes (CNTs). The physical properties of CNTs have improved the common cobalt catalyst currently used in industry. Carbon nanotubes have high surface area, a very stable for FTS activity and, contrary to other common supports, do not interact with the catalyst active phase to produce undesirable compounds. Moreover, CNTs differ from graphite in their purity and by their cylindrical form, which increases the metal dispersion and allows confinement of the particles inside the tubes. Thus, carbon nanotubes as a new type of carbon material have shown interesting properties, favoring catalytic activity for FTS cobalt catalyst. Their surface area can be modified from 170 to 214 m^2/g through acid treatment. The CNT support lowers the amount of Ru promoter needed to increase the catalyst activity up to 80 % CO conversion and potassium promoter increases the selectivity for α-olefins. The olefin to paraffin (O/P) ratio for Co/CNT and CoK/CNT are 0.76 and 0.90, respectively. Moreover, the Co-Fe bimetallic catalysts supported on CNT have proved to be much more attractive in terms of alcohol formation, up to 26.3 % for the Co10Fe4/CNT. The structural characteristics of CNTs have shown to be suitable for use as catalytic support materials for FTS using microemulsion preparation method as applied to produce nanoparticle catalysts. Microemulsion technique results show uniform nanoparticle that are easy to reduce. In addition, the confinement of the particles inside the CNT has improved the lifetime of the catalyst by decreasing the rate of sintering. The deactivation rate at high FTS activity is linear ($X_{CO} = -0.13\ t_{(hr)} + 75$) and at low FTS activity is related to a power law expression of order 11.4 for the cobalt particles outside the tubes and 30.2 for the cobalt particles inside the tube. The optimized catalyst studied

was the CoRuK/CNT catalyst. The best kinetic model to describe the CoRuK/CNT catalyst is: $-r_{H_2+CO} = \frac{18.5\times10^{-5} P_{H_2}^{0.39}}{(1+7.2\times10^{-2} P_{CO}^{0.72} P_{H_2}^{0.1})^2}$.

ACKNOWLEDGMENTS

First, I would like to thank my friends and family for believing in my aptitude to achieving this work successfully and by giving me strength and encouragements.

I would like to record my special gratitude to Dr. Ajay Kumar Dalai, my supervisor, for guidance, for believing in my research abilities, for financial support, for constructive comments and for helping me improve my English writing skills. I also gratefully acknowledge Dr. Nicolas Abatzoglou, my co-supervisor who inspired my passion in renewable energy and R & D researches during my chemical engineering undergraduate studies. He taught me professionalism and makes me to believe in my research potential.

I'm thankful for comments, interest and time spent on reviewing the drafts of this thesis and during committee meeting by Dr. Hui Wang, Dr.Jafar Soltan, Dr. Robert Scott and Dr.Catherine Niu. A special thank to the Department of Chemical Engineering where I have always feel welcome and efficiently served. I would also like to thank Dr. Pereira for serving as the external examiner and for his very constructive comments. Many thanks to the visiting professor Dr. Ahmad Tavasoli for scientific discussions and information which improved my knowledge and research in Fischer-Tropsch synthesis area.

I have always thought that a successful research is achieved with team work. This thesis wouldn't have been thriving without the outstanding technical assistance of Richard Blondin (gas and liquid characterization), Dragon Cekic (order assistance, safety), Christopher A. Dorval Dion (research assistant), Tom Bonli (XRD characterization) and Charles Bertrand (TEM catalysts characterization). Also, I thank all my fellow students in the Catalysis and Chemical Engineering labs in the department of Chemical Engineering at the University of Saskatchewan for help and friendly working atmosphere. I would also acknowledge the financial support of NSERC, NRCan, Enerkem and the University of Saskatchewan.

Finally, sincere and infinite thanks to my dearest significant others, my father, my mom and brothers and sisters for being part of my successful life.

Table of Contents

List of Tables

List of Figures

INDEX

Abbreviations

AC	Activated Carbon
AES	Atomic Emission Spectroscopy
ASF	Anderson-Schultz-Florey
BET	Brunauer, Emmet and Teller
CNT	Carbon nanotubes
EXAFS	Extended X-Ray Absorption Fine Structure
EDX	Energy Dispertive X-Ray spectroscopy
FBR	Fixed bed reactor
FT	Fischer-Tropsch
FTS	Fischer-Tropsch synthesis
GTL	Gas to Liquid
HC	Hydrocarbons
ICP	Inductively Coupled Plasma
MARR	Mean Absolute Relative Residuals
Micro FBR	Micro Fixed Bed Reactor
MWCNT	Multi walled carbon nanotubes
ROH	Alcohol chain
RSS	Residual sum of square
S	Surfactant
SEM	Scanning electron microscopy
TEM	Transmission electron microscopy
TGA	Thermogravimetric analysis
THF	Tetrahydrofurane
TPD	Temperature programmed desorption
TPR	Temperature programmed reduction
W	Water
WGS	Water-gas shift
XANES	X-ray Absorption Near Edge Structure
XPS	X-ray photoelectron spectroscopic
XRD	X-Ray diffraction

Nomenclature

A	Arhenius constant
Co	Cobalt
CO	Carbon monoxide
CO_2	Carbon dioxyde
CH_4	Methane
CH_n	Hydrocarbons chain
E	Energy of activation

Fe	Iron
g_{HC}	gramme of hydrocarbons
H	Hydrogen
h	hour
HNO_3	Nitric Acid
K	Potassium
k	Kinetic constant
K_n	Knudsen number
min	minute
MPa	Mega Pascal
P_{CO}	Partial pressure of CO
P_{H2}	Partial pressure of H_2
R	H_2 to CO ratio
R	Ideal gas constant
R^2	Sum of squares
$-r_A$	Global rate
Ru	Ruthenium
T	Temperature

Greek letters

α	Chain growth probability
λ	Mean free path
η	Order of the reaction
σ	Catalyst pore diameter
w	Weight percentage (W/W%)
ω	Water to surfactant ratio

Chapter 1: Introduction and Background

1.1 Project Motivation

The worldwide high demand of transportation fuel, decrease in conventional oil reserves and the world's commitment for the reduction and control of green house gas (GHG) emissions constitute one of the main driving forces for the continuously growing interest in Fischer Tropsch synthesis (FTS) technologies [De Klerk, 2009a; De Klerk, 2009b, Nel and De Klerk, 2009]. Traditional research on the production of bio-diesel has largely focused on waste oil transformation. FTS offers an alternative method for the production of diesels and enables to add value to syngas or natural gas via production of premium quality products free of nitrogen, sulfur, aromatics, and metals [De Klerk, 2009a]. Virtually unlimited markets already exist for GTL diesel engines since it can be used as a transportation fuel directly or blended to improve the performance of conventional diesels [Jun et al., 2004]. The Fischer-Tropsch process using synthesis gas derived from biomass gasification process is also considered carbon neutral (95 % carbon closure) [Mann and Spath, 1997]. Moreover, the National Renewable Energy Laboratory (NREL) in United States shows that the net energy production from biomass is highly positive: one unit of energy consumed from the fossil fuel produces approximately 16 units of electricity from biomass that can be sent to the grid [Mann and Spath, 1997]. The catalytic conversion of synthesis gas (i.e., CO and H_2 mixtures) leads to a large variety of products such as paraffins, olefins, alcohols, and aldehydes. The most desired products are those containing low amount of methane and oxygenates, high alkene/alkane ratio, and high C_5^+ content. However, there is a need for improvement in FTS catalyst research area in terms of products selectivity, catalyst deactivation and support optimization. The novelty of this research project is to use a new FTS catalyst support that demonstrates significant improvement for the FTS process. This catalyst has never been extensively characterized and tested in a fixed bed reactor.

1.2 Background of Fischer- Tropsch Synthesis

The FTS was invented in 1923 by Franz Fischer and Hans Tropsch during the German fuel crisis after World War I but hasn't been economically successful until the 1980s. The application of FTS at an industrial level started in Germany in 1935. The FT process was built in South Africa in 1960's and 1970's as oil sanctions were being introduced and the government needed a way to provide petrol and diesel in the country. Now, SASOL is operating in South Africa with three coal-based-plants using iron based catalyst [De Klerk, 2009a, Nel and De Klerk, 2009]. There is also a plant in Malaysia where natural gas is used as a raw material and one in Germany where the gas from biomass is used to produce liquid fuel.

The Fischer-Tropsch process involves the synthesis of hydrocarbon fuels from a gas mixture of carbon monoxide (CO) and hydrogen (H_2). The FTS process has shown to be catalyzed by certain transition metals, with Co, Fe, and Ru presenting the highest activity [Bechara et al., 2001; Iglesia, 1997; Jacobs et al., 2002; Oukaci et al., 1999; Tavasoli, 2005]. The Fischer-Tropsch synthesis can be a low temperature process (200 – 250 ^{o}C) or high temperature process (300 – 350 ^{o}C) [Folger, 2002], depending on the catalyst used. The pressure can be high (3MPa) or low (0.1MPa) depending on the product requirement and catalysts used. According to the literature, the space velocity used in a fixed bed micro reactor is around 1000 – 3600 h^{-1} [Itkulova and Zakumbaeva, 2002]. The Fischer-Tropsch main reaction is highly exothermic (Eq.1.1); the heat of reaction needs to be removed rapidly in order to avoid temperature increase which would result in undesired reaction such as deactivation of catalyst due to coking and sintering [Kuntze et al., 1995]. Therefore, the reactors used should be designed to avoid undesired products such as methane and CO_2.

$$CO + H_2 \longrightarrow -CH_2 + H_2O$$
$$\Delta H_R = -152 \text{ kJ/mol} \qquad (1.1)$$

Two main reactors used for the FTS are continuous stirred tank reactor (CSTR) and fixed bed reactor (FBR) [Dry, 2001; Everson and Mulder, 1993; Folger, 2002;]. CSTR or commonly called, slurry reactor, has low pressure drop and is more appropriate for

exothermic reactions [Folger, 2002b]. The synthesis gas is bubbled through heavy oil containing solid catalysts. Figure 1.1 shows the flow scheme of a slurry reactor.

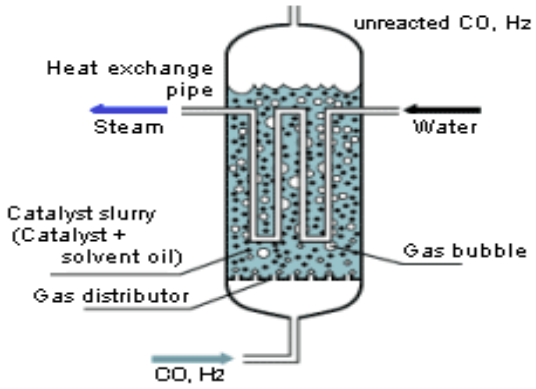

Figure 1. 1: Slurry reactor [Fogler, 2002]

Fixed bed reactors have the highest conversion per mass of catalyst and usually produce high amount of C_{5+} products. In the case of wax production, fixed bed reactors offer an advantage in that the wax product can be easily separated from the catalyst. In a slurry system, special devices are required to continuously remove the wax product. Currently, industries such as SASOL are using cobalt-based catalyst in fixed bed reactors [Dry, 2001]. The disadvantages of the fixed bed reactor are: high pressure drop, high heat transfer resistances and inefficient temperature control. The following figure shows the schematic of a fixed bed reactor.

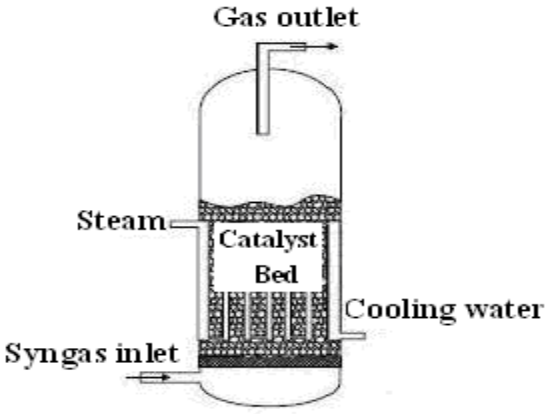

Figure 1. 2: Fixed bed reactor [Dry,2001]

Table 1.1 shows the main reactions of the FTS.

Table 1. 1 : Reactions involved in Fischer-Tropsch Synthesis [Van der Laan and Beenacker, 1999]

Main reactions	
1. Paraffins	$(2n + 1)H_2 + nCO \rightarrow C_nH_{2n+2} + nH_2O$
2. Olefins	$2nH_2 + nCO \rightarrow C_nH_{2n} + nH_2O$
3. WGS reaction	$CO + H_2O \leftrightarrows CO_2 + H_2$
Side reactions	
4. Alcohols	$2nH_2 + nCO \rightarrow C_nH_{2n+2}O + (n - 1)H_2O$
5. Catalyst oxidation/reduction	(a) $M_xO_y + yH_2 \rightleftarrows yH_2O + xM$
	(b) $M_xO_y + yCO \leftrightarrows yCO_2 + xM$
6. Bulk carbide formation	$yC + xM \leftrightarrows M_xC_y$
7. Boudouard reaction	$2CO \rightarrow C + CO_2$

The desirable reactions produce paraffins and olefins. The objective of the process is to produce an olefin/paraffins ratio higher than 1 to enable the α-olefin readsorption steps [Madon et al., 1993]. The water-gas-shift (WGS) is considered to be an undesirable reaction. However, this side reaction can be useful for lean hydrogen syngas feed. In fact, the water gas shift reaction (WGS) produces hydrogen at the same time it produces carbon dioxide. The undesirable reactions are the catalyst oxidation and the carbide compounds formation. Both of these side reactions will increase the catalyst deactivation. As an example, catalyst oxidation enhances the sintering of the catalyst particle. The highly desired products are C_5 to C_{20} hydrocarbons (Naphta C_5-C_{11}, Diesel C_{13}-C_{20} and Wax > C_{20}) [Van der Laan and Beenacker, 1999]. The primary products of FTS are linear olefins with terminal double bonds (70-80 mol %) and linear paraffins [Schulz et al., 2002].

The initial FTS reactions steps involve CO hydrogenation and dissociative CO adsorption (Eq.1.2) [Guczi et al., 1986; Tago et al., 2000]. All reactions involving C-C bond breakage or formation are considered as structure sensitive. Fischer-Tropsch synthesis also involves polymerization reactions. Due to these two types of reactions, the more plausible mechanism for the hydrocarbon formation is the carbide mechanism (-CH_2-) [Schulz et al., 2002; Wojciechowski, 1988]. In this mechanism, the -CH_2- group is the monomer that polymerizes to long hydrocarbon chains [Dry, 2001].

$$CO \longrightarrow CO^{*} \xrightarrow{+H_2} -CH_2 + H_2O \qquad (1.2)$$

Figure 1.3 shows different steps of the chain growth mechanism:

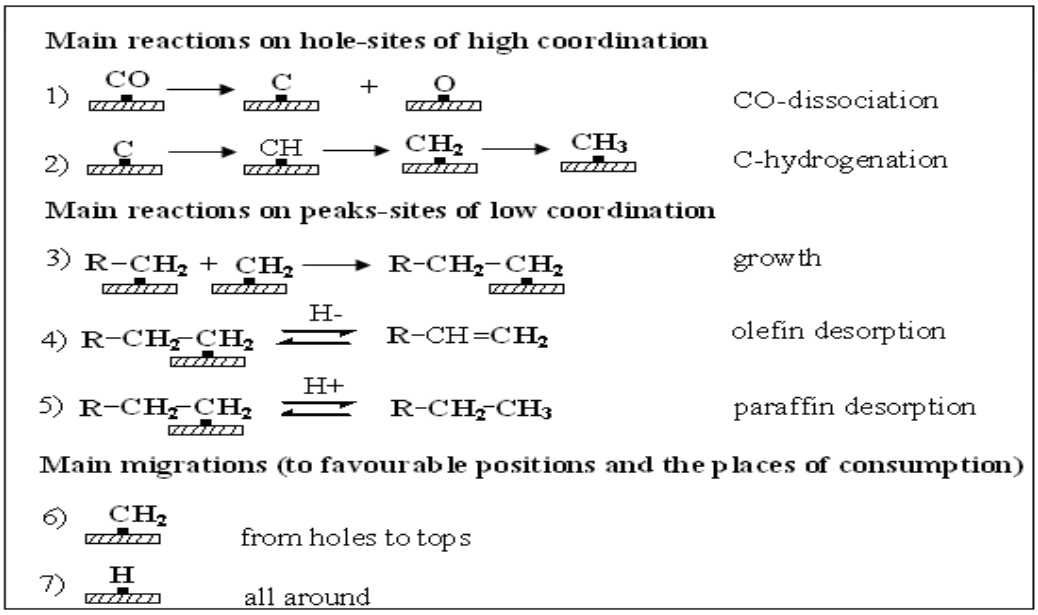

Figure 1. 3: Fischer-Tropsch polymerization mechanism [Schulz et al., 2002; Van der Laan and Beenacker,1999]

In this mechanism, the first steps are the dissociative adsorption of CO and H_2 to form the $-CH_2-$ monomer by hydrogenation (see Figure 1.3). Dissociative adsorption involves, using CO as an example, a carbon atom adsorbing dissociatively from the oxygen atom on the catalyst surface. The hydrogenation step (2) of the carbon site will then lead to the formation of the hydrocarbon monomer $-CH_2-$. Then, the monomer (step 3) initiates the chain growth, which occurs with the addition of an alkyl on the monomer to produce either olefin or paraffin (4-5). The chain termination reaction begins with removal of hydrogen during the hydrocarbon growth process. The re-adsorption of α-olefin is a secondary reaction that permits the production of longer hydrocarbon chains. The formation of the main products such as α-olefins and paraffins is then assumed as associative desorption of hydrogen as shown in equation 1.3. Then an alkyl species

together with a hydrogen atom dissociatively desorbs via hydrogen abstraction (see equation 1.4) to form a hydrocarbon chain [Van der Laan and Beenacker, 1999].

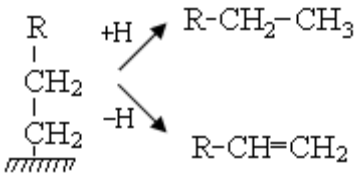

(1.3)

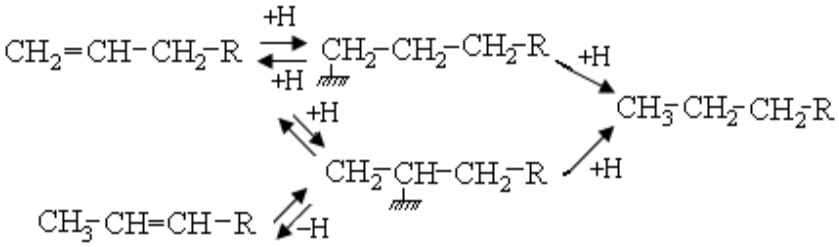

(1.4)

The chain growth probability (α) of the FTS process is determined by the Anderson-Schultz- Flory (ASF) model [Iglesia, 1997]. According to this model, the polymerization process in FTS is assumed to initiate on the surface of the catalyst by a monomer that contains one carbon atom, while chain growth takes place by the addition for one monomer at time [Elbashir and Roberts, 2005]. Example of ASF calculation is shown in Appendix A.

The process parameters have significant influence on product selectivity in Fischer-Tropsch synthesis. Table 1.2 summarizes the effects of each important parameter on product selectivity.

Table 1. 2: Effects of process parameters on FTS selectivity [Van der Laan and Beenacker, 1999]

Parameter	Chain branching	Olefin Selectivity	Alcohol selectivity	Carbon Deposition	Methane Selectivity
Temperature	↑	*	↓	↑	↑
Pressure	↓	*	↑	*	↓
H_2/CO	↑	↓	↓	↓	↑
Conversion	*	↓	↓	↑	↑
Space velocity	*	↑	↑	*	↓
iron catalyst	↓	↑	↑	↑	↓

Note: Increase with increasing parameter. | Decrease with increasing parameter.↓
Complex relation:*

According to Table 1.2, increasing temperature decreases chain length and alcohol selectivity and increases chain branching, carbon deposition and methane selectivity. Another important parameter is the pressure. Increasing the pressure will decrease the chain branching and the methane selectivity and increase the chain length and the alcohol selectivity. The ratio of synthesis gas (H_2/CO) will also influence the selectivity of the synthesis. Thus, increasing H_2/CO ratio decreases the hydrocarbon chain length, the olefin selectivity, the carbon deposition and the alcohol selectivity but increases the chain branching and the methane selectivity. Increasing the conversion decreases the olefin selectivity and increases the carbon deposition on the catalyst and the methane selectivity. The conversion of the FTS reactions is defined as the ratio of the total moles of CO consumed during the reaction over the total inlet moles of CO (Eq.1.5). The selectivity is defined as the ratio of the total moles of CO converted into CH_x over the total moles of CO consumed during the reaction (Eq.1.6). Finally, the yield is defined as return of the initial moles of carbon transformsed into hydrocarbon products (Eq.1.7).

$$\text{CO Conversion (\%)} = X_{CO} = \frac{\text{moles of inlet CO} - \text{moles of outlet CO}}{\text{moles of inlet CO}} \times 100\% \tag{1.5}$$

$$C_x \text{ Selectivity (\%, x = 2,3,4 ...)} = S_{Cx} = \frac{\text{moles of } C_x \text{ produced}}{\text{moles of inlet CO - moles of outlet CO - moles of } CO_2 \text{ produced}} \times 100\%$$

$$S_{C5+} = C_{5+} \text{ selectivity} = 1 - S_{CH4} - S_{C2} - S_{C3} - S_{C4} \tag{1.6}$$

$$\text{Yield (\%)} = \frac{\text{Total mole of C transformed into hydrocarbons chain}}{\text{Total inlet mole of C}} \times 100\% \tag{1.7}$$

1.2.1 Cobalt Catalysts for FTS

The FTS process is catalyzed by transition metals such as Co, Fe, and Ru presenting the highest activity [Bechara et al., 2001; Dry, 1981; Iglesia, 1997; Jacobs et al., 2002; Oukaci et al., 1999; Tavasoli, 2005]. Among them, cobalt catalysts are preferred because of their high activity for FTS, high selectivity to linear hydrocarbons, low activity for the water gas shift (WGS) reaction, stability toward deactivation by water

(a by-product of the FTS reaction), and their low cost compared to ruthenium [Bechara et al., 2001; Dry, 2001; Iglesia, 1997; Kuntze et al., 1995; Oukaci et al., 1999; Tavasoli et al., 2005]. Despite the high cost of cobalt, it has higher activity and longer life compared with Fe. Moreover, cobalt catalysts have a high dispersion of the active metal (Co^o) on the support surface and a high resistance to oxidation [Tavasoli et al., 2007]. Thus, Co based catalysts are considered as a good compromise between performance and cost.

The catalyst support is a physical material that supports the active phase (metal) of the catalyst by increasing its surface area. In order to achieve high surface active sites (Co^o), cobalt precursors are dispersed on these most frequently used porous carriers; SiO_2, Al_2O_3, and to a lesser extent TiO_2 being the most frequently used [Berge et al.,2000; Jacobs et al., 2002; Tavasoli et al., 2005]. Extensive studies have been done using cobalt catalyst supported on Al_2O_3. Alumina is often used as a support for cobalt catalysts due to favourable mechanical properties [Melene and Prinsloo, 2007]. Also, alumina support allows high cobalt dispersion on its surface [Bechera et al., 2001; Jacobs et al., 2002]. Silica support, according to the literature, has high local surface area (200 to 220 m^2/g) and titania support is characterized by its high methanation turnover rates [Iglesia, 1997; Li et al., 2002]. Activated carbon (AC) has aslo been studied as a FTS catalyst support. It shows higher C_1-C_{20} selectivity and olefins products than oxidic supports. The syngas conversion increases with cobalt loading. CO conversion of 56 % is achieved with 15 %.wt of cobalt loading on AC [Ma et al., 2004]. The porous structure of AC decreases the mass transfer limitation. AC is resistant to acidic or basic media and stable at high temperature [Ma et al., 2004, Serp et al., 2003]. A drawback for this support is the formation of cobalt carbides (Co_2C) during the reduction step of the catalyst. Thus, the activity of FTS reactions over co-based catalyst supported on AC decreases due to the formation of carbon-cobalt phase during the activation step [Xiang et al., 2005].

To optimize the hydrocarbon products selectivity (heavy hydrocarbon) with cobalt catalyst, the temperature of the reactor has to be between 210 and 230 ^oC according to SASOL industry [Espinoza and Steynberg, 1999]. The temperature should not exceed 250 ^oC as it lowers the formation of high hydrocarbon compounds (Figure 1.4). The main influence of the temperature is on the % CO conversion and on the

hydrocarbon chain length [Iglesia, 1997]. In fact, high temperature increases the H_2 mobility at the catalyst surface and then increases the % CO conversion [Tavasoli et al., 2007]. Also, temperature enhances the termination of paraffins against chain growth and then leads to a lower selectivity of C_{5+} and olefin to paraffin ratio (O/P). Figure 1.4 shows the influence of temperature on carbon chain length.

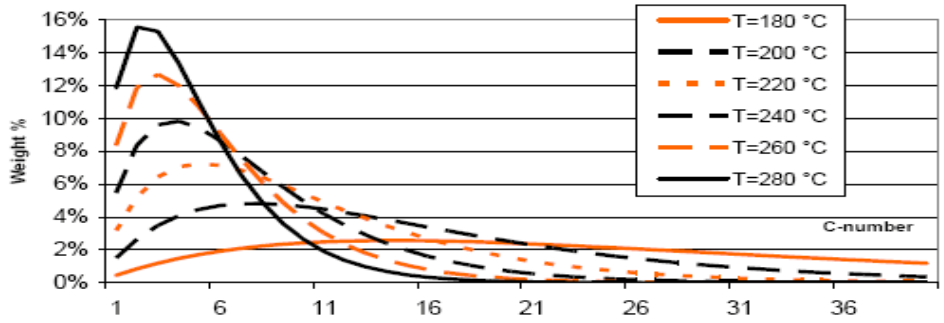

Figure 1. 4: Influence of temperature on the carbon chain length with Co-catalyst [Mann and Spath, 1997]

The desired pressure range for FTS reaction with cobalt catalyst is between 0.1 to 3 MPa. The catalyst performs better at a pressure lower then 3 MPa based on the following data from SASOL process (Figure 1.5) [Espinoza and Steynberg, 1999]. The optimum pressure seems to be at 20 bar (2 MPa) according to the product selectivity.

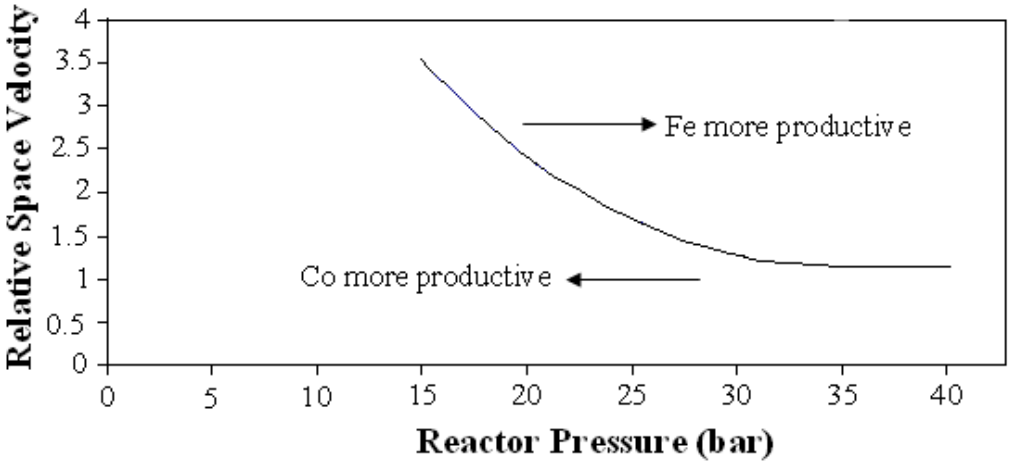

Figure 1. 5: Comparison between iron (240 ^{o}C) and cobalt (220 ^{o}C) based catalysts [Espinoza and Steynberg, 1999]

The feedstock ratio H_2/CO mostly influences the carbon chain length and O/P ratio and the C_{5+} selectivity. Figure 1.6 shows the influence of H_2/CO ratio on hydrocarbon chain length for the FTS reactions.

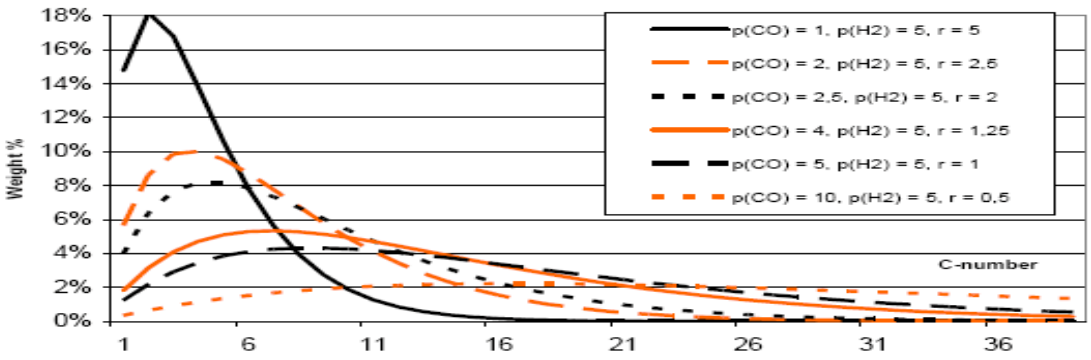

Figure 1. 6: Influence of H_2/CO ratio on the carbon chain length [Mann and Spath, 1997]

Then, higher partial pressure of CO increases CO adsorption at the catalyst surface and then increases the hydrocarbon chain growth [Yates and Satterfield, 1991]. Also, increasing the growth of -CH_2- will increase O/P ratio. The desired product (diesel) is around a carbon chain length of C_{11} to C_{20}. According to Figure 1.6, the recommended H_2/CO ratio should be between 1 and 2.

1.2.2 Carbon nanotubes as FTS Catalyst Support

The drawback of commonly used oxidic catalyst support was the reactivity toward metal cobal during catalyst preparation. The activity resulted in the formation of mixed compounds that are reducible at high temperature [Berge et al., 2000; Jacobs et al., 2002; Tavasoli et al., 2005]. Carbon nanotubes (CNT) provide a relatively inert support, suggesting that this is a unique system for the FTS catalyst study [Bahome et al., 2005; Bezemer et al., 2004;Tavasoli et al., 2008a; Tavasoli et al., 2008b; Tavasoli et al., 2007]. CNT, when used as a cobalt catalyst support in a FTS slurry reactor, allows better metal dispersion control and minimize the metal phase interaction and formation of mixed compounds with the support [Tavasoli et al., 2007]. Since CNTs have been considered as FTS catalysts supports, researchers have demonstrated that CNTs outperformed the commonly used FTS Al_2O_3, TiO_2, SiO_2 supports. Figure 1.7 results shows that CNT as a catalyst support for Fischer-Tropsch in a slurry reactor can increase the performance of the Co-catalyst compared to alumina supports [Tavasoli et al., 2007; Ya-Huie et al., 2005].

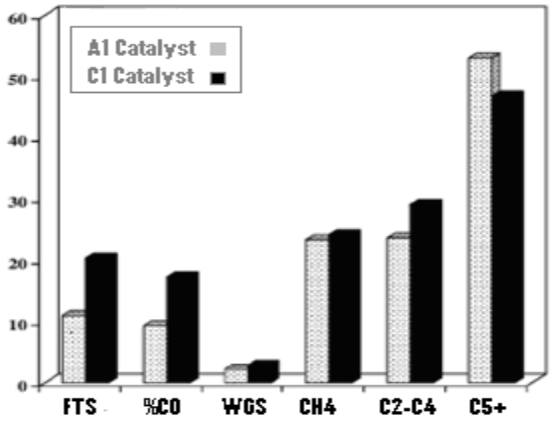

Figure 1. 7: FTS rate, % CO conversion, WGS rate and product selectivity of 15% Co/Alumina (A_1) and 15% Co/CNT (C_1) catalysts (T=220 ^oC, P=1 bar and H_2/CO =2) [Tavasoli et al., 2007]

Co/CNT catalyst significantly improved the %CO conversion and FTS rate (gHC produced/ g cat./ h). The methane selectivity and C_2-C_4 light gases selectivity slightly increases and the selectivity of liquid C_5^+ products are slightly decreasing. Some research has also been done with activated carbon as a support and the results show that this carbon support has resistance to acidic or basic media. Carbon supports are stable at high temperature and have high olefins selectivity compared to other supports [Ma et al., 2004]. Carbon nanotubes possess similar properties and in most cases outperform activated carbon for FTS [Tavasoli et al., 2007]. Chen et al. also observed that the confinement of the Fe particles within the CNT enables better reducibility and leads to higher rates of the CO dissociative adsorption on the metal surface [Chen et al., 2008]. As a new type of carbon material, CNTs have the appropriate pore-size distribution favoring maximum metallic dispersion [Pan et al., 2007]. Their special and steady structural characteristics and morphology are quite suitable for use as catalytic support materials [Bahome et al., 2005; Bezemer et al., 2004; Serp et al., 2003; Tavasoli et al., 2008b]. Carbon nanotubes can interweave during the growth, resulting in the formation of mechanically strong tangled agglomerates (as shown in Figure 1.8). The agglomerates facilitate an open pore volume, a pore size distribution, a predominant mesoporous structure, a high filterability as a result of low mass transfer limitation. They also have high thermal conductivity. Thus, the heat can be dispersed effectively along the CNTs,

which is another advantage for the exothermic FT reactions [Keyser et al., 2007]. Figure 1.8 shows a TEM picture of CNTs and its structural properties.

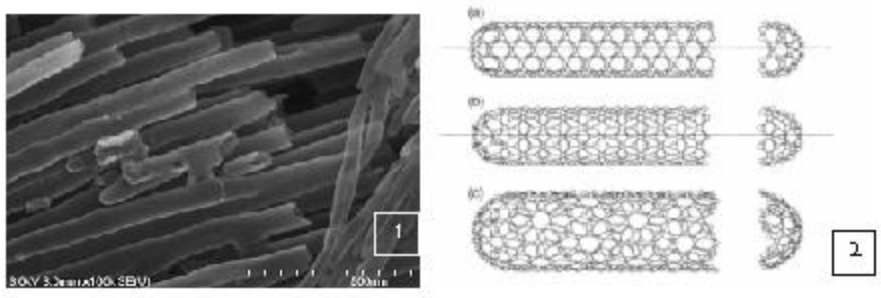

Figure 1. 8 : (1) TEM picture of CNTs produced at University of Saskatchewan by CVD method (2) CNT structural properties: (a) Arm chair, (b) Zigzag and (c) Helicoid [Dresselhaus et al., 1995]

Decrease in mass transfer limitation using mesoporous cobalt catalyst support has been reported in the open literature. According to Table 1.3, mesoporous support increases the %CO conversion and C_{5+} selectivity for FTS reaction related to the low mass transfer resistance inside the catalyst pores. Mesoporous scale is in ascending order for Table 1.3.

Table 1. 3: Fischer-Tropsch product distribution with various mesoporous zirconia-supported cobalt catalysts [Liu et al., 2005]

Sample	CO(%)	C_1(%)	C_5^+(%)	C_{18}^+(%)	$C_{12}C_{18}$(%)
Co/PM Z-3	13.58	44.91	36.36	1.03	9.56
Co/PM Z-5	42.41	24.40	46.46	1.95	14.01
Co/PM Z-7	81.03	12.15	69.86	12.87	20.31
Co/PM Z-12	86.12	10.61	86.69	19.23	32.32

Reaction conditions: T=230^{o}C, P= 2MPa, GHSV = 1000 h^{-1}, H_2/CO =2

Thus, CNT have many unique structural properties and have attracted increasing attention as a novel support media for heterogeneous catalysis [Serp et al., 2003].

1.2.3 Catalysts Preparation

Support Functionalization

A catalyst support is not merely a carrier but it may also contribute to the activity of the catalyst. The acid-base and textural properties of support catalysts play an important role in FT synthesis [Reuel and Bartholomew, 1984]. In addition, the use of an

inert support enhances C-C chain growth probability, and hydrocarbon formation would be favored by the presence of micropores since mass-transfer resistance is fairly low. Li et al., have indicated that using carbon as a support to provide an inert, poorly interacting surface could moderate the catalytic behavior of metals such as iron and cobalt [Li et al., 2003]. Their surface properties can be modified through different treatment to satisfy special needs (defects, acid functional groups). According to the literature, acid treatment not only breaks carbon nanotubes but also introduces a large number of functional groups on the support surface [Li et al., 2003; Pan et al., 2007]. The acidic surface groups significantly influence the preparation of CNT supported catalysts. Since the impregnation method entails contacting the CNT with the solution of the catalyst precursor and CNT, like other carbon materials, are essentially hydrophobic in nature, they have really low affinity for solvents such as water. The acidic groups decrease the hydrophobicity of the CNT and make the surface more accessible to the aqueous solution for the metal deposit [Pan et al., 2007]. Therefore, more metallic precursors are attached to the nanotubes and metal particles are dispersed more homogenously. It can also create some defects on the CNT surface, which increases the cobalt metal deposition.

Metal loading

The loading of the catalyst is defined as the concentration of active metal on the catalyst surface. For the Co-catalyst, according to the literature, variation of the loading is usually between 5 to 30 wt. % [Rohr et al., 2000]. Since, cobalt is expensive it is vital that a minimum amount is used without sacrificing activity. This is achieved by obtaining a high dispersion of Co on a suitable high area of support. The amount of loading influences the catalytic characteristic of the support surface. Indeed, as it is shown in Figure 1.9, CO-conversion increases with increasing the cobalt loading.

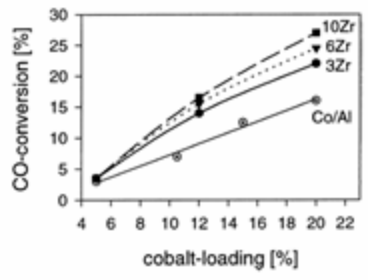

Figure 1. 9: Influence of cobalt loading on alumina support on % CO conversion [Li and Coville, 2001]

Low Co loading (< 15 wt.%) leads to high catalyst dispersion and high loading leads to low CH_4 selectivity and increases C_{12}-C_{20} formation [Bechera et al., 2001; Leonardos, 2005]. Increasing the amount of cobalt on the catalyst surface increases the cobalt particle size, which is due to agglomeration of the cobalt crystallites. The efficiency of the loading onto the catalyst will depend on the use of the catalyst preparation method.

The incipient wetness impregnation is a common method for metal loading on a catalyst support that enhances metal dispersion on the support [Keyser et al., 2007]. This method consists of loading the support with a metal nitrate solution in a small amount of water. The amount of added water is calculated from the pore volume of the support. In that case, this ensures that the support will adsorb all the metal aqueous solution. Characterization analysis from literature shows that crystallite size of the metal is more geometrically uniform on the surface of the support with this method [Benzemer et al., 2006]. These advantages of incipient wetness impregnation loading method ensure an increase in hydrocarbon formation of the FTS [Mirzaei et al., 2006]. The disadvantage of the incipient wetness impregnation technique is it results in wide particle size distribution and the non uniform composition when using bimetallic catalysts.

As mentioned previously, FTS implies structure sensitive reactions where both catalytic activity and selectivity are dependent on metal particle size [Klabunde et al., 1994]. It is well documented that CO hydrogenation mechanism is influenced by the noble metal particle size of the catalyst [Bezemer et al., 2006; Kim et al., 1997; Ojeda et al., 2004]. Thus, control of the chemical and physical parameter, especially the metal particle size, is significant for FTS catalytic reactions. Microemulsion, a novel catalyst preparation method, has been developed to produce synthesized nanoparticles. This new method enables the control of the catalyst metal particle size. The reverse water-in-oil (w/o) microemulsion allows mono-dispersed nanometer particles size [Kishida et al., 1995]. The Microemulsion system is defined as water, oil, and amphiphile (surfactant). This system is an optically isotropic and thermodynamically stable solution. The size of the metallic particle depends on the water droplets size in the microemulsion. The water-to-surfactant ratio (ω) will determine the size of the water droplets. An increase in the water-to-surfactant ratio (ω) will increase the average diameter of the droplets. For

example, Cu nanoparticles prepared in a system consisting of ionic surfactant, cyclohexane, and water increased from 2 to 10 nm as ω changed from 1 to 10 [Lisiecki and Pileni, 1993]. This catalyst preparation method to produce nanosized metal particles becomes attractive since the widespread use of these particles in heterogeneous catalysts [Yasima and Falk, 2003]. The disadvantage of the microemulsion preparation technique is that it is difficult to immobilize the nanoparticles on catalyst supports without large aggregation and the metal loading should not exceed 10 wt. % [Ericksson et al., 2004].

1.2.4 Cobalt FTS catalyst deactivation

One of the most insidious problems in catalysis is the loss of catalytic activity that occurs as the reaction proceeds on the catalyst. Despite that the deactivation of cobalt catalysts has been studied extensively, it has not been exactly identified what fraction of catalyst deactivation is due to re-oxidation of cobalt; cobalt support interactions, cobalt aluminate formation (in case of alumina support), sintering, and refractory coke deposition [Tavasoli et al., 2008c, Tavasoli et al., 2008d]. It is important to study in detail the contribution of each deactivation feature to the total catalyst deactivation. For Co/Al_2O_3, the % CO conversion decreased from 80 to 68 % after 350 h and stayed constant at 68 % until 1000h [Tavasoli et al., 2008c]. Water is one of the products of the FTS that can cause catalyst deactivation [Hilmer and Schanke, 1999]. Water increases the oxidation and metal cobalt interaction with the support which also enhances the coke formation [Hilmer and Schanke, 1999].

1.2.5 Promoters for FTS Cobalt Catalysts

A promoter is a small amount of a substance that increases the activity, selectivity and stability of the catalyst. The literature has presented different types of promoters: structural or structure promoters, electronic promoters, textural promoters, stabilizers, and catalyst-poison-resistant promoters. Since many of the above-mentioned effects tend to overlap in practice, it is sometimes difficult to precisely define the observed function of a promoter [Morales and Weckhuysen, 2006]. In addition, the degree to which additives modify a catalyst's activity in the positive or negative manner is also dependent on the amount of the additive, the support oxide under consideration, and the exact preparation method, causing them to act either as a promoter or a poison. Many

promoters have been used to improve the efficiency of FTS cobalt catalysts such as Ru, Ce, Zr, B, Mg, Re, and K [Anderson, 2001; Everson and Mulder, 1993; Itkulova and Zakumbaeva, 2002; Li and Coville, 1999; Li and Coville, 2001; Ma et al., 2004; Mirzaei et al., 2006; Tago et al., 2000; Tavasoli et al., 2008c; Xiong et al., 2004; Ya-Huei et al., 2005]. Among them, three promoters Ru, Re and K have garnered more attention since they improve the performance of FTS catalysts with alumina supports.

Ruthenium is the most studied noble metal promoter and it has been frequently shown to play a role both in structural and electronical promotion [Morales and Weckhuysen, 2006]. This promoter increases Co F-T activity without modifying the chemical reactivity of exposed Co surface atoms. Ru inhibits the deactivation of the catalyst by keeping the Co surface clean and hence preventing carbon deposition on the Co particles [Morales and Weckhuysen, 2006]. According to the literature, the appropriate ratio for Ru and Co on Co/Al_2O_3 is $Ru/Co < 0.008$ [Hosseini et al., 2004]. Then, the more desired amount of ruthenium for 20 wt. % Co is in between 0.5 to 1 wt. %. Higher purcentage of Ru content of 1.5 to 2 wt. % leads to decrease in CO hydrogenation activity [Hosseini et al., 2004]. The C_{5+} selectivity remained almost unaffected by ruthenium loading [Hosseini et al., 2004; Bazin et al., 2003].

Rhenium (Re) prevents agglomeration during the reaction steps and the results show high Co dispersion on the surface of the catalyst when Re is added [Iglesia, 1997]. High FT conversions (>30 %) have been noticed with 0.34 wt. % Re on 10 wt. % Co catalyst supported on TiO_2 [Ronning et al., 2001]. Rhenium increases the cobalt catalyst activity and prevents the formation of cobalt surface phases. It has been shown a bimetallic interaction resulting in Re-Co bond formation. Moreover, the average cluster size decreased with increasing Re loading [Li and Coville, 1999].

Potassium is more qualified as a support promoter than an active metal promoter. It will interact with both the Co phase and the support [Duvenhage and Coville, 2005; Huffman et al., 1994; Raje et al., 1998]. It has been shown that the K inhibits the reduction of Co/SiO_2 in H_2 at 200 ^oC. This promoter inhibits the reduction of the cobalt catalyst because the catalyst is more oxidized than the unpromoted catalyst. However, potassium will enhance the olefins content of the products with a K/Co ratio of 0.0025 to 0.03 [Huffaman et al., 1994]. It will also increase the specific activity of the catalyst. But

high loading of K/Co > 0.01 will do the reverse phenomenon. In the case of Co catalyst, potassium decreases FT activity and CH_4 selectivity and increases WGS activity [Bazin et al., 2003].

1.2.6 FTS Co/Fe Bimetallic Catalysts

Since the discovery of the FT reaction in the 1920s, the industrial catalysts of choice have been cobalt and iron. Both Co and Fe are typically used when combined with a range of supports and promoters that permit further control over the product spectrum. A viable methodology that has been developed for controlling the property of a metal is that of alloying. Alloys have been used in the FT reaction to obtain the desired selectivity of the FT products spectrum. In particular, it has been reported that an alloy of the two most active catalysts, Fe and Co, have generated product streams in the FT reaction richer in olefins than expected from either Fe or Co catalysts [Duvenhage and Coville, 2002; Jacobs et al., 2002; Mirazaei et al.,2005]. It is also reported that Fe/Co complex is easier to reduce than the individual metals [Duvenhage and Coville, 2002]. The following figure shows the %CO conversion for different Co/Fe alloys [Pena O'Shea et al., 2007].

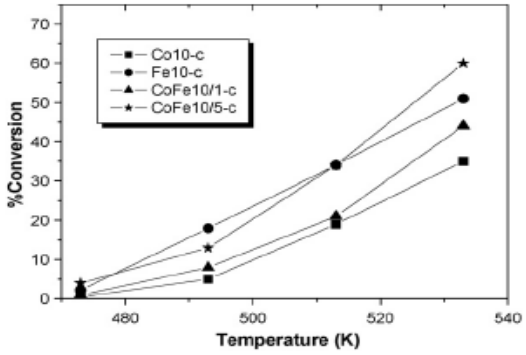

Figure 1. 10: % CO conversion for mono and bimetallic catalyst in a fixed –bed reactor (P=20bar, H_2/CO= 2) [Pena O'Shea et al., 2007]

This figure shows clearly that addition of small amount (< 4 wt. %) of iron on cobalt catalyst increases the selectivity of Fischer-Tropsch Synthesis.

1.2.7 Kinetics studies of FTS cobalt catalyst

Several studies have investigated the kinetics of FTS on cobalt catalyst [Anderson, 1956; Brötz, 1949; Iglesia et al., 1993; Sarup and Wojciechowski, 1989;

Yates and Satterfield, 1991; Zennaro et al., 2000] .Yates and Satterfield, Sarup and Wojciechowski, Iglesia et al, studied the kinetics of relevant cobalt catalyst supported on Al_2O_3, SiO_2 and Kiselgurh showing reaction orders for H_2 and CO rate in the range of 0.5 to 2 and -1.0 to 0.65, respectively. The activation energies for these studies cover a range of 98-103 kJ/mol [Brötz, 1949; Iglesia et al., 1993; Sarup and Wojciechowski, 1989; Yates and Satterfield, 1991]. However, the activation energy of the Co/TiO_2 catalyst studied by Zennaro el al. was in the range of 83.4 kJ/mol [Zennaro et al., 2000]. The support, promoters, heat-mass transport, and catalyst deactivation influence the kinetics [Anderson, 1956; Ribeiro et al., 1997; Zennaro et al., 2000]. Assurances of the absence of pore diffusion, mass transfer, and heat transfer limitation increase the reliability of the studied kinetic model [Anderson, 1956; Folger, 2002; Ribeiro et al., 1997; Zennaro et al., 2000]. Properties and knowledge of the reaction mechanism also allows to determine if the studied models are physically or chemically reasonable [Sarup and Wojciechowski, 1989; Yates and Satterfield, 1991]. Heterogeneous catalysts are effective only if the external and internal mass transfer resistances are reduced so that the reactants can reach the catalytic surface. Often, pore diffusion limits the overall rate of reaction in the case of a heterogeneous catalyst [Smith, 1981]. Figure 1.11 shows the mass transfer and internal pore diffusion in the case of catalyst pellet.

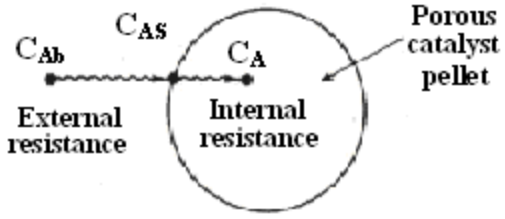

Figure 1. 11: Mass transfer and internal diffusion imply in a catalyst pellet [Fogler, 2002]

External mass transfer resistance is influenced by the boundary layer thickness where the change in concentration of reactant from bulk concentration to surface concentration takes place. At low velocities, mass transfer boundary layer thickness is large and diffusion limits the reaction. To eliminate external mass transfer resistance, the reaction process should be operating at high velocity or using satisfactory small catalyst particle sizes [Satterfield, 1970]. The internal mass transfer resistance occurs when the reactants

diffuse from the external surface into and through the pores within the catalyst. The Weisz-Prater criterion is used to determine if internal mass transfer limits the reaction [Fogler, 2002]. Example of Weisz-Prater criterion calculation and mass transfer diffusion evaluation are shown in Appendix B. Heat-transfer also influences the kinetics of a catalytic reaction. Therefore, in a fixed-bed reactor, transport rates are normally defined in terms of an average heat–or-mass transfer coefficient [Smith, 1981]. The average coefficient can be applied to all the outer surface of a pellet. The global rate ($-r_A$) is calculated by simultaneous solution of mass and energy balance equations. If the objective is to find the intrinsic rate of reaction, the global rate is directly obtained from the experimental measurements [Folger, 2002]. Therefore, it is important to study the effects of such operational parameters (P, T, H_2/CO and flow rate), on the reaction rate, and then to eliminate the effects of physical processes. The energy of activation can be determined by varying reaction temperature for adsorption and surface process ($k = Ae^{-E/R_gT}$) and varying the flow rate and partial pressure will allow evaluating various rate equations according to various reaction mechanisms of reactions [Smith, 1981]. The literature proposes different models for cobalt FTS catalyst kinetics. Wojciechowski created an empirical kinetic equation (Eq.1.8) for the reaction for FTS cobalt catalyst:

$$-r_{CO} = \frac{aP_{CO}^{\alpha}P_{H_2}^{\beta}}{(1+bP_{CO}^{ci}P_{H_2}^{di})^2} \tag{1.8}$$

where, α and β are the reaction order with respect to CO and H_2 respectively. The parameters a and b are the kinetic constant and the adsorption constant, respectively. The reaction order is normally around 0 or 1 or 2 [Wojciechowski, 1988]. The Langmuir–Hinshelwood model in Eq.1.9 based on catalyst surface adsorption studies, proposes a bimolecular surface reaction for FTS with cobalt, which is indicated by the exponent 2 at the denominator of the equation [Wojciechowski, 1988]. Also, in Eq. 1.9 the rate of the reaction is influence by the partial pressure of CO and the partial pressure of H_2.

$$-r_{CO} = \frac{aP_{CO}P_{H_2}}{(1+bP_{CO})^2} \tag{1.9}$$

Table 1.4 shows the kinetic models based on the carbide mechanism developed by many researchers on catalysis area.

Table 1. 4: Summary of kinetics studies of the Fischer-Tropsch synthesis on cobalt bases catalysts [Van der Laan et al., 1999; Wojciechowski, 1988; Yates and Satterfield, 1991]

Study	Rate Equations
Power Law	$-r_{H_2+CO} = aP_{H2}^{\alpha}P_{CO}^{\beta}$
Rautavuoma	$-r_{CO} = \frac{aP_{H_2}^{\alpha}P_{CO}^{\beta}}{(1+bP_{CO}^{\beta})^3}$
Sarup and Wojciechowski	$-r_{H_2+CO} = \frac{aP_{H_2}^{\alpha}P_{CO}^{\beta}}{(1+bP_{CO}^{\beta})^2}$
Sarup and Wojciechowski	$-r_{H_2+CO} = \frac{aP_{H_2}^{\alpha}P_{CO}^{\beta}}{(1+bP_{CO}^{\nu}P_{H_2}^{o})^2}$
Anderson	$-r_{H_2+CO} = \frac{aP_{H_2}^{\alpha}P_{CO}^{\beta}}{(1+bP_{CO}^{\beta}P_{H_2}^{\alpha})^2}$
Iglesia	$-r_{H_2+CO} = \frac{aP_{H_2}^{\alpha}P_{CO}^{\beta}}{1+bP_{CO}^{\beta}}$

Statistical methods require obtaining the best fit of the equation to the kinetic data. Then, powerful iterative methods can be used to solve the model equations.

1.3 Knowledge Gaps

There is no open literature on the cobalt-CNT support catalyst using a fixed bed reactor for the FTS as well as on the novel microemulsion nano-catalyst preparation technique to produce Co/CNT FTS catalyst. The kinetic development of the Co/CNT support catalyst in term of FTS has never been reported in literature.

1.4 Research Objectives

The main research objective is to demonstrate that the carbon nanotubes are suitable as a novel support for FTS cobalt catalyst. To achieve this goal, catalysts were developed for use in Fischer-Tropsch synthesis by evaluation of the support functionalization and the process parameters. The deactivation mechanism was also studied to identify the stability of this novel catalyst. In order to optimize this new developed catalyst, improvement of catalyst efficiency with increasing loadings of active cobalt on the CNT support and promoter loading (Ru, Fe, K) have been studied. Moreover, a new nano-catalyst preparation technique, the microemulsion, was also investigated to study the FTS reaction sensitivity to different particle sizes. Finally, the kinetic model of the optimized catalyst was developed in terms of FTS.

1.5 Organization of the Thesis

The thesis is organized according to the University of Saskatchewan guidelines for manuscript-based-theses. The data and analysis are presented as a series of journal manuscripts. The bulk of the thesis consists of a series of literary publications of the research that were compiled over the course of the project. These manuscripts were written and submitted for publications as each stage of the Ph.D project was completed. The manuscripts presented in Chapters 2-6 have all been published in peer-reviewed journals. The manuscript for Chapter 7 was written in the final phase of the Ph.D project and has only recently been completed and submitted for review to The Canadian Journal of Chemical Engineering. In each manuscript-based chapter, three issues are discussed in addition to the manuscript itself: the contribution of the Ph.D candidate, the contribution of the paper to the overall study and relevant material not in the manuscript (if required). Chapters 1 and 8 are original text in this thesis included to introduce the subject matter and discuss the summary and recommendations of the project. The corresponding references are found at the end of each chapter. Supplementary materials are given in the Appendices at the end of this document.

1.6 Manuscript Content of the Thesis

The following section describes the specific topic of each chapter and the way in which it addresses the overall objectives of the thesis. This manuscript-based thesis is divided into 8 Chapters.

In order to assist the sustainability of this new FTS Co/CNT catalyst and to show the influence of acid treatment (support functionalization) on the CNT support, Chapter 2 discusses about the screening of the Co/CNT catalyst and the influence of acid treatment on CNT support. Chapter 2 reports interesting catalytic properties of CNT-supported cobalt catalysts and show distinct advantages compared to Co/Al_2O_3 catalysts. Although, CNT-supported cobalt catalysts are more expensive, necessitating a longer life-time. Catalyst stability is one of the main performance variables in Co-based FTS catalysts. Therefore, Chapter 3 describes the deactivation study on Co/CNT catalyst and also discusses about the effects of particles confinement inside the carbon nanotubes on activity, selectivity and lifetime of the Co/CNT catalyst. Increasing the cobalt loading or addition of promoter at the surface of the catalyst was used to improve the Co-based FTS catalysts performance. Chapter 4 shows that by increasing the Co wt. % loading of the catalyst up to 30 wt. % and by adding Ru and K promoters, the Co/CNT performance is improved. Alloys can be used for controlling property of transition metals at the catalyst surface. Co and Fe are typically used in combination as FTS catalysts. Chapter 5 discusses the influence of iron (Fe) addition on Co/CNT catalysts. FTS mechanism is conducted by structure sensitive reactions such as CO dissociative adsorption that are influenced by the structure and size of the cobalt particle. Microemulsion catalyst preparation technique enables controlling the particle size on the catalyst surface as well as producing nanosized particle. Chapter 6 describes the influence of cobalt particle size on the reducibility, activity and selectivity of Co/CNT FTS catalyst and compares the previous results using the wetness incipient impregnation catalyst preparation method. This new Co/CNT catalyst study would not have been complete without a kinetic study. Chapter 7 describes the kinetic study of the optimized catalyst under representative reaction conditions in the absence of heat and mass transport limitation. It also reports significance of statistical measurement of data and the development of the the phenomenological kinetic model that takes into account the physical and chemical

properties of synthesis gas consumption on the Co/CNT catalyst surface. General discussion, the achievement of research objectives and recommendations of the thesis are provided in Chapter 8. Appendices summarize calculations such as the ASF distribution (A), the Weisz-Prater criterion (B), the Sherrer Equation (C) and the mass balance (D).

1.7 References

Anderson. R.B., "Experimental method in Catalytic Research," in: "Catalysis vol 4," P.H. Emmet, Eds., Reinhold, New York (1956), Chap.1-2 and 3.

Anderson, R.B., "Catalytic properties of Co/Al_2O_3 system for hydrocarbon synthesis," Applied Catalysis A: General **207**, 343-353 (2001)

Bahome, M.C., L.L. Jewell, D. Hildebrant, D.Glasser and N.J.Coville, "Fischer–Tropsch synthesis over iron catalysts supported on carbon nanotubes," Applied Catalysis A: General **287**, 60-67 (2005).

Bazin, D., I.Kuovacs, J. Lynch and L.Guczi, "Ru-Co/Na bimetallic catalysts: insitu Exafs study of Co-K and Ru-K absorption edges,"Applied Catalysts A: General **242**, 179-186 (2003).

Bechara, R., D.Balloy and D.Vanhove, "Catalytic properties of Co/Al_2O_3 system for hydrocarbon synthesis," Applied Catalysis A: General **207**, 343-353 (2001).

Berge, V.P.J., J. van de Loosdrecgt, S. Barradas and A. M. van der Kraan, "Oxidation of cobalt based Fischer–Tropsch catalysts as a deactivation mechanism," Catalysis Today **58**, 321-334 (2000).

Bezemer, G. L., J.H. Bitter, H.P.C.E Kuipers, H. Oosterbeek, J.E Holewijn, X. Xu, X., F. Kaptejin, A. Jos Van Dillen and K.P de Jong, "Cobalt Particle size Effects in the Fischer-Tropsch Reaction studied with Carbon Nanofiber Supported Catalysts," Journal of American Chemical Society **128**, 3956-3964 (2006)

Bezemer, G.L., A.V. Laak, A. J. V. Dillen and K.P. Jong, "Cobalt Supported on Carbon Nanofibers - A Promising Novel Fischer-Tropsch Catalyst," Studies in Surface Science and Catalysis **147**, 259-264 (2004).

Brötz, W., Elecktrochem **53**, 301-306 (1949)

Chen, W., Z. Fan, X. Pan, X. Bao, "Effect of Confinement in Carbon Nanotubes on the Activity of Fischer-Tropsch Iron Catalyst," Journal of American Chemical Society **130**, 9414-9419 (2008).

De Klerk, A.,"Can Fischer-Tropsch syncrude be refined to on-specification diesel fuel," Energy & Fuel **23**, 4593-4604 (2009a).

De Klerk, A.,"Catalysts important in the refining of Fischer-Tropsch syncrude to fuels, Preparation Paper Americain Chemical Society Division," Fuel Chemistry **54**, 16-117 (2009b).

Dresselhaus, M.S.,G. Dresselhaus,R. Saito., "Physics of Carbon nanotubes," Carbon **33**, 883-891 (1995).

Dry, M.E., "High quality diesel via the Fisher-Tropsch process: A review," Journal of chemical technology and biotechnology **77**, 43-50 (2001).

Dry, M.E.,"The Fischer-Tropsch Synthesis,"in "Catalysis, Science and Technology Vol.1,"J.R. Anderson and M.Boudart, Eds., Springer, Berlin (1981), p.159-255.

Duvenhage, D.J., N.J.Coville, "Fe:Co/TiO_2 bimetallic catalysts for the FT reaction Part2: The effect of calcination and reduction temperature," Applied Catalysis A:General **233**, 63-75 (2002)

Duvenhage, D.J., and N.J Coville, "Effect of K, Mn and Cr on the Fischer-Tropsch activity of Fe:Co/TiO_2 catalysts," Catalysis Letters **104**, 129-133 (2005).

Elbashir, N.O. and C.B. Roberts, "Enhanced Incorporation of α-Olefins in the Fischer−Tropsch Synthesis Chain-Growth Process over an Alumina-Supported Cobalt Catalyst in Near-Critical and Supercritical Hexane Media," Industrial and Engineering Chemistry Research **44**, 505-521 (2005).

Eriksson, S. U. Nylen, S.Rojas and M.Boutonnet, "Preparation of catalysts from microemulsion and their applications in heterogeneous catalysis," Applied Catalysis A: General **265**, 207-219 (2004).

Espinoza, R.L. A.P. Steynberg, "Low temperature Fischer-Tropsch synthesis from a Sasol perspective," Applied Catalysis A: General **186**, 13-26 (1999).

Everson, R. C. H. Mulder, "Fischer-Tropsch reaction with supported ruthenium catalysts," Journal of Catalysis **143**, 166-174 (1993).

Folger, H. S, "Elements of Chemical Reaction Engineering 3^{th} ed," in " Physical and Chemical Engineering Sciences," Upper Saddle River, Eds., New Jersey (2002), pp.21, 581-684, 770, 758.

Guczi, L., Z.Schay, K.Matusek, I.Bogyay, "Surface structure and selectivity control in the CO + H_2 reaction over FeRu Bimetallic catalysts," Applied Catalysis **22**, 289-309 (1986).

Hilmer, A.H., D.Schanke, "Study of the effect of water on alumina supported cobalt," Applied Catalysis A: General **186**, 169-188 (1999).

Hosseini, S.A., A.Taeb, F.Feyzi and F.Yaripour,"Fischer-Tropsch synthesis over Ru promoted Co/γ-Al_2O_3 catalysts in CSTR," Catalysis Communications 5,137-143 (2004).

Huffaman, G.P N., Shah, J.Zhao, F.E.Huggins, T.E.Hoost, S.Halvorsen and J.G.Goudwin,"In-situ XAFS investigation of K-promoted Co catalysts," Journal of Catalysis **151**, 17-25 (1994).

Iglesia, E., "Design, synthesis, and use of cobalt-based Fischer-Tropsch synthesis catalysts," Applied Catalysis A: General **161**, 59-78 (1997).

Iglesia, E., S.C. Reyes, S.L. Soled, "Computer-Aided Design of Catalysts," in "E.R. Becker,"C,J.Pereira, Eds., Dekker, New-York (1993).

Itkulova, S., G.D. Zakumbaeva, **"**The bimetallic co-containing supported catalysts for the production of high value hydrocarbons from carbon dioxide and methane via synthesis-gas," MOKL 57, 265-270 (2002).

Jacobs, G., T.K Das, Y. Zhang, J. Li, G. Racoillet and B.H. Davis, "Fischer–Tropsch synthesis: support, loading, and promoter effects on the reducibility of cobalt catalysts," Applied Catalysis A:General **233**, 263-281 (2002).

Jun, K.W., H.S.Roh, K.S.Kim, J.S. Ryu, K.W.Lee, "Catalytic investigation for Fischer-Tropsch synthesis from bio-mass derived syngas," Applied Catalysis A: General **259**, 221-226 (2004).

Keyser, M. M. and F. F. Prinsloo, "Loading of Cobalt on Carbon Nanofibers," Studies in Surface Science Catalysis **163**, 45-73 (2007).

Kim, W-Y., T Haoka, M. Kishiba and K. Wakabayshi, "Hydrogenation of carbon monoxide over zirconia-supported palladium catalysts prepared using water-in-oil microemulsion," Applied Catalysis A: General **155**, 283-289 (1997).

Kishida, M., T. Fujita, K.Umak, "Novel preparation of metal-supported catalysts by colloidale microparticles in water-in-oil microemulsions catalytic hydrogenation of carbon dioxide," Journal of the Chemical Society, Chemical Communication , 763-764 (1995)

Klabunde, K.J., Y.X.Li, A.Khaleel, in: G.C. Hadjipanayis, " Nanophase Materials," R.W. Siegel (Eds), Kluwer Academic Publishers, Netherlands (1994), p.757.

Kuntze, T., K.Hedden and A.Jess, "Kinetics of the Fisher-Tropsch-Synthesis using a Nitrogen-Rich Synthesis Gas," Erdgasanwendung **2**, 67-71(1995).

Leonardos, M., "Cobalt catalyst for the synthesis of Fischer-Tropsch, catalyst support, processes for the preparation of the support and catalyst and use of catalyst," WO/2005/085390. Rio de Janeiro (2005)

Li, C., Ke Yao, J.Liang, "Influence of acid treatment on the activity of carbon nanotube-supported catalysts," Carbon **41**, 858-860 (2003).

Li, J., N.J Coville, "The effect of boron on the catalyst reducibility and activity of Co/TiO_2 Fischer-Tropsch catalysts," Applied Catalysis A: General **181**, 201-208 (1999).

Li, J.L. and N.J.Coville, "Effect of Boron on the sulfur poisoning of Co/TiO_2 Fischer-Tropsch catalysts," Applied Catalysts A: General **208**, 177-184 (2001)

Lisiecki, I., M.P.Pileni, "Synthesis of Copper metallic clusters using reverse micelles as microreactors,"Journal of American Chemical Society **115**, 3887-3896 (1993).

Liu, Y., K.Fang, J.Chen, Y.Sun, "Effect of pore size on the performance of mesoporous zirconia-supported cobalt Fischer-Tropsch catalyst,"Green Chemistry **9**, 611-615 (2007).

Ma, W-P., Y-J.Ding, L-W. Lin, "Fisher-Tropsch Synthesis over Activated-Carbon-Supported Cobalt Catalyst: Effect of Co Loading and Promoters on Catalyst Performance," Industrial and Engineering Chemistry Research **43**, 2391-2398 (2004).

Madon, R.J., E.Iglesia, "The Importance of Olefin Readsorption and H_2/CO Reactant Ratio for Hydrocarbon Chain Growth on Ruthenium Catalysts," Journal of Catalysis **139**, 576-590 (1993).

Mann, M.K, Spath, P.L, "Life Cycle Assessment of a Biomass Gasification Combined-Cycle System," NREL (1997), Report No. TP-430-23076.

Melene, M. Keyser and Frans F. Prinsloo, "Loading of Cobalt on Carbon Nanofibers", Catalysts and Catalysis, 45-72 (2007)

Mirzaei,A.A., R. Habibpour, E. Kashi, "Preparation and optimization of mixed iron cobalt oxide catalyst for conversion of synthesis gas to light olefins," Applied Catalysis A: General **296**, 222-231 (2005).

Mirzaei, A.A., M. Faizi, R. Habibpour, "Effect of preparation on the catalytic performance of cobalt manganese oxide for conversion of synthesis gas to light olefins," Applied Catalysis A: General **306**: 98-107 (2006).

Morales. F, M. Weckhuysen, "Promotion effects in Co-based Fischer-Tropsch Catalysis," Catalysis **19**, 1-40 (2006).

Nel, R.J.J, A. De Klerk, "Overview of FT aqueous product refining strategies," Fuel Chemistry **54**, 118-119 (2009).

Ojeda, M., S.Rojas, M.Boutonnet, F.J.Perez-Alonso, F. Javier Garcia-Garcia and J.L.G Fierro, "Synthesis of Rh nano-particles by the microemulsion technology: Particle size effect on the CO+H_2 reaction," Applied Catalysis A: General **274**, 33-41 (2004).

Oukaci, R., J.G.Goodwin Jr. and A. H. Singleton, "Effect of Titanium Doping on the Activity of Alumina-Supported Cobalt-Based Fischer-Tropsch Catalysts," Applied Catalysis A: General **186**, 129-144 (1999).

Pan, X., Z. Fan, W. Chen, Y. Ding, H. Luo and X. Bao, "Enhanced ethanol production inside carbon-nanotube reactors containing catalytic particles," Nature **6**, 507-511 (2007).

Patzlaff, J., Y. Liu, C. Graffmann, J. Gaube, "Studies on product distributions of iron and cobalt catalyzed Fischer–Tropsch synthesis," Applied Catalysis A: General **186**, 109–119 (1999).

Pena O'shea, V.A., M.C. Alvarez-Galvan, J.M.Campos-Martin, J.L.G. Fierro, "Fischer-Tropsch-Synthesis on mom-and bimetallic Co and Fe catalysts in fixed bed and slurry reactors," Applied Catalysis A: General **326**, 65-73 (2007).

Raje, A.P., R.J.O'Brien, B.H.Davis, "Effect of potassium promotion on iron-based catalysts for fischer-tropsch synthesis," Journal of Catalyst **180**, 36-43 (1998).

Rautavuoma, A.O.I and H.S. van der Bann, " Kinetics and Mechanism of the Fischer-Tropsch Hydrocarbon Synthesis on a Cobalt on Alumina Catalyst," Applied Catalysis **1**, 247-272 (1981).

Reuel, R.C and C.H. Bartholomew, "Effects of support and dispersion on the CO hydrogenation activity/selectivity properties of cobalt," Journal of Catalysis **85**, 78-88 (1984).

Ribeiro, F.H., A.E. Schach von Wittenau, C.H. Bartholomew and G.A. Samorjai, "Reproducibility of Turnover Rates in Heterogeneous Metal Catalysis: Compilation of Data and Guidelines for Data Analysis," Catalysis Review Science Engineering **39**, 49-76 (1997).

Ronning, M., D.G.Nicholson and A. Holmen, "In-situ Exafs study of the bimetallic interaction in a rhenium-promoted alumina supported cobalt Fischer-Tropsch catalyst," Catalysis Letters **72**, 141 (2001).

Rohr, F.,O.A. Lindvag, A. Holmen, E.A. Blekkan, "Fischer-Tropsch synthesis over cobalt catalysts supported on zirconia-modified alumina," Catalysis Today **58**, 247-254 (2000).

Sarup, B., and B.W. Wojciechowski,"Studies of the Fischer-Tropsch Synthesis on a cobalt catalyst II. Kinetics of carbon monoxide conversion to methane and higher hydrocarbon," The Canadian Journal of Chemical Engineering **74**, 62-74 (1989).

Satterfield, C., "Mass Transfer in Heterogeneous Catalysis," Cambridge, Massachussetts Institute of Technology, (1970).

Serp, P., M. Corrias and P. Kalck, "Carbon nanotubes and nanofibers in catalysis," Applied Catalysis A: General **253,** 337-358 (2003).

Schulz, H., Z. Nie, F.Ousmanov, "Construction of the Fischer-Tropsch regime with cobalt catalysts," Catalysis Today **71**, 351-360 (2002).

Smith, J.M., "Chemical Engineering Kinetics," McGraw-Hill, Inc., US (1981), p.450-517

Tago, T., T.Hanaoka, P.Dhupatemiya, H.Hayashi, M.Kishida, K.Wakabayashi, "Effects of Rh content on catalytic behavior in CO hydrogenation with Rh–silica catalysts prepared using microemulsion," Catalysis Letter **64**, 27-31 (2000).

Tavasoli A., "Catalyst composition and its distribution effects on the enhancement of activity, selectivity and suppression of deactivation rate of FTS cobalt catalysts," Ph.D. Thesis, University of Tehran (2005).

Tavasoli, A., Y. Mortazavi, A. Khodadadi and K. Sadagiani, "Effects of different loadings of Ru and Re on physico-chemical properties and performance of 15% Co/Al_2O_3 FTS catalysts," Iranian Journal of Chemistry and Chemical Engineering **35**, 9-15 (2005).

Tavasoli, A., K. Sadaghiani, A. Nakhaeipour and M. G Ahangari, "Raising distillate selectivity and catalyst lifetime in Fischer-Tropsch synthesis by using a novel dual-bed reactor," Iranian Journal of Chemistry and Chemical Engineering **26**, 1-9 (2007).

Tavasoli, A., R.M. Abbaslou, M. Trépanier and A.K.Dalai, "Fischer-Tropsch synthesis over cobalt supported on carbon nanotubes in a slurry reactor," Applied Catalysis A: Genreal **345**, 134-142 (2008 a)

Tavasoli, A., K.Sadaghiani and K. Khorashe, A.A. Seifkordi, A.A. Rohani and A. Nakhaeipour, "Cobalt supported on carbon nanotubes: a promising novel Fischer-Tropsch synthesis catalyst," Fuel Processing Technology **89**, 491-498 (2008 b).

Tavasoli, A., R.M.M. Abbaslou, M.Trépanier and A.K. Dalai, "Morphology and deactivation behavior of Co-Ru/Al_2O_3 Fischer-Tropsch synthesis," The Canadian Journal of Chemical Engineering **86**, 1070-1080 (2008 c).

Tavasoli, A., R.M.M. Abbaslou, A.K. Dalai, "Deactivation behavior of ruthenium promoted promoted Co/γ-Al_2O_3 catalysts in FTS," Applied Catalysis A: General **346**, 58-64 (2008 d).

Van der Laan, G. P., A.A.C.M. Beenacker, "Kinetics and selectivity of the Fischer-Tropsch Synthesis: A Litterature review," Catalysis Review Science and Engineering **41**, 255-318 (1999).

Wojciechowski, B.W., "The kinetics of the Fischer-Tropsch synthesis," Catalysis Review Science and Engineering **30**, 629-702 (1988).

Xiang, J., Y.Ding, T.Wang, L.Yan, W.Chen, H. Zhu and Y.Lu, "The formation of Co_2C species in activated carbon supported cobalt-based catalysts and its impact on Fischer-Tropsch reaction," Catalysis Letters **102**, 265-269 (2005).

Xiong, H., Y.Zhang, K. Liew, J.Li, "Catalytic performance of zirconium-modified Co/Al_2O_3 for Fisher-Tropsch synthesis," Journal of Molecular Catalysis A: Chemical **231**, 145-151 (2005).

Ya-huei, C., H. Jianli , C. Chunshe, G.Yufei , W.Yong, "Preparation of a novel structured catalyst based on aligned carbon nanotube arrays for a microchannel Fisher-Tropsch synthesis reactor," Catalyst Today **110**, 47-52 (2005).

Yasima, M. and L.K.L. Falk, "Structure and catalytic properties of nanosized alumina supported platinum and palladium particles synthesized by reaction in microemulsion," Journal of Colloid and Interface Science **268**, 348-356 (2003).

Yates, I.C and C. N. Satterfield, "Intrinsic Kinetics of the Fischer-Tropsch Synhtesis on a Cobalt Catalyst," Energy & Fuels **5**, 168-173 (1991).

Zennaro, R., M.Tagliabue and C.H. Bartholomew, "Kinetics of Fischer-Tropsch synthesis on titania-supported cobalt," Catalysis Today **58**, 309-319 (2000).

Chapter 2: Fischer-Tropsch synthesis over carbon nanotubes supported cobalt catalysts in a fixed bed reactor: Influence of acid treatment

A similar version of this chapter has been published in the Fuel Processing Technology journal:

Trépanier, M., A. Tavasoli., A.K. Dalai., N. Abatzoglou, Fischer-Tropsch synthesis over carbon nanotubes supported cobalt catalysts in a fixed bed reactor: Influence of acid treatment, Fuel Processing Technology 90 (2009) 367-374.

The material discussed in this chapter was also included in an oral paper presentation at the following conference:

Trépanier, M., A. Tavasoli, A.K Dalai and N. Abatzoglou, (June 2008) Fischer-Tropsch synthesis over Carbon nanotubes supported cobalt catalysts in a fixed bed reactor: Influence of acid treatment, 20th Canadian symposium on Catalysis, Kingston, Canada.

Contribution of Ph.D Candidate

FTS fixed bed reactor fabrication, development of the cobalt supported CNT catalysts, characterization and catalysts studies were performed by Mariane Trépanier. Ahmad Tavasoli provided guidance in the catalyst preparation methodology and the selection of operations conditions for the catalyst screening. Drs.Dalai and Abatzoglou provided the main idea of the research project and financial support. The data analysis and interpretation was performed by Mariane Trépanier and the submitted manuscript was written by Mariane Trépanier, while Drs. Tavasoli and Dalai provided editorial input.

Dr. Ahmad Tavasoli was a visiting professor from the Research Institute of Petroleum Industry in Tehran, Iran. He was at the University of Saskatchewan for 1 year (2008-2009) in the Chemical Engineering Department. Dr. Ajay K.Dalai, thesis

supervisor, is the Associate Research and Partnerships Dean at the University of Saskatchewan and Canada Research Chair in Bioenergy. Dr. Nicolas Abatzoglou is the Head of department of Chemical Engineering at the Université de Sherbrooke and co-supervisor of the Ph.D research project.

Contribution of this manuscript to Overall Study

The primary goal of this Ph.D research is to demonstrate that the carbon nanotubes are suitable as a novel support for FTS cobalt catalyst. Therefore, Co/CNT FTS catalyst was evaluated as a novel avenue for gas to green diesel production using syngas. Within the literature gap on FTS support, as discussed in Chapter 1, support must be treated before metal loading to optimize the performance of the catalyst. Thus, the Co/CNT catalysts were developed for use in Fischer-Tropsch synthesis by optimization of the support with acid treatment. The support functionalization improved the cobalt loading by opening the caps and adding defects on the CNT support. This part of the research also evaluated Co/CNT catalyst at different FTS process parameters (temperature, H_2/CO ratio) to study their influence on the FTS activity and selectivity.

2.1 Abstract

The influence of acid treatment on carbon nanotubes (CNT) supported cobalt catalysts for Fischer–Tropsch synthesis (FTS) is discussed in this paper. CNTs were first treated with 30 wt. % HNO_3 at 25 and 100 °C for 14 h, respectively. Cobalt catalysts supported on fresh and acid treated carbon nanotubes were prepared using the incipient wetness impregnation method with a cobalt loading of 10 wt. %. The catalysts were extensively characterized by BET, XRD, TPR and TEM, and Raman spectroscopy. The TEM analyses of the acid treated support catalysts showed that the major parts of the cobalt particles were homogenously distributed inside the nanotubes. Raman I_D/I_G band intensity ratios as an indication of the quality of carbon nanotubes for catalyst supports, increased with acid treatment. The FTS activity (g HC produced/g cat./h) and selectivity (the percentage of the converted CO that appears as a hydrocarbon product) of the catalysts were assessed and compared with the as-prepared CNT supported 10 wt. %

cobalt catalyst using a fixed bed micro-reactor. The acid treatments at 25 and 100 °C respectively, (a) increased the BET surface area by 18 % and 25 %; (b) decreased the cobalt particle size and increased the cobalt dispersion; (c) increased by 10 and 50 % the reducibility of the catalysts and (d) increased the FTS activity and % CO conversion by 36 and 114 %. Finally, the product selectivity showed a distinct shift to lower molecular weigh hydrocarbons.

2.2 Introduction

The actual high energy costs and World's commitment to Kyoto's Protocol for green houses gas (GHG) emissions reduction and control constitute the main driving forces for the continuously growing interest in FTS technologies. The FTS process has shown to be catalyzed by certain transition metals, with Co, Fe, and Ru presenting the highest activity [Bechara et al., 2001; Dry et al., 1981; Iglesia, 1997; Jacobs et al., 2002; Oukaci et al., 1999; Tavasoli, 2005]. Among them, cobalt catalysts are preferred for FTS based on natural gas because of their high activity for FTS, high selectivity to linear hydrocarbons, low activity for the water gas shift (WGS) reaction, more stable toward deactivation by water (a by-product of the FTS reaction), and low cost compared to Ru [Bechera et al., 2001; Iglesia, 1997; Tavasoli et al., 2005]. In order to achieve high surface active sites (Co^o), cobalt precursors are dispersed on porous carriers, with SiO_2, Al_2O_3, and to a lesser extent TiO_2 being the most frequently used [Berge et al., 2000; Jacobs et al., 2002; Tavasoli et al.,2005; Tavasoli 2005]. A drawback of these support materials is their reactivity toward cobalt, which during preparation or catalysis results in the formation of mixed compounds that are reducible only at high reduction temperatures [Berge et al., 2000; Jacobs et al., 2002; Tavasoli et al., 2005; Tavasoli 2005].To avoid these problems, the use of carbon as a support has been explored [Bezemer et al., 2004; Reuel and Bartholomew, 1984; Serp et al., 2003]. Activated carbon has many advantages if utilized as FTS catalyst support (resistance to acidic or basic media, stable at high temperatures, etc.). Carbon nanotubes (CNT) possess similar properties and in most cases outperform activated carbon for FTS [Serp et al., 2003; Tavasoli, 2005]. Carbon nanotubes as a new type of carbon material have interesting properties favoring catalytic activity [Pan et al., 2007]. Their special and steady structural characteristics and

morphology are quite suitable for use as catalytic support materials [Bahome et al., 2005; Bezemer et al., 2004; Pan et al., 2007; Serp et al., 2003; Tavasoli et al., 2007a; Tavasoli et al., 2008a]. Especially, their surface properties can be modified through different treatment to satisfy special needs. However, how these treatments affect the properties of the catalysts supported on CNTs has rarely been reported. This work is part of a larger Canadian endeavor to evaluate the techno-economic feasibility of using FTS with new nanocatalyst formulations to convert fossil-derived or renewable gaseous fuels into green diesel.

In this study, the influence of different types of acid treatment of CNTs on the physico-chemical properties of the catalysts and FTS activity and selectivity is investigated.

2.3 Experimental

2.3.1 Catalyst preparation

Multiwall purified (N95%) Mknano-MWCNT was used as support materials for the preparation of cobalt FTS catalysts. The Mknano-MWCNT have been characterized extensively. The characteristics of the CNT are shown on Table 2.2. Three different catalysts have been prepared with loadings of 10 wt. % cobalt using incipient wetness impregnation method with aqueous solution of cobalt nitrate ($Co(NO_3)_2.6H_2O$, 99.0%) (Table 2.1).

Table 2. 1: Composition of catalysts

Catalysts Name	**C_a**	**C_b**	**C_c**
Supports	Fresh-CNTs	Cold treated (25 ^oC) CNTs with 30 wt.% HNO_3	Hot treated (100 ^oC) CNTs with 30 wt.% HNO_3
Wt.% Co	10	10	10

Before loading the catalyst supports with cobalt, hot and cold acid treatment has been done on the CNTs. The first catalyst was prepared using as-prepared CNT (C_a). The support of the second catalyst have been treated with 30 wt. % HNO_3 at 25 °C over night (C_b) and finally, the support of the third catalyst was treated with 30 wt. % HNO_3 at

100 °C over night (C_c). Catalysts were dried at 120 °C. The calcination temperature of the catalysts was determined by TGA analysis of the dried catalyst and the CNT supported catalysts were calcined at 350 °C (determined by TGA) for 3 h with a heating rate of 10 °C/min under argon flow. It is noted that before the treated CNTs were washed and dried at 120 °C with distilled water before cobalt loading.

2.3.2 Catalyst characterization

Perkin Elmer TG/DTA Thermogravimetric differential thermal analyzer was used to measure weight changes of the sample when heated under a flow of argon (flow rate of 40 ml/min) at a constant heating rate of 10 °C/min.

The surface area, pore volume, and average pore radius of the CNTs and catalysts were measured by an ASAP-2000 system from Micrometrics using BJH pore size distribution method. The samples were degassed at 200 °C for 2 h under 50 mTorr vacuum and their BET area, pore volume, and average pore radius were determined.

The morphology of CNTs and catalysts was characterized by Transmission Electron Microscopy (TEM). Sample specimens for TEM studies were prepared by ultrasonic dispersion of the CNTs and catalysts in ethanol. The suspensions were dropped onto a carbon coated copper grid. TEM investigations were carried out using a Hitachi H-7500 (120 kV).

The samples were also characterized by scanning electron microscopy (SEM). SEM analysis was carried out using a Hitachi S-4700 at 3 kV. Sample specimens for SEM were prepared by ultrasonic dispersion of samples in methanol. The suspensions were dropped onto a carbon support cover with a thin silica layer which allows seeing carbon nanotubes at high resolution.

Raman analyses of the CNTs were carried out with a Raman imaging (Renishaw System 2000) microscope (wire version, 1.3) with laser excitation wavelength of 514 nm, an exposure time of 30 s, microscope objective of 50, continuous grating within the wave number range of 3500–150 cm^{-1} and laser power of 25 %.

XRD measurements of the CNTs and calcined catalysts were conducted with a Philips PW1840 X-ray diffractometer with monochromatized Cu/K_α radiation. Using the

Scherrer equation, the average size of the Co_3O_4 crystallites in the calcined catalysts was estimated from the line broadening of a Co_3O_4 peak at 2θ of 36.8°.

Temperature programmed reduction (TPR) spectra of the calcined catalysts were recorded using a CHEMBET-3000, equipped with a thermal conductivity detector. The catalyst samples were first purged in a flow of helium at 150 °C, to remove traces of water, and then cooled to 40 °C. The TPR of 100 mg of each sample was performed using 3.1 % hydrogen in nitrogen gas mixture with a flow rate of 40 cm^3/min. The samples were heated from 40 to 900 °C with a heating rate of 10 °C/min.

2.3.3 Reaction set-up and experimental outline

The catalysts were evaluated in terms of their Fischer–Tropsch synthesis (FTS) activity (g HC produced/g cat./h) and selectivity (the percentage of the converted CO that appears as a hydrocarbon product) in a fixed bed micro-reactor. Prior to the activity tests, the catalyst activation was conducted according to the following procedure. The catalyst (0.5 g) was placed in the reactor and pure hydrogen was introduced at a flow rate of 30 ml/min. The reactor temperature was increased from room temperature to 380 °C at a rate of 10 °C/min, maintained at this activation condition for 14 h and the catalyst was reduced *in-situ*. After the activation period, the reactor temperature was decreased to 180°C under hydrogen flow. The FTS reactor system is shown in Figure 2.1.

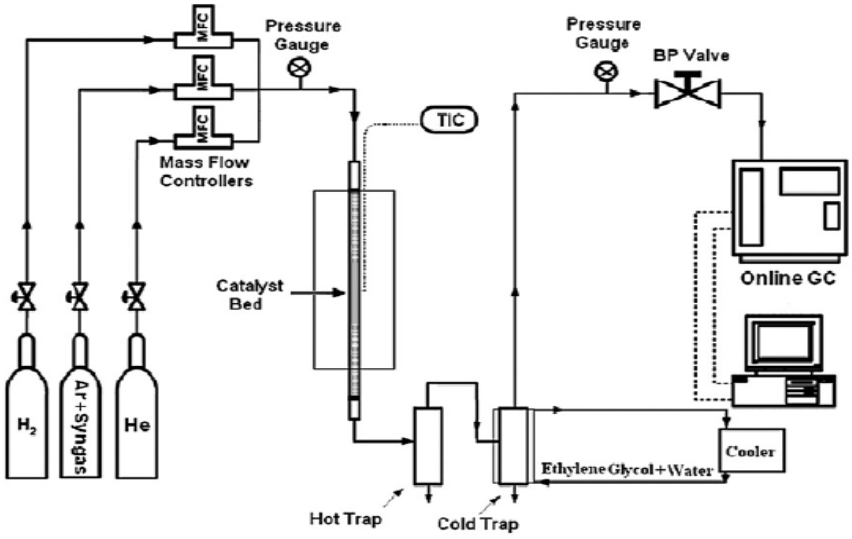

Figure 2. 1: Experimental Set-up for FTS

Brooks 5850 mass flow controllers were used to add H_2, CO and argon at the desired rate to the reactor. Argon was used as internal standard gas in the reactor feed. The mixed gases entered through to the top of the fixed bed reactor. The temperature of the reactor was controlled via a PID temperature controller. Synthesis gas with a flow rate of 30 ml/min (H_2/CO ratio of 2) was introduced and the reactor pressure was increased to 2 MPa. The reactor temperature was then increased to 220 °C at a rate of 1 °C/min. Products were continuously removed from the vapor and passed through two traps, one maintained at 100 °C (hot trap) and the other at 0 °C (cold trap). The uncondensed vapor stream was reduced to atmospheric pressure through a pressure letdown valve. The composition of the outlet gas stream quantified using an on-line GC-2014 Shimadzu gas chromatograph. The contents of the hot and cold traps were removed every 12 h, the hydrocarbon and water fractions separated, and then analyzed by Varian 3400 GC.

2.4 Results and discussion

2.4.1 Catalysts characterization

The TGA technique was used to investigate the presence of any decomposable materials in the uncalcined C_a catalysts [Tavasoli et al., 2008a]. Figure 2.2 shows the results of thermogravimetric analysis for C_a catalyst.

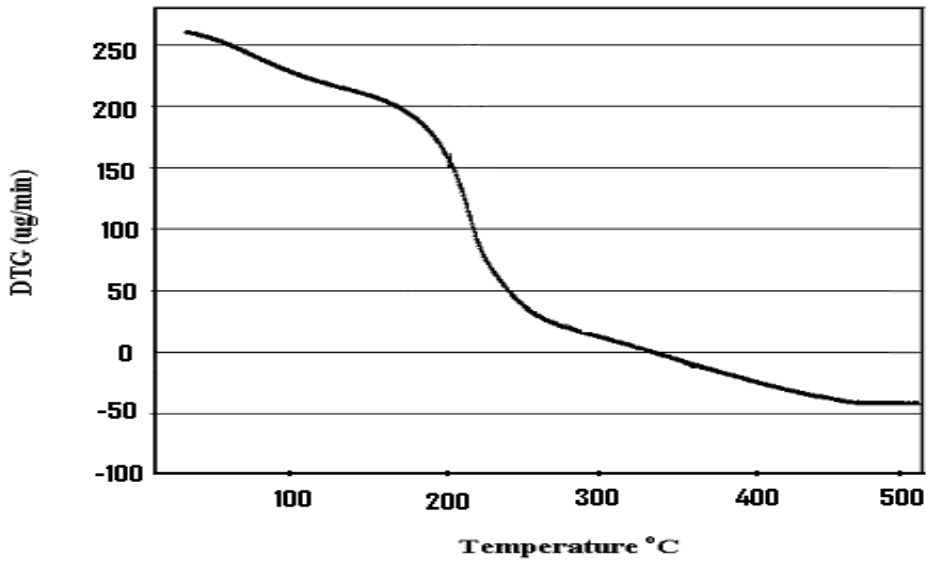

Figure 2. 2: Thermogravimetric analysis of C_a (Fresh-CNTs) under argon flow.

Results show that the rapid weight loss started below 200 °C and continued up to a temperature of 350 °C. Since after this temperature, the weight lost of the catalyst is negligible, it seems that calcination of the CNT supported catalysts at 350°C for 3 h was expected to remove all the displaceable water and counter ions present in the catalyst. Figure 2.3 shows the TEM image of the fresh and treated CNTs.

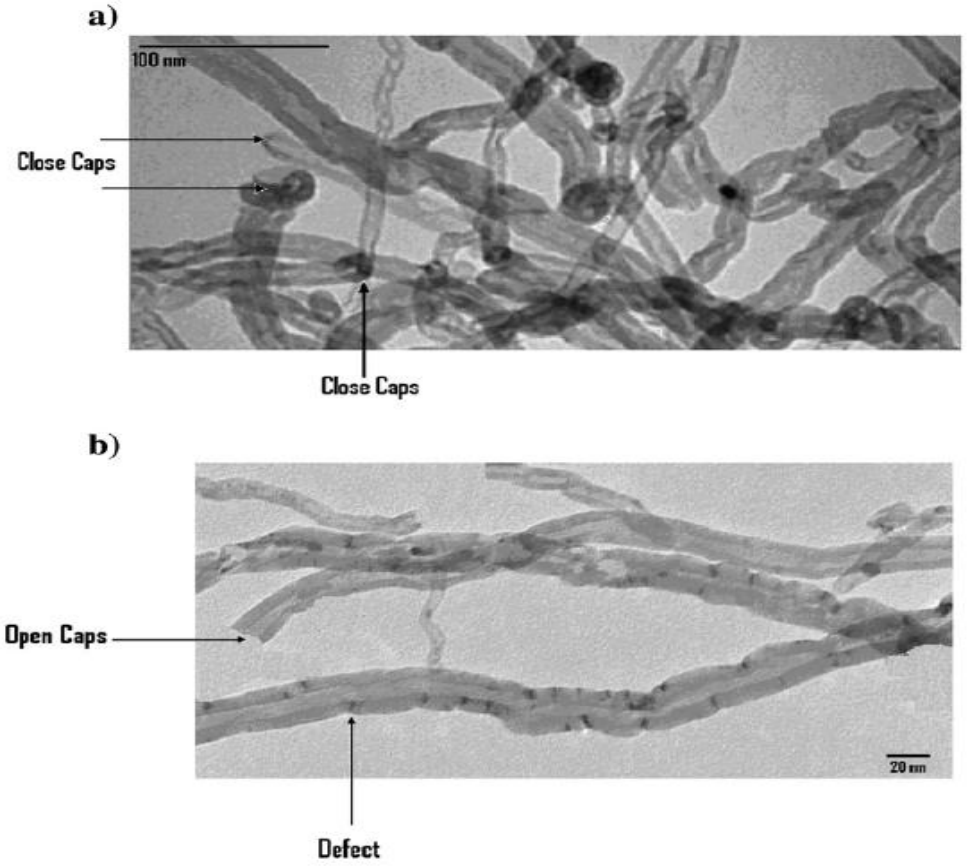

Figure 2. 3: TEM image of CNT supports (a) Fresh-CNT showing close caps of the nanotubes, (b) Hot acid treated CNT with 30 wt.% HNO_3 the defects of the nanotubes.

As shown, treatment with acid opened the caps of the closed tubes and created some defects on the outer surface of the CNTs. Figure 2.4 shows the TEM of cobalt loaded catalysts.

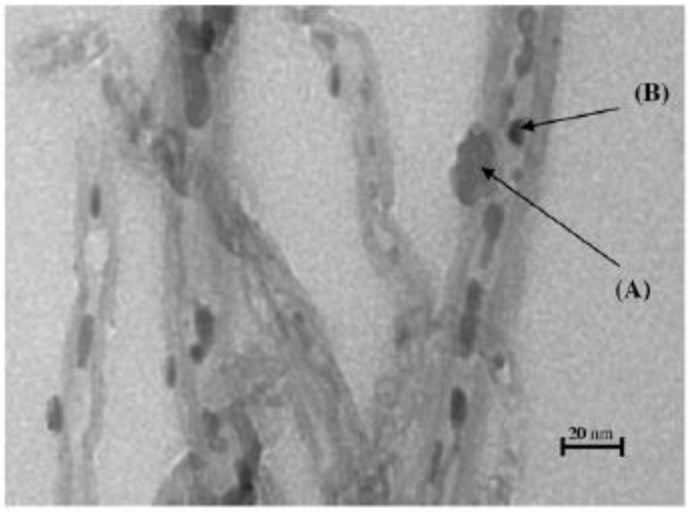

Figure 2. 4: TEM image showing cobalt particles with high dispersion for the acid treated loaded catalyst and showing the open caps of the CNTs: (A) Outside, (B) Inside.

It demonstrates the encapsulated cobalt particles on a selected tube with higher resolution. As shown, the majority of the cobalt particles were distributed inside the tubes and the rest on the outer surface of the CNTs, this distribution has already been observed on cobalt nanofiber-supported catalyst [Winter et al., 2005]. In addition, Figure 2.5 shows the scanning electron microscopy (SEM) picture of the catalysts, which displays more efficiently the cobalt particles outside the tube.

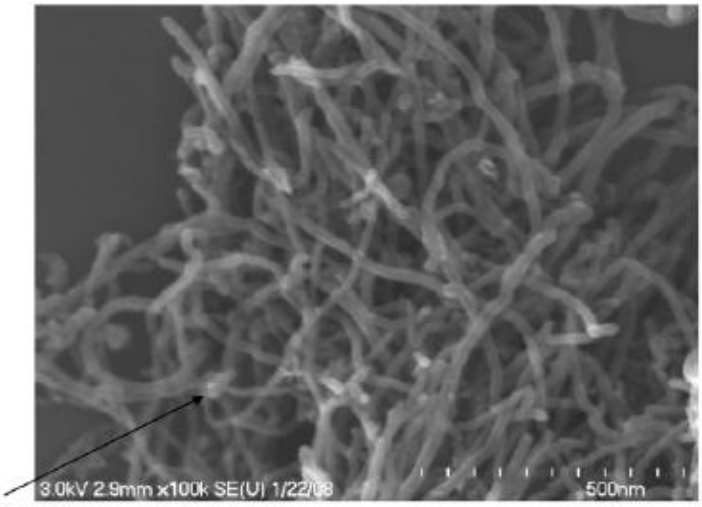

Figure 2. 5: SEM image of 10 wt. % cobalt catalyst supported on acid treated CNT at 100 °C with 30 % HNO_3 (C_c).

The particles inside the tubes are fairly uniform and the most abundant ones are 4–10 nm in size (Figure 2.4) in accordance with the average inner diameter of the CNTs, whereas those on the outer surface have grown to about 5–20 nm (Figure 2.4). Obviously, the CNT channels have restricted the growth of the particles inside the tubes [Winter et al., 2005].

Also, Table 2.2 shows the results of surface area measurements of 10 wt. % cobalt loaded catalysts.

Table 2. 2: BET surface area and porosity data

Supports/Catalysts	BET (m^2/g)	Pore Volume (Single point) (cm^3/g)	Average Pore Radius (nm)
Fresh -CNT	170	0.49	5.7
Cold-CNT	201	0.53	5.6
Hot-CNT	214	0.58	5.5
C_a	162	0.49	6.3
C_b	170	0.51	6
C_c	192	0.56	5.8

For C_a catalyst the loading of 10 wt. % Co decreased the surface area to 162 m^2/g and for C_b and for C_c catalysts it decreased from 201 to 170 m^2/g for cold treated and from 214 to 192 m^2/g for the hot treated one. The results show that the BET surface area of the catalysts is lower than that of the CNTs which indicates pore blockage due to cobalt loading on the supports. Furthermore, the pore blockage for the acid treated CNT supported catalysts is higher than the as prepared catalyst. Results of surface area measurements are shown in Table 2.2. The BET surface area of acid treated CNTs increased from 170 to 201 for the cold treated and to 214 m^2/g for the hot treated CNTs at 100 °C. At the same time, the pore volume of the CNTs are increased from 0.49 to 0.53 cm^3/g for the cold treated CNT at 25 °C and to 0.58 cm^3/g for hot treated CNT. The average pore diameter is decreased for both treated CNTs.

Figure 2.6 displays Raman spectra of the CNTs.

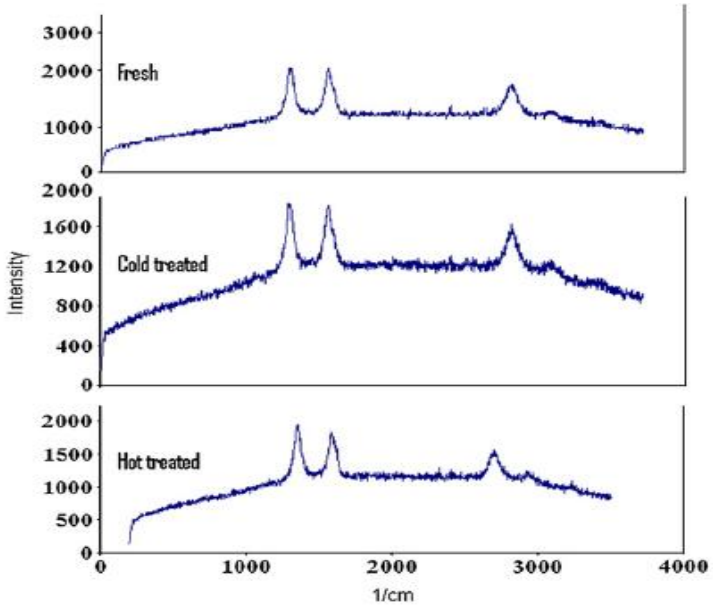

Figure 2.6: Raman spectroscopy for the CNTs support without cobalt.

It shows the D-band tangential Raman modes at 1350 cm^{-1} for disordered carbon and the G-band peak at 1582 cm^{-1} for ordered carbon [Dresselhaus et al., 2002]. Also, Raman I_D/I_G band intensity ratios are presented in Table 2.3.

Table 2. 3: Raman Spectroscopy for CNTs supports

CNT	I_D	I_G	I_D/I_G
Fresh	2143	2170	0.98
Cold treated	1814	1785	1.02
Hot treated	1926	1513	1.27

The I_D/I_G band ratios as an indication of the quality of carbon nanotubes for catalyst supports, increased with acid treatment. Acid treatment at 25 °C and 100 °C increased the I_D/I_G from 0.98 to 1.02 and to 1.27, respectively. This shows that the amount of defects on the CNT surface increases with acid treatment, which in turn leads to better metal dispersion on the acid treated CNTs surface and as well as higher catalyst activity.

XRD patterns of the supports, calcined catalysts and the standards for Co_3O_4 and CoO are shown in Figures 2.7 and 2.8.

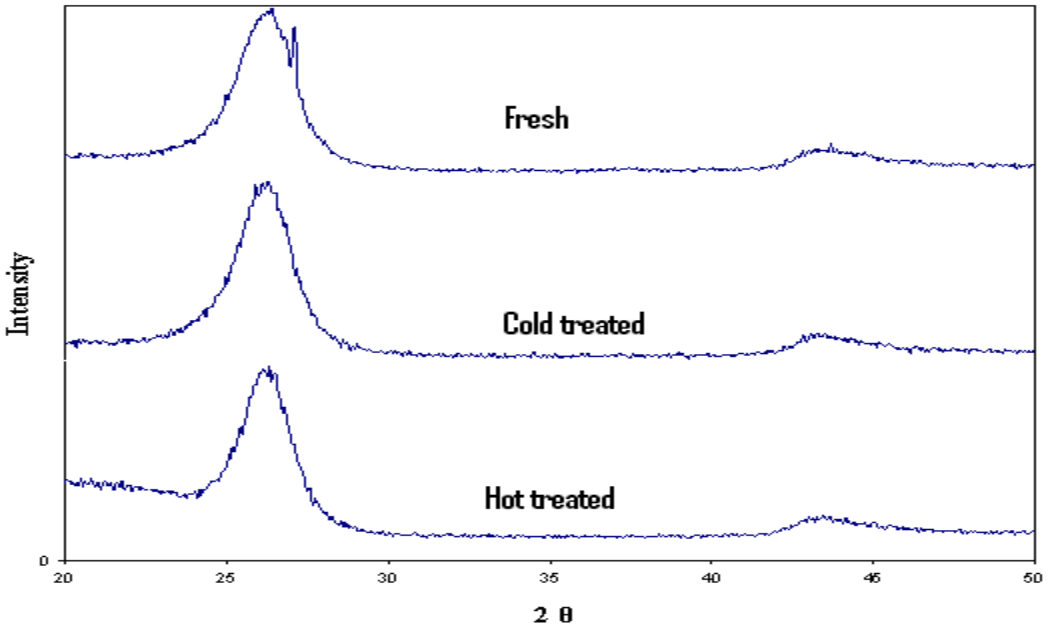

Figure 2. 7: XRD patterns of CNTs Fresh, CNTs cold treated and CNTs hot treated support.

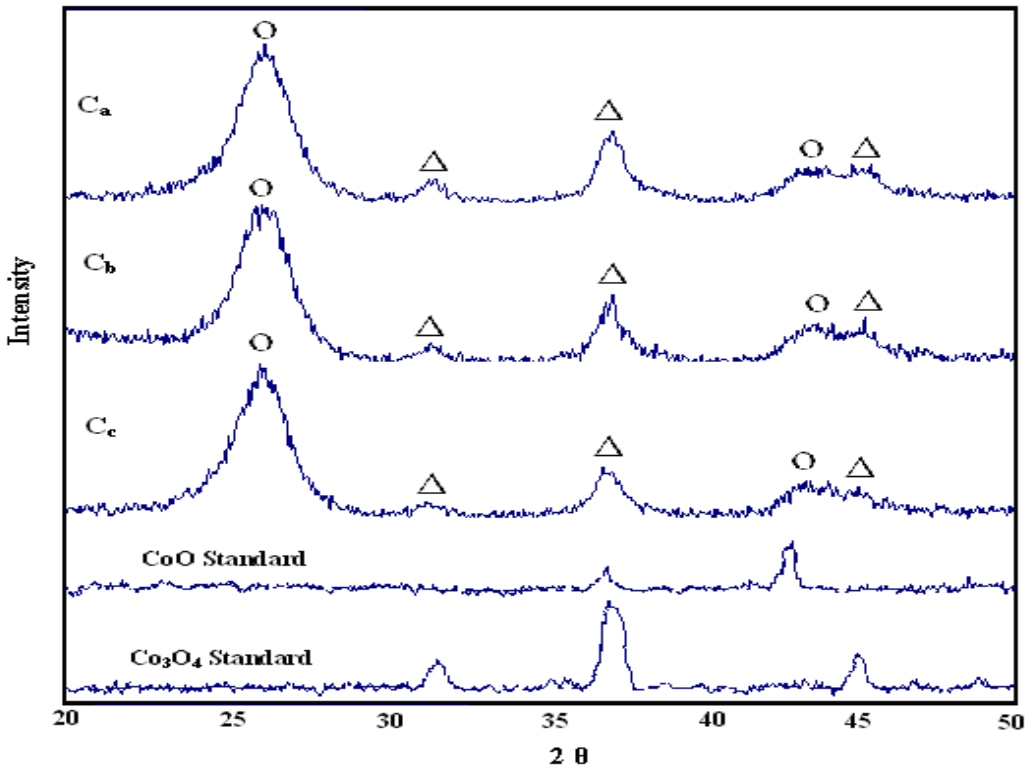

Figure 2. 8: Fig. 8. XRD patterns of calcined C_a, calcined C_b, and calcined C_c catalysts (The crystalline phases indicated are as follows: Δ, Co_3O_4; O, CNT).

The peaks at 2θ of 25° and 43° on Figures 2.7 and 2.8 correspond to those of carbon nanotubes. Also, in the case of Fresh CNT, the small peak at 2θ of 27° is due to impurities. While the other peaks at 2θ of 32, 36.8 and 45° in the spectrum of catalysts in Figure 2.8 are related to different crystal planes of Co_3O_4 and CoO [Jongsomjit et al., 2001]. The peak at 36.8° is the most intense peak corresponding to Co_3O_4 in XRD spectrum. In the XRD spectrum of the catalyst no peak was observed indicating formation of cobalt support compounds. Table 2.4 shows the average Co_3O_4 particle size of the catalysts calculated from XRD spectrum and Scherrer equation with the peak at 36.8° [Tavasoli et al., 2008a].

Table 2. 4: XRD and TPR data

Catalysts	XRD d_{Co3O4} (nm)	1st TPR peak (°C)	2nd TPR peak (°C)	Reducibility Ratio
C_a	9.9	384	481	1
C_b	9.8	371	456	1.1
C_c	8.9	363	448	1.5

This Table represents that the maximum average Co_3O_4 crystallite size is for C_a catalyst and the minimum is for C_c catalyst. Increasing the BET surface area and also opening the caps on the closed CNTs apparently lead to better distribution of the metal particles and as a result lower cobalt cluster sizes. Also as shown by TEM pictures of the fresh and hot treated CNTs (Fig. 2.3 a and b), acid treatment at 25 and 100 °C increased the amount of defects on the CNT surface which are considered as anchoring site for metal particles. Acid treatment not only breaks carbon nanotubes but also introduce a large number of functional groups on the nanotubes [Li et al., 2003; Winter et al., 2005]. The acidic surface groups significantly influence the preparation on CNT supported catalysts. Since the impregnation method entails contacting the CNT with the solution of the catalyst precursor and CNT, like other carbon materials are essentially hydrophobic in nature, they have a really low affinity for solvents such as water. The acidic groups decreased the hydrophobicity of the CNT and make the surface more accessible to the aqueous solution of the metal deposit [Li et al., 2003; Winter et al., 2005]. Therefore, more metallic

precursors are attached to the nanotubes and metal particles are dispersed more homogeneously, leading to small diameters on the whole as indicated by XRD results in Table 2.4.

Breaking the tube leads to shorter tubes as well as lower internal mass transfer limitations for reactants and desorption of products. The acidic functional groups also increase the adsorption of hydrogen on catalyst surface, which in turn leads to higher FTS rate. Temperature programmed reduction (TPR) is a powerful tool to study the reduction behavior of oxidized phases; in some cases it is also possible from the reduction profiles of supported oxides to obtain useful information about the degree of interaction of the active metal with the support [Tavasoli et al., 2005; Tavasoli et al., 2007b]. The TPR spectra of the calcined catalysts and CNT are shown in Figure 2.9.

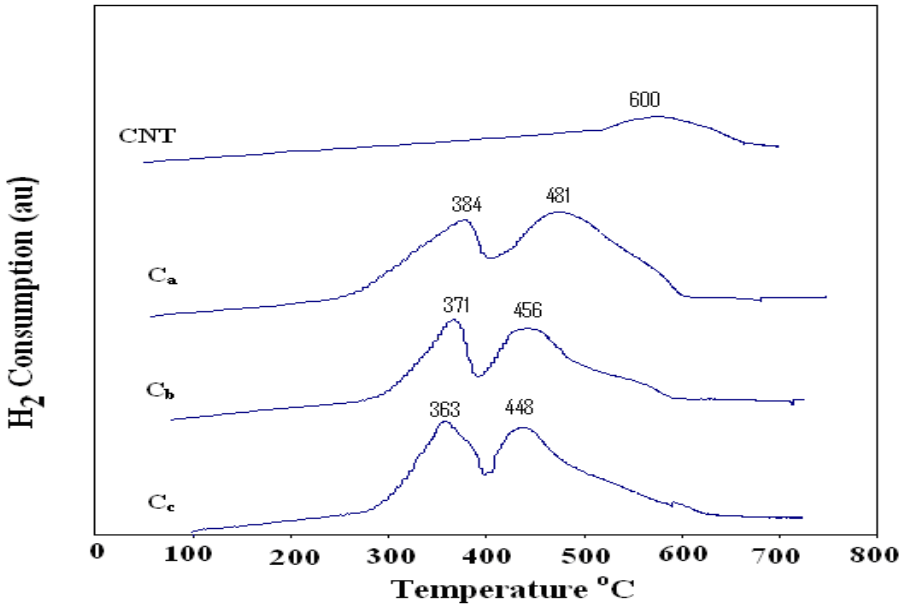

Figure 2. 9: TPR spectra of the calcined catalysts C_a, C_b, C_c and CNT.

In the TPR profile of all catalysts the first peak is typically assigned to the reduction of Co_3O_4 to CoO, although a fraction of the peak likely comprises the reduction of the larger, bulk-like CoO species to Co°. The second peak is mainly assigned to the second step reduction CoO to Co°. This peak also includes the gasification of support which extends the TPR spectra to higher temperatures of 600 °C as indicated by TPR of CNT support. As shown in this Figure, treatment of CNT's with acid shifts the reduction of cobalt species to lower temperature. Treatment of CNT at 25 °C decreased the first TPR

peak from 384 °C to 371 °C and the second TPR peak from 481 °C to 456 °C. Also treatment of CNT at 100 °C decreased the first TPR peak from 384 °C to 363 °C and the second TPR peak from 481 °C to 448 °C. Since treatment opens the caps and also breaks the tubes at imperfections, it makes reduction of cobalt particles easier and shifts the TPR peaks to lower temperatures. Table 2.4 also shows reducibility ratio for catalysts during TPR tests. The reducibility ratio for the whole TPR profile is defined by the ratio of the areas of the corresponding peaks to that for C_a catalyst. This is proportional to the amount of hydrogen consumed. As shown in Table 2.4, acid treatment at 25° and 100 °C enhances hydrogen consumption and as a result the reducibility of cobalt oxides is increased, by about 10 % and 50 %, respectively. It is to be noted that to calculate the exact amount of hydrogen consumption by catalysts; we decreased the area of the TPR peaks by the amount of hydrogen consumption due to gasification of CNT.

2.4.2 Fischer-Tropsch synthesis

Figure 2.10 shows the variations of CO conversion with the time on stream (TOS) for the C_a, C_b and C_c catalyst. The catalysts showed different stability pattern within a time period of 48 h.

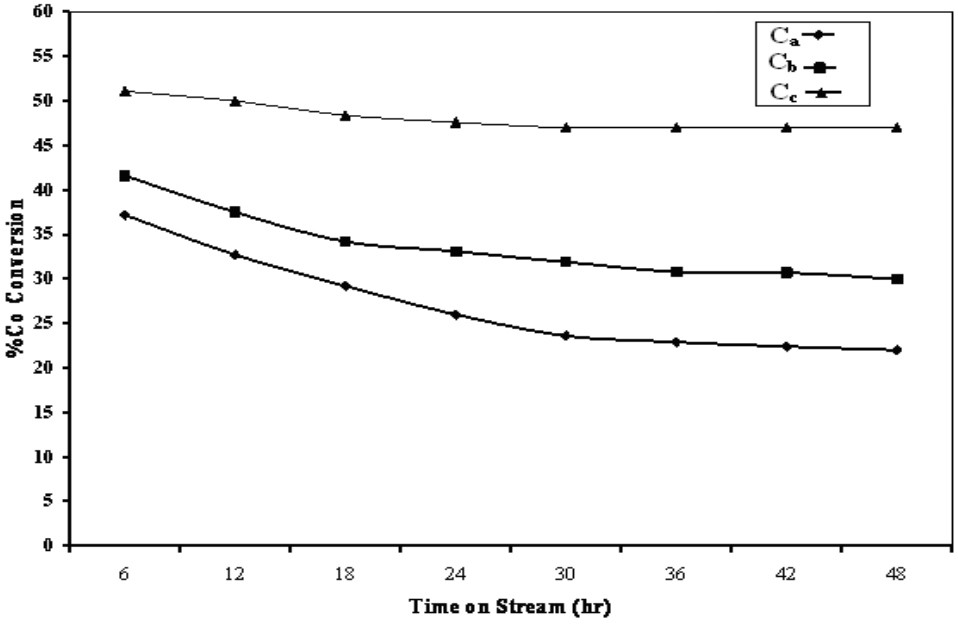

Figure 2. 10: Variation of % CO conversion with time on stream for 10 wt.% Co catalysts supported on Fresh CNT (C_a), Cold treated CNT (C_b) and Hot treated CNT (C_c).

A glance at the Figure 2.10 shows that Co catalyst supported on the CNTs treated with nitric acid at 100 °C is more stable. In the case of C_a catalyst, syngas conversion drops quickly from a conversion of 37.2 % to 22 % during 48 h (41 % decreases in CO conversion). For C_c catalyst there is a slow deactivation from 51.1 % CO conversion to 47 % within 48 h (8 % decreases in CO conversion). The stability of the catalyst may be attributed to the extent of functional groups and defects and/or the structure and morphology of CNT supports. As discussed earlier, the Raman analysis revealed that acid treatment at 100 °C could produce defects on the CNT surface. The defects on the surface can act as anchoring sites for stable metal particles on the support surface and hence lower catalyst sintering rate. Further investigation into the other factors related to catalyst deactivation would be valuable. The results of Fischer–Tropsch synthesis rate (g HC produced/ g cat/ h), water gas shift reaction rate and percentage CO conversion at steady state condition (after 48 h FT synthesis) at 220^o and 230 °C, 2 MPa, and a H_2/CO ratio of 1 and 2 for C_a catalysts are given in Figure 2.11.

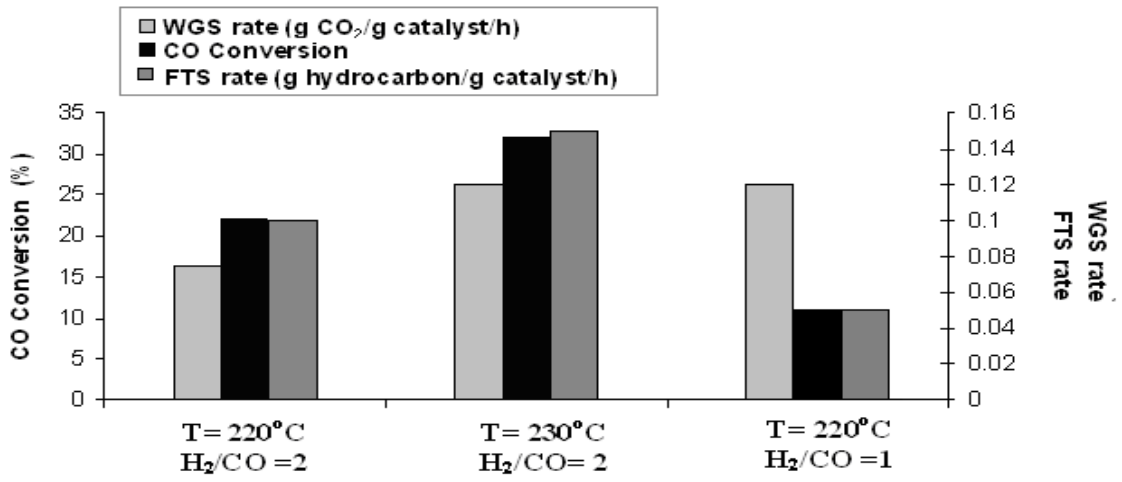

Figure 2. 11: Influence of T and H_2/CO ratio on % CO conversion, WGS rate (g CO_2/g catalyst/h) and FTS rate (g hydrocarbons/g catalyst/h).

It is to be noted that a blank FTS at 220 °C, 2 MPa, and a H_2/CO ratio of 2 did not show significant CO conversion when fresh, cold treated and hot treated CNT as catalysts were charged to the reactor. FT synthesis rate is equal to the gHC produced/g cat./h and water

gas shift reaction rate is equal to the formation rate of CO_2 (R_{FCO2}) and can be defined by [Bahome et al., 2002; Jacobs et al., 2002]:

$$R_{WGS} = R_{FC02} = gCO_2 produced/gcat*h^{-1} \quad (2.1)$$

Figure 2.11 reveals that the activity of cobalt catalyst supported on CNT is comparable to industrial FT synthesis catalysts [Tavasoli et al., 2008b]. Figure 2.11 also reveals that the FTS rate and CO conversion are strongly dependent on the reaction temperature and H_2/CO ratio. In accordance to other FTS catalysts, this figure shows that increasing the FT synthesis temperature from 220° to 230 °C increases the % CO conversion by 45 % and FTS rate by about 50 %. Increasing the FTS temperature increases the mobility of hydrogen on the catalyst surface which in turn leads to higher CO conversion and FTS rate [Tavasoli et al., 2005; Tavasoli et al., 2007a]. At the same time, WGS reaction rate increases by about 64 %. The increase of the WGS reaction rate or CO_2 formation rate can be attributed to the increase in water partial pressure, due to an increase in FTS reaction rate [Tavasoli et al., 2005]. Decreasing the H_2/CO ratio from 2 to 1 decreased the % CO conversion and also the FTS rate by about 50 %. Decreasing the H_2/CO ratio will increase partial pressure of CO on the gas phase resulting in an increase in the amount of CO adsorbed on the catalyst surface. The decreasing of FTS rate can be explained by the kinetic rate equation of cobalt based FTS catalysts in which the partial pressure of CO is in the denominator [Wojciechowski, 1988; Yates and Satterfield, 1991].

Table 2.5 shows the effects of temperature and H_2/CO ratio on the selectivity of Fischer–Tropsch synthesis products at steady state condition (after 48 h FT synthesis).

Table 2. 5: Influence of T and H_2/CO ratio on the selectivity of C_a

Process parameters	**T= 220°C H_2/CO =2**	**T= 230°C H_2/CO= 2**	**T= 220°C H_2/CO =1**
CH_4(%)	16	20	7
C_5+ (%)	72	60	87
O/P	0.98	0.28	1.38

Comparison of the product distributions of the hydrocarbon products for C_a catalyst at 220° and 230 °C, clearly demonstrates that product distribution shows a distinct shift to lower molecular weight hydrocarbons at higher temperature. Calculations show that the methane selectivities for C_a catalyst at 220° and 230 °C are 16 % and 20 %, respectively. Also the selectivity to liquid C_{5+} products for C_a catalyst at 220° and 230 °C are 72 % and 60 %, respectively and the olefin to paraffin ratio decreased from 0.98 to 0.28. Increasing the mobility of hydrogen with increasing the temperature will enhance the termination to parraffins against chain growth. The results of Table 2.5 also show that the liquid C_{5+} selectivity increases from 72 to 87 % with decreasing the H_2/CO ratio from 2 to 1. Increasing the partial pressure of CO increases the amount of adsorbed CO on the catalyst surface and will increase the chain growth and decrease the termination reaction to paraffins. Table 2.5 also shows that the amount of olefin to paraffin ratio is increased from 0.98 to 1.38 with decreasing the H_2/CO ratio from 2 to 1. Figure 2.12 shows the amount of % CO conversion, FTS rate and WGS rate for the different catalysts at steady state condition (after 48 h FT synthesis).

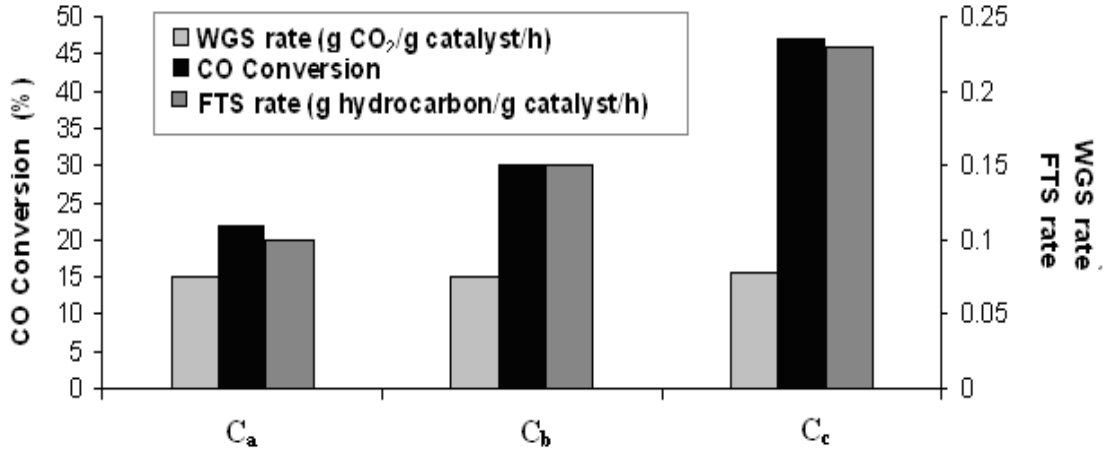

Figure 2. 12 : % CO conversion, WGS rate (g CO_2/g catalyst/h) and FTS rate (g hydrocarbons/gcatalyst/h) for C_a, C_b and C_c.

This figure shows that acid treatment of the support dramatically increases the FTS rate and % CO conversion. Treatment of support at 25 °C increased the % CO conversion from 22 to 30 %, while treatment of support at 100 °C increased the % CO conversion to 47 %. At the same time, WGS reaction rate increased by 0.8 and 4.8 %, respectively. The

results of catalyst characterization show that the acid treatment on CNTs increased the BET surface area, increased the catalyst reducibility, and decreased the particle size and the metal dispersion. All these effects can be evidences for increasing the number of surface active Co^o sites and as a result the FTS reaction rate [Berge et al., 2000; Li et al., 2003; Mirzaei et al., 2006]. But as shown on Figure 2.12 the CO conversion is increased by about 114 % which cannot be only due to the mentioned effects. It is well known that the exterior surfaces of the CNTs are electron-rich, whereas the interior ones are electron-deficient [Tavasoli et al., 2008b], which could influence metal and metal oxide particles in contact with either surface. The confinement of the nanoparticles (as shown in Fig.2.4) within the CNTs, will lead to the particular interaction of the interior nanotubes surface with the metal particles, which benefits the dissociative adsorption of CO. Since the chemisorption of reactants is the rate determining step on FTS reaction, one cobalt particle which is located inside the tubes must be more active than the one on the outer surface of the CNT. As mentioned, acid treatment opened the caps and then increased the population of cobalt particles inside the tubes. The more active cobalt clusters inside the tubes can be the reason for CO conversion enhancement. Acid treatment not only breaks carbon nanotubes but also introduces a large number of functional groups on the nanotubes [Li et al., 2003; Van Steen et al., 2002]. Breaking the tubes leads to shorter tubes as well as lower internal mass transfer limitation for reactants and desorption of products. The acidic functional groups also increase the adsorption of hydrogen on catalyst surface, which in turn leads to higher FTS rate. Also theoretical studies on non-catalytic gas phase reactions have prefigured that confinement within small channels could increase the density of reactants, and hence create a locally higher pressure, which will favor syngas conversion to hydrocarbons in the case of acid treated catalysts [Pan et al., 2007; Tavasoli et al., 2008b]. Table 2.6 compares the hydrocarbon products distribution for all the catalysts at steady state condition (after 48 h FT synthesis).

Table 2. 6: Selectivity of C_a, C_b and C_c catalysts (T=220 °C, P=2 MPa and H_2/CO=2)

Catalysts	**C_a**	**C_b**	**C_c**
CH_4 (%)	16	21	25
C_5^+ (%)	75	73	68
O/P	0.98	0.37	0.56

As shown in Table 2.6 methane selectivity is increased and liquid C_{5+} selectivity is decreased for acid treated catalysts. As mentioned before, treatment of support with acid will produce acidic functional groups that will increase the amount of hydrogen adsorbed on the catalyst surface and then enhance the termination reactions to paraffin instead of chain growth to heavier hydrocarbons. As shown in Table 2.6, the olefin to paraffin ratio decreases from 0.98 to 0.56 when CNT is treated with acid. Lower amount of olefin to paraffin ratio in the final products of C_c catalyst, confirms higher rate of termination reactions to paraffin. Figure 2.13 shows the liquid hydrocarbon distribution for all the catalysts at steady state condition (after 48 h FT synthesis).

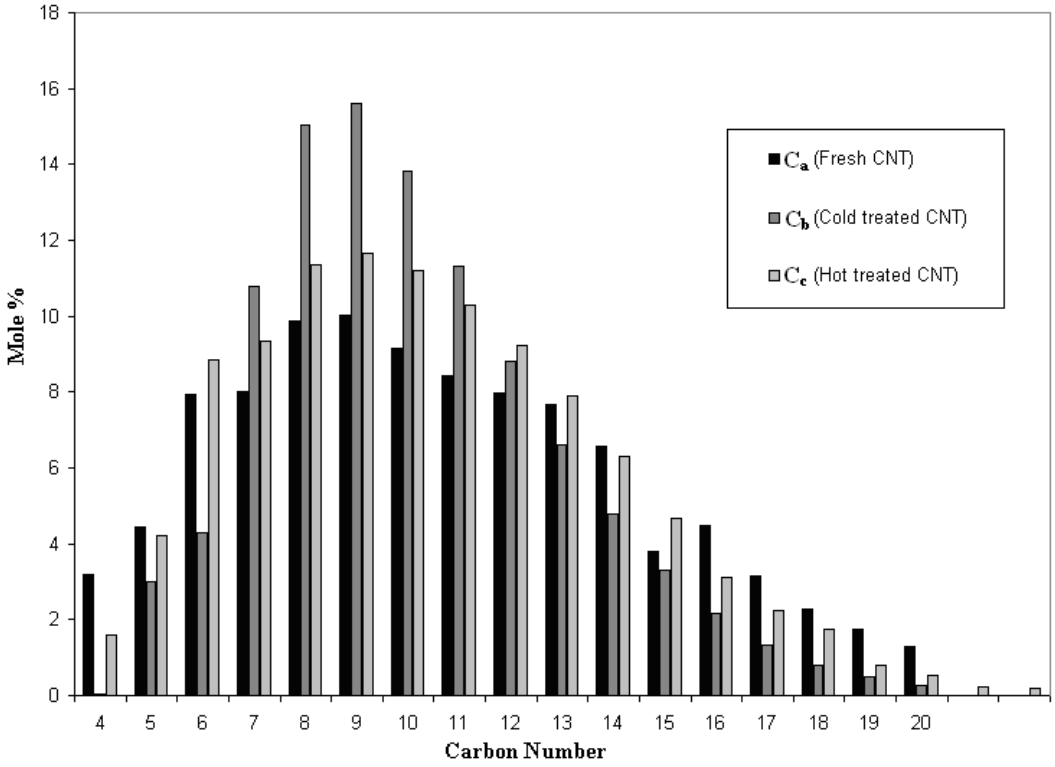

Figure 2. 13: Hydrocarbon products distribution for C_a, C_b and C_c catalysts.

As shown in this figure, the hydrocarbon distribution shows a distinct shift to lower molecular weight hydrocarbons for acid treated catalysts compared to the fresh catalyst. It is believed that in FTS the larger cobalt particles are more selective to higher molecular weight hydrocarbons and the smaller particles are selective for methane and light gases [Tavasoli, 2005, Tavasoli et al., 2008b]. As shown in Figure 2.6, the dispersion of active metal increases with acid treatment. Increasing the dispersion leads smaller cobalt cluster

sizes. This is confirmed with the results from XRD experiments. It seems that in C_a catalyst, which has larger cobalt clusters (Table 2.4), the steric hindrance for dissociative adsorption of CO and $–CH_2–$ monomer and addition of this monomer to the growing chain is less. On the other hand, chain propagation and growth probability at the surface of the large clusters of C_a catalyst is more than that of the smaller clusters of C_b and C_c catalysts.

2.5 Conclusions

Acid treatment of carbon nanotubes at 25 and 100 °C opens the caps, breaks carbon nanotubes and introduces a large number of defects and acidic functional groups on the nanotubes. Treatment of cobalt FTS catalyst support with 30 % HNO_3 acid at 25 and 100 °C, increases the BET surface area by 18 and 25 %, decreases the cobalt particle size and increases the cobalt dispersion. Furthermore, it has been demonstrated that the reducibility of the catalysts improves by 10 and 50 % with acid treatment of CNT support at 25° and 100 °C and most of the cobalt particles were homogenously distributed inside the tubes. The FTS activity and % CO conversion increases by 36 and 114 % by treatment of CNT support with 30 % HNO_3 acid at 25 and 100 °C. The product selectivity shows a distinct shift to lower molecular weight hydrocarbon products when CNT are treated with nitric acid.

2.6 References

Bahome, M.C., L.L. Jewell, D. Hildebrant, D.Glasser and N.J.Coville, "Fischer–Tropsch synthesis over iron catalysts supported on carbon nanotubes," Applied Catalysis A: General **287**, 60-67 (2005).

Bechara, R., D.Balloy and D.Vanhove, "Catalytic properties of Co/Al_2O_3 system for hydrocarbon synthesis," Applied Catalysis A: General **207**, 343-353 (2001).

Berge, V.P.J., J. van de Loosdrecgt, S. Barradas and A. M. van der Kraan, "Oxidation of cobalt based Fischer–Tropsch catalysts as a deactivation mechanism," Catalysis Today **58**, 321-334 (2000).

Bezemer, G.L., A.V. Laak, A. J. V. Dillen and K.P. Jong, "Cobalt Supported on Carbon Nanofibers - A Promising Novel Fischer-Tropsch Catalyst," Studies in Surface Science and Catalysis **147**, 259-264 (2004).

Dresselhaus, M.S, A. Jorio, G. Dresselhaus, R. Saito, A. Filho, G. Souza, M.A. Pimenta, "Raman Spectroscopy of nanoscale carbons and an isolated carbon nanotube," Molecular Crystal Liquids Crystal **387**, 21-29 (2002)

Dry, M.E.,"The Fischer-Tropsch Synthesis,"in "Catalysis, Science and Technology Vol.1,"J.R. Anderson and M.Boudart, Eds., Springer, Berlin (1981), p.159-255.

Iglesia, E., "Design, synthesis, and use of cobalt-based Fischer-Tropsch synthesis catalysts," Applied Catalysis A: General **161**, 59-78 (1997).

Jacobs,G., T.K Das, Y. Zhang, J. Li, G. Racoillet and B.H. Davis, "Fischer–Tropsch synthesis: support, loading, and promoter effects on the reducibility of cobalt catalysts," Applied Catalysis A:General **233**, 263-281 (2002).

Jongsomjit, B., J. Panpranot and J.G. Goodwin Jr., "Co-support compound formation in alumina supported cobalt catalysts," Journal of Catalysis **204**, 98-109 (2001).

Li, C., Ke Yao, J.Liang, "Influence of acid treatment on the activity of carbon nanotube-supported catalysts," Carbon **41**, 858-860 (2003).

Mirzaei, A.A., M. Faizi, R. Habibpour, "Effect of preparation on the catalytic performance of cobalt manganese oxide for conversion of synthesis gas to light olefins," Applied Catalysis A: General **306**: 98-107 (2006).

Oukaci, R., J.G.Goodwin Jr. and A. H. Singleton, "Effect of Titanium Doping on the Activity of Alumina-Supported Cobalt-Based Fischer-Tropsch Catalysts," Applied Catalysis A: General **186**, 129-144 (1999).

Pan, X., Z. Fan, W. Chen, Y. Ding, H. Luo and X. Bao, "Enhanced ethanol production inside carbon-nanotube reactors containing catalytic particles," Nature **6**, 507-511 (2007).

Reuel, R.C and C.H. Bartholomew, "Effects of support and dispersion on the CO hydrogenation activity/selectivity properties of cobalt," Journal of Catalysis **85**, 78-88 (1984).

Serp, P., M. Corrias and P. Kalck, "Carbon nanotubes and nanofibers in catalysis," Applied Catalysis A: General **253,** 337-358 (2003).

Tavasoli A.,"Catalyst composition and its distribution effects on the enhancement of activity, selectivity and suppression of deactivation rate of FTS cobalt catalysts," Ph.D. Thesis, University of Tehran (2005).

Tavasoli, A., Y. Mortazavi, A. Khodadadi and K. Sadagiani, "Effects of different loadings of Ru and Re on physico-chemical properties and performance of 15% Co/Al_2O_3 FTS catalysts," Iranian Journal of Chemistry and Chemical Engineering **35**, 9-15 (2005).

Tavasoli, A., K. Sadaghiani, A. Nakhaeipour and M. G Ahangari, "Raising distillate selectivity and catalyst lifetime in Fischer-Tropsch synthesis by using a novel dual-bed reactor," Iranian Journal of Chemistry and Chemical Engineering **26**, 1-9 (2007a).

Tavasoli, A., A.M. Rashidi, K. S. Zadeh, A. Karimi, A.A. Kodadadi, Y. Mortazavi, "Carbon nanotubes supported cobalt catalyst for converting synthesis gas into hydrocarbons," EP patent 1782885 A1 (2007b).

Tavasoli, A., R.M. Abbaslou, M. Trépanier and A.K.Dalai, "Fischer-Tropsch synthesis over cobalt supported on carbon nanotubes in a slurry reactor," Applied Catalysis A: Genreal **345**, 134-142 (2008 a)

Tavasoli, A., K.Sadaghiani and K. Khorashe, A.A. Seifkordi, A.A. Rohani and A. Nakhaeipour, "Cobalt supported on carbon nanotubes: a promising novel Fischer-Tropsch synthesis catalyst," Fuel Processing Technology **89**, 491-498 (2008 b).

Van Steen, E. and F. F. Prinsloo, "Comparison of preparation methods for carbon nanotubes supported iron Fischer–Tropsch catalysts," Catalysis Today **71**, 327-334 (2002).

Winter, F., G. Meeldijk, A. Jos van Dillen, J.W. Geus and K.P. de Jong, "TEM and XPS studies to reveal the presence of cobalt and palladium particles in the inner core of carbon nanofibers, Carbon **43**, 327-332 (2005).

Wojciechowski, B.W.,"The kinetics of the Fischer-Tropsch synthesis," Catalysis Review Science and Engineering **30**, 629-702 (1988).

Yates, I.C and C. N. Satterfield, "Intrinsic Kinetics of the Fischer-Tropsch Synhtesis on a Cobalt Catalyst," Energy & Fuels **5**, 168-173 (1991).

Chapter 3: Effects of confinement in carbon nanotubes on the activity, selectivity, and lifetime of Fischer-Tropsch Co/CNT catalysts

A similar version of this chapter has been published in Journal of Chemical Engineering and Data:

Tavasoli, A., M. **Trépanier,** A.K. Dalai., N. Abatzoglou, Effects of Confinement in Carbon Nanotubes on the Activity, Selectivity, and Lifetime of Fischer-Tropsch Co/Carbon Nanotube Catalysts, Journal of Chemical Engineering Data 55 (2010) 2757-2763.

The topics discussed in this chapter are also published as a refered proceeding paper and have been presented in an oral paper at the following conference:

Trépanier, M., A.Tavasoli, A.K.Dalai, and N. Abatzoglou, (August 2009) Deactivation Studies on CNT supported cobalt Fischer-Tropsch catalyst, 8th World conference in Chemical Engineering, Montreal, Canada.

Contribution of Ph.D Candidate

The laboratory experiments for the deactivation study of the Co/CNT were performed by Mariane Trépanier. Ahmad Tavasoli provided complementary results from Research Institute of Petroleum Industry in Tehran laboratory and guidance in the writing of the submitted manuscript. Drs.Dalai and Abatzoglou provided editorial assistance, the main idea of the research project and financial support. The data analysis interpretation of the results and the paper writing was performed by Mariane Trépanier.

Contribution of this manuscript to Overall Study

The primary goal of this Ph.D research is to demonstrate that the carbon nanotubes are suitable as a novel support for FTS cobalt catalyst. Chapter 2 shows that Co catalyst supported on CNT are suitable for FTS reactions in terms of activity and

selectivity. However, catalyst stability is also an important variable in the Co/CNT-catalyzed FT process. Once the catalyst lifetime study was completed, the deactivation factors and mechanism were identified. This study also demonstrated that carbon nanotubes as a catalyst support is a novel avenue to decrease sintering phenomenon during catalytic process.

3.1 Abstract

The effects of electronic properties of the inner and outer surfaces of carbon nanotubes (CNTs) on the deactivation of cobalt Fischer-Tropsch (FT) catalysts were studied. The comparative characterization of the fresh and used 0.20 *w* (mass fraction) Co/CNT catalysts by transmission electron microscopy (TEM), X-ray diffraction (XRD), temperature-programmed reduction (TPR), Brunnauer-Emmett-Teller analysis (BET), and H_2 chemisorption showed that cobalt reoxidation, cobalt-support interactions, and sintering are the main sources of catalyst deactivation. TEM showed that continuous FT synthesis for 480 h increased the average Co particle size located inside the pores from (7 to 8.5) nm, while the average Co particle size located outside of the tubes increased from (11.5 to 25) nm. XRD analysis of the used catalyst confirmed cobalt reoxidation, interaction between cobalt and CNTs, and the creation of carbide phases. At a higher percent CO (%CO) conversion and H_2O partial pressure, the deactivation rate is zero order and independent of the number of active catalyst sites. In this case, the main deactivation mechanisms are cobalt reoxidation and metal support interactions. At lower % CO conversion and H2O partial pressure, the deactivation rate can be simulated with power law expressions of the order of 11.4 for the particles outside the tubes and 30.2 for the particles inside the tubes. In this case, the main deactivation mechanism is sintering. Because of the electron deficiency of the inner sides of the CNTs, the interaction between the cobalt oxides and the support is stronger; leading to lower rates of sintering as compared with the particles located on the outer layers of the CNTs. Regeneration recovered the catalyst activity with 9.1 % of the total activity loss.

3.2 Introduction

Fischer-Tropsch synthesis (FTS) is a promising option for the environmentally friendly industrial production of chemicals and fuels from biomass, coal, and natural gas

where a high performance catalyst plays an essential role [Dry, 1999; Michiel et al., 2002]. In the FTS process, the catalyst activity, selectivity, and lifetime are influenced by the nature and structure of support, nature of metal phase, metal dispersion, metal loading, and catalyst preparation method [Bukur et al., 1990; Zhang et al., 2003]. Cobalt catalysts are believed to deactivate less rapidly and yield higher linear alkanes than iron counterparts due to high chain growth probability. Thus, cobalt catalysts are considered to be the best candidates for syngas to clean liquid fuel requirements [Michiel et al., 2002]. Most studies on cobalt FTS catalysts have been carried out with the metals supported on silica, alumina, or titania. Other families of supports with carbonaceous bases such as activated carbon have also been investigated for FT reactions [Bezemer et al., 2006; Guczi et al., 2006; Ma et al., 2006; Serp et al., 2003; Tavasoli, 2005; Tavasoli et al., 2008a; Tavasoli et al., 2008b]. As a FTS catalyst support, activated carbon has many advantages including resistance to acidic or basic media and stability at high temperatures. Carbon nanotubes (CNTs) possess similar properties and outperform activated carbon in most cases [Serp et al., 2003]. The unique properties of CNTs such as uniform pore size distribution, meso- and macropore structure, inert surface properties, and resistance to acid and base environments can play an important role in many catalytic reactions [Serp et al., 2003]. In our previous work we have reported interesting catalytic properties of CNT-supported cobalt catalysts prepared by the sequential aqueous incipient wetness impregnation method [Tavasoli et al, 2008a; Trépanier et al., 2009]. From a catalytic activity standpoint, the FT synthesis rate and percent CO (% CO) conversion obtained by CNT-supported cobalt catalysts were (40 to 45) % higher than that obtained with alumina-supported cobalt catalysts with the same cobalt loading in both fixed bed and slurry reactors [Tavasoli et al., 2008a; Tavasoli et al., 2008b]. CNTs also caused a slight decrease in the FTS product distribution to lower molecular weight hydrocarbons, requiring a smaller hydrocracker in the product upgrading section [Trépanier et al., 2009].

Co/CNT-catalyzed FT synthesis is advantageous in carbon utilization as compared to processes using Co/Al_2O_3, Co/SiO_2, or Co/TiO_2 catalysts, but CNT-supported cobalt catalysts are more expensive necessitating a longer catalyst lifetime [Bezemer et al., 2006; Tavasoli, 2005; Tavasoli et al., 2008a]. Therefore, catalyst stability

is an important performance variable in the Co/CNT-catalyzed FT process. In the case of silica, alumina, and titania-supported cobalt catalysts, the potential causes of cobalt FTS catalyst deactivation includes (a) oxidation of the cobalt surface, (b) cobalt support interactions and formation of mixed compounds that are reducible only at high reduction temperatures, (c) sintering, (d) refractory coke formation, (e) loss of metal cobalt because of attrition, and (f) heteroatoms poisoning (i.e., sulfur) [Tavasoli et al., 2007a; Jacobs et al., 2002; Jacobs et al., 2004]

The present work investigates the deactivation properties of CNT-supported cobalt catalysts during continuous FT synthesis for 480 h in a fixed-bed micro-reactor, considering different deactivation mechanisms. The main objective of this work is to study the effect of electronic properties of the inner and outer surfaces of the CNTs on the deactivation of Co/CNT catalysts.

3.3 Experimental section

3.3.1 Catalyst Preparation

Purified multi-wall carbon nanotubes (MWCNT) were used as support material for the preparation of the FTS catalyst. Prior to impregnation, the support was treated with 0.30*w* (mass fraction) HNO_3 at 100 °C overnight, washed with distilled water, and dried at 120°C for 6 h. The purified CNTs were loaded with 0.20 *w* cobalt using sequential incipient wetness impregnation of cobalt nitrate solution ($Co(NO_3)_2 \cdot 6H_2O$ 99.0 %, Merck). After each impregnation step, the catalyst was dried at 120 °C for 6 h and calcined at 350 °C for 3 h at a heating rate of 10 °C· min^{-1} under argon flow. The cobalt loadings of the calcined fresh and used catalysts were verified by an inductively coupled plasma atomic emission spectroscopy (ICP-AES) system.

3.3.2 Catalyst characterization

Morphology of the support and the fresh and used catalysts was studied by transmission electron microscopy (TEM). Sample specimens for the TEM studies were prepared by ultrasonic dispersion of the catalysts in ethanol and the suspensions dropped onto a copper grid. TEM investigations were carried out using a Hitachi H-7500 (120

kV). Several TEM micrographs were recorded for each sample and analyzed to determine the particle size distribution.

The surface area, pore volume, and average pore radius of the support and the fresh and used catalysts were measured by an ASAP-2010 system from Micromeritics. The samples were degassed at 200 °C for 4 h under 50 mTorr vacuum, and their Brunnauer-Emmett-Teller (BET) area, pore volume, and average pore radius were determined.

X-ray diffraction (XRD) measurements of the support and the fresh and used catalysts were conducted with a Philips PW1840 X-ray diffractometer with monochromatized Cu/KR radiation. Using the Scherrer equation, the average size of the cobalt oxide crystallites in the calcined fresh and used catalysts were estimated from the line broadening of the cobalt oxide peaks.

Temperature programmed reduction (TPR) spectra of the fresh and used catalysts were recorded using a Micromeritics TPD-TPR 290 system, equipped with a thermal conductivity detector. To remove traces of water, the catalyst samples were first purged in a flow of argon at 100 °C and then cooled to 40 °C. The TPR of 50 mg of each sample was performed using 5.1 % hydrogen in argon gas mixture with a flow rate of 40 $cm^3 \cdot min^{-1}$. The samples were heated from (40 to 800) °C with a heating rate of 10 $°C \cdot min^{-1}$.

The amount of chemisorbed hydrogen on the fresh and used catalysts was measured using the Micromeritics TPD-TPR 290 system. 0.25 g of the sample was reduced under hydrogen flow at 400 °C for 12 h and then cooled to 100 °C under hydrogen flow. To remove the weakly adsorbed hydrogen, the flow of hydrogen was then switched to argon at the same temperature, for about 30 min. The temperature-programmed desorption (TPD) of the samples was obtained by increasing the temperature of the samples to 400 °C with a ramp rate of 20 $°C \cdot min^{-1}$ under argon flow. The TPD spectrum was used to determine the cobalt dispersion and its surface average crystallite size using the following equations [Jacobs et al., 2002; Tavasoli et al., 2007b]

$$\text{Calibration value } (l_{gas}/\text{area units}) = \frac{\text{loop volume} \times \% \text{ analytical gas}}{\text{mean calibration area} \times 100} \qquad (3.1)$$

$$H_2 \text{ uptake (moles/g}_{cat}) = \frac{\text{analytical area from TPD} \times \text{calibration value}}{\text{sample weight} \times 24.5} \quad (3.2)$$

$$\%D_{\text{Total Co}} = \frac{H_2 \text{ uptake} \times \text{atomic weight} \times \text{stoichiometry}}{\%\text{ metal}} = \frac{\text{number of Co}^o \text{ atoms on the surface} \times 100}{\text{total number of Co}^o \text{ atom}} \quad (3.3)$$

$$\%D_{\text{reduced Co}} = \frac{\text{number of Co}^o \text{ atoms on the surface} \times 100}{\text{total number of Co}^o \text{ atom} \times \text{fraction reduced}} \quad (3.4)$$

$$\text{diameter (nm)}_{\text{total Co}} = \frac{6000}{\text{density} \times \text{maximum area} \times \text{dispersion}} \quad (3.5)$$

$$\text{diameter (nm)}_{\text{reduced Co}} = \frac{6000}{\text{density} \cdot \text{maximum area} \times \text{dispersion} \times \text{fraction reduced}} \quad (3.6)$$

3.3.3 Reaction Setup and Experimental Outline

The catalyst was evaluated in terms of FTS activity ($g_{HCproduced} \cdot g_{cat}^{-1} \cdot h^{-1}$) and selectivity (the percentage of the converted CO that appears as hydrocarbon products) in a fixed-bed micro reactor. The reactor temperature was controlled via a PID temperature controller. Brooks 5850 mass flow controllers were used to add H_2, CO, and argon at the desired rate to the reactor. Argon was used as an internal standard gas in the reactor feed. Prior to the activity tests, the catalyst activation was conducted according to the following procedure: The catalyst (1 g) was placed in the reactor, and pure hydrogen was introduced at a flow rate of 60 mL$\cdot$ min^{-1}. The reactor temperature was increased from room temperature to 380 °C at a rate of 10 °C$\cdot$ min^{-1} and maintained at this activation condition for 20 h, and the catalyst was reduced in situ. After the activation period, the reactor temperature was decreased to 180 °C under flowing hydrogen.

The synthesis gases entered through the top of the fixed-bed reactor at a flow rate of 52.4 mL$\cdot$ min^{-1} (H_2/CO ratio of 2). The reactor pressure was increased to 2 MPa, and the temperature was increased to 220 °C at a rate of 10 °C$\cdot$ min^{-1}. Products were continuously removed from the vapor and passed through two traps, one maintained at 100 °C (hot trap) and the other at 0 °C (cold trap). The uncondensed vapor stream was reduced to atmospheric pressure through a back-pressure regulator. The composition of the outlet gas stream was determined using an online GC-2014 Shimadzu gas

chromatograph. Contents of the hot and cold traps were removed every 24 h and analyzed by a Varian 3400 GC liquid chromatograph.

After 480 h of the first FT synthesis step, the flow of synthesis gas was switched off, and the catalyst was rereduced (second treatment step) in a flow rate of 60 mL· min^{-1} H_2 at 270 °C for 20 h. The second FT synthesis step was carried out under the same conditions and the activity ($g_{HCproduced} \cdot g_{cat}^{-1} \cdot min^{-1}$) and selectivity of the system measured. The third treatment step of the catalyst was performed at 380 °C for 20 h, cooled to 220 °C, and carried out under the same conditions as the previous synthesis steps. The products were analyzed under the same conditions as the first synthesis step. The catalytic bed was treated by helium flow for 3 h at 270 °C to remove the heavy waxes inside the catalyst pores. The temperature of the reactor was lowered to 20 °C, and the catalyst was passivated with pulses of dry air to stop further oxidation. The used catalyst was discharged and characterized extensively.

3.4 Results and Discussion

3.4.1 Characterization Overview

A sample of the purified CNT material was analyzed by TEM. The purified product consisted of an interwoven matrix of tubes (Figure 3.1) comprised of multiwalled CNTs.

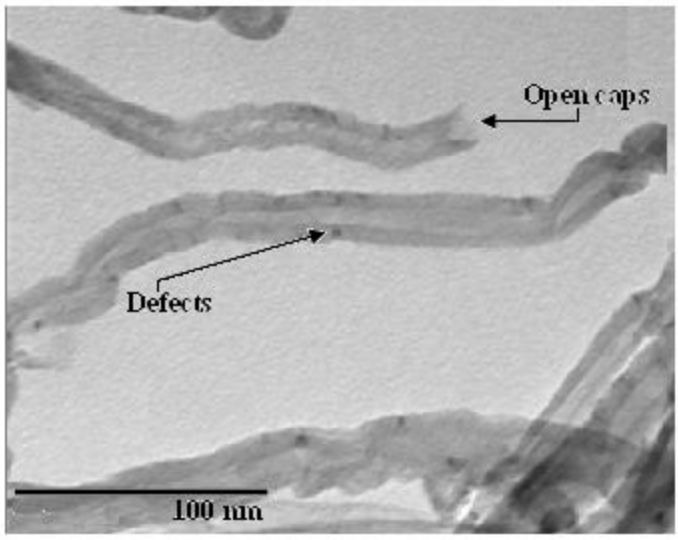

Figure 3. 1: TEM image of the CNTs as support material after acid treatment.

The TEM image of calcined fresh catalyst revealed that the catalyst particles were well-dispersed inside the tubes and also on the perimeter of the tube walls (Figure 3.2).

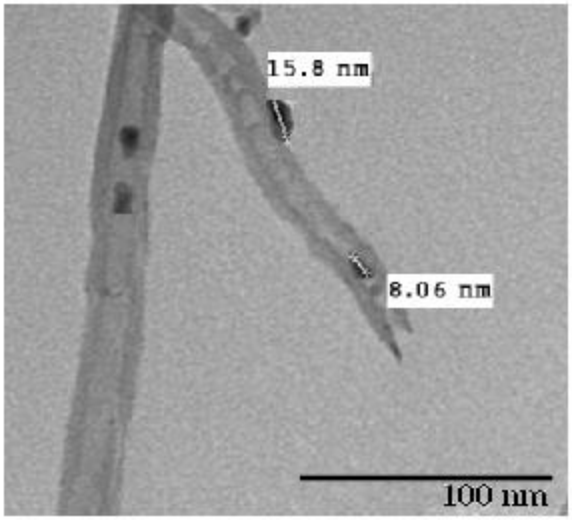

Figure 3. 2: TEM image of the calcined fresh catalyst.

Dark spots represent the cobalt nano-particles which are attached either inside or outside the nanotubes. This figure shows that the majority of the cobalt particles, about (65 to 70) %, are distributed in the inner pores of the CNTs. This can be attributed to the tubular morphology of CNTs that can induce capillary forces during the impregnation process. The particle sizes were calculated using the following equation $d = (4ab/\pi)^{0.5}$ where a and b are the dimensions of the particles as seen in the TEM image. In the fresh catalyst, the size of the cobalt oxide particles located inside the CNTs are fairly uniform with the most abundant in the range of (4 to 11) nm, which is accordance with the average inner diameter of the CNTs (12 nm). The cobalt oxide particles located on the outer surface have grown to about 16 nm (Figure 3.2). Clearly, the CNT channels restricted particle growth inside the tubes. A bar graph depicting the size distribution of the total particle populations inside and outside the tubes for the calcined catalyst is shown in Figure 3.3.

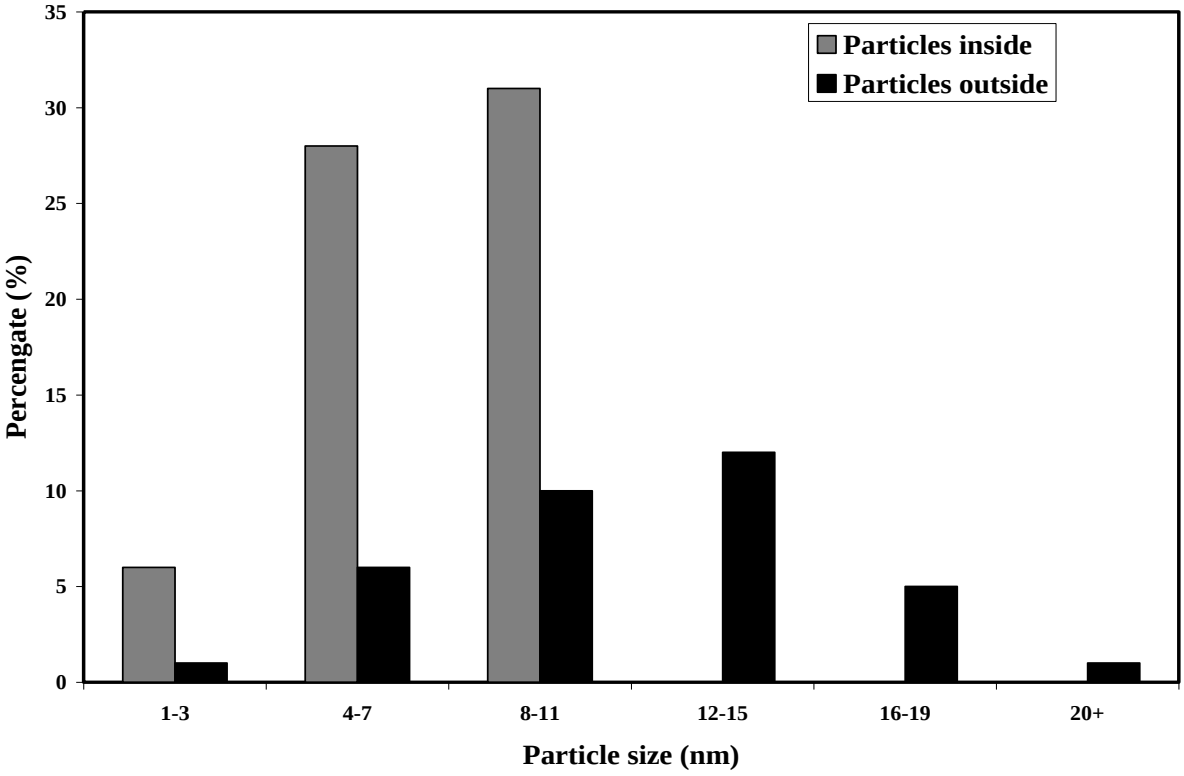

Figure 3. 3: Cobalt oxide particle size distribution of the used catalyst.

This figure shows that the average particle size of the particles located on the inner surface of the tubes is about 7.2 nm with a standard deviation of 2.3 nm and that of the particles located on the outer surface of the tubes is about 11.5 nm with a standard deviation of 4.1 nm.

Figure 3.4 shows a TEM picture of the used catalyst, which shows that particles inside the CNTs are still small (4 to 11) nm while the particles attached to the outer surfaces of the CNTs have grown significantly (i.e., > 40 nm).

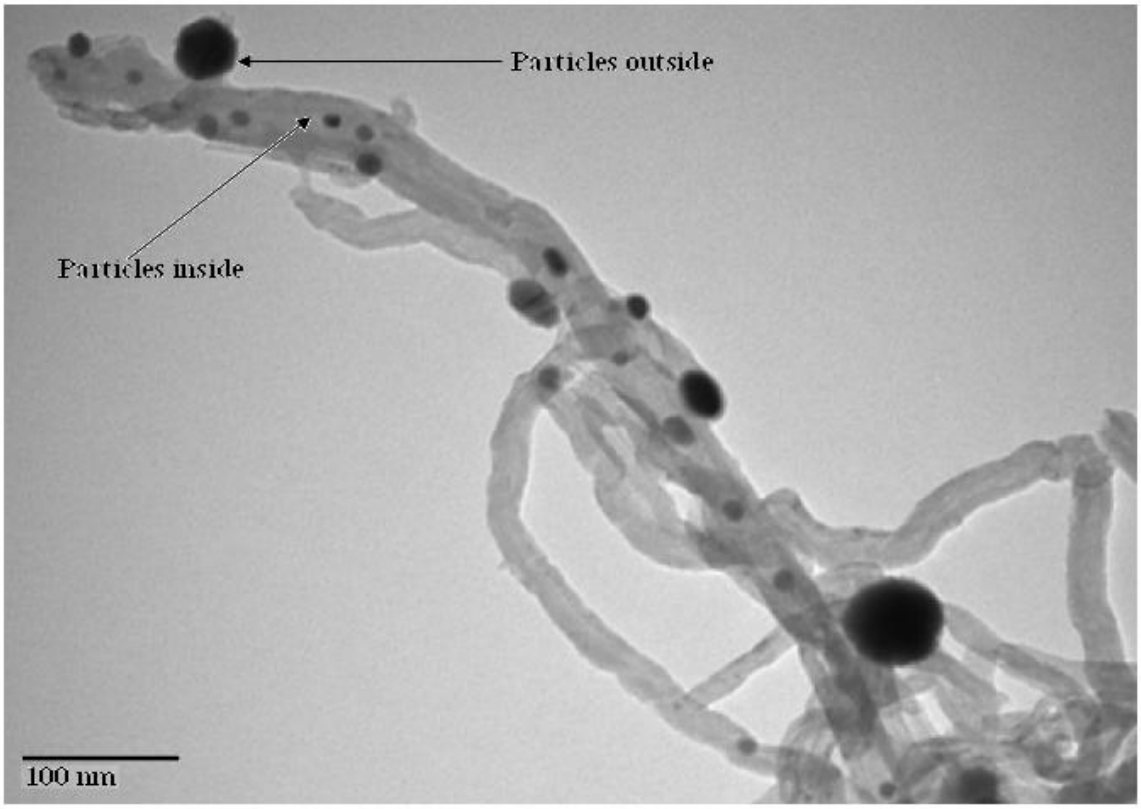

Figure 3. 4: TEM image of the used catalyst.

There is no significant cobalt oxide agglomeration inside the CNT channels, a phenomenon related to both the interaction of the metal site with the inner surface of the tubes and to the spatial restriction of the CNT channels. However, on the exterior surface most of the nanoparticle agglomerated, resulting in lower metal site dispersion under FT reactions. The tubular morphology of the graphene layers make CNTs different compared to other carbonaceous supports. The studies by Chen et al. reveal that the deviation of the graphene layers from planarity causes the π-electron density to shift from the concave inner surface to the convex outer surface, leading to an interior electron-deficient surface and an exterior electron-enriched surface [Chen et al., 2008; Menon et al., 2000 Pan et al., 2007] This characteristic can influence the structure and electronic properties of metals in contact with either surface of the CNTs. It can be concluded that, due to the electron deficiency of the inner sides of the CNTs, the interaction between the cobalt oxides and the support could be stronger, thus leading to lower rates of sintering than that

of the particles located on the outer layer of the CNTs. Furthermore, since the particles inside the tubes are rather less mobile, the sintering occurrence is considerably limited.

A bar graph depicting the size distribution of the total cobalt oxide particle populations inside and outside the tubes for the used catalyst is presented in Figure 3.5.

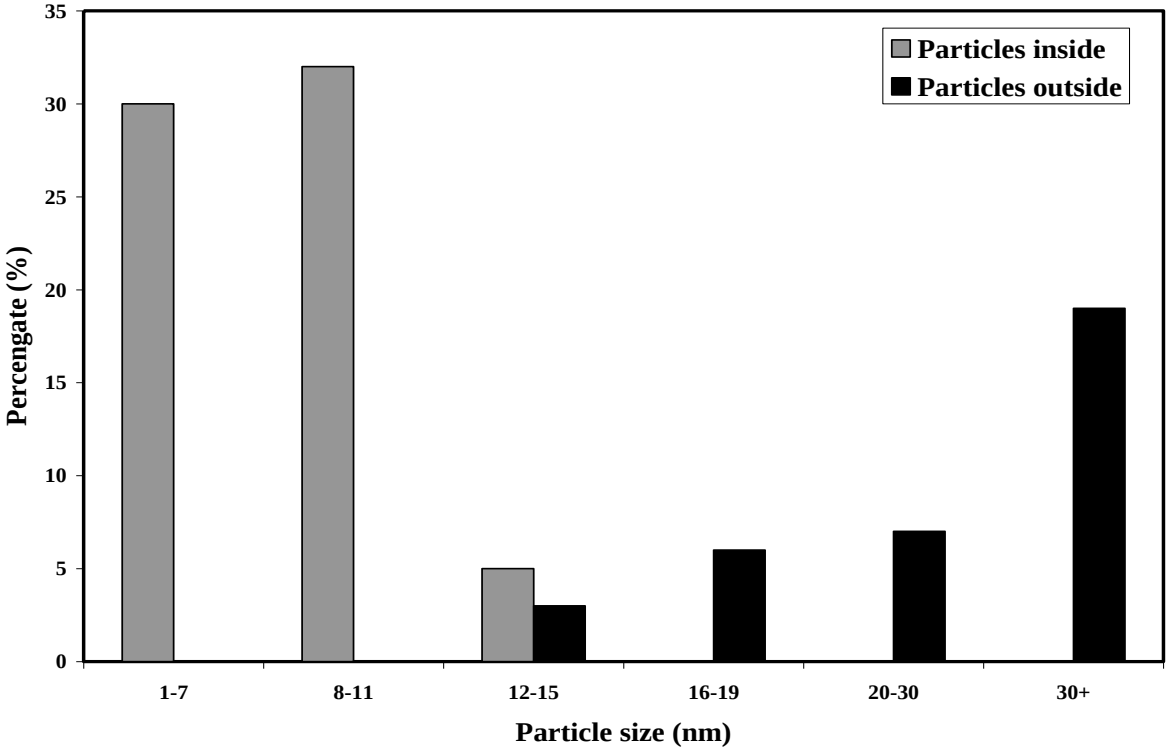

Figure 3. 5: Cobalt oxide particle size distribution of the used catalyst.

Comparing Figures 3.3 and 3.5 clearly shows that the sintering rate of the particles located on the outer surface of the CNTs is more significant than for particles on their inner surface. In the case of the particles located on the inner surface of the tubes, the average particles size increased from (7 to 8.5) ± 2.3 nm, and that of the particles located on the outer surface of the tubes increased from (11.5 to 25) ± 4.1 nm.

Table 3.1 shows the metal contents for both the fresh calcined and the used catalysts.

Table 3. 1: BET Surface Area, Porosity, XRD, and TPR Data for the Fresh and Used Catalysts

Catalysts/ Support	ICP (wt.%)	BET (m^2/g)	Pore volume (cm^3/g)	Pore Radius (nm)	XRD d(nm)	1st TPR peak (^oC)	2nd TPR peak (^oC)
CNT	-	210	0.6	6.1	-	-	-
Fresh catalyst	19.8	163	0.47	5.8	8.5	330	428
Used Catalyst	19.7	121	0.36	5.9	17	270	380

ICP analyses of the catalysts revealed that the metal contents of the catalysts was similar and close to the targeted metal content of 0.20 *w* Co. Table 3.1 also shows the results of the BET surface area measurements of the purified CNTs, fresh and used catalysts. In the case of the fresh calcined catalyst, a loading of 0.20 *w* Co decreased the surface area from (210 to 163) $m^2 \cdot g^{-1}$ and the pore volume from (0.6 to 0.47) $cm^3 \cdot g^{-1}$, indicating pore blockage due to cobalt loading on the support. After 480 h of FT synthesis, the catalyst BET surface area and the pore volume were further decreased from (163 to 121) $m^2 \cdot g^{-1}$ and from (0.47 to 0.36) $cm^3 \cdot g^{-1}$, respectively. Sintering of the particles and pore blockage during the FT synthesis causes a decrease in BET surface area and pore volume.

Figure 3.6 shows the XRD profiles of the purified CNTs and the fresh and used catalysts.

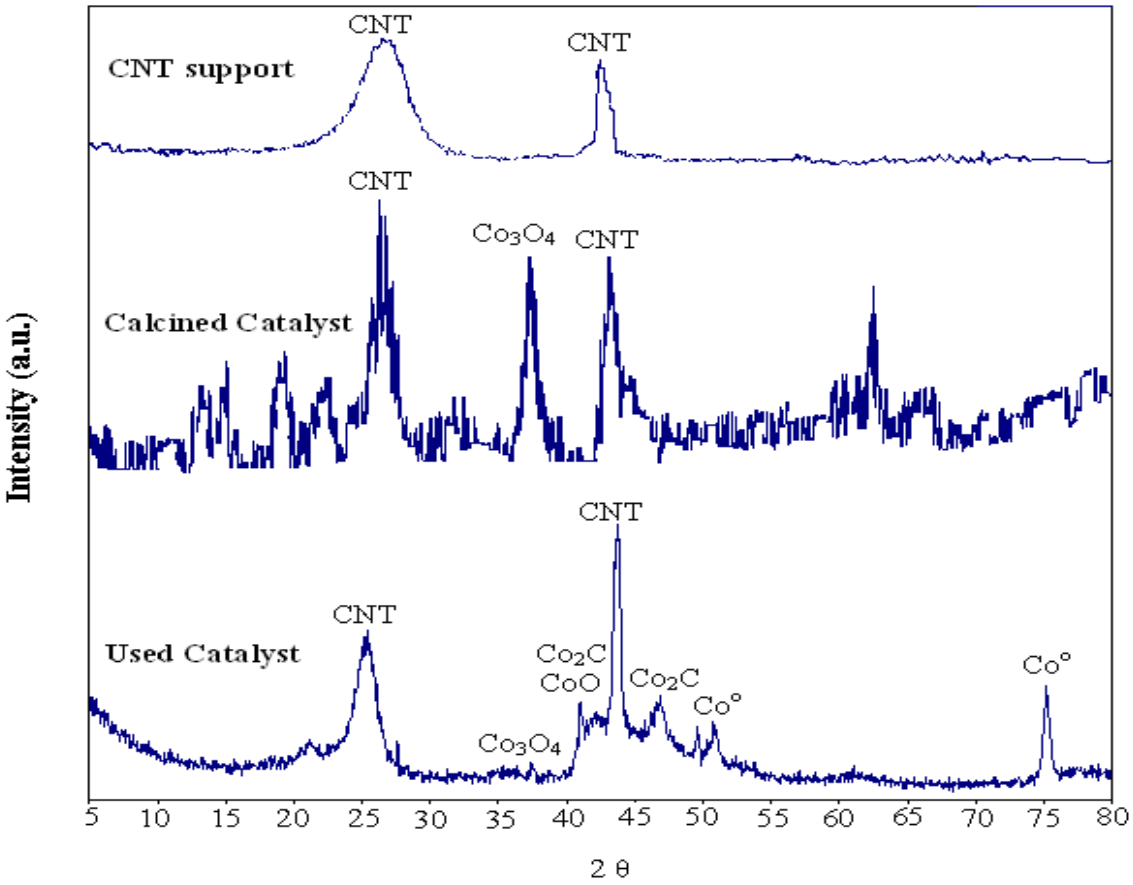

Figure 3. 6: XRD spectra for the pure CNTs, fresh and used 0.20 *w* Co/CNT catalysts

The peaks at 2θ of 25° and 43° correspond to graphite layers (multiwall CNTs), while the other peak in the spectrum of the fresh catalyst (36.8°) relates to the crystal planes of Co_3O_4 [Jacobs et al., 2002]. No peak was observed indicating formation of cobalt-support compounds in the fresh catalyst XRD spectrum. For the used catalyst, the peaks for CNT remain at a 2θ value of 25° and 43°. The peak at 42.5° in the XRD spectrum clearly indicates the presence of CoO compounds [Jacobs et al., 2002; Tavasoli et al., 2008c]. Co_3O_4 compounds were also observed in the spectrum of the used catalyst, but with a smaller peak than for the fresh catalyst at 36.8°. The metallic cobalt structure (Co°) is observed from the XRD pattern of the used catalyst at 51.5° [Jacobs et al., 2002; Tavasoli et al., 2008c]. Furthermore, the peak at a 2θ value of 47° correlates well with the Co_2C species [Jacobs et al., 2002]. Peaks for Co_2C may also be present at 36.8° and 45.7°, but these peaks are hidden in the broad peak of Co_3O_4 and CNT. The presence of Co_2C can

be attributed to either cobalt CNT interaction or a Co/carbon reaction during the CO dissociative adsorption. Although a fraction of the cobalt clusters may oxidize in the presence of significant amounts of water formed during FT synthesis with high conversions, it is probable that a fraction of cobalt oxide is formed during the discharge and passivation step at room temperature. Table 3.1 shows the average cobalt oxide particle size of the fresh and used catalysts calculated from the XRD spectra and the Scherrer equation. In agreement with the results of the TEM analyses, XRD results show that there is a significant particle growth in the course of the FTS reaction. On the basis of the XRD profiles and the TEM studies, there is good agreement between the data for the average particle size calculated.

The activation of the fresh and used catalysts in a hydrogen atmosphere was proven by TPR experiments (Figure 3.7).

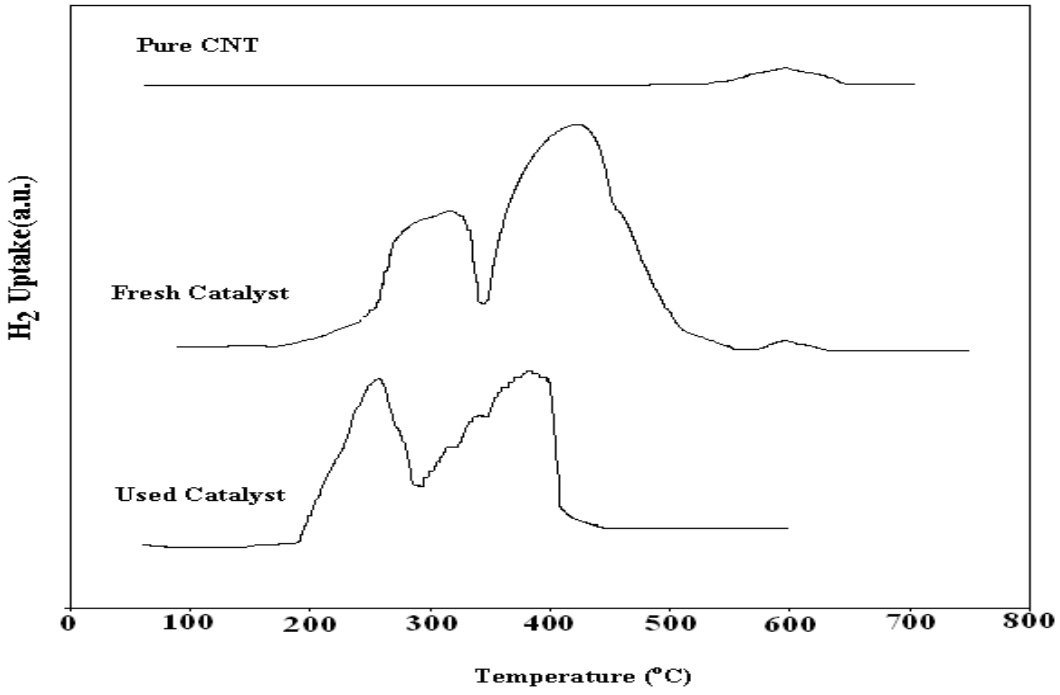

Figure 3. 7: TPR profile for the pure CNTs, calcined fresh and used 0.20 *w* Co/CNT catalysts.

The low temperature peak at (300 to 400) °C is typically assigned to the reduction of Co_3O_4 to CoO, although a fraction of the peak may be due to the reduction of the larger, bulk-like CoO species to Co° [Tavasoli et al., 2008b]. The second broad peak at (400 to

500) °C is assigned to the reduction of small CoO to Co° species and includes the reduction of cobalt species that interact with the support. The small peak at about 600 °C in is assigned to the gasification of the CNT [Trépanier et al., 2009]. For the used catalyst, the peaks shifted to lower temperatures, indicating that the reduction of the cobalt oxides occurred at lower temperatures than for the fresh calcined catalyst (Figure 3.7). According to Table 3.1, 480 h of FT synthesis decreased the first TPR temperature peak from (330 to 270) °C and the second TPR peak from (428 to 380) °C, suggesting an easier reduction process. A low reduction temperature can be due to either an easier reduction of larger cobalt particles (TEM and XRD) or to the presence of less stable oxides (XRD). However, in the case of the used catalyst the total H_2 consumption is lower, indicating a decrease in catalyst porosity due to particle growth and differentiation of the cobalt species (i.e., carbides). Therefore, it has been shown that the interaction of the metal oxide nanoparticles with the inner and outer CNT surfaces can affect the reduction behavior of the metal oxides [Chen et al., 2008; Pan et al., 2007]. The electron deficiency of the interior CNT surface can facilitate the reduction of the metal oxides located in the inner surface of the tubes as compared with the particles located in the outer surface of the tubes [Chen et al., 2008; Pan et al., 2007]. Sintering of the particles attached to the outer surface of the tubes during FT synthesis (as confirmed by TEM pictures) increased the ratio of the number of particles located inside the tubes to the number of particles located on the outer surface. In fact the ratio of the easily reducible particles to the total particles increased in the course of the FT reaction which could be another reason for the lower TPR peak temperature of the used calcined catalyst. In addition, it is important to note that the cobalt particles of the used catalyst are partially reduced according to the XRD spectra. Thus, the reduction will occur at lower temperature.

Results of H_2 chemisorption for the fresh and used catalysts are shown in Table 3.2.

Table 3. 2: Percentage Dispersion and Crystallite Sizes of Unreduced and Reduced Cobalt Particles in 0.20 *w* Co/CNT Catalyst Determined by H_2 TPR

Catalysts	μ mole H_2 desorbed /g cat.	% Red.	% Dispersion (Tot. Co)	% Dispersion (Red. Co)	dp (nm) (Tot. Co)	dp (nm) (Red. Co)
Fresh catalyst	221.4	63.9	10.4	16.3	9.9	6.3
Used Catalyst	178.9	53.4	8.4	15.7	17.5	9.4

The data show that the hydrogen consumption for the used catalyst is lower than that of the fresh calcined catalyst. The percentage of reduction and dispersion calculated based on the total cobalt concentration were decreased by about 10 %. The reduced cobalt also decreased significantly. In agreement with the TEM and XRD data, the particle diameters calculated on the basis of both the total cobalt and the reduced cobalt increased significantly with time on stream.

3.4.2 Fischer-Tropsch Synthesis

Table 3.3 presents the FT synthesis rate ($g_{HC} \cdot g^{-1}_{cat} \cdot h^{-1}$), % CO conversion, chain growth probability, and different product selectivity during first 12 h of FT synthesis.

Table 3. 3: FT Synthesis Results for 12 h (220 °C, 2 MPa, H_2/CO =2, GSHV =3000 h^{-1})

% CO Conversion	FT synthesis rate (gHC/g cat/hr)	α	CO_2 selectivity	CH_4 selectivity	C_2-C_4 selectivity	C_{5+} selectivity
74.6	0.4192	0.86	1.2	13.7	5.4	79.7

The FT synthesis productivity (0.4192 $g_{CH} \cdot g^{-1}_{cat} \cdot h^{-1}$) of the 0.20 *w* Co/CNT catalyst is greater than that of the commercial Al_2O_3, SiO_2, and TiO_2-supported cobalt based FT synthesis catalysts [Jacobs et al., 2004; Tavasoli et al., 2008b; Tavasoli et al., 2008c]. However, its product distribution (13.7 % CH_4, 5.4 % C_2-C_4, and 79.7 % C_{5+} selectivity) shows a shift to the lower molecular weight hydrocarbons. It is to note that the FT

synthesis rate of the commercial Al_2O_3, SiO_2, and TiO_2 supported cobalt catalysts is between (0.25 and 0.32) $g_{CH} \cdot g^{-1}_{cat} \cdot h^{-1}$, and the CH_4 and C_{5+} selectivities are (4 to 6) % and (86 to 93) %, respectively [Tavasoli et al., 2008c]

Figure 3.8 presents the CO conversion changes with time on stream of FT synthesis with 0.20 *w* Co/CNT catalysts.

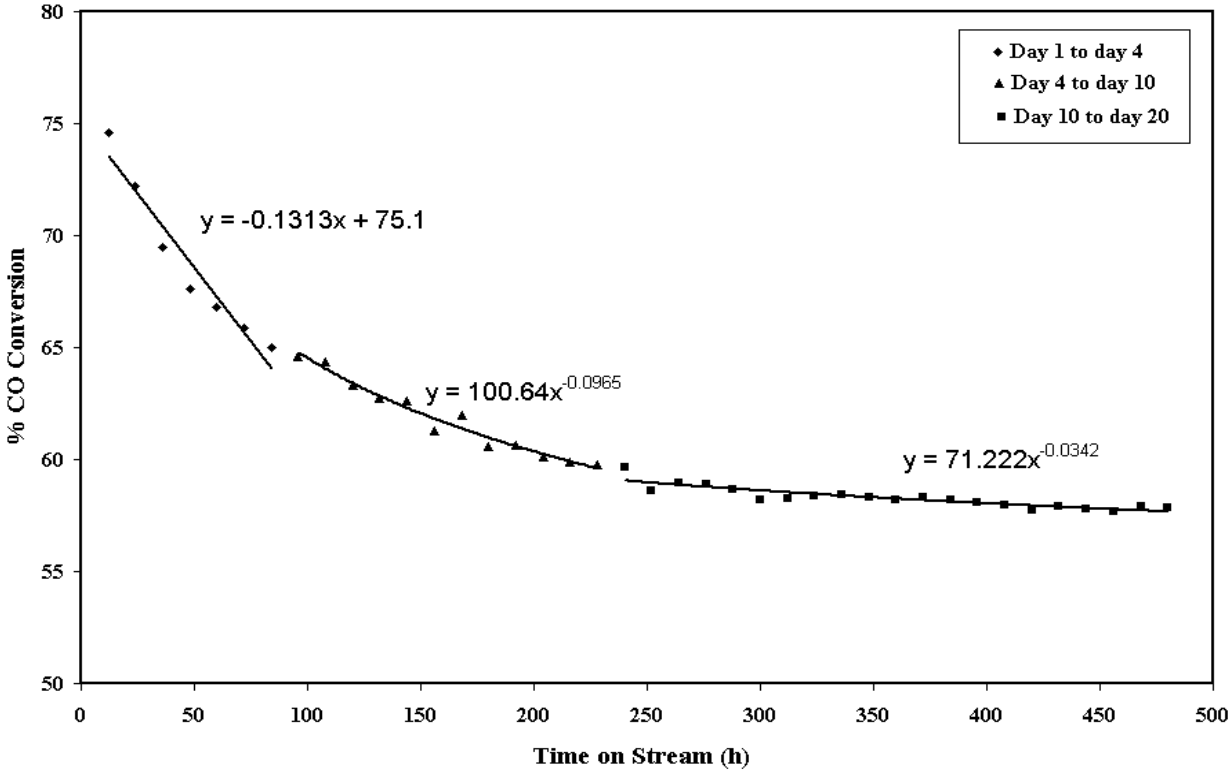

Figure 3. 8 : %CO conversion with time on stream (*T* = 220 °C, *P* = 2 MPa, $H_2/CO=2$).

Three different deactivation steps are clearly distinguishable (1) during the first 4 days, the %CO conversion drops by 10 %, (2) during days 5 to 10, the %CO conversion drops by 4.7 %, and (3) during days 11 to 20, the %CO conversion drops by only 0.73 % and reaches a plateau region. The loss of active sites significantly decreases during the first 240 h of continuous FT synthesis. As Figure 3.8 shows, the profiles of declining curves of the first, second and third step deactivations are different. For the first step, the deactivation curve is steeply sloped, then is moderated for the second step, and slowly levels off for the final step. The loss of activity for the first deactivation step can be simulated with the following linear correlation:

$$X_{CO} = -0.13T_{hr} + 75.1 \quad (3.7)$$

The linear deactivation mode suggests that the order of the deactivation rate to %CO conversion is zero. This reveals that during the first four days, the FTS deactivation rate is independent of the number of catalyst active sites and that deactivation is caused by exterior factors [Bartholomew, 2001; Tavasoli et al., 2007a; Tavasoli et al., 2008c]. It has been suggested that in FT synthesis on cobalt-based catalysts at high conversions, the loss of activity is caused by water-induced oxidation of cobalt [Jacobs et al., 2002; Jacobs et al., 2004; Tavasoli et al., 2007a; Tavasoli et al., 2008c; Tavasoli et al., 2008d].This deactivation process entails cobalt redox transformation with no support participation. Another reason for this type of activity loss is the formation of more refractory forms of oxidized cobalt generated by cobalt support interactions [Tavasoli et al., 2008c; Tavasoli et al., 2008d]. The extent of this type of deactivation also depends on the partial pressure of water produced during FT synthesis. It was recommended that water promotes interaction between cobalt oxide species and support [Jacobs et al., 2002; Jacobs et al., 2004]. Thus, the larger deactivation observed during the first 4 days of FT synthesis can be due to higher partial pressure of water as an exterior factor present in the catalytic bed of the reactor [Jacobs et al., 2002; Jacobs et al., 2004; Tavasoli et al., 2007a; Tavasoli et al., 2008c; Tavasoli et al., 2008d]. In other words, a CNT-supported cobalt catalyst is more susceptible to reoxidation and cobalt-support interactions at higher water partial pressures. Thermodynamic studies on the stability of nanosized metallic cobalt crystallites in water/syngas mixtures show that, under realistic FTS conditions the oxidation of bulk metallic cobalt is not feasible, unless the water partial pressure relative to the hydrogen and carbon monoxide partial pressures is in excess of (50 to 60) % [Kiss et al., 2003; Van Steen et al., 2005]. However, the oxidation of small cobalt crystallites to Co(II)O or the formation of an oxide shell might be thermodynamically feasible under specific conditions. The stability of nanosized crystallites, which are related to dispersion of cobalt particles, is dependent on the ratio of surface energy to the overall system energy that may vary with crystallite size, morphology, the starting crystal phase, and the ratio of the partial pressure of water relative to the partial pressure of the syngas. It is

shown that spherical cobalt crystallites with a diameter less than 4.4 nm are not stable, thus leading to higher catalyst deactivation under industrial FT conditions [Bartholomew, 2002; Bezemer et al., 2006; Tavasoli et al., 2008d]. The decrease in %CO conversion during the first 4 days may come from the oxidation of these nanosized cobalt crystallites.

For the second and third deactivation steps, the catalyst deactivation could be simulated with the following power law expressions:

Second step: $X_{CO} = 100.64 T_{hr}^{-0.0965}$ (3.8)

Third step: $X_{CO} = 71.22 T_{hr}^{-0.0342}$ (3.9)

Assuming the deactivation rate is: $-\frac{dX}{dt} = KX^{n}$ (3.10)

After integration and data reduction by least-squares, the power order (n) can be determined as 11.4 and 30.2 for the second and the third deactivation steps, respectively. These values are in the range that ordinary metal catalysts would experience during sintering [Bartholomew, 2001]. The low n value (11.4) for the second deactivation step demonstrates that the rate of sintering during this step was significantly higher than that for the third step. The TEM test results showed that the rate of sintering of the particles located on the outer surfaces of the CNT is higher than that of the particles located on the inside of the tubes. The zone with the higher sintering rate (Figure 3.8, step 2) can be attributed to the sintering of the particles located in the outer layers of the tubes, and the zone with the lower sintering rate (Figure 3.8, step 3) can be attributed to the sintering of the particles located inside the tubes. The results of H_2 chemisorptions and reoxidation tests shown in Table 3.2 confirm the cluster growth during the 480 h reaction. A FT synthesis temperature of 220 °C is low to enhance the cluster growth at the catalyst surface, but the water vapor increases the oxidation-reduction cycles on the catalyst surface that in turn leads to cluster growth or sintering. These results verify that, to have a Co/CNT catalyst with a longer lifetime, it is necessary to distribute the active metal particles in the inner layers of the CNTs. Introducing functional groups and defects on the

CNT surfaces can also act as anchoring sites for the cobalt particles and hence decrease sintering rate of the cobalt particles which are located on the outer layer of the CNTs [Trépanier et al., 2009].

The regeneration of the used catalyst at (270 and 380) °C increased %CO conversion from (57.9 to 63.5) % and from (63.5 to 67.1) %, respectively. The total activity recovery after the third regeneration step at 380 °C (about 9.1 %) is close to the total activity loss during the first deactivation step (about 10 %). Since the catalyst deactivation due to sintering is an irreversible process, the activity recovery can be assigned to the reduction of reoxidized cobalt and the reduction of cobalt species that interacted with the support (Figure 3.8, step 1).

The uncondensed vapor stream of the cold trap was reduced to atmospheric pressure through a pressure letdown valve, and the composition of this stream was quantified using an online gas chromatograph. The contents in the hot and cold traps were removed every 24 h. The hydrocarbon and water fractions were separated and analyzed using a Varian CP 3400 GC. Figure 3.9 shows the methane and C_{5+} liquid hydrocarbon selectivity variations with time on stream.

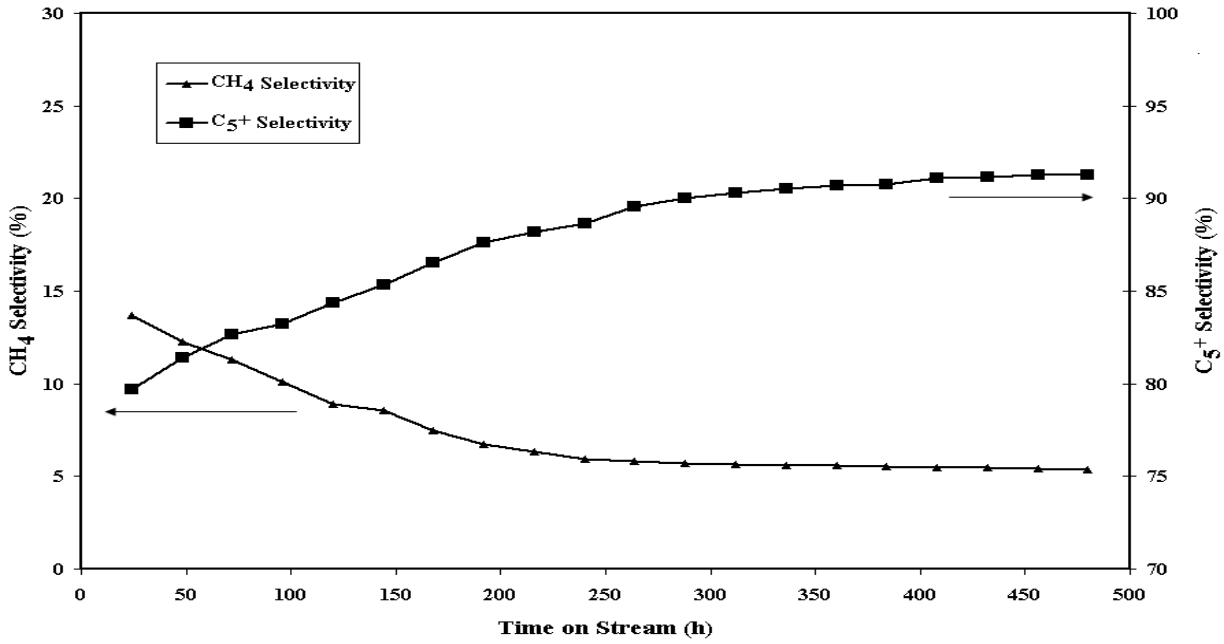

Figure 3. 9: Products selectivity with time on stream (*T* = 220 °C, *P* = 2 MPa, H_2/CO=2).

This figure displays that, during 480 h FT synthesis at 220 °C and 2 MPa, CH_4 selectivity decreases and C_{5+} selectivity increases with time on stream. The studies of Bezemer et al. have shown that the larger cobalt particles are more selective to higher molecular weight hydrocarbons and smaller ones are selective to methane and light gaseous hydrocarbons [Bezemer et al., 2006] It can be concluded that sintering of the smaller particles leads to enhancement of C_{5+} selectivity and suppression of CH_4 production with time on stream.

As discussed earlier, most of the cobalt particles are located inside the CNTs. Confinement of the reaction intermediates inside the pores can enhance their contact with cobalt particles, favoring the growth of longer chain hydrocarbons. In addition, the inner sides of the CNTs are electron-deficient and can enhance the dissociation of CO resulting in the production of higher hydrocarbons chain. Increasing the ratio of the particles located inside the tubes to the particles located outside the tubes is believed to be the main reason for enhancement of C_{5+} selectivity and suppression of CH_4.

3.5 Conclusions

Cobalt catalysts supported on CNTs have shown two different types of deactivation mechanisms: cobalt oxidation and sintering. Sintering is the main source of irreversible deactivation in the CNT-supported cobalt FT synthesis catalysts. The deposition of cobalt particles inside the CNT pores improves the catalytic behavior of the Co/CNT catalyst, which is likely due to the difference in the electronic properties of the inner and outer surface of the CNTs and cobalt particle confinement effects. Because of the electron deficiency of the inner sides of the CNTs, the interaction between the cobalt oxides and the support is stronger, leading to lower rates of sintering as compared with the particles located on the outer layers. Also, the physical encapsulation of the metal particles inside the pores reduces the metal site sintering. Confinement of reaction intermediates inside the channels increases the contact time with active metal sites, resulting in the production of heavier hydrocarbons.

3.6 References

Bartholomew, C. H., “Mechanism of catalyst deactivation,” Applied Catalysis A: General **212**, 17–60 (2001).

Bezemer, G.L., P.B. Radstake, V.Koot, A.J. van Dillen, J.W. Geus, K.P. de Jong, "Preparation of Fischer–Tropsch cobalt catalysts supported on carbon nanofibers and silica using homogeneous deposition-precipitation," Journal of Catalysis **237,** 291-302 (2006).

Bukur, D.B., X. Lang, D. Mukesh, W.H. Zimmerman, M.P. Rosynek and C. Li, "Binder/support effects on the activity and selectivity of iron catalysts in Fischer-Tropsch synthesis," Industrial and Engineering Chemistry Research **29**, 1588-1599 (1990).

Chen, W., Z. Fan, X. Pan, X. Bao, "Effect of Confinement in Carbon Nanotubes on the Activity of Fischer-Tropsch Iron Catalyst," Journal of American Chemical Society **130**, 9414-9419 (2008).

Dry, M.E., "Fischer-Tropsch reactions and environment," Applied Catalysis A: General **189**, 185-190 (1999).

Guczi, L., G. Stefler, O. Geszti, Z. Koppany, Z. Konya, E. Molnar, M.I Urbanc, J. Kiricsi, "CO hydrogenation over cobalt and iron catalysts supported over multiwall carbon nanotubes: Effect of preparation," Journal of Catalysis **244**, 24–32 (2006).

Jacobs,G., T.K Das, Y. Zhang, J. Li, G. Racoillet and B.H. Davis, "Fischer–Tropsch synthesis: support, loading, and promoter effects on the reducibility of cobalt catalysts," Applied Catalysis A:General **233**, 263-281 (2002).

Jacobs, G., P.M. Patterson, T. Das, M. Luo, B. Davis, "Fischer- Tropsch synthesis: Effect of water on Co/Al2O3 catalysts and XAFS characterization of reoxidation phenomena," Applied Catalysis A: General **270**, 65–76 (2004).

Kiss, G., C.E. Kliewer, G.J. DeMartin, C.C. Culross, J.E. Baumgartner, "Hydrothermal deactivation of silica-supported cobalt catalyst in Fischer-Tropsch synthesis," Journla of Catalysis **217**, 127–140 (2003).

Ma, W-P, E.L. Kugler, J. Wright and D.B. Dadyburjor, "Mo-Fe catalysts supported on Activated Carbon for synthesis of liquid fuels by the Fischer-Tropsch Synthesis process: Effect of Mo addition on reducibility, activity, and hydrocarbon selectivity," Energy & Fuels **20**, 2299–2307 (2006).

Menon, M., A.N. Andriotis, G.E. Froudakis, "Contrasting bonding behaviors of 3*d* transition metal atoms with graphite and C_{60}," Physique Letters **320**, 425–431 (2000).

Michiel, J.A., M.J.A. Tijmensen, A.P.C. Faaij, C.N. Hamelinck and M.R.M. Van Hardeveld, "Exploration of the possiblities for production of Fischer-Tropsch liquids and power via biomass gasification, Biomass and Bioenergy **23**, 129-152 (2002).

Pan, X., Z. Fan, W. Chen, Y. Ding, H. Luo and X. Bao, "Enhanced ethanol production inside carbon-nanotube reactors containing catalytic particles," Nature **6**, 507-511 (2007).

Serp, P., M. Corrias and P. Kalck, "Carbon nanotubes and nanofibers in catalysis," Applied Catalysis A: General **253,** 337-358 (2003).

Tavasoli A.,"Catalyst composition and its distribution effects on the enhancement of activity, selectivity and suppression of deactivation rate of FTS cobalt catalysts," Ph.D. Thesis, University of Tehran (2005).

Tavasoli, A., K. Sadaghiani, A. Nakhaeipour and M. G Ahangari, "Raising distillate selectivity and catalyst lifetime in Fischer-Tropsch synthesis by using a novel

dual-bed reactor," Iranian Journal of Chemistry and Chemical Engineering **26**, 1-9 (2007a).

Tavasoli, A., A.M. Rashidi, K. S. Zadeh, A. Karimi, A.A. Kodadadi, Y. Mortazavi, "Carbon nanotubes supported cobalt catalyst for converting synthesis gas into hydrocarbons," EP patent 1782885 A1 (2007b).

Tavasoli, A., R.M. Abbaslou, M. Trépanier and A.K.Dalai, "Fischer-Tropsch synthesis over cobalt supported on carbon nanotubes in a slurry reactor," Applied Catalysis A: Genreal **345**, 134-142 (2008 a)

Tavasoli, A., K.Sadaghiani and K. Khorashe, A.A. Seifkordi, A.A. Rohani and A. Nakhaeipour, "Cobalt supported on carbon nanotubes: a promising novel Fischer-Tropsch synthesis catalyst," Fuel Processing Technology **89**, 491-498 (2008 b).

Tavasoli, A., R.M.M. Abbaslou, M.Trépanier and A.K. Dalai, "Morphology and deactivation behavior of Co-Ru/Al_2O_3 Fischer-Tropsch synthesis," The Canadian Journal of Chemical Engineering **86**, 1070-1080 (2008 c).

Tavasoli, A., R.M.M. Abbaslou, A.K. Dalai, "Deactivation behavior of ruthenium promoted promoted Co/γ-Al_2O_3 catalysts in FTS," Applied Catalysis A: General **346**, 58-64 (2008 d).

Trépanier, M., A. Tavasoli, A.K. Dalai and N. Abatzoglou, " Fischer-Tropsch synthesis over carbon nanotubes supported cobalt catalysts in a fixed bed reactor: Influence of acid treatment," Fuel Processing Technology **90**, 367-374 (2009 a).

Van Steen, E., M. Claeys, M.E., Dry, J. Van de Loosdrecht, E.L. Viljoen, J.L. Visagie, "Stability of nanocrystals: thermodynamic analysis of oxidation and re-

reduction of cobalt in water/hydrogen mixtures," Journal of Physical Chemistry B **109**, 3575–3577 (2005).

Zhang, J., J. Chen, J. Ren, Y. Li and Y. Sun, "Support effect of Co/Al_2O_3 catalysts for FTS," Fuel 82, 581-586 (2003).

Chapter 4: Co, Ru and K loadings effects on the activity and selectivity of carbon nanotubes supported cobalt catalyst in Fischer-Tropsch synthesis

A similar version of this chapter has been published in Applied Catalysis A: General:

Trépanier, M., A. Tavasoli, A.K. Dalai., N. Abatzoglou, Co, Ru and K loadings effects on the activity and selectivity of carbon nanotubes supported cobalt catalyst in Fischer-Tropsch synthesis. Applied Catalysis A: General 353 (2009) 193-202

The work discussed in this chapter was also included in paper presentations at the following conferences:

Trépanier, M., A.Tavasoli, A.K. Dalai and N. Abatzoglou, (October 2008) Effects of different loadings Co, Ru and K on physico-chemical properties and performance of Carbon nanotubes supported Co FTS catalysts, 58th CSChe Conference, Ottawa, Canada.

Contribution of Ph.D Candidate

The laboratory experiments, data analysis and results interpretation for the optimized catalysts study was performed by Mariane Trépanier. Ahmad Tavasoli provided guidance in the results and discussion while writing the submitted manuscript. Drs.Dalai and Abatzoglou provided editorial assistance, the main idea of the research project and financial support. The submitted manuscript was written by Mariane Trépanier.

Contribution of this manuscript to Overall Study

Chapters 2 and 3 demonstrated the potential of carbon nanotubes as suitable support for FTS cobalt catalyst in a fixed bed reactor. A secondary goal of the Ph.D research is to optimize the performance of the new by developed Co/CNT catalyst.

Cobalt loadings and addition of promoters have been studied. In order to minimize the cost of the newly developed catalyst, catalytic performance for wide cobalt loading has been evaluated. This phase of the research also demonstrates that commonly used promoters for cobalt FTS catalyst such as ruthenium (Ru) and potassium (K), enhance the FTS activity and selectivity of the Co/CNT catalyst. Finally, Chapter 4 contributed to this study by indicating the accurate wt. % of cobalt loading and wt. % of promoters needed to optimize Co/CNT catalyst efficiency.

4.1 Abstract

An extensive study of Fischer–Tropsch synthesis (FTS) on carbon nanotubes (CNTs) supported cobalt catalysts with different loadings of cobalt, ruthenium and potassium is reported. Up to 30 wt. % of Co, 1 wt. % of Ru and 0.0066 wt. % of K were added to the catalyst by co-impregnation method. The physicochemical properties, activity and selectivity of the catalysts were assessed. For the 15 wt. % Co/CNT catalyst, most of the metal particles were homogeneously distributed inside the tubes and the rest on the outer surface of the CNTs. Increasing the Co loading to 30 wt. % increased the amount of Co on the outer surface of the CNTs, increased the cobalt cluster sizes and decreased the reduction temperature and dispersion. Increasing the Co loading from 15 to 30 wt. % increased the CO conversion from 48 to 86 % and the C_{5+} selectivity from 70 to 77 %. Ruthenium was found to enhance the reducibility of Co_3O_4 to CoO and that of CoO to Co^o, increase the dispersion and decrease the average cobalt cluster size. However, potassium was responsible in shifting the reduction temperatures to higher temperatures. 0.5 wt. % Ru increased the FTS rate of 15 wt. %Co/CNT catalyst by a factor of 1.4 while the addition of 0.0066 wt. % K decreased the FTS rate by a factor of 7.5. Both promoters enhanced the selectivity of FTS towards the higher molecular weight hydrocarbons however; the effect of Ru is less pronounced. Potassium increased the olefin to paraffin ratio from 0.73 to 3.5 and the C_{5+} selectivity from 70 to 87 %.

4.2 Introduction

High energy cost is the main driving force of currently increasing interest in the Fischer–Tropsch synthesis (FTS) for the conversion of natural gas to liquid fuels (GTL). The catalytic synthesis of hydrocarbons from CO and H_2 syngas mixtures leads to a large

variety of products such as paraffins, olefins, alcohols and aldehydes. The most desired products are those with low methane, low oxygenate, high alkene/alkane ratio, and high C_{5+} contents. Due to high chain growth probability, lower deactivation rate, low water gas shift activity, and quite low price, cobalt catalyst is considered to be the best candidate for syngas to clean liquid fuels requirements [Dry, 2001]. However, the activity and selectivity of Co containing catalysts still need improvement. Various studies have been performed on the influence of promoters and loadings on cobalt-based catalysts supported on Al_2O_3, SiO_2 and TiO_2 [Bechera et al., 2001; Dry , 2001; Iglesia et al., 1988; Jacobs et al., 2002; Li et al., 2002; Rohr et al., 2000]. Increase in the amount of cobalt loadings and promoter addition to cobalt catalyst appears to improve the FTS activity of cobalt catalyst. It has been shown that, for cobalt catalysts supported on Al_2O_3, SiO_2 and TiO_2 oxide supports higher the cobalt loading (>15 wt. %Co) increases FTS activity, increases cobalt particle size due to agglomeration of cobalt crystallites and leads to low selectivity of CH_4 and high selectivity of C_{12}–C_{40} parrafins [Bechera et al., 2001; Dry, 2001; Iglesia et al., 1988; Jacobs et al., 2002; Li et al., 2002; Rohr et al., 2000]. However, the maximum loading of cobalt depends on the support characteristics [Tavasoli et al., 2005]. For cobalt catalysts supported on Al_2O_3, SiO_2 and TiO_2, noble metals such as ruthenium are typically used to decrease the reduction temperature of the cobalt oxides and increase the dispersion of the cobalt clusters [Jacobs et al., 2002]. Also synergistic bimetallic interactions between Co and Ru increase FTS rate and C_{5+} selectivity [Iglesia et al., 1993]. In addition, in the case of metal-oxide supported cobalt catalysts alkali promoters such as potassium improves the selectivity of the catalyst [Iglesia et al., 1988]. It has been shown that potassium promoter enhances the selectivity towards longer hydrocarbons and increases the olefin to paraffin (O/P) ratio [Huffman et al., 1994]. However, K promoter decreases FTS rate compared to unpromoted cobalt catalyst [Huffman et al, 1994].

Al_2O_3, SiO_2 and TiO_2 supported cobalt catalysts have been commercialized and now being used by different companies in industrial scale. Major drawback of these supports and catalysts is their reactivity towards cobalt. Using these metal-oxides as cobalt catalyst support can lead to the formation of mixed compounds that are reducible only at high reduction temperatures. Indeed, a catalyst support is not merely a carrier but

it may also contribute to the activity of the catalyst. The acid–base and textural properties of supported catalysts play an important role in FTS. Earlier studies have indicated that using carbon as a support to provide an inert, poorly interacting surface could moderate the catalytic behavior of metals such as iron, cobalt and ruthenium [Bahome et al., 2005; Bahome et al., 2007; Tavasoli et al., 2007; Tavasoli et al., 2008c;]. Carbon nanotubes provide a relatively inert support, suggesting that this is a unique system for the study of the catalytic behavior of metals since it provides reduced support interactions [Bahome et al., 2007; Bezemer et al., 2004; Tavasoli et al., 2007; Tavasoli et al., 2008a; Tavasoli et al., 2008b;]. Also, carbon nanotubes as a new type of carbon material have appropriate pore-size distribution favoring maximum metallic dispersion [Bezemer et al., 2004; Tavasoli et al., 2007; Tavasoli et al., 2008a; Tavasoli et al., 2008b]. Their special and steady structural characteristics and morphology are quite suitable for use as catalytic support materials [Bezemer et al., 2004; Tavasoli et al., 2007; Tavasoli et al., 2008a; Tavasoli et al., 2008b].

The present work was undertaken with the aim of exploiting the beneficial effects of carbon nanotubes as cobalt FTS catalyst support. Due to high cost of cobalt, it is important to determine the appropriate loading of cobalt to maximize the availability of active cobalt surface sites for participation in the reaction. In this work a series of Co/CNT catalysts were prepared with different loadings of cobalt (15–30 wt. %). The effect of the cobalt loading on the physico-chemical properties of the catalysts is investigated. Also a series of ruthenium and potassium promoted catalysts with different amounts of Ru and K loadings have been formulated. It is important to determine the optimum loading of these promoters for maximizing the availability of the active metal for catalyzing the Fischer–Tropsch (FT) reaction.

4.3 Experimental

4.3.1 Catalyst preparation

Purified (>95 %) Mknano-MWCNT was used as support materials for the preparation of FTS catalysts. Prior to impregnation, the support was treated with 30 wt. % HNO_3 at 100 ^oC over night, washed with distilled water, and dried at 120 ^oC for 6 h. All catalysts were prepared with incipient wetness impregnation of cobalt nitrate

($Co(NO_3)_26H_2O$ 99.0 %, Merck) solution on treated Mknano-MWCNT as the support. Using sequential impregnation method Co15, Co22 and Co30 catalysts were prepared with cobalt loadings of 15, 22 and 30 wt. %. After each impregnation step, the catalyst was dried at 120 ^oC and calcined at 350 ^oC for 3 h with a heating rate of 10 ^oC/min under argon flow. Ru promoted Ru.25(Co15), Ru.5(Co15) and Ru1(Co15) catalysts were prepared with fixed amount of cobalt (15 wt.%) and different amounts of Ru (0.25, 0.5 and 1 wt. %) using co-impregnation of aqueous solutions of cobalt nitrate($Co(NO_3)_26H2O$), and ruthenium (III) nitrosylnitrate. Also potassium promoted K.0016(Co15), K.0033(Co15) and K.0066(Co15) catalysts were prepared with constant amount of cobalt (15 wt.%) and different amounts of K (0.0016, 0.0033 and 0.0066 wt.%) using co-impregnation of aqueous solutions of cobalt nitrate and potassium nitrate (KNO_3). All promoted catalysts were dried at 120 ^oC for 6 h and calcined at 350 ^oC under argon flow for 3 h with a heating rate of 10 ^oC/min. The loadings were verified by an inductively coupled plasma (ICP) AES system.

4.3.2 Catalyst characterization

The treated CNTs and Co15, Co22 and Co30 unpromoted catalysts were characterized by transmission electron microscopy (TEM). Sample specimens for TEM studies were prepared by ultrasonic dispersion of the catalysts in methanol. The suspensions were dropped onto a carbon-coated copper grid. TEM investigations were carried out using a Hitachi H-7500 (120 kV).

The surface area, pore volume, and average pore radius of the catalysts were measured by an ASAP-2000 system from Micromeritics. The samples were degassed at 200 ^oC for 2 h under 50 mTorr vacuum and their BET area, pore volume, and average pore radius were determined. XRD measurements of the pure CNTs and calcined catalysts were conducted with a Philips PW1840 X-ray diffractometer with monochromatized Cu/Kα radiation. Using the Scherrer equation, the average size of the Co_3O_4 crystallites in the calcined catalysts was estimated from the line broadening of a Co_3O_4 peak at 2θ of 36.8^o.

Temperature programmed reduction (TPR) spectra of the calcined catalysts were recorded using a CHEMBET-3000, equipped with a thermal conductivity detector. The

catalyst samples were first purged in a flow of helium at 150 ^{o}C, to remove traces of water, and then cooled to 40 ^{o}C. The TPR of 100 mg of each sample was performed using 3.1% hydrogen in nitrogen gas mixture with a flow rate of 40 cm_3/min. The samples were heated from 40 to 800 ^{o}C with a heating rate of 10 ^{o}C/min. The amounts of chemisorbed hydrogen on the Co and Co/Ru catalysts were measured using the Micromeritics TPD TPR 290 system. 0.25 g of the calcined catalyst was reduced under hydrogen flow at 400 ^{o}C for 20 h and then cooled to 50 ^{o}C under hydrogen flow. Then the flow of hydrogen was switched to argon at the same temperature, which lasted for about 30 min in order to remove the physisorbed hydrogen. Afterwards, the temperature programmed desorption (TPD) of the samples was obtained by increasing the temperature of the samples, with a ramp rate of 20 ^{o}C/min, to 400 ^{o}C under the argon flow. The resulting TPD spectra were used to determine the cobalt dispersion and its surface average crystallite size. The % dispersion and particle diameter are calculated by the formula below [Tavasoli et al., 2008a; Tavasoli et al., 2008c].

$$\text{Calibration value } (l_{gas}/\text{area units}) = \frac{\text{loop volume} \times \%\ \text{analytical gas}}{\text{mean calibration area} \times 100} \tag{4.1}$$

$$H_2 \text{ uptake } (\text{moles}/g_{cat}) = \frac{\text{analytical area from TPD} \times \text{calibration value}}{\text{sample weight} \times 24.5} \tag{4.2}$$

$$\%D_{\text{Total Co}} = \frac{H_2 \text{ uptake} \times \text{atomic weight} \times \text{stoichiometry}}{\%\ \text{metal}} = \frac{\text{number of Co}^{o}\ \text{atoms on the surface} \times 100}{\text{total number of Co}^{o}\ \text{atom}} \tag{4.3}$$

$$\%D_{\text{reduced Co}} = \frac{\text{number of Co}^{o}\ \text{atoms on the surface} \times 100}{\text{total number of Co}^{o}\ \text{atom} \times \text{fraction reduced}} \tag{4.4}$$

$$\text{diameter (nm)}_{\text{total Co}} = \frac{6000}{\text{density} \times \text{maximum area} \times \text{dispersion}} \tag{4.5}$$

$$\text{diameter (nm)}_{\text{reduced Co}} = \frac{6000}{\text{density} \cdot \text{maximum area} \times \text{dispersion} \times \text{fraction reduced}} \tag{4.6}$$

The amount of chemisorbed carbon monoxide (CO uptake) on the Co15 catalyst and potassium promoted catalysts were measured via injection of pulses of pure CO to the

reduced catalysts after TPD of the samples. The resulting spectra were used to determine the amount of chemisorbed carbon monoxide (micro moles of CO/g of catalyst).

4.3.3 Reaction setup and experimental outline

The catalysts were evaluated in terms of their FTS activity ($g_{HCproduced}$ /gcat./h) and selectivity (the percentage of the converted CO that appears as a hydrocarbon products) in a fixed bed microreactor. The temperature of the reactor was controlled via a PID temperature controller. Brooks 5850 mass flow controllers were used to add H_2, CO and argon at the desired rate to the reactor. Argon was used as internal standard gas in the reactor feed. Prior to the activity tests, the catalyst activation was conducted according to the following procedure. The catalyst (1 g) was placed in the reactor and pure hydrogen was introduced at a flow rate of 60 ml/min. The reactor temperature was increased from room temperature to 380 ^{o}C at a rate of 10 ^{o}C/min, maintained at this activation condition for 20 h and the catalyst was reduced in situ. After the activation period, the reactor temperature was decreased to 180 ^{o}C under flowing hydrogen.

The mixed gases entered through to the top of the fixed bed reactor. Synthesis gas with a flow rate of 60 ml/min (H_2/CO ratio of 2) was introduced and the reactor pressure was increased to 2 MPa. The reactor temperature was then increased to 220 ^{o}C at a rate of 10 ^{o}C/min. Products were continuously removed from the vapor and passed through two traps, one maintained at 100 ^{o}C (hot trap) and the other at 0 ^{o}C (cold trap). The uncondensed vapor stream was reduced to atmospheric pressure through a back pressure regulator. The composition of the outlet gas stream was determined using an on-line GC-2014 Shimadzu gas chromatograph. The contents of hot and cold traps were removed every 24 h. The hydrocarbon and water fractions were separated, and then analyzed by Varian 3400 GC liquids analyzer.

4.4 Results and discussion

4.4.1 Characterization overview

A sample of the purified CNT material was analyzed by TEM. The purified product is comprised of an interwoven matrix of tubes (Figure 4.1) that is shown to be comprised of multi-walled carbon nanotubes (MWCNTs).

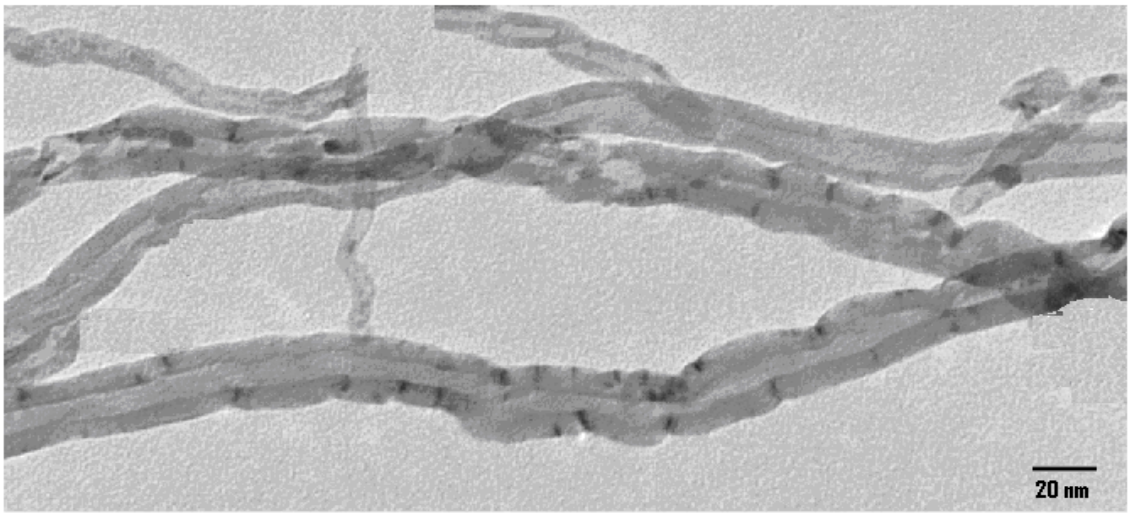

Figure 4. 1: TEM image of the purified CNT as support material after purification showing the open caps and defects on the surface of the CNT.

The TEM images of unpromoted Co15 catalysts revealed that the catalyst particles are well dispersed inside the tubes and as well as on the perimeter of the tube walls (Figure 4.2).

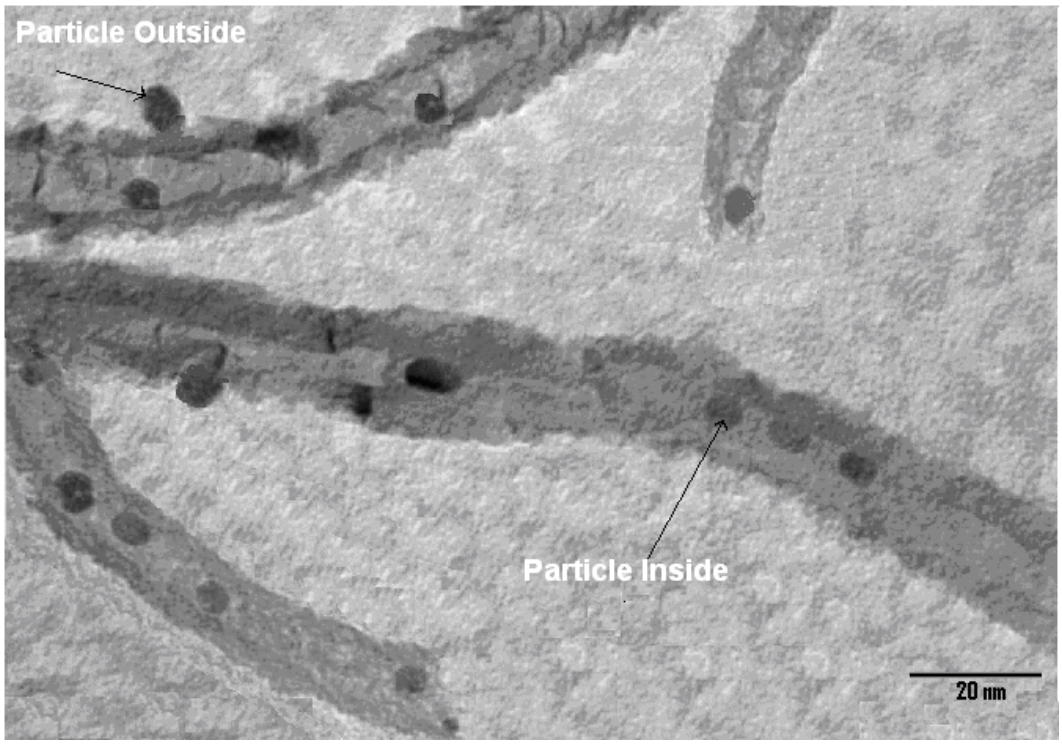

Figure 4. 2: TEM image of cobalt particles uniformly distributed inside the CNT of Co15 catalysts (60 kV)

The particles inside the tubes are fairly uniform and the most abundant ones are 3–10 nm in size in accordance with the average inner diameter of the CNTs, whereas those on the outer surface have grown to about 8–15 nm (Figure 4.2). The CNT channels have restricted the growth of the particles inside the tubes. A bar graph depicting the size distribution of the particles which is taken using 10 TEM pictures of unpromoted Co15, Co22 and Co30 catalysts is shown in Figure 4.3.

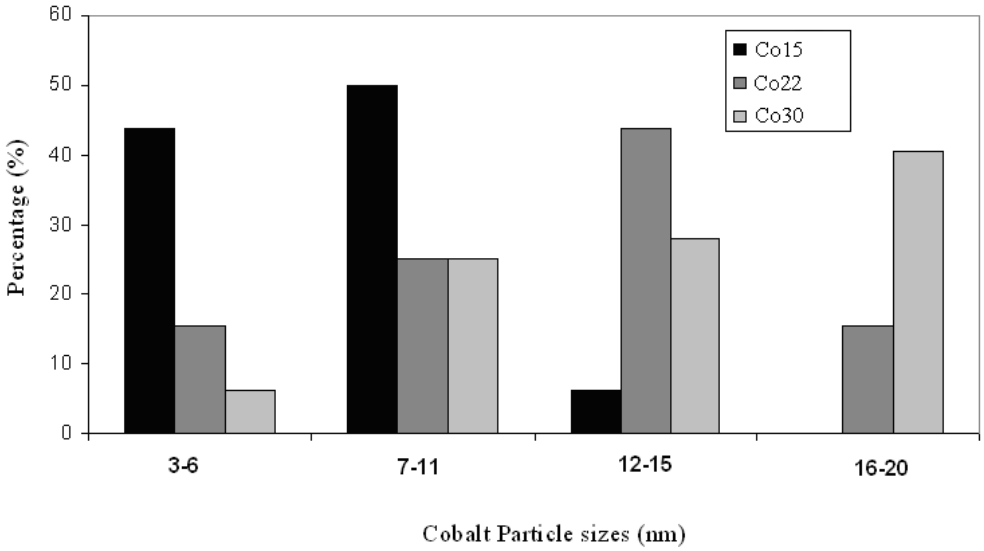

Figure 4. 3: A bar graph depicting the size distribution of the cobalt particles of Co15, Co22 and Co30 catalysts based on TEM pictures.

This figure shows that by increasing the cobalt loading from 15 to 30 wt.%, the average cobalt particles size increases from 8 ± 2nm to 16 ± 3 nm . Results of surface area measurements are shown in Table 4.1.

Table 4. 1: BET surface area and porosity data

Catalysts/Support	%Co	%Ru	%K	BET (m^2/g)	Pore volume (cm^3/g)	Average pore radius (nm)
CNT	-	-	-	210	0.60	6.1
Co15	15	-	-	160	0.50	5.7
Co22	22	-	-	154	0.45	5.6
Co30	30	-	-	145	0.41	5.5
Ru.25(Co15)	15	0.25	-	161	0.49	5.7
Ru.5(Co15)	15	0.5	-	160	0.50	5.8
Ru1(Co15)	15	1.0	-	159	0.50	5.7
K.0016(Co15)	15	-	0.0016	160	0.51	5.7
K.0033(Co15)	15	-	0.0033	161	0.51	5.7
K.0066(Co15)	15	-	0.0066	162	0.50	5.7

These results show that the BET surface area of Co15, Co22 and Co30 unpromoted catalysts decreases from 210 to 160, 154 and 145 (m^2/g), respectively. At the same time, the pore volumes of the catalysts are decreased from 0.60 to 0.50, 0.45 and 0.41 (cm^3/g), respectively. The lower BET surface area and pore volume of the Co15, Co22 and Co30 catalysts compared to that of the pure CNTs indicates some pore blockage due to cobalt loading on the support. Increasing the amount of cobalt loading increases the pore blockage. Due to low amounts of K and Ru, the BET area, pore volume and average pore radius of the Ru and K promoted catalysts are very close to those of unpromoted Co15 catalyst.

X-ray diffraction patterns of the support and calcined catalysts are shown in Figures 4.4 and 4.5.

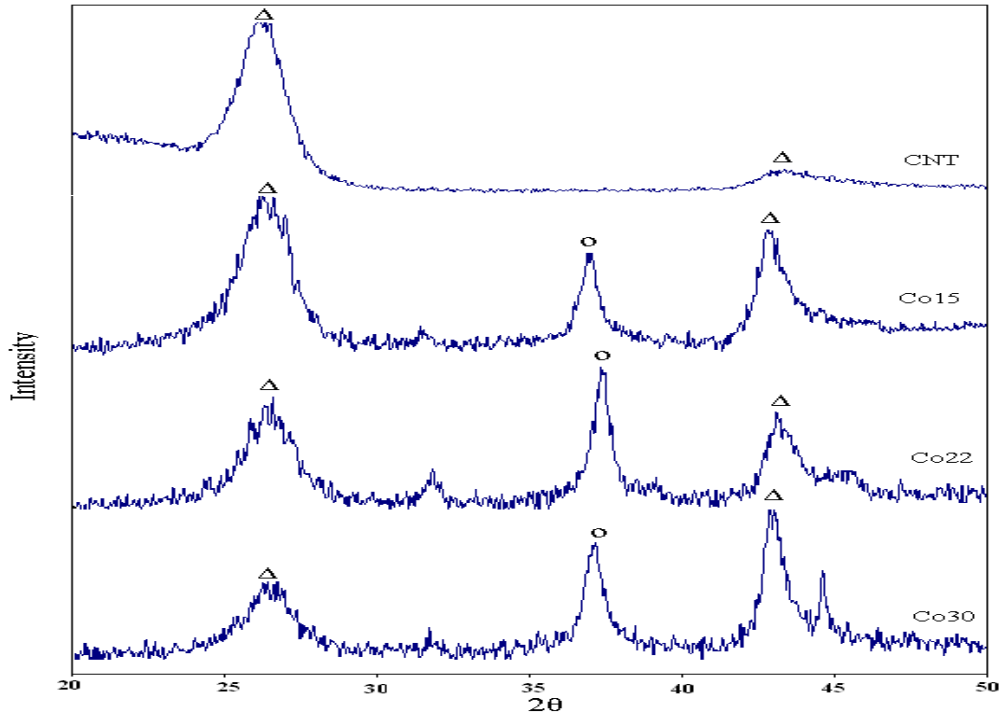

Figure 4. 4: XRD spectra for pure CNT, Co15, Co22 and Co30 catalysts O: Co_3O_4 (36.8^o), Δ: CNT.

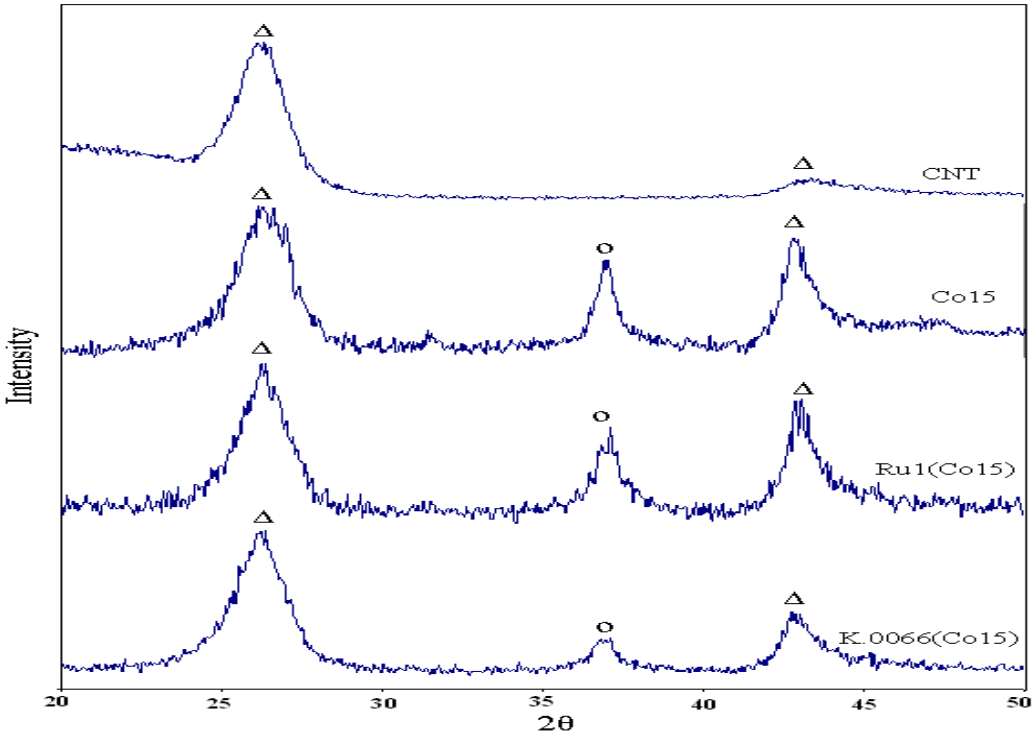

Figure 4. 5: XRD spectra for pure CNT and Co15, Ru1(Co15) and K_0066(Co15) catalysts O: Co_3O_4 (36.8^o), Δ : CNT.

In the XRD spectrum of the support CNT and all the catalysts, peaks at 25° and 43° correspond to carbon nanotubes, while the other peaks in the spectrum of the catalysts are related to different crystal planes of Co_3O_4 [Bezemer et al., 2004]. The peak at 36.8° is the most intense peak of Co_3O_4 in XRD spectrum of all the catalysts. Due to low amounts of Ru and K promoters in the XRD spectrum of promoted catalysts no peak was observed indicating diffraction lines of Ru oxide and K oxides (Figure 4.5). Table 4.2 shows the average Co_3O_4 particle size of the catalysts calculated from XRD spectrum and Scherer equation at 36.8° [Bechera et al., 2001]. As shown in Table 4.2, the average particle size of Co_3O_4 increases from 9.6 to 13 and 16 nm by increasing the cobalt loading from 15 to 22 and 30 wt.%, respectively which is also confirmed by TEM pictures of the unpromoted Co15, Co22 and Co30 catalysts (Figure 4.3). Agglomeration of cobalt particles is the main reason of increasing the average cobalt particle sizes. Table 4.2 also shows that by addition of Ru to the Co15 catalyst the average particle size slightly decreases while by addition of K to the Co15 catalyst, the average particle size remains unchanged.

Table 4. 2: XRD and TPD data

Catalysts	XRD (d_{Co3O4}) nm	1st TPR peak (°C)	2nd TPR peak (°C)	Reducibility ratio
Co15	9.6	330	500	1.00
Co22	13	313	490	1.30
Co30	16	310	485	1.70
Ru.25(Co15)	-	320	477	1.15
Ru.5(Co15)	-	315	452	1.35
Ru1(Co15)	9.4	290	450	1.36
K.0016(Co15)	-	330	505	0.98
K.0033(Co15)	-	335	510	0.97
K.0066(Co15)	9.6	335	512	0.94

The activation of the catalysts in hydrogen atmosphere was disclosed by temperature programmed reduction (TPR) experiments. The TPR spectra of the calcined Co15, Co22 and Co30 catalysts and CNTs support are shown in Figure 4.6.

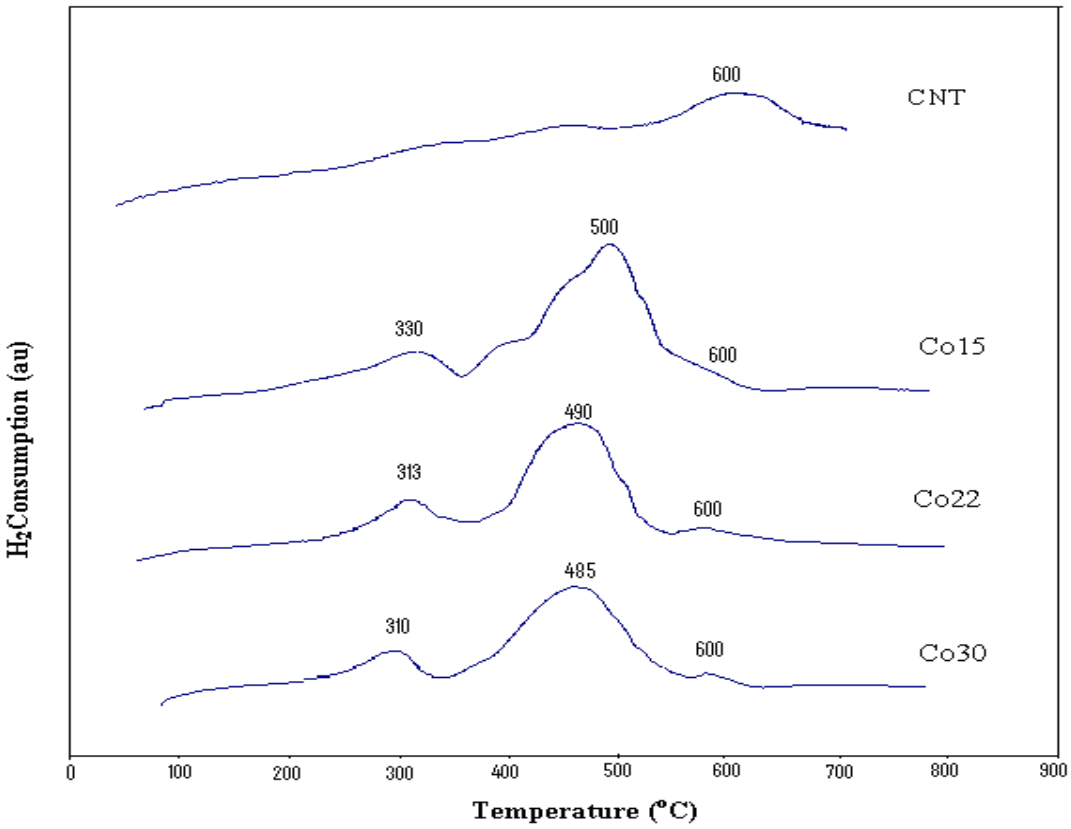

Figure 4. 6: TRP profiles of the calcined unpromoted catalysts (Co15, Co22 and Co30) and purified CNT.

In this figure, the TPR profile of Co15 catalyst shows the first peak at 330 ^{o}C which is typically assigned to the reduction of Co_3O_4 to CoO, although a fraction of the peak likely comprises the reduction of the larger, bulk-like CoO species to Co^{o} [Tavasoli et al., 2008a]. In the TPR profile of Co15 catalyst the second peak at 500 ^{o}C, is mainly assigned to the second step reduction, which is due to the reduction of CoO to Co^{o}. This peak also includes the reduction of cobalt species that interact with the support [Tavasoli et al., 2008a]. The small peak at about 600 ^{o}C in the TPR spectra of Co15 catalyst can be assigned to the gasification of support as indicated by TPR of pure CNT support at about 600 ^{o}C. As shown in Figure 4.6, increasing the cobalt loading significantly decreases the relative intensity of the second reduction peak shoulder and causes it's tailing to get

shorter, suggesting a higher degree of reduction. The relative contribution of the species reducing at high temperatures to the overall reduction pattern decreased and the maximum temperature for these species shifted to lower temperatures, indicating a lower strength of interaction, with increasing cobalt loading. Table 4.2 shows the peak temperatures obtained from TPR profiles for the catalysts under consideration shown in this table, increase in the cobalt loading shifts both TPR peaks to the lower temperatures, suggesting an easier reduction process. Increase in cobalt loading from 15 to 30 wt. % results in a decrease in the temperature of the first TPR peak from 330 to 310 ^{o}C and the temperature of the second TPR peak from 500 to 485 ^{o}C. This indicates that by increasing the cobalt loading, the amount of the species reduced at high temperature, decreases. These differences are attributed to the increasing in the average cluster size (Table 4.2 and Figure 4.3) and the resulting loss of interaction with the support. To have a better understanding, the TPR peaks for the Co15, Co22, and Co30 catalysts have been divided into two parts. The first part is defined from 25 to 500 ^{o}C and the second part is defined from 500 to 800 ^{o}C. The area under the TPR peaks for both parts have been calculated by integration. The areas of the peaks are proportional to the amount of H_2 consumption on each section. The results show that by increasing the cobalt loading from 15 to 22 and 30 wt.%, the ratio of H_2 consumption of part two (500–800 ^{o}C) to the H_2 consumption of part one (25–500 ^{o}C) decreased from 0.75 to 0.52 and 0.42, respectively. This can confirm that by increasing the cobalt loading, the amount of the species reduced at high temperatures, decreases suggesting an easier reduction for the higher loaded catalysts. Figure 4.7 shows the TPR profiles of the ruthenium promoted catalysts.

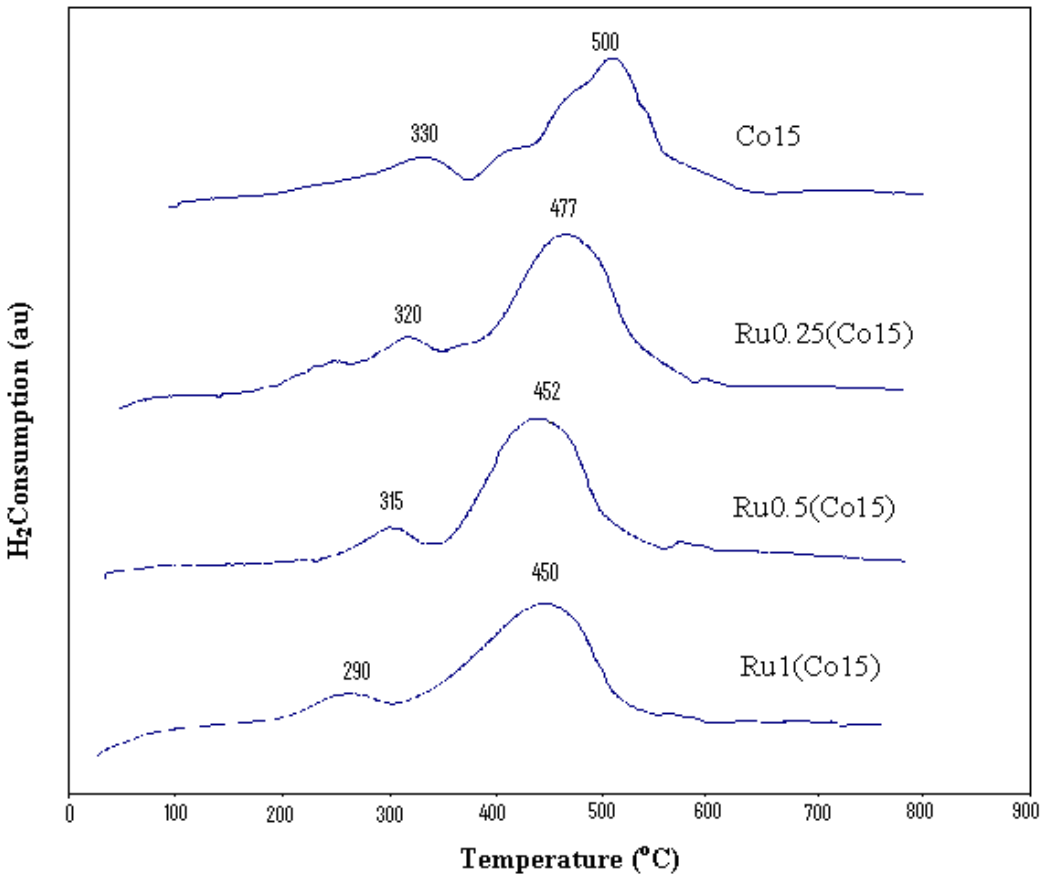

Figure 4. 7: TRP profiles of the calcined Co15 and Ru promoted catalysts: Ru.25(Co15), Ru.5(Co15) and Ru1(Co15).

This figure shows that the addition of small amounts of Ru to the cobalt catalyst shifts both TPR peaks significantly to the lower temperatures. Addition of 1 wt. %Ru to the Co15 catalyst results in a decrease in the temperature of the first TPR peak from 330 to 290 ^{o}C and that of the second TPR peak from 500 to 450 ^{o}C. Table 4.2 also shows the reducibility ratio for the whole TPR profile, defined by the ratio of the areas of the corresponding peaks to that for Co15 catalyst. This is proportional to the amount of hydrogen consumed. The addition of 0.25 and 0.5 wt. %Ru to the Co15 cobalt catalyst, results in a significant improvement in the reducibility of the catalyst (Table 4.2). Increasing the Ru loading to 1 wt. % only resulted in a marginal effect in the catalyst reducibility. The Ru enhances the reducibility of both Co_3O_4 and other Co oxide species, as indicated by the reducibility ratios (Table 4.2 and Figure 4.7). As shown in Figure 4.7 the reducibility of the first peak is enhanced more than the second one. Das et al. have

showed that the reduction of ruthenium oxide occurs at temperatures lower than that of the cobalt. They have concluded that reduced Ru enhances the reduction of cobalt oxides, by spillover of hydrogen from Ru to the cobalt oxide. Ruthenium may also enhance the reduction of smaller cobalt species that strongly interacts with the alumina support [Das et al., 2003].

Figure 4.8 shows the TPR profiles of potassium promoted catalysts.

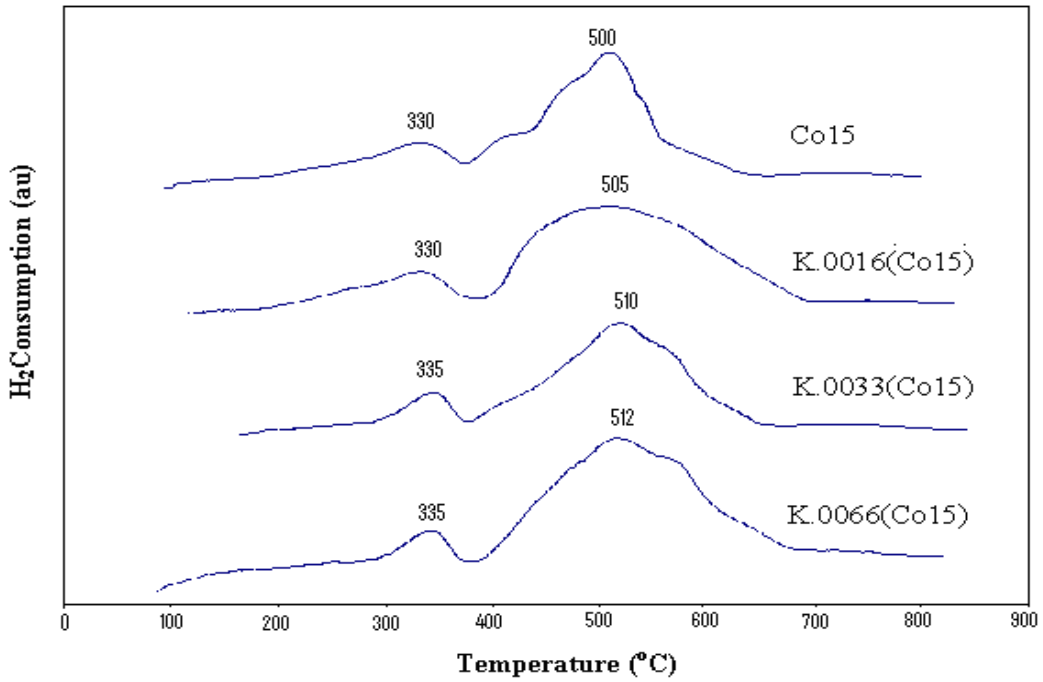

Figure 4. 8: TRP profiles of calcined Co15 and K promoted catalysts: K.0016(Co15), K.0033(Co15) and K.0066(Co15).

This figure shows that addition of potassium to the Co15 catalyst slightly increases the temperature of the first and the second TPR peaks. In addition, it indicates that by addition of potassium to the Co15 catalyst, the tailing of the second TPR peak becomes broader slightly, suggesting difficult reduction process for small cobalt species due to higher interaction with support. The peak indicating gasification of CNT is strongly overshadowed by broad tailing of the second TPR peak. Also the results of Table 4.2 show that the reducibility of the catalyst slightly decreases upon promotion of the catalyst with different amounts of potassium. Comparing the data in Figures 4.7 and

4.8 shows that ruthenium promoted cobalt catalysts are reduced more easily than those promoted with potassium.

The results of hydrogen temperature programmed desorption (TPD) of the Co and Co/Ru catalyst are given in Table 4.3.

Table 4. 3: H_2 Chemisorption results

Catalyst	H_2 uptake (μ mole H_2 desorbed /g cat.)	CO uptake (μ mole CO desorbed /g cat.)	%Dispersion	d_p (nm)
Co15	120.09	30.32	9.3	10.9
Co22	172.16	-	8.2	12.5
Co30	221.06	-	6.8	15.3
Ru.25(Co15)	155.50	-	12.1	8.5
Ru.5(Co15)	231.03	-	17.9	5.7
Ru1(Co15)	228.16	-	17.7	5.8
K.0016(Co15)	-	82.25	-	-
K.0033(Co15)	-	110.32	-	-
K.0066(Co15)	-	115.20	-	-

This table shows that in the case of Co15, Co22 and Co30 catalysts, the hydrogen uptake increases with increasing the amount of cobalt added up to 30 wt.%. Also the percentage dispersion of the cobalt crystallites calculated based on the total amount of cobalt decreases significantly. In addition, Table 4.3 shows that increasing the amount of cobalt causes a remarkable increase in cobalt particle size, which is due to the agglomeration of the cobalt crystallites with increasing the cobalt loading. Larger cobalt clusters have lower interaction with support and thus reduce more easily. Table 4.3 also shows the results of hydrogen temperature programmed desorption (TPD) for Ru

promoted catalysts. This table shows that by addition of ruthenium to the 15 wt. % Co/CNT catalyst, the hydrogen uptake increases with the amount of Ru added up to 0.5 wt. % then levels off. Also addition of 0.25, 0.5 and 1 wt. % Ru to the Co15 catalyst increased the percentage dispersion from 9.3 to 12.1, 17.9 and 17.7 %, respectively. However the Co particle sizes decreased by addition of Ru promoter to the catalyst. This may be due to the reduction of smaller cobalt crystallites when the catalysts are promoted by Ru. These crystallites have higher interaction with the support. Table 4.3 also shows the results of CO chemisorption on the Co15 and K promoted catalysts. As shown in this table CO uptake increases significantly by addition of alkali promoter to the Co15 catalyst. Addition of 0.0016 wt. % and 0.0033 wt. % of K increased the CO uptake by a factor of 2.72 and 3.36, respectively. Addition of 0.0066 wt. % of K resulted in a marginal increase in the CO uptake. This data show that addition of K to cobalt catalyst significantly increases the CO chemisorption rate on the catalyst surface.

4.4.2 Fischer-Trospch Synthesis

The catalytic activity and product selectivity data have been calculated after initial catalyst stability within first 24 h. Figure 4.9 presents the results of %CO conversion, FTS rate (g HC produced/g cat./min) and water gas shift reaction rate for Co15, Co22 and Co30 catalysts.

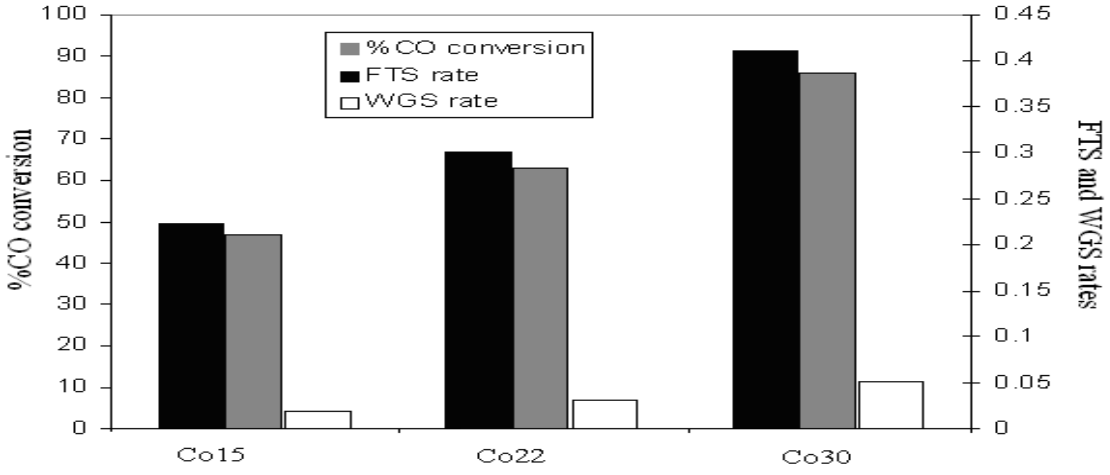

Figure 4. 9 : %CO conversion, FTS rate (g HC/g cat./h) and WGS rate (g CO2/g cat. h) for Co/CNT catalysts loading (Co15, Co22 and 30Co)

This figure reveals that with increasing the amount of cobalt loading FTS rate shows a remarkable increase. % CO conversion increased from 48 % in the case of Co15 catalyst to 63 % and 86 % for Co22 and Co30 catalysts, respectively. At the same time increasing the Co loading from 15 to 22 and 30 wt. % enhanced the FTS rates by 28 and 70 %, respectively. Comparing the results of Figure 4.9 and Table 4.3 reveals that the FTS rate increases, in accordance with the amount of hydrogen uptake, with increasing the cobalt loading up to 30 wt. %. However, the FTS rate keeps on increasing, in contrast to the percentage dispersion, with addition of cobalt loading up to 30 wt.%. Increasing the cobalt loading increases the number of surface active sites available for FTS and hence increases the % Co conversion and FTS rate. Therefore, the maximum concentration of surface Co^o sites and FTS activity are achieved for the 30 wt. % cobalt sample presenting a high dispersion and highest reducibility. However, this loading may not be the optimum loading and to determine the proper loading it is necessary to test the loadings above the 30 wt. %. Figure 4.9 also presents the effect of the cobalt loading on the water gas shift reaction. Water gas shift reaction rate is equal to the formation rate of carbon dioxide (R_{FCO2}) and can be defined by:

$$R_{WGS} = R_{FCO2} = g_{CO2} \text{ produced/g cat/min} \qquad (4.7)$$

This figure shows that, the water gas shift reaction rate increases by increasing the cobalt loading. This may be attributed to the tendency of larger cobalt particles for H_2O adsorption, which participate in the water-gas shift reaction, and leads to the production of CO_2 [Jacobs et al., 2004]. Also, the increase in the CO_2 formation rate can be attributed to the increase in water partial pressure, due to increase in FTS reaction rate [Tavasoli et al., 2005]. Figure 4.10 shows the variations of CO conversion rate, FTS rate and WGS rate with H_2 uptake determined by H_2 chemisorption tests for Co15, Co22 and Co30 catalysts.

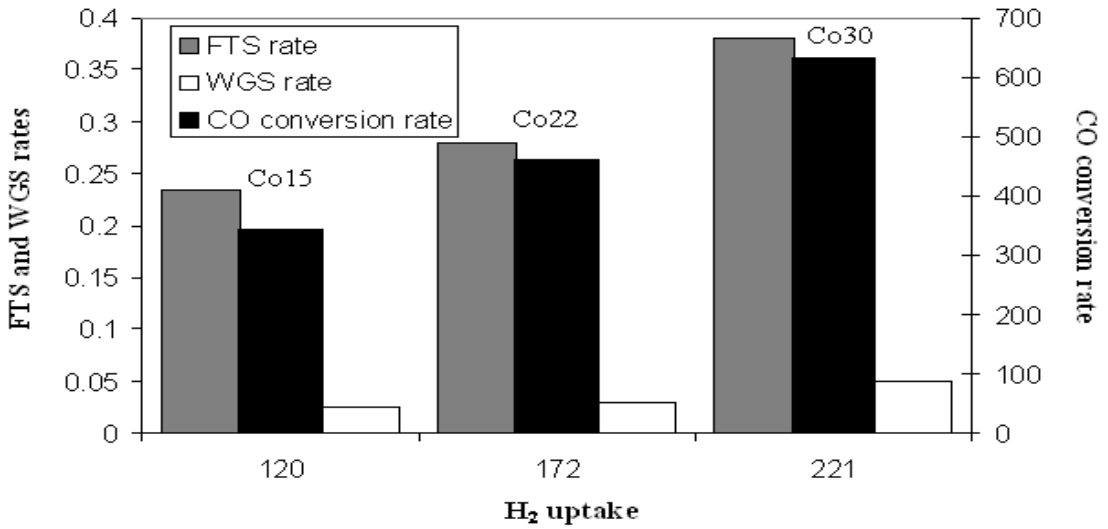

Figure 4. 10: Variation of CO conversion rate (µ mole CO/g cat.min), FTS rate (g HC/g cat./h) and WGS rate (g CO_2/g cat.h) with H_2 uptake (µ mole H_2 desorbed /g cat.) of Co15, Co22 and 30Co catalysts.

The CO conversion rate is defined as:

$R_{conv.CO}$ = [%CO conv. × CO flow (ml/min) × molar volume (1 atm, 25^{o}C) (µ mole/ ml)] / g cat.

(4.8)

This figure shows that the CO conversion rate, FTS rate and WGS rate increase with the amount of hydrogen uptake. Increasing H_2 uptake increases the reduced cobalt surface atoms which in turn lead to enhancement of the mentioned parameters. Table 4.4 shows the effect of cobalt loading on the selectivity of FTS to CH_4, C_2–C_4 light gases hydrocarbons and C_{5+} liquid products.

Table 4. 4: Products selectivity

Catalysts	CH_4%	(C_2-C_4) %	C_5+%	CO_2%	Olefin/Paraffin	α
Co15	23	5.0	70	2	0.73	0.767
Co22	18	3.9	75	3.1	0.78	0.789
Co30	16	3.0	77	4	0.82	0.810
Ru.25(Co15)	19	3.4	74.5	2.8	0.79	0.792
Ru.5(Co15)	17.4	3.3	76	3.3	0.83	0.807
Ru1(Co15)	17	3.1	77	3.3	0.84	0.815
K.0016(Co15)	10	4.2	80	5	2	0.821
K.0033(Co15)	7	4.3	81	7	3	0.830
K.0066(Co15)	4	4.5	87	4	3.5	0.836

It clearly shows that, the methane and C_2–C_4 light gaseous hydrocarbons selectivity are reduced and the selectivity of C_{5+} liquid hydrocarbons increased by increasing the cobalt loading. Moving upward from the 15 to 30 wt. % cobalt loaded catalyst (increasing the average cluster size from 8 to 16 nm), results in 10 % improvement in the C_{5+} selectivity of the catalysts. At the same time the 30 wt. % catalyst, showed 30% lower selectivity to methane. Figure 4.11 presents the C_{5+} product distributions for Co15, Co22 and Co30 catalysts.

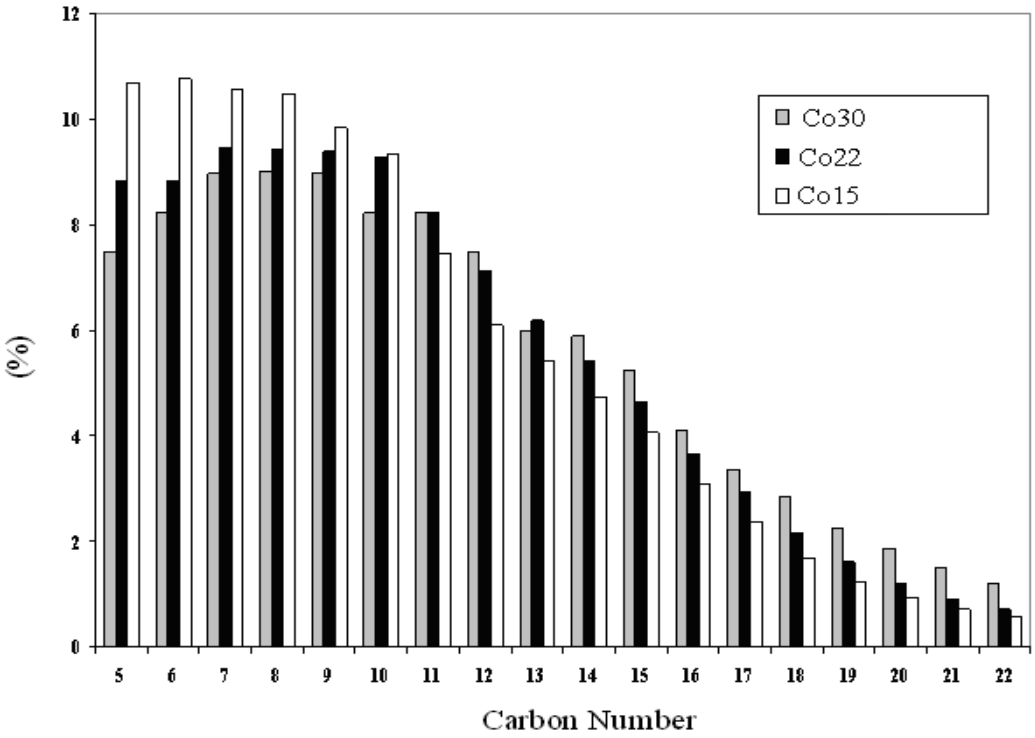

Figure 4. 11: C_{5+} liquid hydrocarbons products distribution of the catalysts with different cobalt loading on the CNT support.

As shown in this figure, product distribution shows a distinct shift to higher molecular weight hydrocarbons with increasing the cobalt loading of catalysts. The results presented in Table 4.4 and Figure 4.11 clearly demonstrate that the larger cobalt particles are more selective to higher molecular weight hydrocarbons and the smaller particles are selective for methane and light gases. It seems that the steric hindrance for dissociative adsorption of CO and $–CH_2–$ monomer and addition of this monomer to the growing chain is less in the larger cobalt clusters. In the other hand, chain propagation and growth probability of the larger clusters is more than the smaller ones. The Anderson–Schultz–Florey (ASF) model is a common model used to describe the chain growth mechanism in FTS. According to this model, the polymerization process in FTS is assumed to initiate on the surface of the catalyst by a monomer that contains one carbon atom, while chain growth takes place by the addition for one monomer at time [Elbashir and Roberts, 2005]. The chain growth probability (α) of FTS products for the catalysts is presented in Table 4.4. The shift to higher molecular weight hydrocarbons is clear from ascending trend in chain growth probability, α, with increasing the cobalt loading of catalysts. Figure 4.12

represents the results of % CO conversion, FTS and WGS reaction rates for Co15 catalyst promoted with different amounts of Ru.

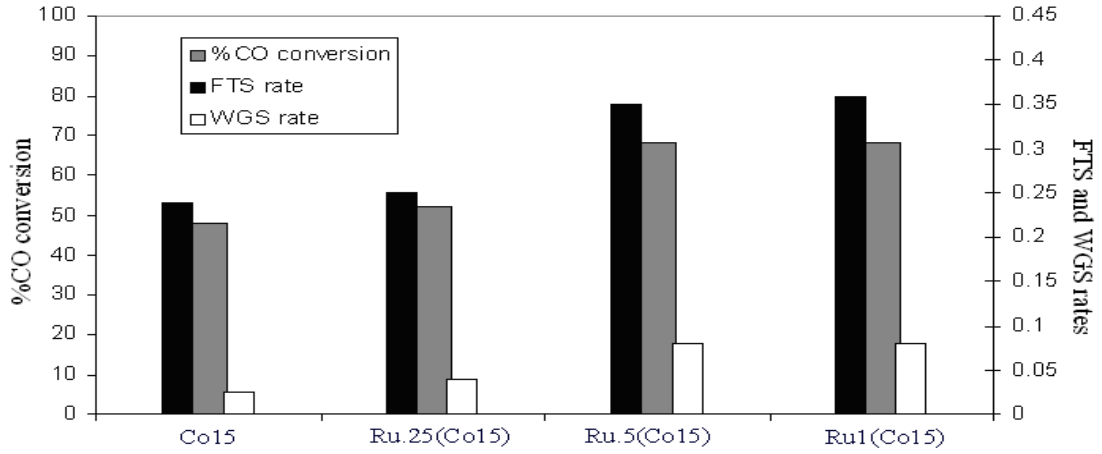

Figure 4. 12 : % CO conversion, FTS rate (g HC/g cat./h) and WGS (g CO_2/g cat.h) for Co15, Ru0.25(Co15), Ru.5(Co15) and Ru1(Co15) catalysts.

This figure reveals that the % CO conversion and FTS rate of the catalyst significantly increases with addition of Ru up to 0.5 % and then levels off. Comparing the data of Figure 4.12 and H_2 chemisorption data in Table 4.3, show that the trend for the % CO conversion and FTS rate are similar to that for the hydrogen uptake. Figure 4.13 shows the variations of CO conversion rate, FTS rate and WGS rate with H_2 uptake determined by H_2 chemisorption tests for Co15, Ru.25(Co15), Ru.5(Co15) and Ru1(Co15) catalysts.

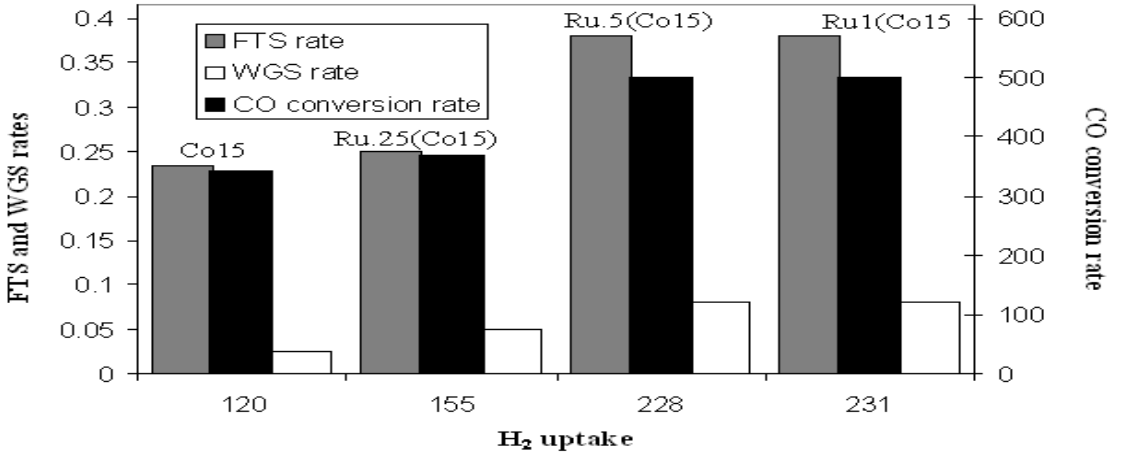

Figure 4. 13 : Variation of CO conversion rate (µ mole CO/g cat.min), FTS rate (g HC/g cat./h) and WGS (g CO_2/g cat.h) with H_2 Uptake (µ mole H_2 desorbed /g cat.) of Co15, Ru0.25(Co15), Ru.5(Co15) and Ru1(Co15) catalysts.

Similar to the results presented in Figure 4.10, this figure shows that the CO conversion rate, FTS rate and WGS rate increase with the amount of hydrogen uptake. Addition of Ru to the cobalt catalyst enhanced % reduction as well as H_2 uptake which increased the reduced cobalt surface atoms and the active site available for FTS and WGS reactions. These results reveal that FT activity of the catalysts is strongly dependent to the surface reduced cobalt sites (Figures 4.7, 4.12 and 4.13). As discussed in the last section of the paper, the reduction of ruthenium oxide occurs at temperatures lower than that of the cobalt. Reduced Ru enhances the reduction of cobalt oxides, by spillover of hydrogen from Ru to the cobalt oxide. Also, ruthenium can enhance the reduction of smaller cobalt species that may not reduce in case of the unpromoted catalyst. Thus Ru increases the number of active surface Co^o sites available for FT reaction in Ru promoted catalysts and hence enhances the % CO conversion, and FTS reaction rate. It is believed that addition of Ru promoter to the cobalt catalysts changes the catalyst morphology. It has been reported that Ru mostly is enriched on the surface of cobalt [Bertole et al., 2002]. Considering the higher FTS activity of Ru with respect to cobalt and its enrichment on cobalt surface may be another cause for the activity improvement in Ru promoted catalysts. However, the benefits due to addition of Ru are not restricted only to the improvements in reducibility and activity of the CNT supported cobalt catalyst. It is to note that the effect of Ru on the activity of cobalt catalysts supported on oxide supports is studied by many researchers [Li et al., 2002; Jacobs et al., 2002; Iglesia et al., 1993]. It has been shown that by addition of 0.5 wt. % of Ru to the 15 wt. % Co/Al_2O_3 catalyst, the % CO conversion is almost doubled [Tavasoli et al., 2005]. Thus our results show that by addition of 0.5 wt. % of Ru to the Co15 catalyst the % CO conversion is increased by only 39 %. This variation of % CO conversion enhancement obtained with CNT support can be attributed to the improvements of the percentage of cobalt reduced due to promotion of the catalyst by Ru. Reduction of cobalt species on the CNT supported catalysts is easier than the reduction of cobalt particles supported on oxide supports. Figure 4.12 also shows that the WGS reaction rate increases with addition of Ru to Co15 catalyst. Increasing of the WGS reaction rate can be attributed to the increase in water partial pressure, due to increase of FTS reaction rate. Table 4.4 shows the effects of Ru promoter on the selectivity of FTS to CH_4, C_2–C_4 and C_{5+} products. It clearly shows that,

in addition to the significant enhancement of the CO conversion (Figure 4.12 and Table 4.4), methane and C_2–C_4 light gaseous products selectivities are reduced and the selectivity of C_{5+} liquid hydrocarbons increases by promoting the cobalt catalyst with of 0.25 wt. % Ru. Ru increases the C_{5+} selectivity by 4.8 %. At the same time the 0.25 wt. % Ru promoted catalyst shows 4 % lower selectivity to methane. Increasing the amount of Ru from 0.25 to 1 wt. % monotonically increases the selectivity to higher molecular weight hydrocarbons. The chain growth probability (α) of FTS products for the unpromoted and promoted catalysts is presented in Table 4.4. The shift to higher molecular weight hydrocarbons is clear from ascending trend in chain growth probability, α, by increasing the amount of Ru promoter. Ru is more selective towards higher molecular weight hydrocarbons than cobalt. Therefore, the improvement in C_{5+} selectivity observed for Ru promoted catalysts as compared to unpromoted catalyst may be due to the Ru enrichment on the cobalt crystallite surface. Figure 4.14 represents the results of % CO conversion, FTS and WGS reaction rates for Co15 promoted with different amounts of K.

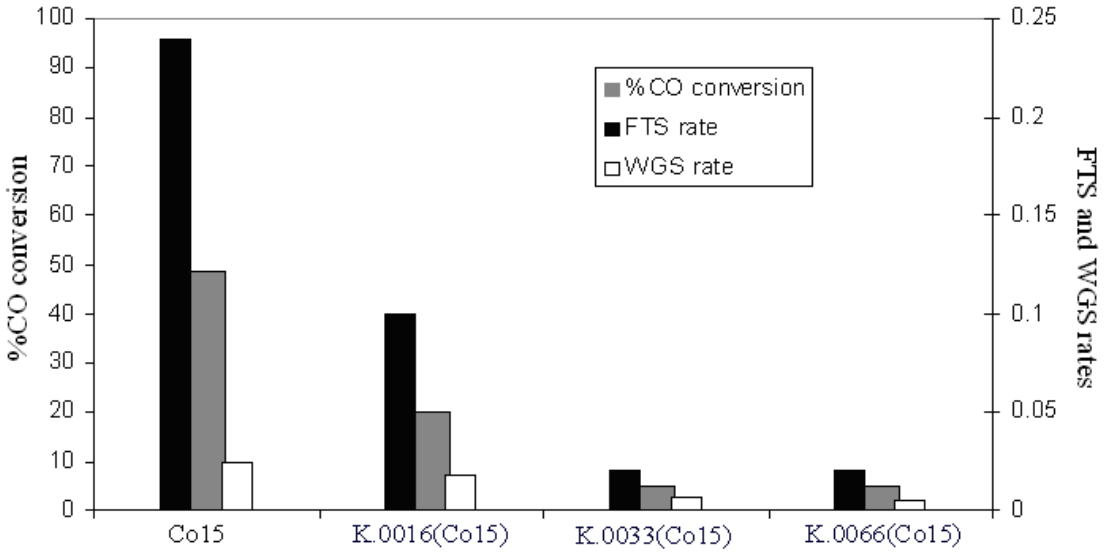

Figure 4. 14 : : % CO conversion, FTS rate (g HC/g cat./h) and WGS rate (g CO_2/g cat.h) for Co15 , K.0016(Co15), K.0033(Co15) and K.0066(Co15) catalysts.

It reveals that the % CO conversion and FTS rate of the Co15 catalyst decreases significantly with addition of small amounts of K. As example, addition of 0.0016, 0.0033 and 0.0066 wt. % of K to the cobalt catalyst decreased the % CO conversion from

48 to 20, 8 and 5 %, respectively (Figure 4.14). Also the FTS rate was decreased with addition of potassium to the cobalt catalyst. However the effects on the WGS rate are less pronounced. It has been shown that the reaction orders and activation energies were not significantly influenced by addition of alkali promoters on the catalysts [Campbell et al., 1982]. The results of CO chemisorption measurements (Table 4.3) on unpromoted and alkali promoted catalysts indicated that CO chemisorption rates increases significantly by addition of K to the catalysts. So it seems that the mobility of hydrogen is significantly restricted upon alkali promotion by blocking the low-coordination edge and corner sites for dissociative adsorption of hydrogen [Uner et al., 1994]. The reduced hydrogen mobilities as well as reduced hydrogen adsorption rates could qualitatively explain the decrease in the %CO conversion and FTS reaction rates. Figure 4.15 shows the variations of CO conversion rate, FTS rate and WGS rate with CO uptake determined by CO chemisorption tests for Co15, K.0016(Co15), K.0033(Co15) and K.0066(Co15) catalysts.

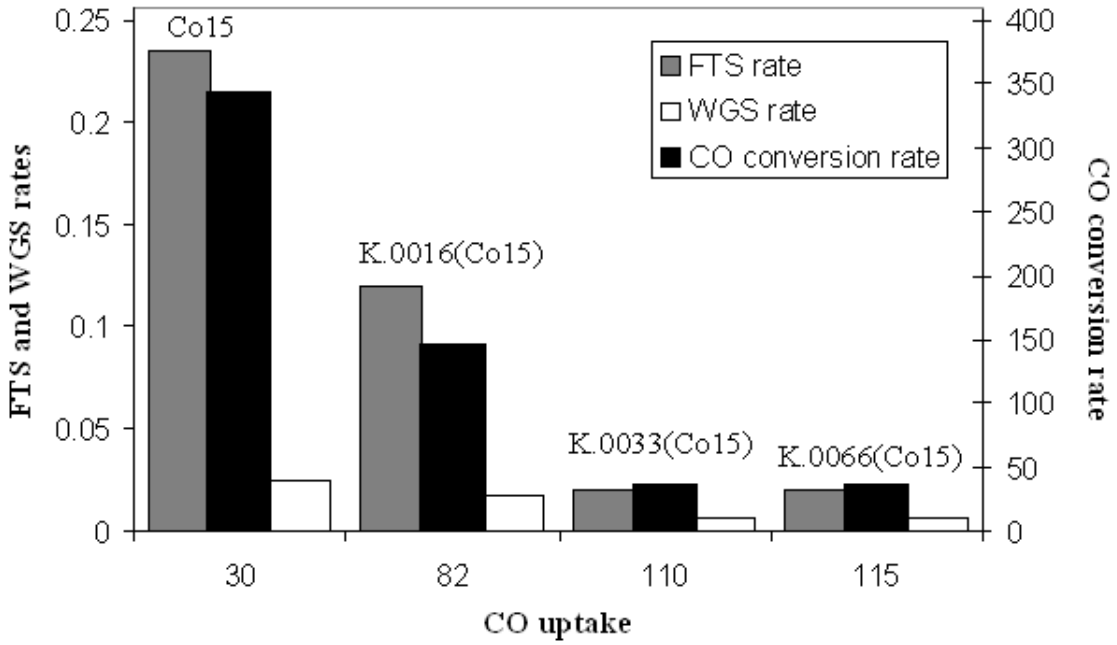

Figure 4. 15: Variation of CO conversion rate (µ mole CO/g cat.min), FTS rate (g HC/g cat./h) and WGS rate (g CO_2/g cat.h) with CO Uptake (µ mole CO desorbed /g cat.) of Co15, K.0016(Co15), K.0033(Co15) and K.0066(Co15) catalysts.

This figure shows that the CO conversion rate, FTS rate and WGS rate decrease with increasing the amount of CO uptake. As discussed, increasing CO uptake decreases the mobility of H_2 in the catalyst surface which in turn leads to lower CO conversion, FTS

and WGS rates [Huffaman et al., 1994]. Table 4.4 shows the effects of K promoter on the selectivity of FTS to CH_4, C_2–C_4 and C_{5+} products. Also the effects of alkali on α-olefin/ n-paraffin ratios are shown in this table. It should be mentioned that the measurements for α-olefin/n-paraffin ratios were taken for C_2–C_8 hydrocarbons. This table demonstrates that the alkali-promoted cobalt catalyst increased a-olefin selectivity considerably. 1-Alkenes are regarded as primary products of the FTS and may be hydrogenated to alkanes or isomerized to 2-alkenes in the course of the reaction. It seems that alkali promoter gives rise to a drastic reduction of these subsequent reactions. CO chemisorption studies on alkali promoted catalysts (Table 4.3) indicated that the mobility of hydrogen was significantly restricted upon alkali promotion by blocking the low-coordination edge and corner sites for dissociative adsorption of hydrogen. The increased CO adsorption rates as well as reduced hydrogen adsorption rates could qualitatively explain the decrease in hydrogenation of 1-alkenes to alkanes and as a result the increased α-olefin/n-paraffin ratios. The results in Table 4.4 also indicate that the alkali-promoted catalysts give rise to lower methane selectivity while improving selectivity towards higher molecular weight hydrocarbons. As may be seen the CH_4 selectivity obtained over K.0033(Co15) catalyst is about 40% lower than that over Co15 catalyst. Also C_{5+} selectivity shows a significant improvement for K.0033(Co15) catalyst as compared to Co15 catalyst. High chain growth was obtained because of the alkalization of the cobalt catalyst; i.e. the alpha of K.0033(Co15) catalyst was about 10 % higher than the alpha parameter for Co15. The decrease in the selectivity of methane can be explained on the basis of partial pressure of hydrogen atoms (Table 4.3) on alkalized catalyst surface which in turn leads to a decrease in the rate of chain termination step to paraffins (i.e. methane) in the course of FT reaction. Increase in the selectivity of higher molecular weight hydrocarbons of cobalt catalyst upon alkali promotion, can be explained by the increased concentration of α-olefins and readsorption and chain initiation of these primary products on catalyst surface which lead to the ultimate desorption of these α-olefins as larger products [Madon et al., 1993]. In a similar work but with a different active metal (i.e. Fe/K/CNT), Bahome et al., have shown that the addition of K to Fe/CNT catalyst, increased the olefinity of the C_2 hydrocarbon from 0.1 to 0.72 %. Also they showed that by addition of K to the Fe/CNT catalyst the alpha value

increased significantly and CH_4 content of the FTS products decreased [Bahome et al., 2005]. Figures 4.16 and 4.17 present the C_{5+} product distributions for Co15, Ru.5(Co15) and K.0016(Co15) catalysts.

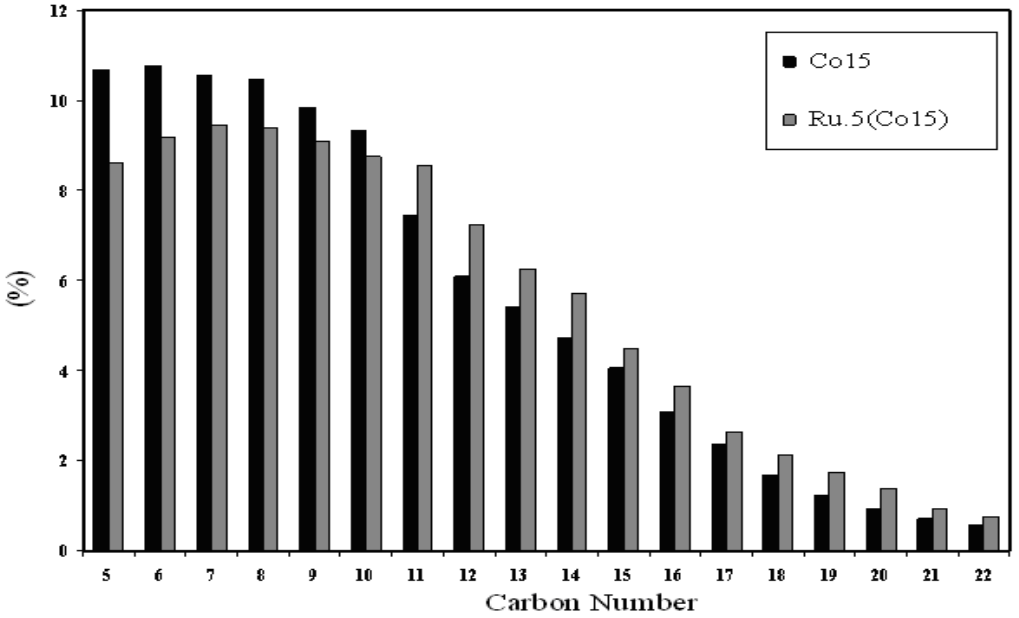

Figure 4. 16 : C_{5+} liquid hydrocarbons products distribution for the Co15 and Ru.5(Co15) catalysts.

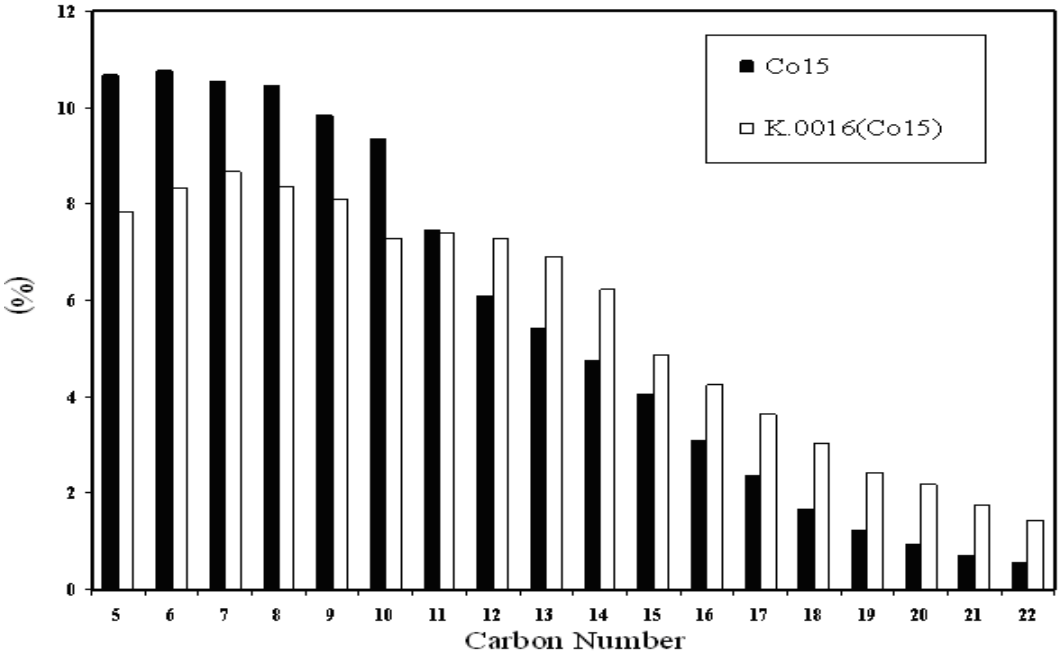

Figure 4. 17 : C_{5+} liquid hydrocarbons products distribution for the Co15 and K.0016(Co15) catalysts

As shown in these figures product distribution shows a distinct shift to higher molecular weight hydrocarbons with addition of Ru and K promoters to the Co15 catalysts.

4.5 Conclusions

Fischer–Tropsch synthesis (FTS) on carbon nanotubes (CNTs) supported cobalt catalysts with different loadings of cobalt, ruthenium and potassium was studied. For the Co15 catalyst, most of the metal particles were homogeneously distributed inside the tubes and the rest on the outer surface of the CNTs. TEM results showed that increas in the Co loading from 15 to 30 wt. % increases the amount of Co on the outer surface of the CNTs and increases the cobalt cluster sizes from 8 to 16 nm. Also, increases the amount of Co decreases the reduction temperature from 500 to 485 ^{o}C and decreases dispersion. Increasing the Co loading from 15 to 30 wt. % increases the CO conversion from 48 to 86 % and the C_{5+} selectivity from 70 to 77 %. Ru promoter enhances the reducibility, increases the dispersion and decreases the average cobalt cluster sizes. Potassium shifts the reduction temperatures to higher temperatures. Ru.5(Co15) increases the FTS rate of Co15 catalyst by a factor of 1.4 while addition of 0.0066 wt.% K decreases the FTS rate by a factor of 7.5. Both promoters enhanced the selectivity of FTS towards the higher molecular weight hydrocarbons. However; the effect of ruthenium is less pronounced. Potassium increased the olefin to paraffin ratio from 0.73 to 3.5 and the C_{5+} selectivity from 70 to 87 %.

Additional Information Not in the Manuscript

This chapter describes Co/CNT catalysts loaded with different amount of Ru or K but do not show any results of mixed promoted catalysts with Ru and K. Additional studies, also described in Chapter 7, show that the optimized catalyst in terms of FTS activity and selectivity is the Ru.5K0.0016 (Co15)/CNT. Table 4.5 shows the complete products selectivity results of this study.

Table 4. 5: Additional products selectivity

Catalysts	CH_4 %	(C_2-C_4) %	C_5+%	CO_2%	Olefin/Paraffin	α
Co15	23	5.0	70	2	0.73	0.767
Co22	18	3.9	75	3.1	0.78	0.789
Co30	16	3.0	77	4	0.82	0.810
Ru.25(Co15)	19	3.4	74.5	2.8	0.79	0.792
Ru.5(Co15)	17.4	3.3	76	3.3	0.83	0.807
Ru1(Co15)	17	3.1	77	3.3	0.84	0.815
K.0016(Co15)	10	4.2	80	5	2	0.821
K.0033(Co15)	7	4.3	81	7	3	0.830
K.0066(Co15)	4	4.5	87	4	3.5	0.836
Ru.5K.0016(Co15)	13.2	3.7	78.5	5.5	0.91	0.90

Mixing of 0.5 wt. % of Ru and 0.0016 wt. % of K as promoter for Co15 catalyst decreases the methane and C_2-C_4 selectivity and increases the C_{5+} selectivity and the chain growth probability. Moreover, the Ru.5K.0016(Co15) shows 70 % CO conversion, which is the higher % CO conversion recorded in this study compare to Co15/CNT catalyst.

4.6 References

Bahome, M.C., L.L. Jewell, D. Hildebrant, D.Glasser and N.J.Coville, "Fischer–Tropsch synthesis over iron catalysts supported on carbon nanotubes," Applied Catalysis A: General **287**, 60-67 (2005).

Bahome M.C, L.L Jewell, D. Hildebrant, D. Glasser, A.K. Datye, N.J. Coville, "Fe Ru small particle bimetallic catalysts supported on carbon nanotubes for use in Fischer–Tröpsch synthesis," Applied Catalysis A: General **328**, 243-251 (2007).

Bechara, R., D.Balloy and D.Vanhove, "Catalytic properties of Co/Al_2O_3 system for hydrocarbon synthesis," Applied Catalysis A: General **207**, 343-353 (2001).

Bertole, C.J, C.A. Mims, G.Kiss, "The Effect of Water on the Cobalt-Catalyzed Fischer–Tropsch Synthesis," Journal of Catalysis **210**, 84-96 (2002).

Campbell, C.T., D.W. Goodman, "A surface science investigation of the role of potassium promoters in nickel catalysts for CO hydrogenation," Surface Science **123**, 413-422 (1982).

Chen, W., Z. Fan, X. Pan, X. Bao, "Effect of Confinement in Carbon Nanotubes on the Activity of Fischer-Tropsch Iron Catalyst," Journal of American Chemical Society **130**, 9414-9419 (2008).

Clayes, M., E. van Steen, "On the effect of water during Fischer-Tropsch synthesis with ruthenium catalyst," Catalysis Today **71**, 419-427 (2002).

Das, T. K., G.Jacobs, P.M. Patterson, W.A. Conner, J.Li, B.H. Davis, "Fischer-tropsch synthesis characterization and catalytic properties of rhenium promoted cobalt alumina catalysts," Fuel **82**, 805-815 (2003).

Dry, M.E., "High quality diesel via the Fisher-Tropsch process: A review," Journal of chemical technology and biotechnology **77**, 43-50 (2001).

Elbashir, N.O. and C.B. Roberts, "Enhanced Incorporation of α-Olefins in the Fischer−Tropsch Synthesis Chain-Growth Process over an Alumina-Supported

Cobalt Catalyst in Near-Critical and Supercritical Hexane Media," Industrial and Engineering Chemistry Research **44**, 505-521 (2005).

Huffaman, G.P N., Shah, J.Zhao, F.E.Huggins, T.E.Hoost, S.Halvorsen and J.G.Goudwin, "In-situ XAFS investigation of K-promoted Co catalysts," Journal of Catalysis **151**, 17-25 (1994).

Iglesia, E., S.L.Soled, R.A. Fiatto, A. Grayson, "Bimetallic Synergy in Cobalt Ruthenium Fischer-Tropsch Synthesis Catalysts," Journal of Catalysis **143**, 345-368 (1993).

Iglesia, E., S.L. Soled, R.A. Fatio, U.S Patent 4794099 (1988)

Jacobs,G., T.K Das, Y. Zhang, J. Li, G. Racoillet and B.H. Davis, "Fischer–Tropsch synthesis: support, loading, and promoter effects on the reducibility of cobalt catalysts," Applied Catalysis A:General **233**, 263-281 (2002).

Jacobs, G., P.M. Patterson, T. Das, M. Luo, B. Davis, "Fischer- Tropsch synthesis: Effect of water on Co/Al2O3 catalysts and XAFS characterization of reoxidation phenomena," Applied Catalysis A: General **270**, 65–76 (2004).

Li, J., G.Jacobs, T.Das, B.H.Davis, "Fischer-Tropsch synthesis: effect of water on the catalytic properties of the ruthenium promoted Co/TiO2 catalyst," Applied Catalysis A: General **233**, 255-262 (2002).

Madon, R.J., E.Iglesia, "The Importance of Olefin Readsorption and H_2/CO Reactant Ratio for Hydrocarbon Chain Growth on Ruthenium Catalysts," Journal of Catalysis **139**, 576-590 (1993).

Rohr, F., O.A. Lindvag, A. Holmen, E.A. Blekkan, "Fischer-Tropsch synthesis over cobalt catalysts supported on zirconia-modified alumina," Catalysis Today **58**, 247-254 (2000).

Tavasoli, A., Y. Mortazavi, A. Khodadadi and K. Sadagiani, "Effects of different loadings of Ru and Re on physico-chemical properties and performance of 15% Co/Al_2O_3 FTS catalysts," Iranian Journal of Chemistry and Chemical Engineering **35**, 9-15 (2005).

Tavasoli, A., K. Sadaghiani, A. Nakhaeipour and M. G Ahangari, "Raising distillate selectivity and catalyst lifetime in Fischer-Tropsch synthesis by using a novel dual-bed reactor," Iranian Journal of Chemistry and Chemical Engineering **26**, 1-9 (2007).

Tavasoli, A., R.M. Abbaslou, M. Trépanier and A.K.Dalai, "Fischer-Tropsch synthesis over cobalt supported on carbon nanotubes in a slurry reactor," Applied Catalysis A: Genreal **345**, 134-142 (2008 a)

Tavasoli, A., K.Sadaghiani and K. Khorashe, A.A. Seifkordi, A.A. Rohani and A. Nakhaeipour, "Cobalt supported on carbon nanotubes: a promising novel Fischer-Tropsch synthesis catalyst," Fuel Processing Technology **89**, 491-498 (2008 b).

Tavasoli, A., R.M.M. Abbaslou, M.Trépanier and A.K. Dalai, "Morphology and deactivation behavior of $Co\text{-}Ru/Al_2O_3$ Fischer-Tropsch synthesis," The Canadian Journal of Chemical Engineering **86**, 1070-1080 (2008 c).

Uner, D.O., M. Pruski, B.C. Gerstein, T.S. King, "Hydrogen Chemisorption on Potassium Promoted Supported Ruthenium Catalysts," Journal of Catalysis **146**, 530-536 (1994).

Chapter 5: Fischer-Tropsch synthesis on mono-and bimetallic Co and Fe catalysts supported on carbon nanotubes

A similar version of this chapter has been published in Fuel Processing Technology:

Tavasoli, A., M. **Trépanier**, R. M.M. Abbaslou, A.K. Dalai. and N. Abatzoglou, Fischer-Tropsch synthesis on mono-and bimetallic Co and Fe catalysts supported on carbon nanotubes. Fuel Processing Technology 90 (2009) 1486-1494.

The work discussed in this chapter was also included in paper presentations at the following conference:

Trépanier, M., A.Tavasoli, A.K. Dalai and N. Abatzoglou, (October 2008), Fischer-Tropsch synthesis on mono- and bimetallic Co and Fe catalysts supported on Carbon nanotubes, 58th CSChe Conference, Ottawa, Canada.

Contribution of Ph. D Candidate

The laboratory experiments, data analysis and results interpretation for the mono- and bimetallic catalysts study were performed by Mariane Trépanier. Dr. Tavasoli provided guidance in the results and discussion while writing the submitted manuscript. The Ph. D student Reza M.M Abbaslou provided the Fe/CNT mono catalyst results as a reference. Drs.Dalai and Abatzoglou provided editorial input, the main idea of the research project and financial support. The submitted manuscript was written by Mariane Trépanier and Dr.A.Tavasoli.

Contribution of this manuscript to Overall Study

The secondary objective of the Ph.D thesis is to optimize the composition of Co/CNT novel catalyst with addition of promoters. It is also important to consider the

bimetallic catalysts. Iron has also been extensively used as FTS catalyst metal. Thus, it can also act as a promoter for Co/CNT catalyst and improve the catalyst performance. This study reveals the influence of iron addition on Co/CNT catalyst on the FTS activity and selectivity. It also reveals that Co/Fe bimetallic catalyst supported on CNT enhances the alcohol selectivity towards FTS products.

5.1 Abstract

An extensive study of Fischer–Tropsch synthesis (FTS) on carbon nanotubes (CNTs)-supported bimetallic cobalt/iron catalysts is reported. Up to 4 wt. % of iron is added to the 10 wt. % Co/CNT catalyst by co-impregnation. The physico-chemical properties, FTS activity and selectivity of the bimetallic catalysts were analyzed and compared with those of 10 wt.% monometallic cobalt and iron catalysts at similar operating conditions (H_2/CO=2:1 molar ratio, P=2 MPa and T=220 °C). The metal particles were distributed inside the tubes and the rest on the outer surface of the CNTs. For iron loadings higher than 2wt. %, Co–Fe alloy was revealed by X-ray diffraction (XRD) techniques. 0.5 wt. % of Fe enhanced the reducibility and dispersion of the cobalt catalyst by 19 and 32.8 %, respectively. Among the catalysts studied, cobalt catalyst with 0.5 % Fe showed the highest FTS reaction rate and percentage CO conversion. The monometallic iron catalyst showed the minimum FTS and maximum water–gas shift (WGS) rates. The monometallic cobalt catalyst exhibited high selectivity (85.1 %) toward C_{5+} liquid hydrocarbons, while addition of small amounts of iron did not significantly change the product selectivity. Monometallic iron catalyst showed the lowest selectivity for 46.7 % to C_{5+} hydrocarbons. The olefin to paraffin ratio in the FTS products increased with the addition of iron, and monometallic iron catalyst exhibited maximum olefin to paraffin ratio of 1.95. The bimetallic Co–Fe/CNT catalysts proved to be attractive in terms of alcohol formation. The introduction of 4 wt. % iron in the cobalt catalyst increased the alcohol selectivity from 2.3 to 26.3 %. The Co–Fe alloys appear to be responsible for the high selectivity toward alcohol formation.

5.2 Introduction

The conversion of natural gas to liquids (GTL) via Fischer–Tropsch (FT) technology is currently of increasing interest. The catalytic synthesis of hydrocarbons

from CO and H_2 mixtures leads to a large variety of products such as paraffins, olefins, alcohols and aldehydes. The most desired products are those with low methane, low oxygenate, high alkene/alkane ratio, and high C_{5+} content. This control is typically achieved by modification of the catalyst, the reactor and/or the reaction conditions [Dry, 1981; Iglesia, 1997].

Since the discovery of the FT reaction in the 1920s, the industrial catalysts of choice have proven to be cobalt and iron. Both Co and Fe are typically used in combination with a range of supports and promoters that permit further control over the products selectivity. A viable methodology that has been developed for controlling the property of a metal is alloying. In particular it has been reported that a mixture of the two most active catalysts, Fe and Co, have generated product streams in the FT reaction richer in olefins and alcohols than expected from either Fe or Co catalysts [Duvenhage and Coville, 1997; Duvenhage and Coville, 2005a; Duvenhage and Coville, 2005b; Pena O'Shea et al., 2003; Pena O'Shea et al., 2007].

In many heterogeneous reactions, the active phase is spread on a support. A catalyst support is not merely a carrier but also a contributor to the activity of the catalyst. The acid-base and textural properties of supported catalysts play an important role in FT synthesis. In addition the use of an inert support enhances C–C chain growth probability, and hydrocarbon formation is favored by the presence of micro-pores since mass-transfer resistance is low and residence time is improved. Earlier studies [Bezemer et al., 2004; Reuel and Bartholomew, 1984; Serp et al., 2003] have indicated that using carbon as a support to provide an inert, poorly interacting surface could moderate the catalytic behavior of metals such as iron and cobalt. In particular, it has been noted that carbon nanotubes (CNTs) provide a relatively inert support which shows low metal–support interactions, suggesting that this is a unique system for the study of the catalytic behavior of metals [Abbaslou et al., 2009; Trépanier et al., 2009]. Also, carbon nanotubes possess a uniform pore-size distribution compared to conventional supports such as activated carbon or alumina. Their special and steady structural characteristics and morphology are quite suitable for use as catalytic support materials [Tavasoli et al., 2007; Tavasoli et al., 2008b].

The present work was undertaken with the aim of studying the performance of Fe/Co bimetallic catalysts supported on CNTs for FTS. In particular, the emphasis is placed on the determination of the best ratio of Fe to Co to maximize the benefits of the bimetallic Fe–Co/CNT catalysts.

5.3 Experimental

5.3.1 Catalyst preparation

Commercial multi-wall carbon nanotubes (MWCNT) (with carbon content over 95wt. % and BET surface area of 170 m^2/g) were used as support materials for the preparation of Fischer–Tropsch synthesis (FTS) catalysts. Prior to impregnation, to increase the purity of the CNTs, the support was treated with 30 wt. % HNO_3 at 100 °C over night, washed with distilled water, and dried at 120 °C for 6 h. CNTs supported cobalt and iron catalysts were prepared by the incipient wetness impregnation method with cobalt nitrate ($Co(NO_3)_2 \cdot 6H_2O$) and iron nitrate ($Fe(NO_3)_3 \cdot 9H_2O$) aqueous solutions. Four bimetallic Co–Fe catalysts, containing a fixed amount of cobalt (10 wt. %) and different amounts of iron (0.5, 1, 2 and 4 wt. %), were prepared and denoted as 10Co0.5Fe/CNT, 10Co1Fe/CNT, 10Co2Fe/CNT, and 10Co4Fe/CNT, respectively. For comparison, a reference catalyst containing 10 wt. % Co and a reference catalyst containing 10 wt. % Fe were also prepared. All impregnates were dried at 120 °C for 6 h and calcined at 350 °C under flowing argon for 3 h with a heating rate of 1 °C/min [Bezemer et al., 2004; Reuel and Bartholomew, 1984]. The loadings were verified by an inductively coupled plasma (ICP) AES system. In order to characterize the catalysts and study alloy formation and compositions, all catalysts were reduced under hydrogen flow at 400 °C for 20 h and then cooled to 50 °C under hydrogen flow. The passivation was made with small pulsation of air inside the furnace at 50 °C to oxidize a thin layer of the catalyst surface.

5.3.2 Catalyst characterization

The CNTs and catalysts were characterized by Transmission Electron Microscopy (TEM). Sample specimens for TEM studies were prepared by ultrasonic dispersion of the

CNTs and catalysts in ethanol. The suspensions were dropped onto a carbon-coated copper grid. TEM investigations were carried out using a Hitachi H-7500 (120 kV).

The samples were characterized by scanning electron microscopy (SEM). SEM analysis was carried out using a Hitachi S-4700 at 3 kV. Sample specimens for SEM were prepared by ultrasonic dispersion of samples in methanol. The suspensions were dropped onto a silica support.

The reduced passivated 10Co4Fe/CNT sample was characterized with the energy-dispersive X-ray (EDX) spectrometer of a scanning electron microscope (SEM/EDX). This analysis was carried out using a Jeol-2900 at 20 kV. Sample specimens for SEM/EDX were prepared by ultrasonic dispersion of samples in methanol. The suspensions were dropped onto a silicium wafer.

The Bruauner, Emett, Teller (BET) surface area, pore volume, and average pore radius of the CNTs and catalysts were measured by an ASAP-2000 system from Micromeritics. The samples were degassed at 200 °C for 2 h under 50 mTorr vacuum and their BET area, pore volume, and average pore radius were determined.

X-ray diffraction (XRD) measurements of the CNTs, calcined catalysts and reduced passivated catalysts were conducted with a Philips PW1840 X-ray diffractometer with monochromatized Cu/Kα radiation.

Temperature programmed reduction (TPR) spectra of the calcined catalysts were recorded using a CHEMBET-3000, equipped with a thermal conductivity detector. The catalyst samples were first purged in a flow of helium at 150 °C to remove traces of water, and then cooled to 40 °C. The TPR of 100 mg of each sample was performed using 3.1 % hydrogen in nitrogen gas mixture with a flow rate of 40 cm^3/min. The samples were heated from 40 to 900 °C with a heating rate of 10 °C/min.

The amounts of chemisorbed CO and percentage reduction for the catalysts were measured using the Micromeritics TPD-TPR 290 system. 0.25 g of the calcined catalyst was reduced under hydrogen flow at 400 °C for 20 h and then cooled to 50 °C under hydrogen flow. Then the flow of hydrogen was switched to argon. In order to remove the adsorbed hydrogen, the temperature programmed desorption (TPD) of the samples was performed by increasing the temperature of the sample with a ramp rate of 10 °C/min, to 400 °C under the argon flow. Then, the sample was reoxidized at 400 °C by pulses of 10

% oxygen in helium to determine the extent of reduction. The percentage reduction was calculated by assuming (mono-metal and bimetallic systems) total oxidation at 400 °C of the reduced Fe and Co sites by O_2 to form Fe_2O_3 and Co_3O_4. Also the amounts of chemisorbed carbon monoxide (CO uptake) were measured via injection of pulses of pure CO to the reduced catalysts after TPD of the samples. The resulting spectra were used to determine the amount of chemisorbed carbon monoxide (micro moles of CO/g of catalyst). The %dispersion is calculated by the formula below [Devenhage and Coville, 1997].

$$\%Dispersion = \frac{1.175 \times (\mu mol / g\,CO)}{(\%metal \times fraction\ reduced)} \tag{5.1}$$

5.3.3 Reaction setup and experimental outline

The catalysts were evaluated in terms of their Fischer–Tropsch synthesis (FTS) activity ($g_{HC\ produced}/g_{cat}./h$) and selectivity (the percentage of the converted CO that appears as a hydrocarbon product) in a fixed bed micro-reactor. The temperature of the reactor was controlled via a PID temperature controller. Brooks 5850 mass flow controllers were used to add H_2, CO and argon at the desired rate to the reactor. Argon was used as internal standard gas in the reactor feed. Prior to the activity tests, the catalyst activation was conducted according to the following procedure. The catalyst (0.5 g) was placed in the reactor and pure hydrogen was introduced at a flow rate of 30 ml/min. The reactor temperature was increased from room temperature to 380 °C at a rate of 10 °C/min, maintained at this activation condition for 14 h and the catalyst was reduced in-situ. After the activation period, the reactor temperature was decreased to 180 °C under flowing hydrogen.

Synthesis gas with a flow rate of 30 ml/min (H_2/CO ratio of 2) was introduced at the top of the fixed bed reactor and the reactor pressure was increased to 2 MPa. The reactor temperature was then increased to 220 °C at a rate of 10 °C/min. Products were continuously removed from the reactor and passed through two traps, one maintained at 100 °C (hot trap) and the other at 0 °C (cold trap). The uncondensed vapor stream was reduced to atmospheric pressure through a pressure let down valve. The composition of

the outlet gas stream quantified using an on-line GC 2014 Shimadzu gas chromatograph. The contents in hot and cold traps were removed every 24 h, the hydrocarbon and water fractions were separated, and then analyzed by Varian 3400 GC.

5.4 Results and discussion

5.4.1 Characterization overview

A sample of the purified CNTs material (95 < carbon, BET surface area of 170.4 m^2/g) was analyzed by TEM. The purified product consisted of an interwoven matrix of tubes (Figure 5.1a) that was shown to be comprised of multi-walled carbon nanotubes. Figure 5.1b shows a high resolution image of the CNT sample presenting graphite layers of multi-wall CNTs. The TEM images of Co10Fe4/CNT catalysts revealed that the catalyst particles were well dispersed inside the tubes and also on the perimeter of the tube walls (Figure 5.2).

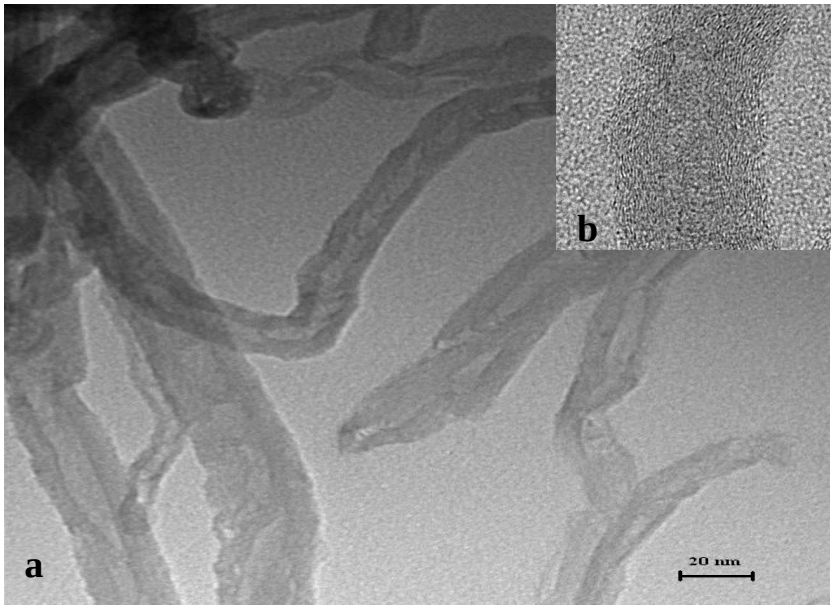

Figure 5. 1: TEM images of the CNT sample a) support material after purification, b) high resolution image showing graphite layers of multi-wall CNTs

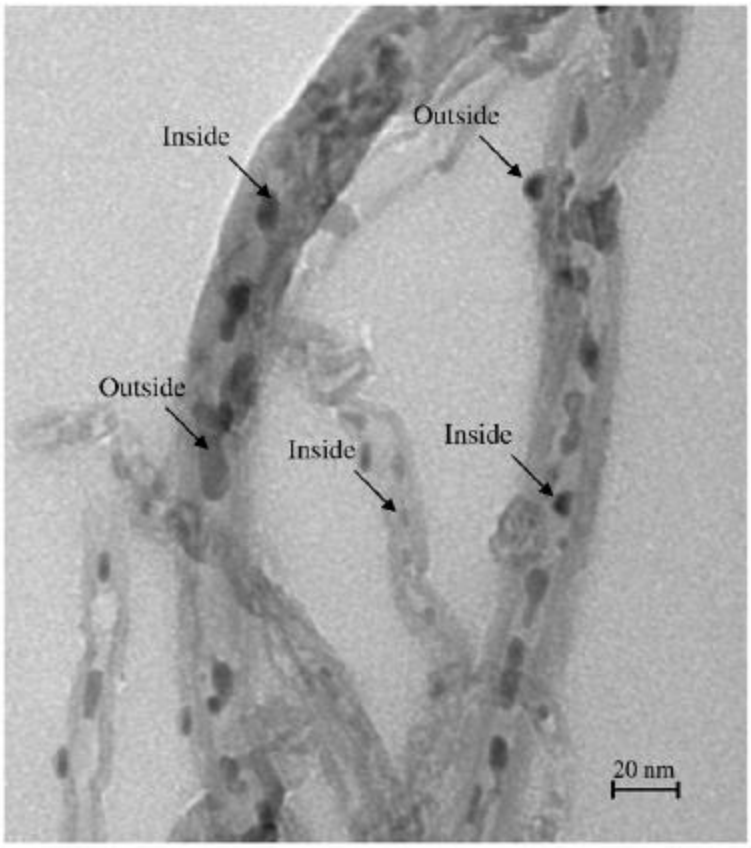

Figure 5. 2:TEM image of the Co10Fe4/CNT catalyst

The particles measurement has been calculated using the equation $d = (4\ a\ b/\pi)^{0.5}$ where *a* and *b* are dimensions of the particles as seen in the TEM image. The iron and cobalt oxide particles were grown to a maximum size of 10 nm, whereas those on the outer surface have grown up to about 12 nm (Figure 5.2). Obviously, the CNTs channels have restricted the growth of the particles inside the tubes. A bar graph depicting the size distribution of the total particles inside and outside the tube was determined based on total particle population taken from several TEM micrographs shown in Figure 5.3.

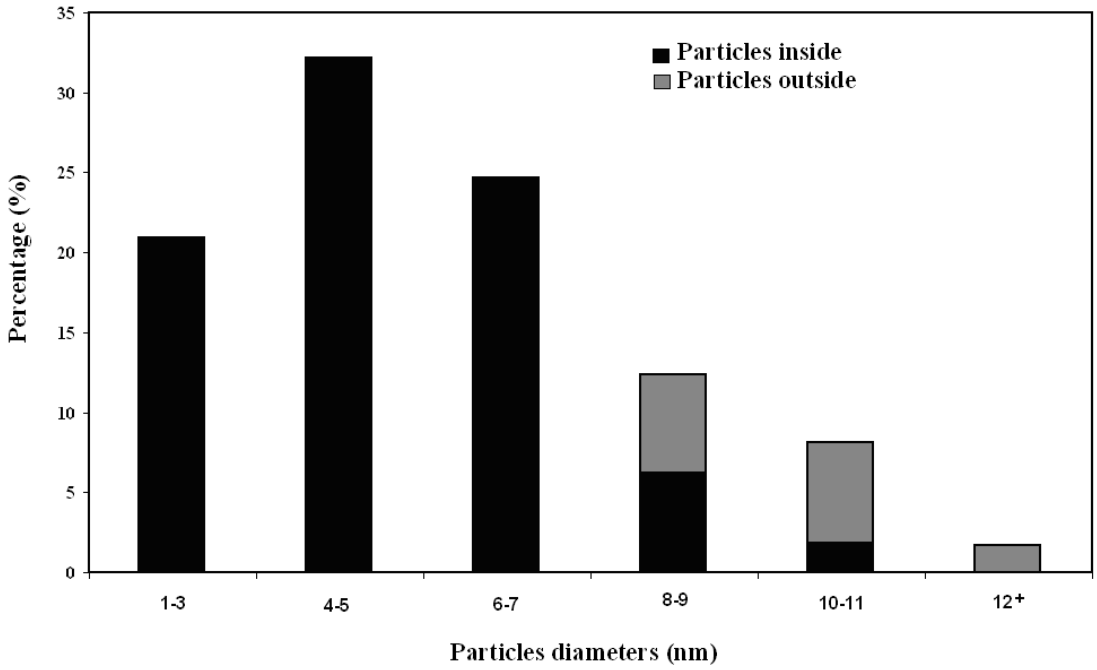

Figure 5. 3: Particle size distribution for the Co10Fe4/CNT catalyst.

In addition to the catalyst particles visible in Figure 5.2, the representative SEM image of the Co10Fe4/CNT catalyst shown in Figure 5.4 reveals the outside of CNT walls.

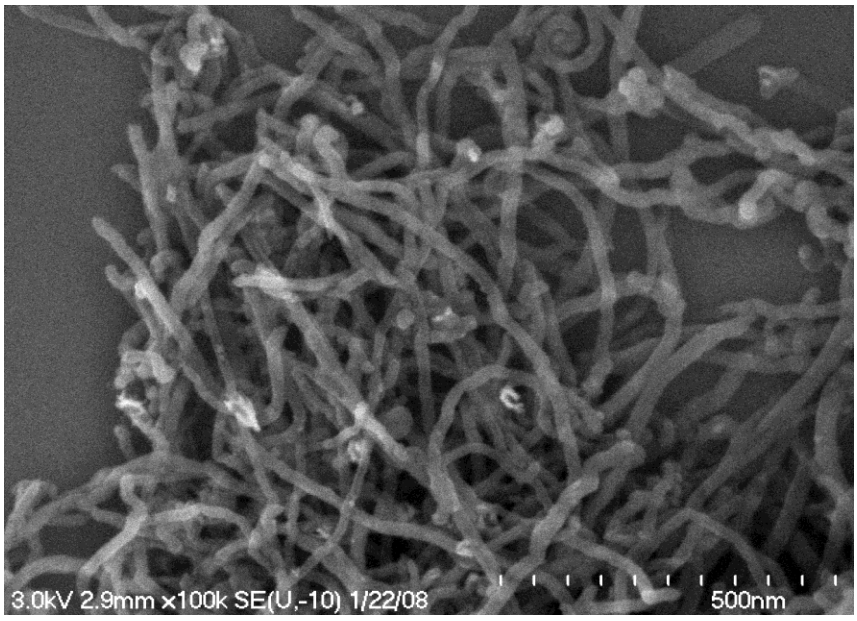

Figure 5. 4: SEM image of the Co10Fe4/CNT catalyst

The SEM picture reveals that the support material is entirely comprised of nanotubes and there are no other impurities such as carbon nanospheres.

Results of surface area measurements are shown in Table 5.1.

Table 5. 1: BET surface area and porosity data for the CNT support, monometallic and bimetallic catalysts

Support/Catalyst	BET (m^2/g)	Pore Volume (Single point) (cm^3/g)	Average Pore Diameter (nm)
CNT	214.1	0.58	10.90
10Co/CNT	192	0.56	11.60
10Co0.5Fe/CNT	188	0.55	11.62
10Co1Fe/CNT	184	0.54	11.76
10Co2Fe/CNT	166	0.53	11.40
10Co4Fe/CNT	156	0.52	10.60
10Fe/CNT	194	0.56	11.60

These results show that the BET surface area of 10 % Co loaded and 10 % Fe loaded monometallic catalysts decreased the surface area from 214 to 192 and 194 m^2/g respectively. At the same time, the pore volume decreased from 0.58 to 0.56 cm^3/g for both samples. The results show that the BET surface area of both catalysts were lower than that of the CNTs, which indicates pore blockage due to cobalt and iron loading on the support. Also in the case of bimetallic catalysts, by increasing the amount of Fe from 0.5 to 4wt. %, the BET area decreased from 188 to 156 m^2/g and the pore volume decreased from 0.55 to 0.52 cm^3/g. Incorporation of cobalt and iron to the CNTs support led to a decrease in both BET areas and pore volumes, and pore blockage increased with increasing amount of Fe.

The structure of the reduced and passivated Co10Fe4/CNT catalyst was studied using energy-dispersive X-ray spectrometry. The resulting spectrum is shown in Figure 5.5.

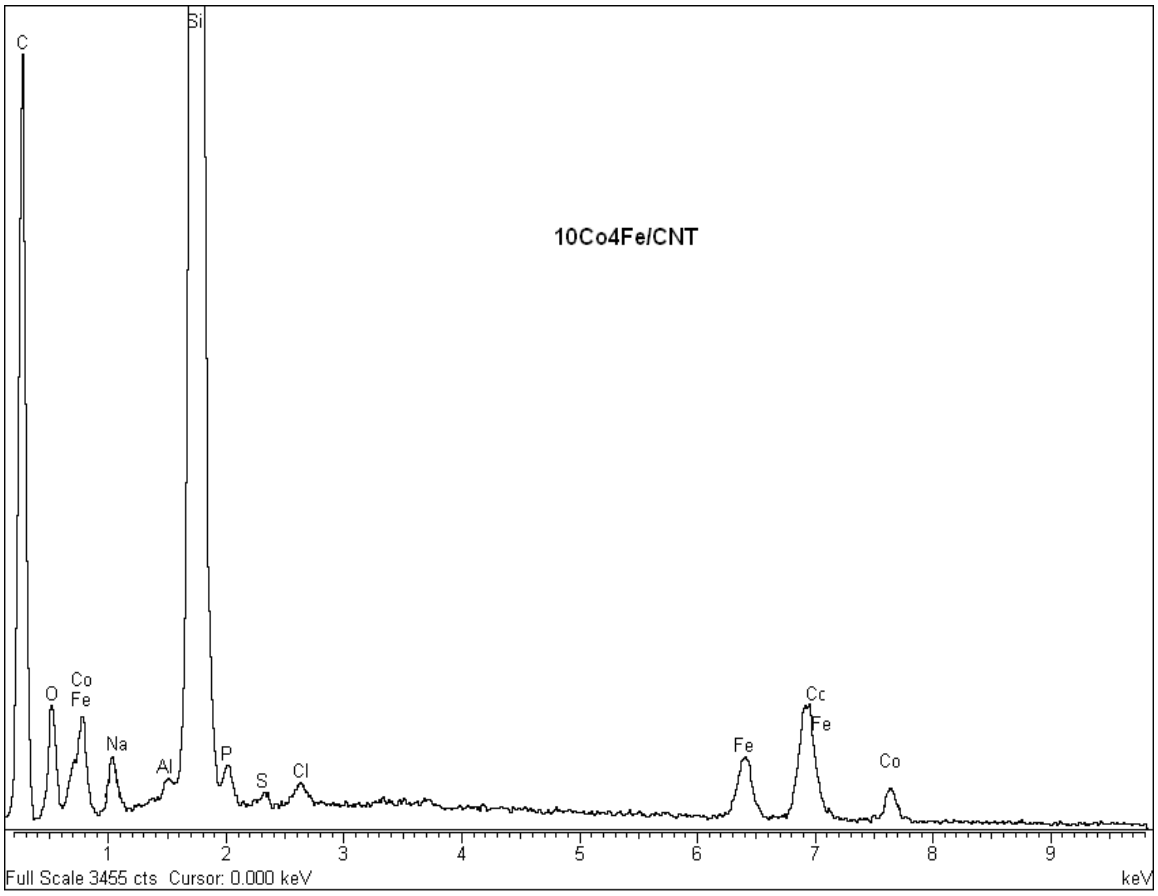

Figure 5. 5: EDX spectra of the Co10Fe4/CNT

As shown in this figure the cobalt particles are present at 0.775, 6.9 and 7.7 keV and iron particles are present at 0.704 and 6.4 keV, respectively. However, the peak at 6.9 keV can also be attributed to metal phase containing both cobalt and iron metals, according to Kozhuharova et al. [Kozhuharova et al., 2005].

The crystal structure of the supported cobalt and iron phases of the calcined and reduced catalysts was revealed by X-ray diffraction. XRD patterns of the support and calcined catalysts are shown in Figure 5.6.

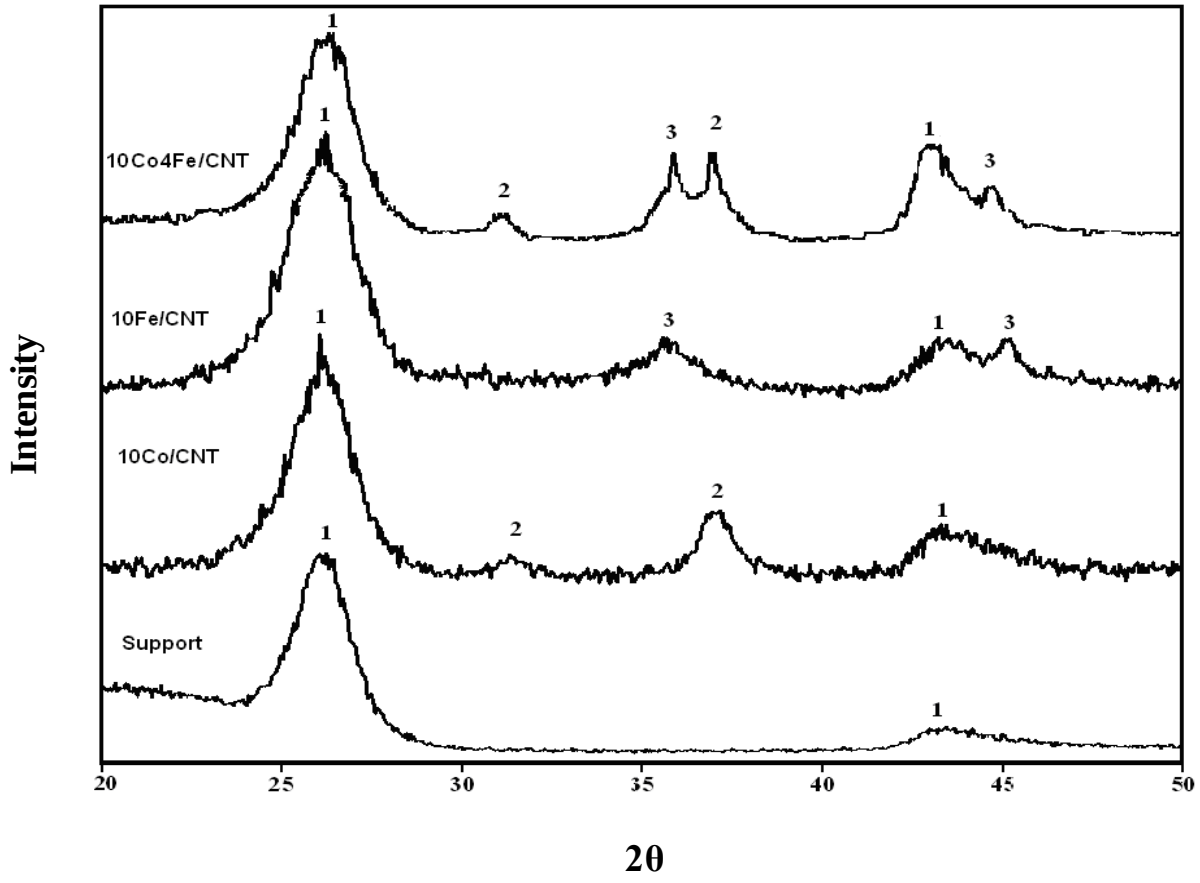

Figure 5. 6: XRD spectra of the CNT support and calcined monometallic and 10Co4Fe/CNT bimetallic catalysts (The crystalline phases indicated are as follows: 1, CNT; 2, Co_3O_4; 3, Fe_2O_3)

In the XRD spectrum of CNTs support and all catalysts, peaks at 25 and 43° correspond to carbon nanotubes [Tavasoli at al., 2008b]. The monometallic 10Co/CNT sample displayed the diffraction lines of the Co_3O_4 spinel at 2θ values of 31.5 and 36.8° [Tavasoli et al., 2008b], whereas the other monometallic 10Fe/CNT sample exhibited the pattern of hematite (Fe_2O_3) at 2θ values of 35.7 and 44.5° [Jothimurugesan et al., 2000]. In the patterns of bimetallic 10Co0.5Fe/CNT catalyst the diffraction lines of Co_3O_4 spinel appeared at 2θ value of 31.5 and 36.8°. However for this catalyst, because of low amounts of iron, only a small peak at 44.5° correlated with Fe_2O_3. The XRD patterns of bimetallic 10Co1Fe/CNT, 10Co2Fe/CNT and 10Co4Fe/CNT catalysts showed the peaks of Co_3O_4 at 2θ values of 31.5 and 36.8° and the peaks of Fe_2O_3 at 2θ values of 35.7 and 44.5°. XRD patterns of the reduced passivated catalysts are shown in Figure 5.7.

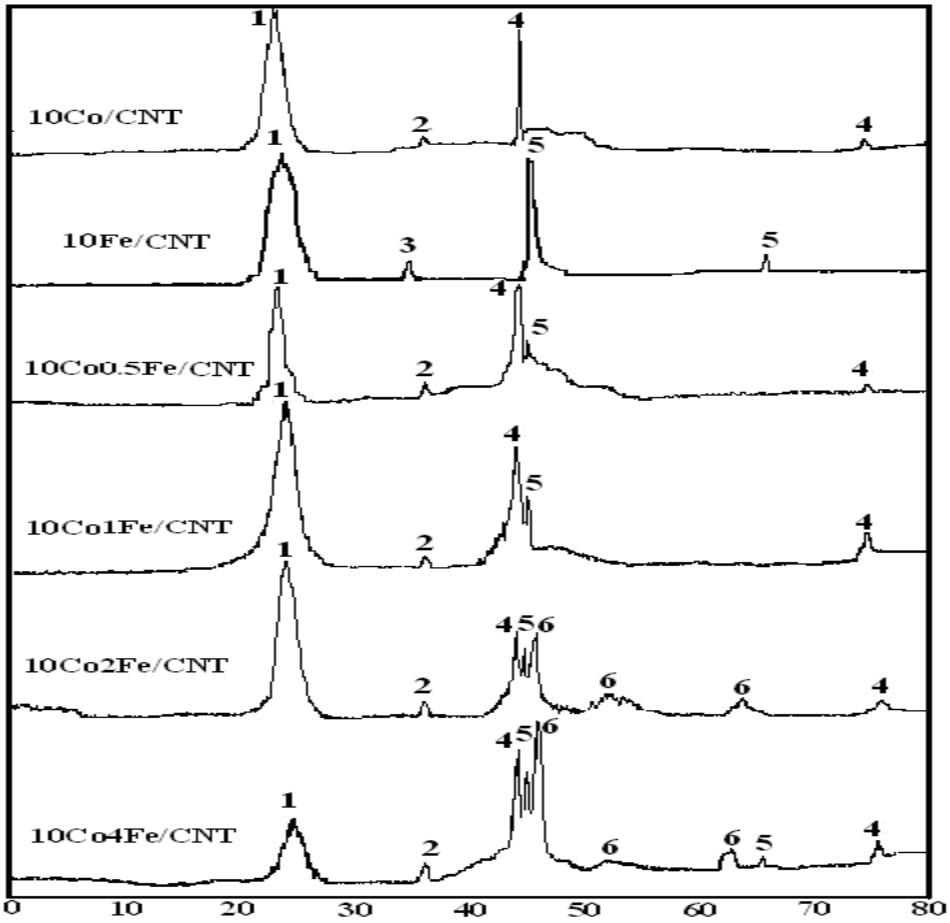

Figure 5. 7: XRD spectra of the reduced bimetallic catalysts (The crystalline phases indicated are as follows: (1) CNT; (2)Co_3O_4 or CoO; (3) Fe_2O_3 ; (4) Co^o ; (5) Fe^o; (6) Fe/Co alloy

In this figure, for all catalysts the peaks for CNTs support appeared only at 2θ value of 25° and the peak at 43° is overshadowed by the peaks of metallic Co and Fe. In the case of reduced monometallic 10Co/CNT catalyst, the peaks at 2θ value of 44 and 77° can be corresponding to metallic cobalt (Co°) [Pena O'Shea et al., 2007]. However a small peak at 2θ value of 36.8° corresponds to cobalt oxides which are produced during the passivation step. This peak was also present in the XRD of all reduced bimetallic catalysts. For reduced monometallic 10Fe/CNT catalyst, the peaks at 2θ values of 44.8 and 66° may correspond to metallic iron (Fe°) [Pena O'Shea et al., 2007]. However, the small peak at 2θ value of 35.7° corresponds to hematite (Fe_2O_3) which is produced during the passivation step. In the case of reduced bimetallic 10Co0.5Fe/CNT and

10Co1Fe/CNT catalysts the diffraction lines of Co° appeared at 2θ values of 44 and 77°. In addition for these catalysts a small peak at 44.8° correlates with Fe°. In the patterns of reduced bimetallic 10Co2Fe/CNT and 10Co4Fe/CNT catalysts not only the diffraction lines of Co° appeared at 2θ values of 44 and 77° and the diffraction lines of Fe° appeared at 2θ values of 44.8 and 66° but also the characteristic diffractions of a bimetallic Co/Fe phase appeared at 2θ values of 45, 53 and 62° [Pena O'Shea et al., 2003; Pena O'Shea et al., 2007; Tihay et al., 2001]. These two peaks were not present at the XRD of other bimetallic Co Fe/CNT catalysts, containing less iron, presumably as a consequence of the development of very low crystal size particles. These results suggest that by increasing the amount of iron in bimetallic catalysts, the interaction between the cobalt and iron increases, thus producing Co/Fe alloys during reduction of the catalysts.

The activation of the catalysts in hydrogen atmosphere was disclosed by temperature programmed reduction (TPR) experiments. The TPR profile of the calcined monometallic catalysts and CNTs support are shown in Figure 5.8.

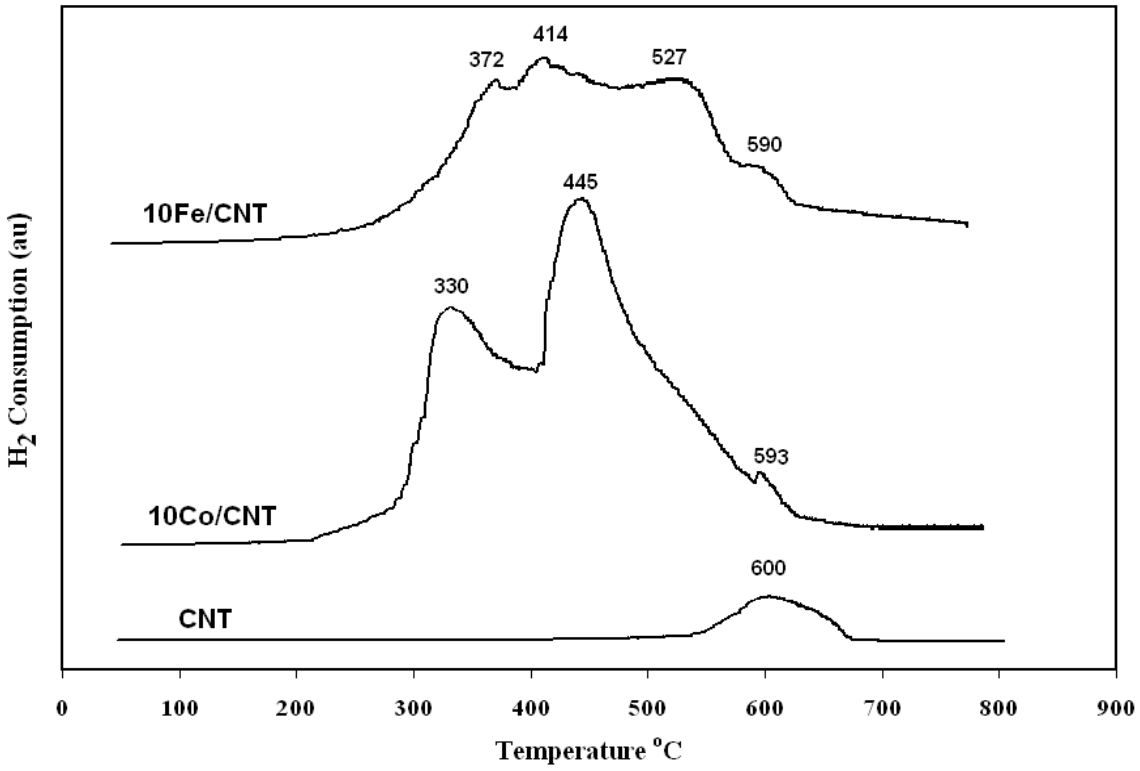

Figure 5. 8: TPR profiles of the support, monometallic 10Co/CNT and 10Fe/CNT calcined catalysts

The first peak of the TPR profile of the monometallic cobalt catalyst was assigned to the reduction of Co_3O_4 to CoO, and the second peak with a broad shoulder was mainly assigned to the second reduction step, which is the reduction of CoO to Co° [Tavasoli et al., 2008b]. This peak also included the reduction of cobalt species that interact with the support, which extend the TPR profile to higher temperatures [Tavasoli et al., 2008a]. Figure 5.8 shows the first reduction peak of Co/CNT at 330°C and the second reduction peak at 445 °C. The small peak at about 593 °C at the TPR profile of 10Co/CNT catalyst was assigned to the gasification of the support, as also indicated by TPR of pure CNTs support at 600 °C. In previous work, Tavasoli et al., studied the temperature programmed reduction of cobalt catalysts (8–40 wt. % cobalt loadings) supported on γ-Al_2O_3 [Tavasoli et al., 2007]. They showed that for Co/γ-Al_2O_3 catalysts, the first TPR peak temperature varied between 360 and 370 °C and the second TPR peak temperature varied between 600 and 620 °C. Comparison of the results for the Co/γ-Al_2O_3 catalyst [Tavasoli et al., 2007] and for Co/CNT catalyst in Figure 5.8 shows that in case of Co/CNT both reduction peaks were shifted significantly to lower temperatures suggesting an easier reduction process. It resulted in a decrease in the temperature of the first TPR peak by 30–40 °C, and the temperature of the second TPR peak by 150–170 °C. This indicates that by using CNTs as support for cobalt catalyst, the reduction temperature of difficult-to-reduce species (450–650 °C) decreased due to a lower degree of interaction between the Co and CNTs support [Bezemer et al., 2004; Reuel and Bartholomew, 1984; Tavasoli et al., 2008b; Tavasoli et al., 2008c].

The TPR of the 10Fe/CNT catalyst was more complex and exhibited four broad peaks at 372, 414, 527 and 590 °C. The first three peaks can be assigned to the following consecutive reduction steps: α-$Fe_2O_3 \rightarrow Fe_3O_4 \rightarrow FeO \rightarrow Fe°$ [Brown et al., 1982]. The fourth small peak in the TPR spectra of this catalyst was due to the gasification of support, as also indicated by TPR of pure CNTs support and monometallic cobalt catalyst. It seems that loading of cobalt and iron on CNTs decreases the gasification temperature of CNTs. It is noted that the relative hydrogen uptake of 10Fe/CNT catalyst was lower than the 10Co/CNT catalyst (Table 5.2). Temperature programmed reduction of iron catalyst (10wt. %) supported on silica has been studied by O'Shea et al. [Pena

O'Shea et al., 2007]. They have shown that for the 10Fe/SiO_2 catalyst, the first, second and third TPR peak temperatures were 371, 520 and 700 °C respectively. Comparing the TPR results of the 10Fe/CNT catalyst with O'Shea et al. TPR studies on the 10Fe/SiO_2 catalyst show that using CNTs as iron catalyst support significantly shifts the TPR peaks to the lower temperatures [Pena O'Shea et al., 2007]. This indicates that by using CNTs as iron catalyst support, the extent of difficult-to-reduce species decreases due to lower degree of interaction between the Fe and CNTs support [Bezemer et al., 2004].

Figure 5.9 shows the TPR profiles of the bimetallic catalysts.

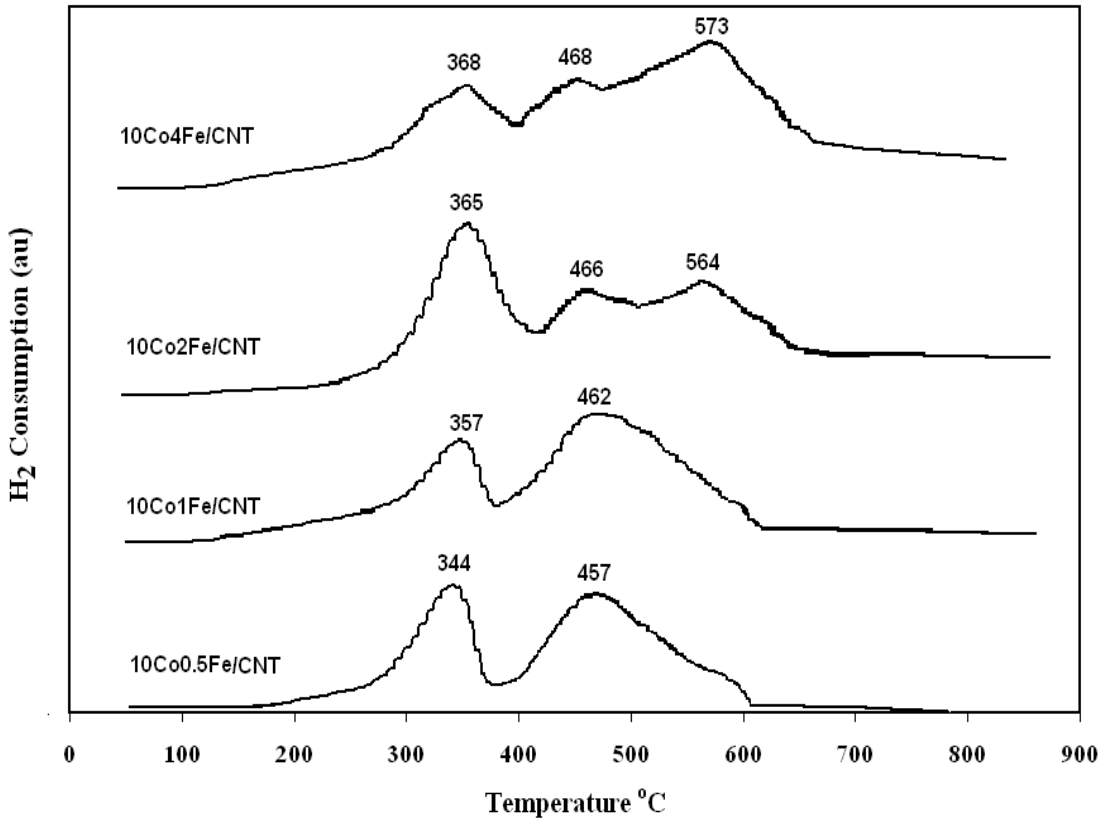

Figure 5. 9: TRP profiles of bimetallic 10Co0.5Fe/CNT and 10Co1Fe/CNT, 10Co2Fe/CNT and 10Co4Fe/CNT calcined catalysts

The TPR profiles of the bimetallic 10Co0.5Fe/CNT and 10Co1Fe/CNT catalysts are similar to that of the Co10/CNT sample, although the positions of the both peaks are shifted toward higher temperatures. Addition of 0.5 wt. % of iron to cobalt catalyst resulted in an increase in the temperature of the first TPR peak from 330 to 344 °C and the temperature of the second TPR peak from 445 to 457 °C. Similarly, the addition of 1

wt. % of iron to cobalt catalyst resulted in an increase in the temperature of the first and second TPR peaks from 330 to 445 °C and from 357 to 462 °C, respectively.

Figure 5.9 also indicates that by addition of 0.5 and 1 wt. % of iron to the cobalt catalyst, the tailing of the second TPR peak becomes broader significantly, suggesting a difficult reduction process for cobalt oxides. There is also the possibility that this broad tailing could correspond to the reduction of a Co–Fe mixed oxide phase. It should be mentioned that the peak indicating gasification of CNTs is strongly overshadowed by the broad tailing of the second TPR peak.

The TPR profiles of the bimetallic catalysts with 2 and 4wt. % of iron are also shown in Figure 5.9. In comparison with 10Co0.5Fe/CNT and 10Co1Fe/CNT catalysts, one additional reduction peak appeared in the temperature range of 550–650 °C. This additional peak was centered at 564 and 573 °C for 10Co2Fe/CNT and 10Co4Fe/CNT catalysts, respectively. It has been suggested that this new peak at the reduction profile of these catalysts with a broad tailing could be related to the formation of a very stable, difficult-to-reduce Fe rich phase, which may be formed in the synthesis of the bimetallic catalysts [Duvenhage and Coville, 1997].

Table 5.2 presents the results of percentage reduction, CO chemisorption and percentage dispersion for all the catalysts.

Table 5. 2: Degree of reduction, Co uptake and percentage dispersion for mono-and bimetallic catalysts

Catalyst	CO uptake (μ mole CO /g cat.)	%Reduction	%Dispersion
10Co/CNT	20.2	48.3	4.9
10Co0.5Fe/CNT	33.8	57.3	6.5
10Co1Fe/CNT	25.2	58.5	4.6
10Co2Fe/CNT	21.0	50.2	4.1
10Co4Fe/CNT	16.7	40.1	3.5
10Fe/CNT	17.8	16.7	12.5

As shown in this table, the percentage reduction for the 10Co/CNT catalyst is about 3 times higher than that for 10Fe/CNT catalyst. Comparing the data in Table 5.2 for the percentage reduction of the 10Co/CNT catalyst (48.3 %) with our previous studies [Tavasoli et al., 2007] on Co/γ-Al_2O_3 catalysts (% reduction between 19.6 and 23 %) it was demonstrated that using CNTs as cobalt catalyst support increased the percentage reduction significantly. This is due to a lower degree of interaction between the Co and CNTs [Bezemer et al., 2004; Reuel and Bartholomew, 1984; Tavasoli et al., 2008b]. This will make more active metal atoms available for reaction in CNTs-supported catalysts in comparison with Co/γ-Al_2O_3 catalysts [Tavasoli et al., 2007]. However, the 10Co/CNT catalyst still shows incomplete reducibility.

As seen in Table 5.2, it is clear that small amounts of Fe enhanced the reducibility of the bimetallic catalysts. However, if Fe is present in high concentrations (i.e. Fe>1 wt. %), the Co catalyst properties are influenced by the Fe properties, which in turns lead in decreasing the percentage of reduction [Pena O'Shea et al., 2003]. Table 5.2 shows that the amount of CO uptake for the 10Co/CNT catalyst was higher than that for 10Fe/CNT catalyst. This table shows that for bimetallic catalysts with increasing the Fe content, CO uptake increased, passing through a maximum at the Fe loading of 0.5 wt. % and then decreased. The data suggested that at higher Fe loadings, the surface has been affected by mixing of the Fe and Co. In contrast to the CO uptake and percentage of reduction, the percentage of dispersion for 10Fe/CNT was higher than that for 10Co/ CNT catalyst. For the bimetallic catalysts, with addition of Fe, percentage of dispersion increased significantly, passing through a maximum at Fe loading of 0.5 wt. % and then decreased (Table 5.2). Thus, it seems that the ratio of Fe to Co plays an important role in controlling the metal dispersion and degree of reduction in the bimetallic system.

5.4.2 Activity and products selectivities results

The catalytic activity and product selectivity data have been calculated after initial catalyst stability within first 72 h. The % CO conversion for the monometallic and bimetallic catalysts is shown in Figure 5.10.

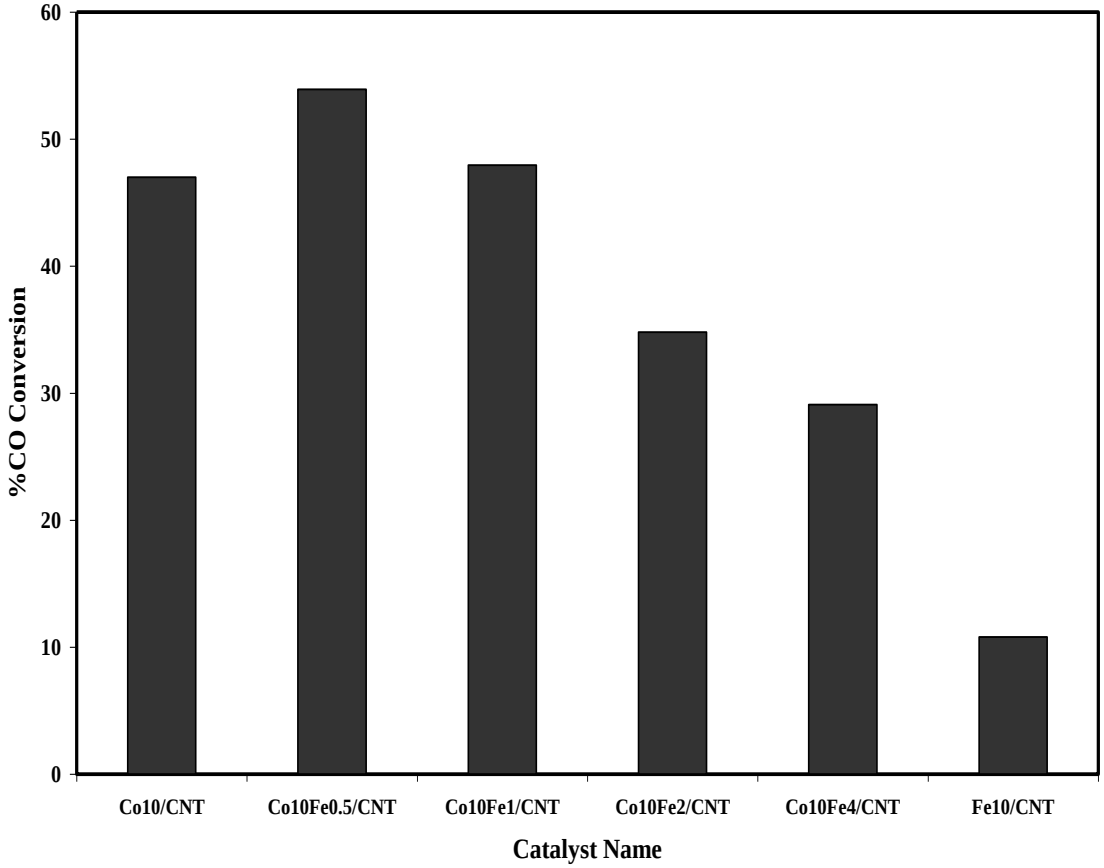

Figure 5. 10: %CO conversion for mono- and bimetallic catalysts

For the monometallic catalysts, the 10Co/CNT catalyst showed a CO conversion of 47% compared to that of 10Fe/CNT catalyst with the CO conversion of 10.8 %. As shown in Figure 5.10, % CO conversion increases with addition of iron to cobalt catalyst with Fe loading of 0.5 wt. % and then decreased. In Table 5.2, we showed that the addition of small amounts of iron (i.e. 0.5 wt. %) to the cobalt catalyst led to an increase in percentage reduction and percentage metal dispersion. Improvements in metal dispersion and reduction created more active metal atoms available for FTS reaction and as a result enhanced the catalyst activity significantly. Increasing the amount of Fe decreased the percentage dispersion which in turn decreases the % CO conversion. The decrease in CO conversion could also be due to Fe enrichment at the surface of the bimetallic catalysts. The higher the iron loading, the more severe this phenomenon would be.

Figure 5.11 shows the FTS reaction rate (Eq. (5.2)) and WGS reaction rate (Eq. (5.3)) for the monometallic and bimetallic catalysts.

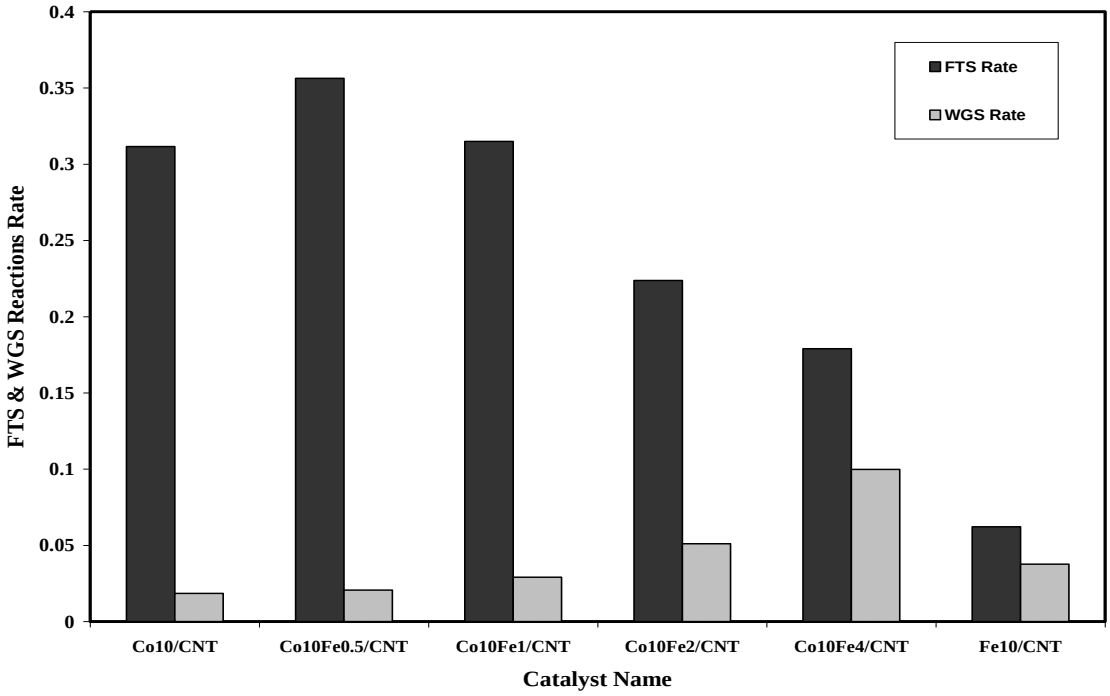

Figure 5. 11: FTS rate (g HC/cat./h) and WGS rate (g CO_2/cat./h) for mono- and bimetallic catalysts

$$R_{FTS}\,(\text{g HC/g cat./h}) = \textit{total mass of hydrocarbons produced / g}\ \text{cat. / h} \quad (5.2)$$

$$R_{WGS}(\text{g } CO_2\text{/g cat./h}) = \textit{total mass of } CO_2 \textit{ produced / g cat. / h} \quad (5.3)$$

The CO_2 formation rate corresponds to the consumption of the CO in WGS reaction (Eq. (5.4)), whereas the difference in the CO consumption in WGS reaction and the total CO conversion gives the consumption of the CO in the FTS reaction (Eqs. (5.5) and (5.6)).

$$CO + H_2O \leftrightarrow CO_2 + H_2 \quad (5.4)$$

$$CO + 2H_2 \leftrightarrow {}^{-}CH_2{}^{-} + H_2O \quad (5.5)$$

(CO converted to hydrocarbons) = (total CO conversion) – (CO converted with WGS reaction) (5.6)

Figure 5.11 shows that the FTS reaction rate increased with addition of iron to cobalt catalyst, which passed through a maximum at Fe loading of 0.5 wt. % and then started to decrease. The same behaviour has been observed by Pena O'Shea et al., with cobalt catalyst promoted with 1 to 4 wt. % of Fe [Pena O'Shea et al., 2007]. The 10Co0.5Fe/CNT catalyst increased the FTS rate by 14.3 %, while addition of 2 and 4 wt. % iron decreased the FTS rate by 28 and 42 %, respectively. This figure also shows that addition of iron to cobalt catalyst increased the WGS reaction rate. The increase in theWGS reaction rate was not significant at low values of the Fe (i.e. 0.5 wt. % of Fe). However, addition of 2 wt. % of Fe or more increased the WGS rate significantly. Figure 5.11 shows that at low values of Fe content (10Co0.5Fe/CNT), the WGS rate followed the FTS rate. This is because the produced H_2O in FT reaction (Eq. (5.3)) is consumed as the reactant in WGS reaction. For the catalysts with Fe loadings higher than 1 wt. %, the data in Figure 5.11 show that the WGS reaction rate accelerated compared to the FTS rate. As discussed in the previous sections, at higher iron loadings the surface of the bimetallic catalysts was enriched with Fe atoms and the catalysts took on the properties of this metal. Figure 5.11 shows that the monometallic Fe10/CNT catalyst had the lowest FTS rate and highest WGS rate compared to the other catalyst studied (Co/CNT and bimetallic catalysts). The higher rate of WGS reaction could be attributed to the lower capacity of iron catalysts for absorbing CO dissociatively.

Product distributions of the catalysts are displayed in Table 5.3.

Table 5. 3: Products selectivity for the mono-and bimetallic catalysts

Catalyst	CH_4%	(C_2-C_4) %	C_5+%	CO_2%	Olefin/Paraffin	Alcohols %
10Co/CNT	9.3	3.8	85.1	1.8	0.56	2.3
10Co0.5Fe/CNT	9.4	3.5	85	2.1	0.96	4.1
10Co1Fe/CNT	9.5	4.8	83	2.7	1.08	5.4
10Co2Fe/CNT	11.2	6	78	4.8	1.32	22.0
10Co4Fe/CNT	12.3	7.8	71	8.9	1.48	26.3
10Fe/CNT	16.9	21.7	46.7	14.7	1.95	10.3

Comparing the selectivities of monometallic catalysts demonstrates that the monometallic cobalt catalyst showed low selectivity to methane and light gaseous hydrocarbons, while its yield of C_{5+} hydrocarbons was high. Monometallic Fe10/CNT catalyst, by contrast, exhibited very high selectivity to lighter hydrocarbons. Also, Table 5.3 shows that the inclusion of iron in the cobalt catalyst changed the molecular weight of products. Addition of 0.5 and 1 wt. % of Fe to the cobalt catalyst did not change the catalyst product selectivity significantly. However, addition of 2 and 4 wt. % of iron to the cobalt catalyst increased the methane selectivity by a factor of 20.4 and 32.3 % and decreased the C_{5+} liquid hydrocarbons selectivity by 8.3 and 16.5 %. The mechanism of hydrocarbon synthesis on the Co and Fe catalysts includes three steps namely initiation, propagation and termination reactions. The higher yield of C_{5+} liquid hydrocarbons and lower production rate of CH_4 for the monometallic cobalt catalyst could be due to the effective participation of olefins in the carbon–carbon chain propagation. On this catalyst, α-olefins of the type R–CH=CH_2 can compete with carbon monoxide and heavier olefins for re-adsorption and chain initiation. Also they can add directly to the growing chains. Thus, the higher average molecular weight for the monometallic cobalt catalyst was due to the secondary chain growth of re-adsorbed α-olefins, whereas the secondary chain growth was negligible for iron catalysts over propagation steps [Patzlaff et al., 1999]. In bimetallic catalysts at higher iron loadings, Fe enriched at the surface of the bimetallic

catalysts and the catalyst took on the properties of this metal, and hence decreased the chain growth by α-olefins readsorption and secondary reactions. Also, it has been suggested that the formation of Co–Fe alloys in bimetallic catalysts decreases the non-alloyed cobalt and hence decreases the chain growth by α-olefins re-adsorption and secondary reactions [Pena O'Shea et al., 2007]. The formation of Co–Fe alloys in the case of 10Co2Fe/CNT and 10Co4Fe/CNT catalysts has been confirmed by XRD tests of the reduced catalysts (Figure 5.7). Table 5.3 also shows that by increasing the amount of iron (Fe wt. % $\geq$ 1) in bimetallic catalysts the selectivity toward C_2–C_4 light gaseous hydrocarbons increased. Table 5.3 also shows that the introduction of iron resulted in changes in olefinity of the products. In these calculations, the hydrocarbons with carbon numbers between 2 and 5 were included. The olefin to paraffin ratio in the FTS products increased with the addition of iron. The higher olefin selectivity found for bimetallic catalysts compared to Co10/CNT monometallic catalyst can be attributed to the high olefin selectivity of iron. As shown in this table the olefin selectivity of Fe10/CNT monometallic catalyst was about 3.5 times higher than that of the Co10/CNT monometallic catalyst. It has been suggested that in iron catalysts the hydrogen mobility is significantly restricted by blocking the low coordination edge and corner sites for dissociative adsorption of hydrogen [Jam et al., 2006]. Reduced hydrogen mobility, as well as reduced hydrogen adsorption rates could explain the decrease in hydrogenation of olefins to paraffins and enhancement of olefin to paraffin ratios. The selectivity of the catalysts towards the alcohols (with carbon numbers up to 5) is shown in Table 5.3. The monometallic Co10/CNT catalyst exhibited a low selectivity for alcohols. The alcohol selectivity of monometallic Fe10/CNT catalyst was about 4.5 times higher than that of the monometallic Co10/CNT catalyst. The higher selectivity of Fe10/CNT catalyst can be attributed to the difficult dissociation of CO on the iron clusters. Table 5.3 shows that introduction of iron into the cobalt catalyst significantly increased the FTS product selectivity towards alcohols. The selectivity toward alcohols depends on the Co/Fe ratio and the maximum alcohol selectivity achieved at the maximum inclusion of iron. The behavior of bimetallic catalysts regarding increased selectivity toward alcohols can be attributed to the presence of Co–Fe alloys [Pena O'Shea et al., 2003; Pena O'Shea et al., 2007; Tihay et al., 2001]. FTS reaction products are alcohols (ROH) and hydrocarbons

(HC), and the relative proportion ROH/HC is highly dependent on the presence of Co–Fe alloys. These results can be rationalized by assuming that two different reaction mechanisms are involved: ROH is formed through a non-dissociative adsorption of CO, whereas hydrocarbon formation follows a dissociative mechanism [Bezemer et al., 2004; Pena O'Shea et al., 2003; Pena O'Shea et al., 2007; Reuel and Bartholomew, 1984]. The change of the ROH/HC ratio with the amounts of Co–Fe alloys is due to competing H- and CO-insertion reactions and variable proportions of molecularly and dissociatively adsorbed CO and H_2 on the surface. As the alcohols were the major reaction products with large amounts of Co–Fe alloy, hydrogenation of adsorbed CO species predominated. However, with lower amounts of Fe the C–O bond splits and ROH formation were strongly inhibited, while methane and other C_{2+} hydrocarbonswere the major reaction products (Table 5.3).

Figure 5.12 shows the distribution of produced alcohols for the monometallic and bimetallic catalysts.

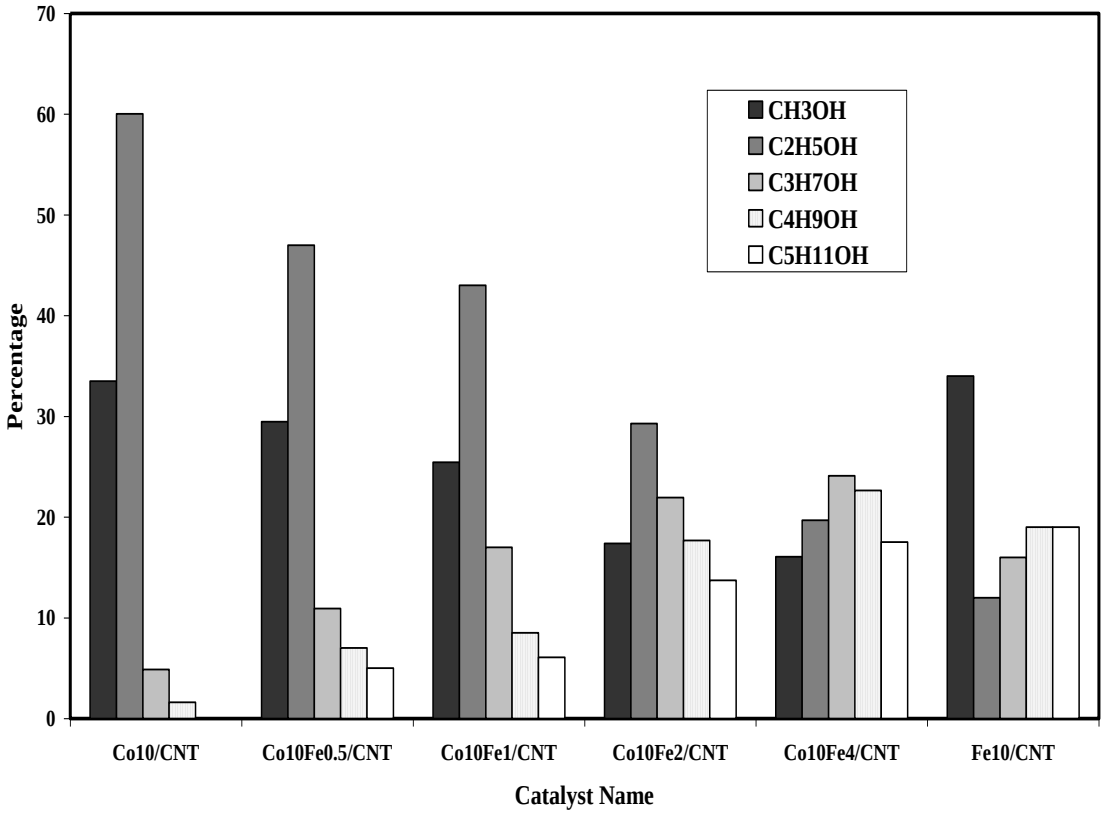

Figure 5. 12: Selectivity towards alcohols for mono- and bimetallic catalysts

As shown the main alcohol product for Co10/CNT catalyst was C_2H_5OH. In the case of Fe10/CNT catalyst, methanol was the main product. However, in the case of this catalyst the selectivity of heavier alcohols was significant. The cobalt catalyst possesses a major capacity for adsorbing CO dissociatively and mainly results in ethanol formation by CO insertion in C_1 adsorbed fragments, while the dissociation of CO is more difficult on the iron based catalyst and methanol formation by hydrogenation of non dissociative CO is the favoured reaction [Tavasoli et al., 2008b]. Figure 5.12 shows that the introduction of iron into the cobalt catalyst increased the selectivity of alcohols with heavier molecular weight. The increase in the amount of iron from 0.5 to 4 wt. % increased the $C_{3+}OH$ alcohols selectivities from 23 to 65 %. It should be noted that the selectivity of monometallic Fe10/CNT catalyst towards $C_{3+}OH$ alcohols was about 53 %. The behavior of bimetallic catalysts regarding increased selectivity toward alcohols may be attributed to the size of Co–Fe alloys clusters. Increasing the amount of iron increased the alloy formation and increases the size of Co–Fe clusters and therefore enhanced the ability of CO insertion reaction, thereby increase in the formation rate of alcohols with heavier molecular weight [Pena O'Shea et al., 2003; Pena O'Shea et al., 2007]. Larger Co–Fe particles were more selective to higher molecular weight hydrocarbons and the smaller particles were selective for methane and light gases. It seems that the steric hindrance for dissociative adsorption of CO and $–CH_2–$ monomer and addition of this monomer to the growing chain were less in the larger metal clusters [Tavasoli et al., 2008b].

5.5 Conclusions

Using CNTs with unique properties such as uniform pore structure, and high surface area with minor metal–support interaction, the effects of Co/Fe ratio on the activity and selectivity of Co–Fe bimetallic catalysts were studied. A series of catalyst containing Fe and Co on carbon nanotubes was prepared, and FT studies revealed that the two metals, when intimately mixed together, had different catalytic characteristics than catalysts containing only one of the Fe and Co metals. Most of the metal particles were homogeneously distributed inside the tubes, and the rest on the outer surface of the CNTs. The structural data obtained by XRD techniques pointed to the formation of Co–

Fe alloys. The small amounts of Fe enhanced the reducibility and dispersion of the bimetallic catalysts. FTS reaction rate and percentage CO conversion increased with addition of iron to cobalt catalyst with a highest CO conversion for the 10Co0.5Fe/CNT. The addition of iron to cobalt catalyst increased the WGS reaction rate. However, the increase in the WGS reaction rate was not significant at low values of the Fe. The monometallic cobalt catalyst exhibited fairly high selectivity (85.1 %) toward C_{5+} liquid hydrocarbons, while addition of small amounts of iron did not change the product selectivity significantly. Monometallic iron catalyst showed lowest selectivity of 46.7 % to C_{5+} hydrocarbons. The olefin to paraffin ratio in the FTS products increased with the addition of iron and monometallic iron catalyst exhibited maximum olefin to paraffin ratio of 1.95. The bimetallic Co–Fe/CNT catalysts proved to be much more attractive in terms of alcohol formation. The introduction of 4 wt. % of iron to the cobalt catalyst increased the alcohol selectivity from 2.3 to 26.3 %. The Co–Fe alloys appear to be responsible for the rather high selectivity toward alcohol formation.

5.6 References

Abbaslou, R.M.M., A. Tavasoli, A.K. Dalai, Effect of pre-treatment on physicochemical properties and stability of carbon nanotubes supported iron Fischer– Tropsch catalysts, Applied Catalysis A: Genereal **355**, 33–41 (2009).

Dry, M.E.,"The Fischer-Tropsch Synthesis,"in "Catalysis, Science and Technology Vol.1,"J.R. Anderson and M.Boudart, Eds., Springer, Berlin (1981), p.159-255.

Duvenhage, D.J., N.J. Coville, "Fe: 10/TiO2 bimetallic catalysts for the Fischer-Tropsch reaction I. Characterization and reactor studies," Applied Catalysis A: Geneneral **153**, 43–67 (1997).

Duvenhage, D.J., and N.J Coville, "Effect of K, Mn and Cr on the Fischer-Tropsch activity of Fe:Co/TiO_2 catalysts," Catalysis Letters **104**, 129-133 (2005 a).

Duvenhage, D.J., N.J. Coville, "Fe:Co/TiO2 bimetallic catalysts for the Fischer-Tropsch reaction: part 3: the effect of Fe:Co ratio, mixing and loading on FT product selectivity," Applied Catalysis A: General **289**, 231–239 (2005b).

Iglesia, E., "Design, synthesis, and use of cobalt-based Fischer-Tropsch synthesis catalysts," Applied Catalysis A: General **161**, 59-78 (1997).

Jam, S., M. Ghalbi Ahangary, A. Tavasoli, K. Sadaghiani, A. Nakhaeipour, "Enhancement of distillate selectivity in Fischer–Tropsch synthesis by using iron and cobalt catalysts in a novel dual-bed reactor," Reaction Kinetics and Catalysis Letters **89**, 71–79 (2006).

Jothimurugesan, K., J.G. Goodwin Jr., K. Santosh, K. Hanwal, J.J. Spivey, "Development of Fe Fischer–Tropsch catalysts for slurry bubble column reactors," Catalysis Today **58**, 335–344 (2000).

Kozhuharova, R., M. Ritschel, D. Elefant, A. Graff, I. Monch, T. Muhl, C.M. Schneider, A. Leonhardt, "(Fe_xCo_{1-x})-alloy filled vertically aligned carbon nanotubes grown by thermal chemical vapor deposition," Journal of Magnesium and Magnétique Materials **290–291**, 250–253 (2005).

Patzlaff, J., Y. Liu, C. Graffmann, J. Gaube, "Studies on product distributions of iron and cobalt catalyzed Fischer–Tropsch synthesis," Applied Catalysis A: General **186**, 109–119 (1999).

Peña O'shea, V.A., M.C. Alvarez-Galvan, J.M.Campos-Martin, J.L.G. Fierro, "Fischer-Tropsch-Synthesis on mom-and bimetallic Co and Fe catalysts in fixed bed and slurry reactors," Applied Catalysis A: General **326**, 65-73 (2007).

Peña O'Shea, V.A., N.N. Menéndez, J.D. Tornero, J.L.G. Fierro, "Unusually high selectivity to C_2+ alcohols on bimetallic CoFe catalysts during CO hydrogenation," Catalysis Letter **88**, 23–128 (2003).

Reuel, R.C and C.H. Bartholomew, "Effects of support and dispersion on the CO hydrogenation activity/selectivity properties of cobalt," Journal of Catalysis **85**, 78-88 (1984).

Serp, P., M. Corrias and P. Kalck, "Carbon nanotubes and nanofibers in catalysis," Applied Catalysis A: General **253,** 337-358 (2003).

Tavasoli, A., A.M. Rashidi, K. S. Zadeh, A. Karimi, A.A. Kodadadi, Y. Mortazavi, "Carbon nanotubes supported cobalt catalyst for converting synthesis gas into hydrocarbons," EP patent 1782885 A1 (2007).

Tavasoli, A., R.M. Abbaslou, M. Trépanier and A.K.Dalai, "Fischer-Tropsch synthesis over cobalt supported on carbon nanotubes in a slurry reactor," Applied Catalysis A: Genreal **345**, 134-142 (2008 a)

Tavasoli, A., K.Sadaghiani and K. Khorashe, A.A. Seifkordi, A.A. Rohani and A. Nakhaeipour, "Cobalt supported on carbon nanotubes: a promising novel Fischer-Tropsch synthesis catalyst," Fuel Processing Technology **89**, 491-498 (2008 b).

Tavasoli, A., R.M.M. Abbaslou, M.Trépanier and A.K. Dalai, "Morphology and deactivation behavior of Co-Ru/Al_2O_3 Fischer-Tropsch synthesis," The Canadian Journal of Chemical Engineering **86**, 1070-1080 (2008 c).

Tihay, F., G. Pourroy, M. Richard-Plouet, A.C. Roger, A. Kiennemann, "Effect of Fischer–Tropsch synthesis on the microstructure of Fe–Co-based metal/spinel composite materials," Applied Catalysis A: General **206**, 29–42 (2001).

Trépanier, M., A. Tavasoli, A.K. Dalai and N. Abatzoglou, " Fischer-Tropsch synthesis over carbon nanotubes supported cobalt catalysts in a fixed bed reactor: Influence of acid treatment," Fuel Processing Technology **90**, 367-374 (2009).

Chapter 6: Synthesis of CNT-supported cobalt nanoparticle catalysts using a microemulsion technique: Role of nanoparticle size on reducibility, activity and selectivity in Fischer-Tropsch reactions

A similar version of this chapter has been published in Applied Catalysis A: General:

Trépanier, M., A. K. Dalai and N. Abatzoglou, Synthesis of CNT-supported cobalt nanoparticle catalysts using a micoremulsion technique: Role of nanoparticle size on reducibility, activity and selectivity in Fischer-Tropsch reactions. Applied Catalysis A: General 374 (2010) 79-86.

The work discussed in this chapter was also included in paper presentations at the following conference:

Trépanier, M, A.K.Dalai and N. Abatzoglou, (March 2010) Microemulsion synthesis of Co nanoparticles supported on CNT: Effects of Nanoparticles Size on reducibility, activity and selectivity in FTS, American Institute of Chemical Engineering (Aiche spring conference), San Antonio, Texas, US.

Contribution of Ph.D Candidate

The laboratory experiments, data analysis and results interpretation were performed by Mariane Trépanier. Drs.Dalai and Abatzoglou provided editorial input, the main idea of the research project and financial support. The submitted manuscript was written and presented by Mariane Trépanier.

Contribution of this manuscript to Overall Study

The previous chapters demonstrated that unpromoted or promoted Co/CNT catalysts are suitable for FTS process in terms of activity and selectivity. They also revealed that FTS process is influenced by catalyst structure properties. In this part of the

research, microemulsion has been used as a new nanocatalyst preparation technique to have a better understanding of the particle size effect on FT reactions using a novel Co/CNT catalyst. The inert property of the CNT allows this study to be performed without undesirable interactions with the support such as observed with the oxidic support (Al_2O_3). Microemulsion catalyst preparation method is used to ensure uniform cobalt nano-particle at different sizes.

6.1 Abstract

The influence of cobalt particle size on catalyst performance in Fischer–Tropsch synthesis (FTS) has been investigated using inert carbon nanotubes (CNT)-supported catalysts. The catalysts were produced by the core reverse micelle reactions with cobalt particles of various sizes (3–10 nm). It has been shown that particle size is proportional to the water-to-surfactant ratio (3–10) used for the catalyst preparation. Very narrow particle size distributions have been produced by the microemulsion technique and at relatively high loading (Co 10 wt. %). Selectivity and activity were found to be dependant on cobalt particle size. The FTS rate increases from 0.36 to 0.44 g_{HC}/g_{cat}./h and the C_{5+} selectivity increases from 89 to 92.5 wt. % with increasing the average cobalt particle size from 2–3 to 9–10 nm, respectively. According to TEM analysis, small Co particles (2–6 nm) are mostly confined inside the CNTs where influence of its electron deficiency in the inside surface has changed the commonly expected catalyst's structure-sensitive results. Finally, the CNT-supported cobalt nanoparticles synthesized by the proposed microemulsion technique increased the CO conversion by 15 % compared to those prepared by incipient wetness impregnation.

6.2 Introduction

There is a renewed interest in Fischer–Tropsch synthesis (FTS) in both academia and industry, largely as a result of the demand for clean and renewable transportation [Bezemer et al., 2006a]. In the Fischer–Tropsch (FT) reaction, syngas (a mixture of CO and H_2), is converted into liquid fuel via catalytic surface polymerization which leads to a large variety of products such as paraffins, olefins, alcohols and aldehydes [Bezemer et al., 2006a; Li et al., 2002; Tavasoli et al., 2008a]. Supported cobalt catalysts are well-known for their activity and selectivity towards FTS. High chain growth probability,

lower deactivation rates, low water-gas shift activity, and low costs make cobalt catalysts the best candidates for converting syngas to clean liquid fuels [Dry, 2001, Jacobs et al., 2002].

Many investigations have been carried out to study the influence of catalyst properties on Fischer–Tropsch synthesis, including the influence of catalyst preparation techniques (such as microemulsion), to have better understanding of the structure sensitive effects in FT catalysis [Bezemer et al., 2006a; Hayashi et al.,2002; Martinez and Prieto, 2007]. A sub-category of structure-sensitive reactions regards the dependence of both catalytic activity and selectivity on catalytic metal particle size [Kim et al., 1997; Ojeda et al., 2004]. It is well documented that the metal particle size of the catalyst is a parameter of importance for the CO hydrogenation mechanism [Bezemer et al., 2006a; Kim et al., 1997; Ojeda et al., 2004]. Microemulsion, a novel technique for catalyst preparation, enables the control of metal particle size with a narrow particle size distribution, regardless of metal content [Eriksson et al., 2004; Kim et al., 1997; Martinez and Prieto, 2007; Tago et al., 2000]. Briefly, a microemulsion consists of nano-sized water droplets surrounded by an oil phase, stabilized by a surfactant [Eriksson et al., 2004]. The size of the cobalt particles formed in water-in-oil (w/o) microemulsions is controlled by changing the micelle size (the water-to-surfactant ratio) [Eriksson et al., 2004]. Hanaoka et al. and Hayashi et al. have shown that the catalysts prepared by water-in-oil microemulsion increases the CO hydrogenation rate, the H2 chemisorption rate and the C_{2+} selectivity [Eriksson et al., 2004; Hanaoka et al., 1997; Hayashi et al., 2002; Kim et al., 1997; Ojeda et al., 2004; Tago et al., 2000]. Also, Hayashi et al. found that the activity of a Fe/SiO_2 catalyst prepared by microemulsion was higher than that of the same average particle size catalyst prepared by incipient wetness impregnation [Hayashi et al., 2002]. However, it has been also shown that cobalt nanoparticles obtained by microemulsion techniques interact strongly with oxygen-carrying ceramic supports (such as Al_2O_3, SiO_2 and TiO_2). Such interactions lead to a decrease of the catalyst reduction efficiency [Bezemer et al., 2006b; Martinez and Prieto, 2007; Saib et al., 2002]. Therefore, oxidic carriers impose serious limitations to the investigation of structure-sensitive effects in FT catalysis because of the co-existence of incompletely reduced cobalt phase, caused by strong interaction with the oxidic carrier [Saib et al., 2002;

Tavasoli et al., 2008a; Tavasoli et al 2008b]. Specifically, nanoparticles synthesized by microemulsion are known to be more difficult to reduce on oxidic carriers. Although, Martine`z et al., has shown that with modifying the catalyst carrier (silylated ITQ-2), high reducibility can be obtained using microemulsion as the catalyst preparation route [Martinez and Prieto, 2007]. Moreover, our previous work has shown that carbon nanotubes (CNT), when used as a cobalt catalyst support, allow a better metal dispersion control and minimize the metal phase interaction (formation of mixed compounds) with the support [Tavasoli et al., 2008a; Trépanier et al., 2009a; Trépanier et al., 2009b]. Chen et al. observed that the confinement of the Fe particles within the CNT enables a better reducibility and leads to higher rates of the CO dissociative adsorption on the metal surface [Chen et al., 2008]. Since the chemisorption of reactants is the rate determining step on FTS reaction, a cobalt particle located inside the tubes must be more active than one on the outer surface of the CNT [Chen et al., 2008; Tavasoli et al., 2008a; Trépanier et al., 2009a; Trépanier et al., 2009b]. Although, it is not clear until now, if this phenomenon is due only because of the metal–CNT walls particular interactions.

This present work compares the proposed microemulsion technique for catalyst preparation with the incipient wetness impregnation method for the control of cobalt metal particle size using CNTs as a catalyst carrier. The influences of cobalt particle size on the FTS Co/CNT catalysts on their activity and selectivity as well as the reducibility were evaluated and reported. A critical discussion allows drawing useful scientific and technical conclusions.

6.3 Experimental

6.3.1 Catalyst preparation

Prior to catalyst preparation, the Mknano-MWCNT (>95%) support was treated with 30 wt. % HNO_3 at 100 ^oC overnight, washed with distilled water, and dried at 120 ^oC for 6 h. Cobalt particles were synthesized in a reverse microemulsion using a nonionic surfactant Triton X-100 (Aldrich) and cyclohexane (C_6H_{12}) as the oil phase. The concentration of cobalt was adjusted using aqueous cobalt nitrate ($Co(NO_3)_2 6H_2O$ 99.0 %, (Merck) up to 10 wt.%. The water-to-surfactant molar ratio (W/S) was varied from 3 to 10. After vigorous stirring, a microemulsion was obtained (15 min). Hydrazine was

added in excess (hydrazine/Co = 10) to improve cobalt nanoparticle formation in the core of the micelles by reducing the cobalt oxide [Dauscher et al., 1993; Eriksson et al., 2004; Martinez and Prieto, 2007]. Then, the appropriate weight of purified carbon nanotubes was added under stirring. During the 3 h of stirring, tetrahydrofurane (THF), an emulsion destabilizing agent, was added drop wise (1 ml/min). A fast addition could lead to fast particle agglomeration and uncontrolled particle deposition on the support (CNT) [Dauscher et al., 1993; Eriksson et al., 2004; Martinez and Prieto, 2007]. The mixture was left to mature and settle slowly overnight and then decanted. The solid sample was recovered by vacuum filtration using ash less 90 mm Ø x 100 circle filtration paper (Whatman1) and washed several times with ethanol. In order to remove the remaining traces of surfactant and nitrates, the catalysts were calcined under argon (Ar) flow at 450 ^{o}C for 3 h and slowly exposed to an oxygen atmosphere during the cooling step. The catalysts prepared by means of this protocol were denoted as $MECo_a$ for a W/S ratio of 3, $MECo_b$ for a W/S ratio of 5 and $MECo_c$ for a W/S ratio of 10 (see Table 6.1). The control catalyst was prepared using the incipient wetness impregnation method (IWCod). Cobalt nitrate ($Co(NO_3)_2 6H_2O$ 99.0 %, Merck) solution was added to the treated CNT as the support up to 10 wt. % Co. After the impregnation step, the catalyst was dried at 120 ^{o}C and calcined at 450 ^{o}C under Ar flow for 3 h and slowly exposed to an oxygen atmosphere during the cooling step. The cobalt loading of 10%.wt in all the calcined catalysts was verified by an Inductively Coupled Plasma Atomic Emission Spectroscopy (ICP-AES) system.

6.3.2 Catalysts characterization

The treated CNTs and the catalysts were characterized by Transmission Electron Microscopy (TEM). Sample specimens for TEM studies were prepared by ultrasonic dispersion of the catalysts in methanol. The suspensions were dropped onto a carbon coated copper grid. TEM investigations were carried out using a Hitachi H-7500 (120 kV).

The surface area, pore volume, and average pore radius of the catalysts were measured by an ASAP-2000 system from Micromeritics. The samples were degassed at

200 ^{o}C for 2 h under 50 mTorr vacuum and their BET area, pore volume, and average pore radius were determined.

XRD measurements of the calcined catalysts were conducted with a Philips PW1840 X-ray diffractometer with monochromatized Cu/Kα radiation. Using the Scherer equation, the average size of the Co_3O_4 crystallites in the calcined catalysts was estimated from the line broadening of a Co_3O_4 peak at 2θ of 36.8^{o}.

Temperature programmed reduction (TPR) spectra of the calcined catalysts were recorded using a CHEMBET-3000, equipped with a thermal conductivity detector. The catalyst samples were first purged in a flow of Ar at 150 ^{o}C, to remove traces of water, and then cooled to 40 ^{o}C. The TPR of 0.1 g of each sample was performed using 3.1 % hydrogen in nitrogen gas mixture with a flow rate of 40 cm^3/min. The samples were heated from 40 to 800 ^{o}C with a heating rate of 10 ^{o}C/min.

The amount of chemisorbed hydrogen (H_2) on the catalysts was measured using the Micromeritics TPD-TPR 290 system. 0.25 g of the calcined catalyst was reduced under H2 flow at 400 ^{o}C for 20 h and then cooled to 70 ^{o}C, always under H_2 flow. Then the flow was switched to Ar at the same temperature; this step, used to remove the physisorbed H_2, lasted for about 30 minutes. The subsequent temperature programmed desorption (TPD) of the samples was obtained by increasing the temperature of the samples, at a ramp rate of 20 ^{o}C/min, to 400 ^{o}C under Ar flow. The resulting TPD spectra were used to determine the cobalt dispersion and its surface average crystallite size. The % dispersion and particle diameter are calculated by the equations below [Tavasoli et al., 2008b]:

$$\text{Calibration value } (l_{gas}/\text{area units}) = \frac{\text{loop volume} \times \%\ \text{analytical gas}}{\text{mean calibration area} \times 100} \quad (6.1)$$

$$H_2 \text{ uptake } (\text{moles}/g_{cat}) = \frac{\text{analytical area from TPD} \times \text{calibration value}}{\text{Mean calibration area}} \quad (6.2)$$

$$\%\ \text{Dispersion} = \frac{H_2 \text{ uptake} \times \text{atomic weight} \times \text{stoichiometry}}{\%\ \text{metal}} = \frac{\text{number of } Co^{o} \text{ atoms on the surface} \times 100}{\text{total number of } Co^{o} \text{ atom}} \quad (6.3)$$

$$\text{diameter (nm)}_{\text{total Co}} = \frac{6000}{\text{density} \times \text{maximum area} \times \text{dispersion}} \quad (6.4)$$

6.3.3 Reaction testing

The catalysts were evaluated in terms of their FTS activity (g HC produced/g_{cat}./h) and selectivity (the percentage of the converted CO that appears as a hydrocarbon product) in a fixed bed microreactor (Figure 6.1).

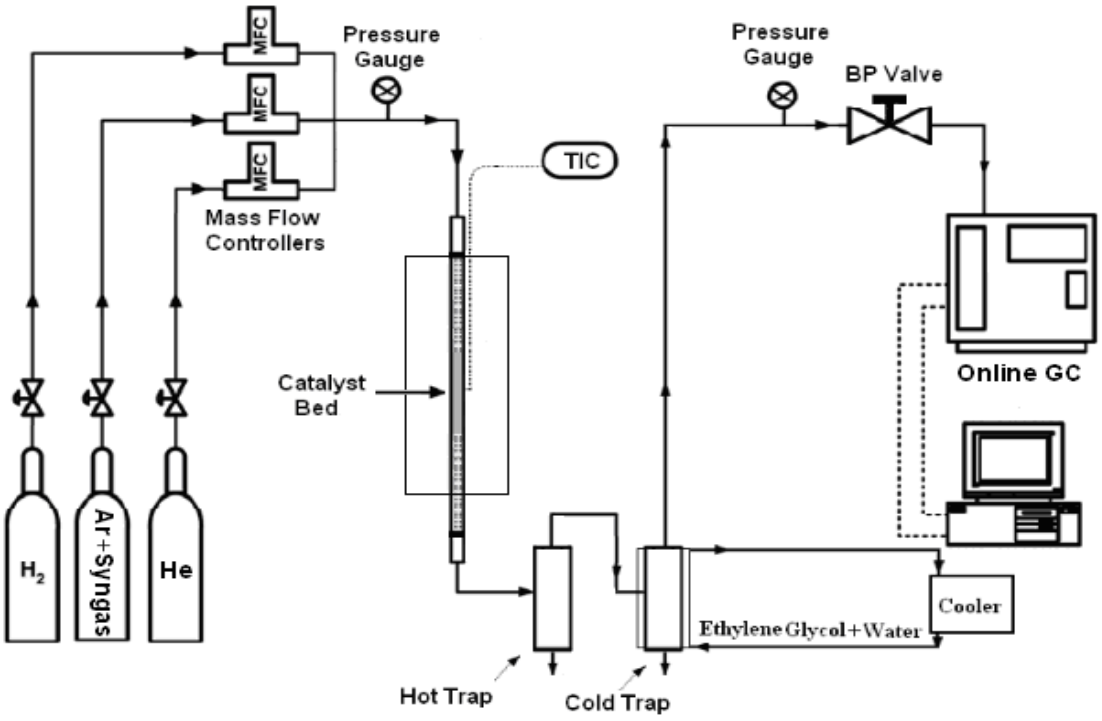

Figure 6. 1: Experimental set-up for FTS

Catalyst activation was conducted first in situ under pure hydrogen at a flow rate of 60 ml/min and a temperature of 380 ^{o}C for 20 h. After the catalyst reduction period, the mixed gases (CO,H_2 and Ar) were fed at a flow of 30 ml/min, a temperature of 220 ^{o}C, a H_2/CO = 2 and a pressure of 2MPa. The products were continuously removed from the reactor and passed through two traps, one maintained at 100 ^{o}C (hot trap) and the other at 0 ^{o}C (cold trap). The uncondensed vapor stream was depressurized to atmospheric pressure through a back pressure regulator. The composition of the outlet gas stream was determined using an on-line GC-2014 Shimadzu gas chromatograph. The contents of hot

and cold traps were removed every 24 h. The hydrocarbon and water fractions were separated, and then analyzed by Varian 3400 GC liquids analyzer.

6.4 Results and discussion

6.4.1 Catalysts characterization

The main purpose of the TEM study is to (1) show the effects of acid treatment (defects and open caps) on the CNT (Figure 6.2), (2) demonstrate the narrow uniformity of the particles made by microemulsion technique (Figure 6.3) and, (3) show the particles that are inside and outside the CNTs (Figure 6.3). Figure 6.2 shows the defects and the open caps which resulted from the acid treatment on the CNT support.

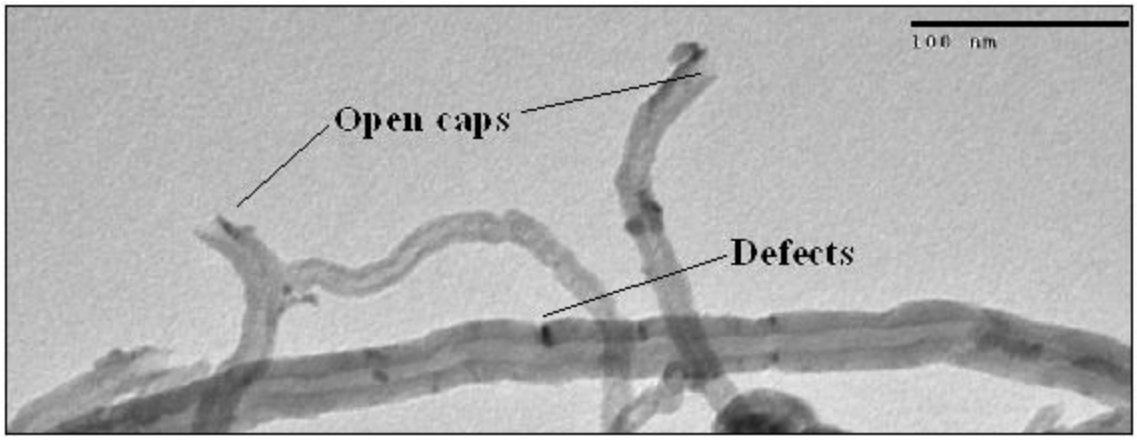

Figure 6. 2: TEM picture showing the effects of acid treatment on the CNT support: formation of open caps and defects.

According to our previous works, the purpose of functionalization of CNT support is to increase the BET surface area and the cobalt dispersion on catalyst surface by allowing cobalt particles to go inside the CNTs [Trépanier et al., 2009a; Trépanier et al., 2009b]. In fact, the inner particles of the CNTs are easier to reduce than the ones located outside the CNTs. Thus, these particles improve the selectivity for FTS products by enhancing the CO dissociative adsorption on the metal surface [Chen et al., 2008; Tavasoli et al., 2008a; Tavasoli et al., 2008b; Trépanier et al., 2009a; Trépanier et al., 2009b]. The TEM images of the catalysts made by the proposed microemulsion preparation route are shown in Figure 6.3(a)–(e).

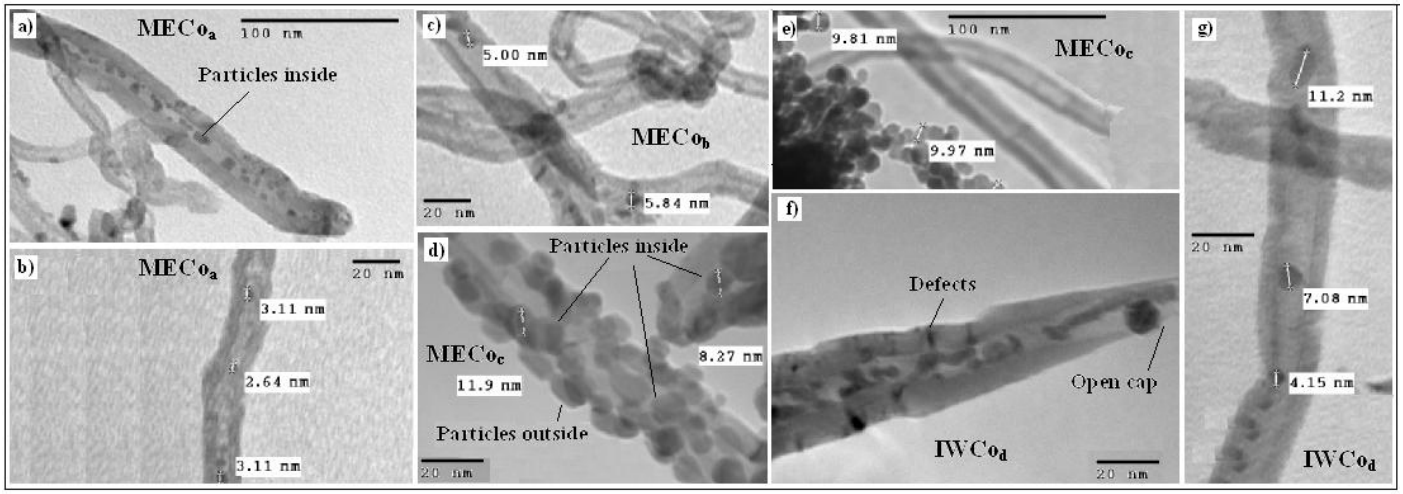

Figure 6. 3: TEM pictures of the calcined catalysts showing (a) the particles inside the CNT for the MECo$_a$ catalyst and the particles size of the (b) MECo$_a$ catalyst (3nm), (c) MECo$_b$ catalyst (5nm), (d) the particle outside and inside the MECo$_c$ catalyst, (e) the particle size of the MECo$_c$ catalyst (10 nm), (f) the defects and the open cap onto the CNT after acid treatment and (g) the particles size of the IWCo$_d$ catalyst

The MECo$_a$ and MECo$_b$ catalyst particles are both dispersed mostly inside the tubes and on the outer surface of the CNT walls. For the MECo$_c$ (9–10 nm) catalyst, the percentage of the particles lying at the outer surface of the CNT walls is higher compared to the other catalysts prepared by microemulsion (Figure 6.3(d)). Indeed, the narrow inner diameter of the CNT channels (8–10 nm) restricted the insertion of particles in sizes close to the channel diameter (10 nm). The average particle sizes for MECo$_a$, MECo$_b$ and MECo$_c$ are linearly depending upon their respective water-to-surfactant ratio (3, 5 and 10). The most abundant particle sizes for the MECo$_a$ catalyst are within the range of 2–3 nm (Figure 6.3(a) and (b)). MECo$_b$ and MECo$_c$ catalysts have Co particle sizes in the range of 5–6 nm and 9–10 nm, respectively (see Figure 6.3(c)–(e)). Figure 6.3(f) and (g) show the TEM images of the IWCo$_d$ catalyst made by the incipient wetness impregnation route. Similar to our previous works, the smaller cobalt particles are lying inside the CNT channels and the larger particles on the outside. The average particle size of the IWCo$_d$ catalyst is within the range of 6–10 nm [Trépanier et al., 2009a; Trépanier et al., 2009b]. In this case, the cobalt particles are formed within the CNT during the impregnation and

calcination steps. CNT channels have restricted the growth of the particles inside the tubes from 4 to 9 nm. Almost all particles of sizes 10 nm and over are lying on the outer surface of the CNT walls.

Figure 6.4 depicts the size distribution of the cobalt particles, which is determined using the population of the total cobalt particles of each $MECo_a$, $MECo_b$, $MECo_c$ and $IWCo_d$ catalysts based on data taken from 10 TEM pictures.

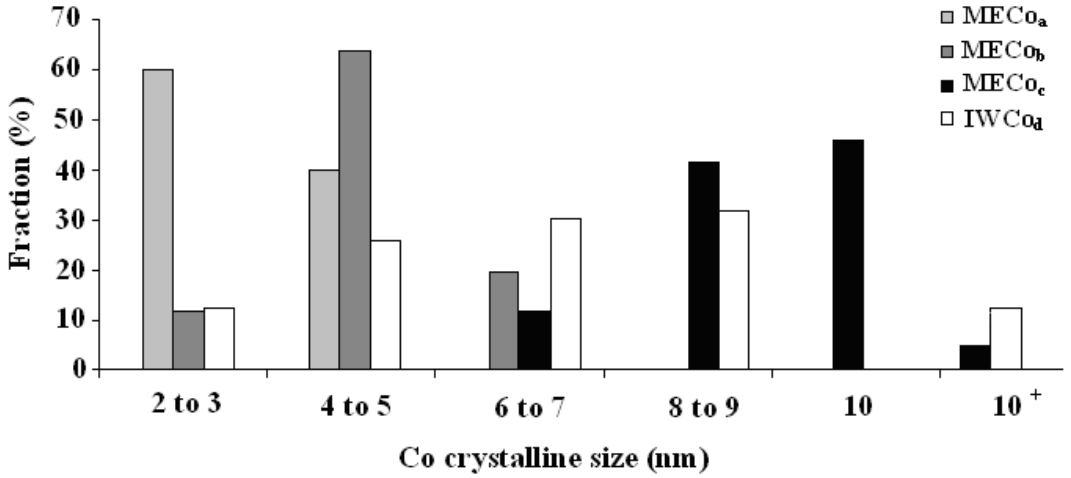

Figure 6. 4: A bar graph depicting the particles size distributions for the calcined $MECo_a$, $MECo_b$, $MECo_c$, $IWCo_d$ catalysts.

This figure, as well as the TEM pictures, shows that microemulsion preparation route enables to control a narrow nanoparticle size distribution with different water to surfactant ratios. For example, Figure 6.4 shows that for the W/S ratio of 3, 5 and 10, the average particle sizes are 2–3 ± 0.27, 5–6 ± 0.53 and 8–10 ± 1 nm, respectively. According to Figure 6.4, the average particle size for the catalyst prepared by incipient wetness impregnation method ($IWCo_d$) is 6–10 ± 1 nm and over. This results is in accordance with our previous work and Tavasoli et al., observation for 10 wt.% Co/CNT [Tavasoli et al., 2008b; Trépanier et al., 2009a; Trépanier et al., 2009b].

Results of the surface area measurements are shown in Table 6.1.

Table 6. 1: Selected catalyst properties

Catalysts	Co (wt. %)	Preparation route	BET (m^2/g)	Pore volume (cm^3/g)	Pore radius (nm)	XRD d (Co_3O_4) nm
CNT	-	-	210	0.63	6.1	-
$MECo_a$	10	Microemulsion	185	0.54	5.5	5.6
$MECo_b$	10	Microemulsion	177	0.54	5.7	7.1
$MECo_c$	10	Microemulsion	173	0.53	6.6	10.5
$IWCo_d$	10	Incipient Wetness	191	0.60	6.8	11.2

These results show that the BET surface area of $MECo_a$, $MECo_b$, and $MECo_c$ catalysts decreases from 185 to 177 and 173 m^2/g, respectively. The pore volumes of different catalysts prepared by microemulsion route did not change and remained at 0.53– 0.54 cm^3/g. The lower BET surface area and pore volume of the $MECo_a$, $MECo_b$ and $MECo_c$ catalysts are comparable to the values obtained for pure CNTs (210 m^2/g, 0.63 cm^3/g), indicating some pore blockage due to cobalt loading on the support. The BET surface area and the pore volume of the IWCod are higher than the catalyst prepared by microemulsion technique (191 m^2/g, 0.60 cm^3/g), indicating less pore blockage.

X-ray diffraction patterns of the calcined catalysts are shown in Figure 6.5.

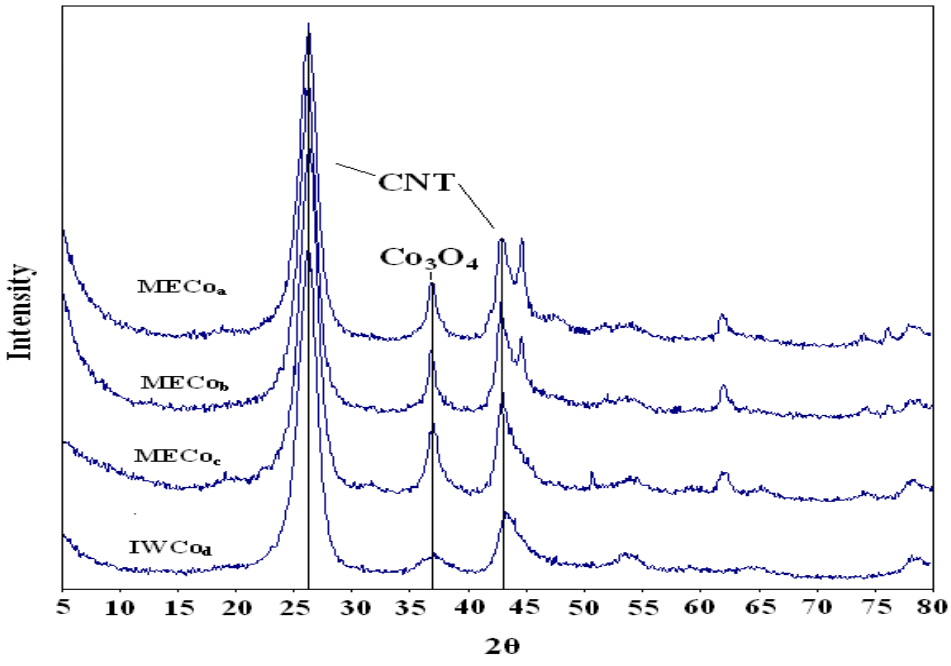

Figure 6. 5: XRD patterns of the calcined catalysts: CNT (25.8° and 43°), Co_3O_4 (36.8°).

In the XRD spectra the peaks at 2θ values of 25° and 43° correspond to the CNT support, while the other peaks in the spectra of the catalysts are related to different crystal planes of Co_3O_4 [Bezemer et al., 2004]. The peak at 2θ value of 36.8° is the most intense one of Co_3O_4 in XRD spectra of all catalysts. Minor peaks were also observed at 44°, 52° and 74°, for the catalysts which correlate with a cubic cobalt structure [Jacobs et al., 2002]. This structure has no influence on the product selectivity [Jacobs et al., 2002]. Table 6.1 shows the average Co_3O_4 particle size of the catalysts calculated from XRD spectra using the Scherer equation at 2θ value of 36.8° [Bechera et al., 2001]. The average Co_3O_4 cluster size was determined after calcinations for the $MECo_a$, $MECo_b$, $MECo_c$ and $IWCo_d$ as approximately 5.6, 7.1, 10.5 and 11.2 nm, corresponding to 4.2, 5.3, 7.6 and 8.5 nm when reduced to metal, respectively. This agrees reasonably well with the cobalt particle diameter obtained with the H_2 chemisorption results (Table 6.2). As shown in Table 6.1, the average particle sizes of Co_3O_4 are linearly correlated with the water-to-surfactant ratio used during the microemulsion catalyst preparation route; the latter is also confirmed by TEM pictures of the $MECo_a$, $MECo_b$, and $MECo_c$ (Figure 6.3). In fact, nanoparticles are formed in the internal structure of the microemulsion, which is determined by the ratio of water-to-surfactant. At high oil concentration, the bicontinuous phase is transformed into a structure of small water droplets within a continuous oil phase (reverse micelles) when surfactant is added (Figure 6.6).

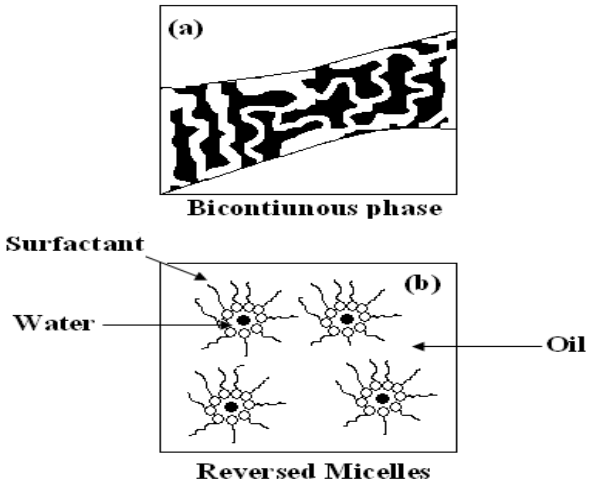

Figure 6. 6: Microemulsion structure at a given concentration of surfactant: (a) Water-in-oil phase, (b) Formation of cobalt particles (black dotes) within the reversed micelles with the addition of surfactant.

Thus, the results show that the size of different droplets determines the cobalt's particle size, depending on the amount of surfactant [Eriksson et al., 2004].

The reducibility of the catalysts in H_2 atmosphere was determined by TPR experiments. The TPR spectra of the calcined $MECo_a$, $MECo_b$, $MECo_c$ and $IWCo_d$ are shown in Figure 6.7 and the specific reduction temperatures are presented in Table 6.2.

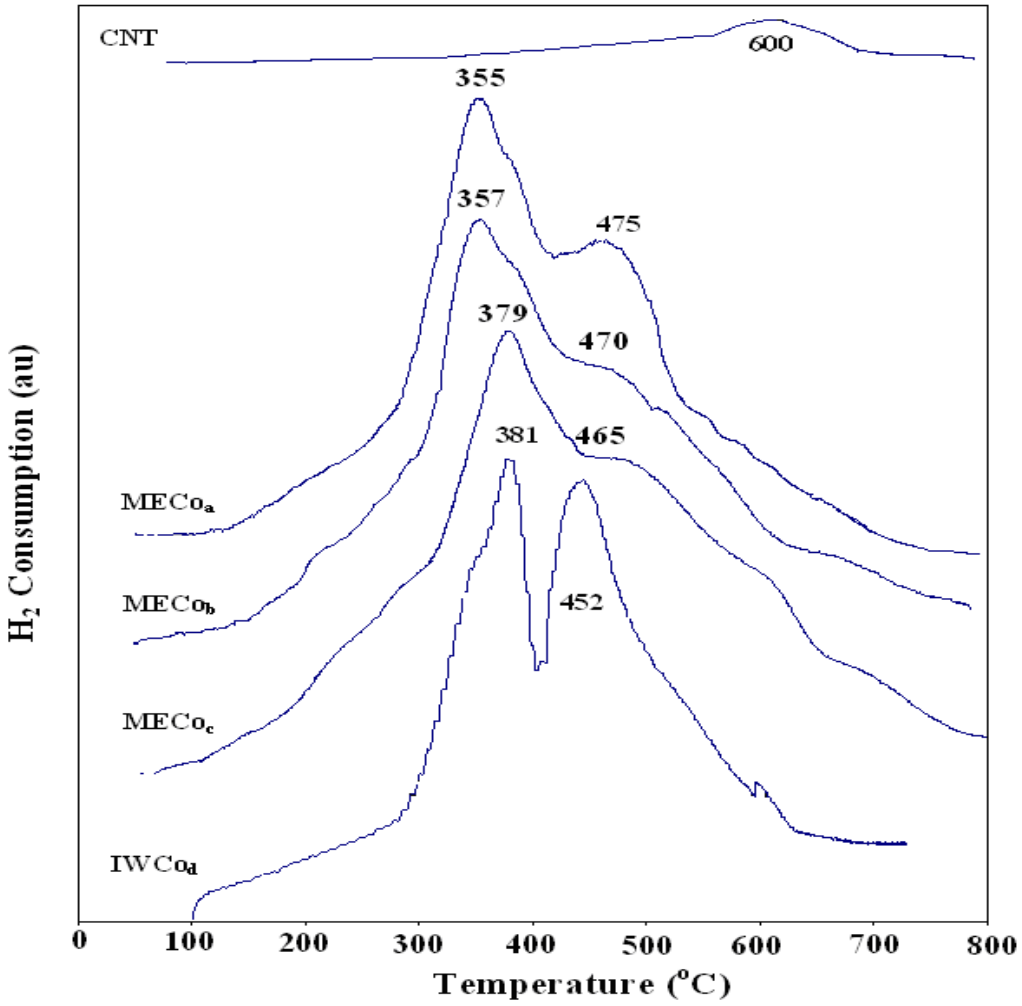

Figure 6. 7: Temperature Programmed Reduction profiles for the calcined $MECo_a$, $MECo_b$, $MECo_c$ and $IWCo_d$ catalysts.

Table 6. 2: TPR and TPD results

Catalysts	1st TPR peak (°C)	2nd TPR peak (°C)	Reductibility ratio	H_2 uptake (μ mole H_2 desorbed /g cat.)	%Dispersion	Co^o d_p (nm)
$MECo_a$	355	475	0.70	526	26.2	3.6
$MECo_b$	357	470	0.85	379	16.8	5.9
$MECo_c$	379	465	0.91	306	13.2	7.8
$IWCo_d$	381	452	1	276	12.8	7.9

The low temperature peak (300–400 °C) is typically assigned to reduction of Co_3O_4 to CoO, although a fraction of the peak likely comprises the reduction of the larger, bulk-like CoO species to Co^o [Huffman et al.,1994; Lin et al., 2004]. The second broad peak is assigned to reduction of small CoO to Co^o species, which also includes the reduction of cobalt species that interact with the support. The small peak at about 600 °C in the TPR spectra of the catalysts can be assigned to the gasification of support as indicated by TPR of pure CNT support at about 600 °C (Figure 6.5).

According to Figure 6.7, the deposition of cobalt nanoparticles synthesized by microemulsion on the CNTs shift the reduction step of the Co_3O_4 to CoO species (first peak) to a lower temperature compared to the catalyst impregnated by the common method; indicating higher reducibility for uniform particles ($MECo_c$). Interestingly, the reduction temperature of the first peak also decreases with decreasing cobalt particle size from 10 to 3 nm. According to the TEM pictures of the catalysts prepared by microemulsion technique, most of the small particles (<9 nm) are inside the tubes, especially for the $MECo_a$ catalyst, which in turn leads to a better interaction with the intern electron deficient walls of the CNTs and favors the reduction of Co_3O_4 species [Chen et al., 2008]. The tubular morphology of the graphene layers make CNTs different compared to other carbonaceous supports. Thus, it is well known that the exterior surfaces of the CNTs are electron-rich, whereas the interior ones are electron-deficient, which could influence metal and metal oxide particles in contact with either surface [Chen et al., 2008; Tavasoli et al., 2008b]. Chen et al. studies reveal that deviation of the grapheme layers from planarity causes π-electron density to shift from the concave inner

surface to the convex outer surface, leading to an interior electron-deficient surface and an exterior electron enriched surface [Chen et al., 2008]. Moreover, Chen et al., have particularly found that particles inside the carbon nanotubes are more catalytically active than particles on the outside surface [Chen et al., 2008].

Although, the second reduction peak for the $MECo_a$, $MECo_b$ and $MECo_c$ catalysts shifts to higher temperatures such as 475, 470 and 465 ^oC compared to 452 ^oC for the $IWCo_d$ catalyst. As expected in case of larger cobalt particle sizes (>10 nm), the catalyst prepared by impregnation ($IWCo_d$) displays better reducibility for the second reduction step. Indeed, the degree of interaction with the metal phase and the support varies with the cobalt particle sizes, larger CoO particles are reduced more easily than smaller CoO particles [Bezemer et al., 2006a; Bezemer et al., 2006b; Trépanier et al., 2009b]. Figure 6.7 also indicates that by decreasing the cobalt particle size, the broad shoulder of the second TPR peak becomes larger, suggesting more difficult reduction process for CoO species with 2–3 nm cobalt particles.

According to Figure 6.7, there is no significant evidence of formation of metal-support compounds on the catalyst surface due to the absence of significant reduction peaks above 500 ^oC. Thus, Tavasoli et al., as well as Martinez et al. have noted that reduction peak present at temperatures above 530 ^oC with oxidic carrier shows formation of cobalt species that are difficult to reduce (oxide compounds). CNT as an inert support for cobalt catalyst do not show any peak related to formation of metal-support compounds as compared to $Co/\alpha\text{-}Al_2O_3$ catalysts suggesting an easier reduction process with CNT than with oxidic carriers [Tavasoli et al., 2008a; Tavasoli et al., 2008b].

Table 6.2 also shows the reducibility ratio of all tested catalysts. The reducibility ratio was correlated to the amount of H_2 consumed (area under the peaks) for each part of the reduction steps (Co_3O_4 to CoO and CoO to Co^o). Thus, to have a better understanding of the compared reducibility of the catalysts, the areas under the TPR peaks have been divided into two parts for $MECo_a$, $MECo_b$, $MECo_c$ and $IWCo_d$ catalysts and were calculated by integration. The areas of the peaks are proportional to the amount of H_2 consumption. The first part is defined from 25 to 450 ^oC and the second part is defined from 450 to 800 ^oC. The results show that by increasing the cobalt particle size from 3 to 5 and 10 nm, the ratio of H_2 consumption of part two (500 to 800 ^oC) to the H_2

consumption of part one (25 to 500 ^{o}C) decreased from 0.6 to 0.54 and 0.49, respectively. This confirms that by increasing the cobalt particle size, the reduction temperature for the species that need to be reduced at high temperatures decreases suggesting an easier reduction for larger cobalt particles. Table 6.2 also shows that the reducibility ratio of the catalyst prepared by microemulsion $MECo_c$ is closer to that of the $IWCo_d$ catalyst. Martinez et al., also observed that microemulsion preparation technique with a less oxidic carrier almost suppresses the formation of cobalt species which are normally difficult to reduce with an oxidic support [Martinez and Prieto, 2007] .Indeed, Ernst et al., have observed that cobalt catalyst particles (1–5 nm) prepared by microemulsion route are usually more difficult to reduce with oxidic support carriers than those produced by incipient wetness impregnation [Ernst et al., 1999].

To conclude, uniformity of nanoparticles synthesized by core reverse micelle as well as particles confined inside the CNT improved the first reduction step of the catalysts, but increased the reduction temperature for the CoO to Co^{o} compounds. Thus, particles within the CNTs are easily reduced because of the confinement phenomenon for the first reduction step but the reducibility is still more influenced by the particle size for the second step of reduction. Therefore, the confinement of Co particles in the CNT channels allowed high catalyst reducibility which does not normally occurs with nanoparticle supported on other common carriers [Chen et al., 2008; Ernst et al., 1999; Martinez et al., 2003; Martinez and Prieto, 2007]. Consequently, no significant reducibility limitations were observed for any of the catalysts studied.

The results of the temperature programmed desorbtion (TPD) of the $MECo_a$, $MECo_b$, $MECo_c$ and $IWCo_d$ catalysts are also given in Table 6.2. This table shows that in case of $MECo_a$, $MECo_b$ and $MECo_c$ catalysts, the hydrogen chemisorption (H_2 uptake) decreases with increasing the cobalt particle sizes up to 10 nm in accordance with the % dispersion of the cobalt particles. Thus, increasing the cobalt particle size decreases the % dispersion from 26.2 to 12.8 % (see Table 6.2).

The H_2 uptake of the $MECo_c$ catalyst is higher than the $IWCo_d$ catalyst, inspite of similar Co particle size (7.8 and 7.9 nm). Martinez et al, have shown that narrow particle size distributions obtained by the microemulsion preparation route are more efficient for H_2 chemisorption than particle size distributions obtained with the impregnation method

[Martinez and Prieto, 2007]. Moreover, Bezemer et al observed that H_2 uptake is directly related to particle size for particles less than 10 nm, a trend which levels-off for bigger particles. This can also explain the similarity of H_2 uptake between the $MECo_c$ and $IWCo_d$ catalysts [Bezemer et al., 2006a].

6.4.2 Activity and product selectivity for FTS

The catalytic activity and product selectivity data have been calculated for runs showing catalyst stability within the first 24 h of operation and have been reproduced twice to confirm the results reproducibility. Figure 6.8 shows the influence of cobalt particles size on FTS rate (g HC produced/g_{cat}./min), olefin/paraffin mass ratio, C_{5+} and methane (CH_4) selectivity.

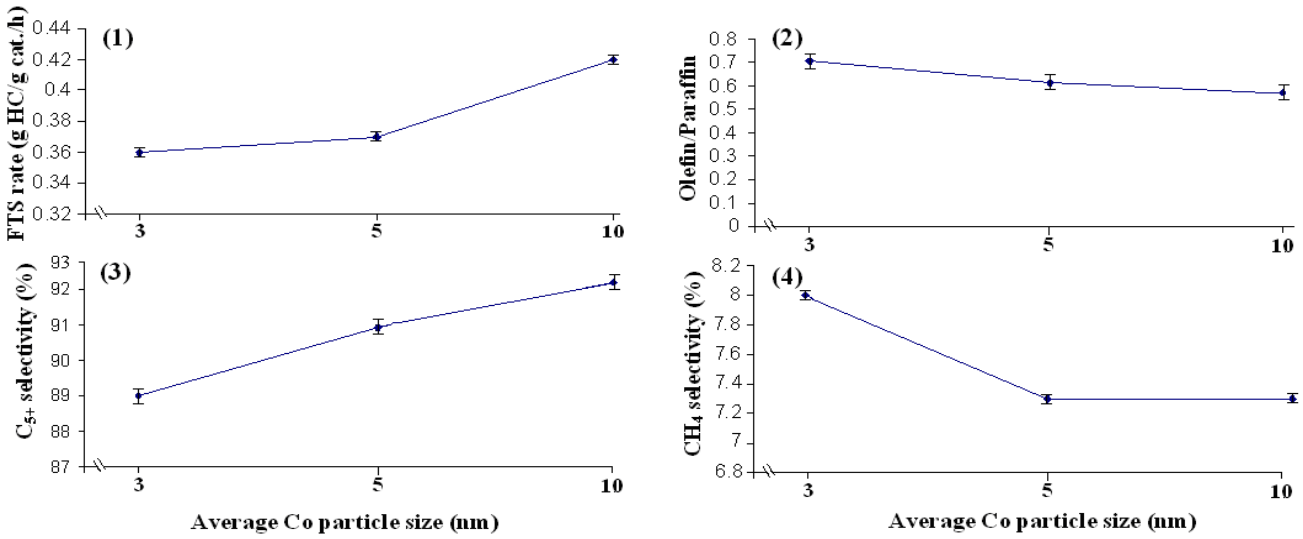

Figure 6. 8: Influence of cobalt particles size on (1) FTS rate (gHC/gcat./h), (2) Olefin to paraffin ratio, (3) C_{5+} selectivity and (4) CH_4 selectivity.

These preliminary results show that the FTS activity decreases as the size of the CNT-supported cobalt particles is decreased to < 10 nm. This is in accordance with Bezemer et al. observations showing lower activity for particles smaller than 10 nm [Bezemer et al., 2006a; Bezemer et al., 2006b]. Bezemer et al. found that the maximum concentration of surface Co^o sites and FTS activity are achieved with catalyst particle sizes less than 10 nm on carbon nanofiber supports [Bezemer et al., 2006a]. In our case, the optimum has

not been evaluated due to the internal CNT diameter restriction and the particle confinement concern in our study. Indeed, Chen et al. observed that particle size is not the only property to have an effect on the FTS activity [Chen et al., 2008]. In our work, the particles are mostly inside the CNT walls for the $MECo_a$, $MECo_b$ and $IWCo_d$ (Figure 6.3). It appears that the particles located inside the CNT and the particle size itself influences the FTS activity [Bezemer et al., 2006a; Bezemer et al., 2006b; Chen et al., 2008]. However, the particle's confinement within CNTs may be more important than the particle size effect for the FTS activity. Figure 6.8 clearly shows that the CH_4 selectivity is reduced with increasing cobalt cluster size. Compared to $MECo_a$ and $MECo_b$ catalysts, the $MECo_c$ catalysts showed 1.2 % lower selectivity to methane. The systematic error of the test was ± 0.1 %which indicates a significant change on the selectivity of methane. The lower production rate of CH_4 for the cobalt catalyst could be due to the effective participation of olefins in the carbon–carbon chain propagation. Thus, on the $MeCo_c$ catalyst, α-olefins of the type R–CH=CH_2 can compete with carbon monoxide and heavier olefins for re-adsorption and chain initiation. Moving upward with average particle sizes from 3 to 10 nm resulted in 4% improvement in the C_{5+} selectivity of the catalyst. Bezemer et al. reported that a minimum cobalt particle size of 8 nm is necessary to give high C_{5+} selectivity [Bezemer et al., 2006a]. According to Figure 6.8, at the range of 2–3 nm the C_{5+} selectivity is already 89 wt. %. This result reveals that the dissociative adsorption of CO and chain growth probability (α-olefins re-adsorbtion) on the propagation step is efficient even with 2–3 nm particles due to beneficial electronic properties of the internal CNT walls. The walls electron deficiency inside the carbon nanotubes enhances the CO chemisorption and enlarges the residence time of the reactants, thus allowing more probability of longer carbon chains to be formed (see higher selectivity observed in C_{5+} compounds) [Chen et al., 2008; Tavasoli et al., 2008b; Trépanier et al., 2009a; Trépanier et al., 2009b]. The selectivity for C_{5+} products on the CNT-supported cobalt catalyst is still higher for larger particles (10 nm). However, when compared to Bezemer et al. results obtained on smaller Co particles (<8 nm) supported on oxidic substrates, the results obtained in our case do not show the same degree of differentiation. This is most probably due to the fact that small particles (<8 nm) confined inside CNTs are more stable than those of the same size supported on oxidic carrier

[Bezemer et al., 2006a; Martinez and Prieto, 2007]. According to Chen et al. the particle sintering is effectively prevented inside CNTs due to spatial restriction of the CNT channels which stabilized the activity and selectivity of the cobalt particles [Chen et al., 2008]. The olefin/paraffin mass ratio decreases from 0.7 to 0.58 with increasing the particle size. Catalysts with high C_{5+} selectivity and cobalt particles smaller than 8 nm usually show a substantial increase in the paraffin over olefin ratio [Martinez ans Prieto, 2007]. It should be mentioned that the measurements for α-olefin/n-paraffin ratios were taken for C_2–C_8 hydrocarbons in this work. Therefore, the slight decreasing might be related to the lower amount of CH_4 for larger cobalt particles that can produce 1-alkene (olefins). 1-alkenes are regarded as primary products of the FTS propagation step and may be hydrogenated to alkanes or isomerized to 2-alkenes in the course of the reaction [Madon and Iglesia, 1993].

Figure 6.9 shows the true boiling point (TBP) distillation curve for all the catalysts (C_{10} to C_{40}).

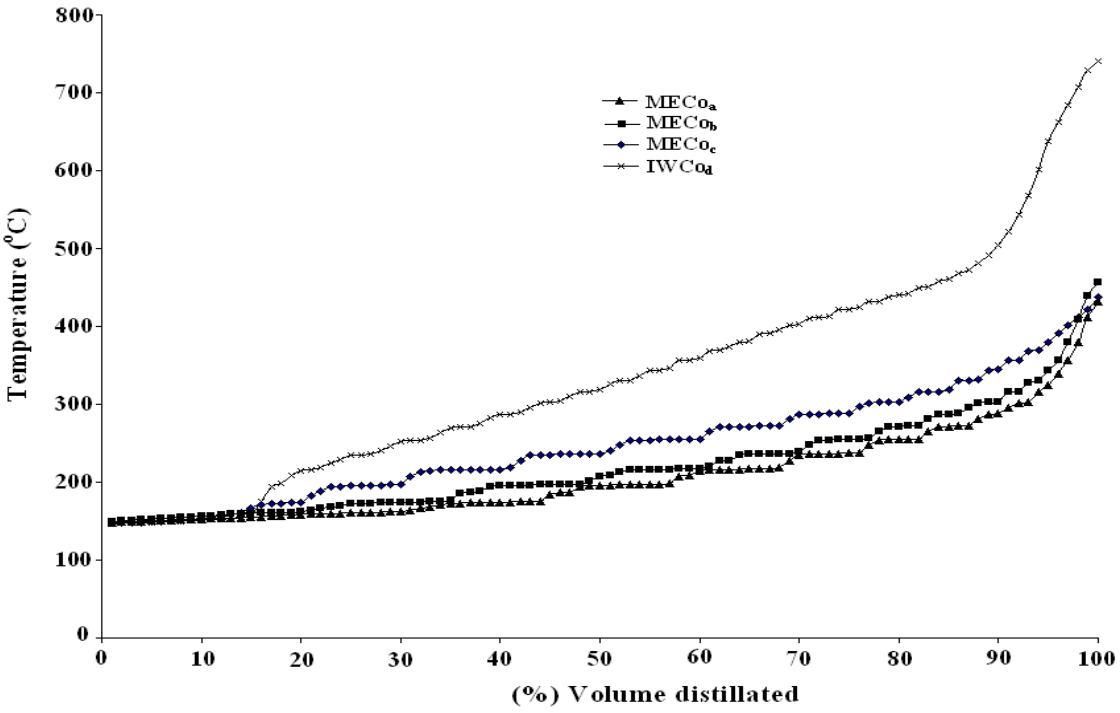

Figure 6. 9: True Boiling Point distribution according to hydrocarbons collected into hot trap for all the catalysts after 24h operation at 220°C, 2 MPa and H_2/CO=2.

The TBP distillation curves show that after the C_{10} hydrocarbon chain, larger cobalt particles are more selective for heavier molecular weight hydrocarbons (Figure 6.9). These results show that with increasing the cobalt cluster size, there is a shift in hydrocarbons to higher molecular weights. It seems that the steric hindrance for dissociative adsorption of CO and -CH_2- monomer and addition of this monomer to the growing chain is better in the larger cobalt clusters. Moreover, Ernst et al. observed that higher reduction degree of cobalt favors the production of higher molecular weight hydrocarbons (waxes) [Ernst et al., 1999].

Figure 6.10 shows the comparative C_{5+} selectivity, olefin/paraffin ratio and CH_4 selectivity for the $MECo_c$ and $IWCo_d$ catalysts.

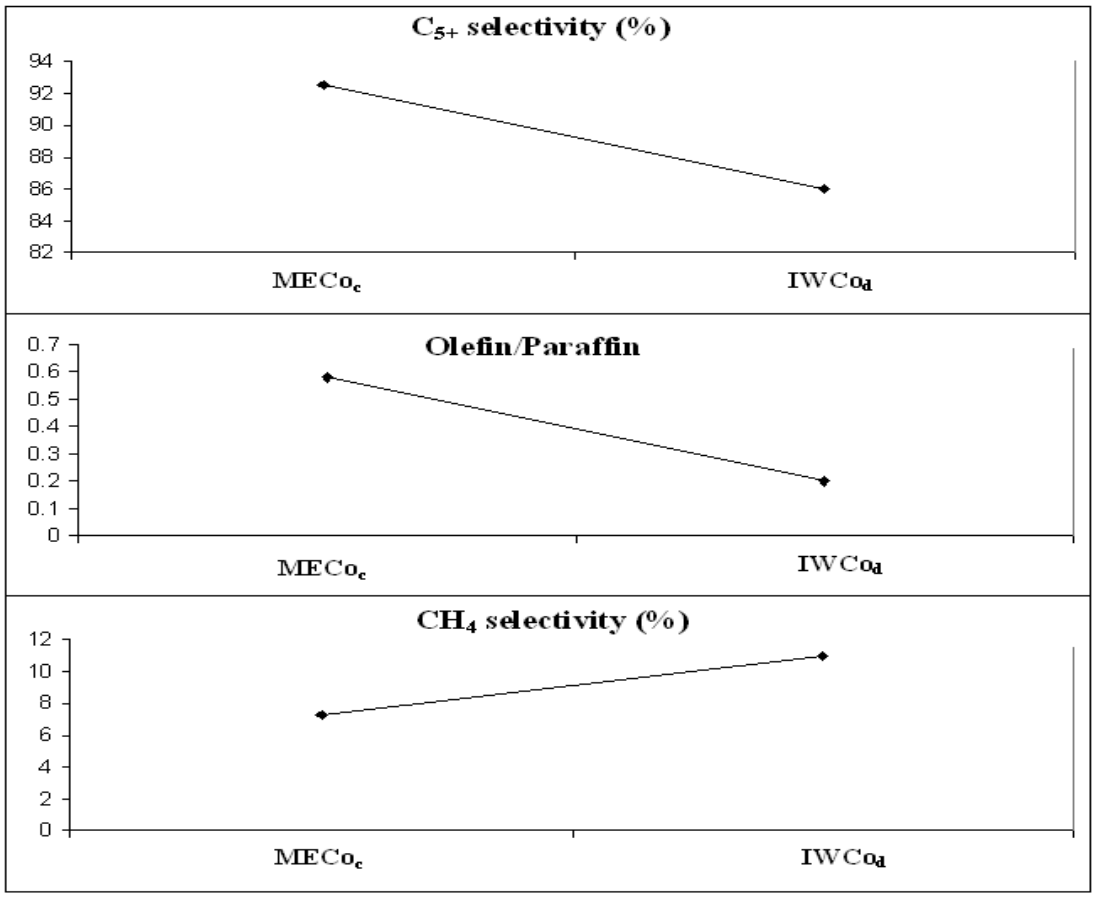

Figure 6. 10: Influence of catalyst preparation route on C_{5+} selectivity, Olefin to paraffin ratio and CH_4 selectivity at 220°C, 2 MPa and $H_2/CO=2$.

The catalyst prepared by the reverse micelle synthesis has higher selectivity for C_{5+} products than that of the $IWCo_d$ catalysts. The same results have been observed by Kim et al. with a zirconia supported palladium catalyst. The uniformity of the particle size improved the hydrogenation of carbon monoxide, which in turn increased the selectivity for C_{5+} products. Although, as shown in Figure 6.9, the catalyst prepared by the conventional impregnation method showed better selectivity for heavier hydrocarbon molecules (C_{10+}),which can be explained by the presence of larger cobalt particle sizes (10+ nm) than the catalyst prepared by the microemulsion route. Large particles (10+ nm) have high potential of re-adsorption and polymer chain initiation on the catalyst's surface [Madon and Iglesia, 1993]. Interestingly, the CH_4 selectivity is lower for the $MECo_c$. The decrease in the selectivity of CH_4 can be explained by the effective participation of olefins in the carbon–carbon chain propagation for the uniform cobalt clusters produced by microemulsion technique. The olefin/paraffin ratio is higher for the $MECo_c$ catalyst. On $MECo_c$ catalyst, α-olefins of the type $R–CH=CH_2$ can compete with carbon monoxide and heavier olefins for readsorption and chain initiation up to chain lengths of C_{11}. The higher H_2 chemisorption on the $MECo_c$ catalyst means higher probability of CHx + H reactions which consequently leads to a higher termination rate after C_{11} hydrocarbon chains. The shift towards olefin production could also indicate lower hydrogenation activities for particles outside the CNT tubes (larger particles) than the particles inside the tubes. As shown in TEM pictures, the $MECo_c$ catalyst has fewer particles inside the tube than $IWCo_d$ catalyst.

Figure 6.11 presents the comparative results of %CO conversion, FTS rate (g $HC_{produced}/g_{cat}$./min) and water gas shift (WGS) reaction rate for $MECo_c$ and $IWCo_d$ catalysts.

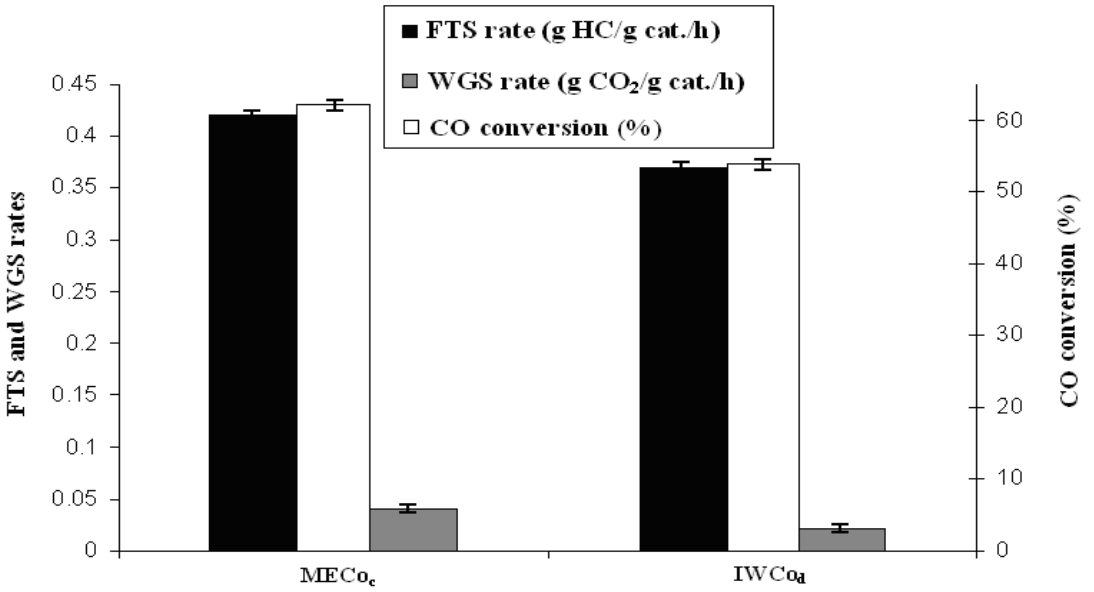

Figure 6. 11: Comparison of FTS (g HC/g_{cat}./h) , WGS rate (g CO_2/g_{cat}.h) and % CO conversion for the catalysts prepared by Microemulsion ($MECo_c$) and Incipient Wetness impregnation ($IWCo_d$) preparation route (220°C, 2 MPa and H_2/CO=2).

It reveals that catalysts prepared through the microemulsion synthesis technique show a higher FTS rate than those prepared by the incipient impregnation preparation route. % CO conversion increased from 54 % in the case of $IWCo_d$ catalyst to 62 % for the $MECo_c$ catalysts. $IWCo_d$ catalyst is characterized by different particle size distribution compared to $MECo_c$ catalyst showing a narrow particle size distribution. The cobalt sites produced by microemulsion are more stable by their uniformity than the ones produced by incipient wetness impregnation [Hayashi et al., 2002]. Martinez et al. observed that a narrow particle size distribution enhances the turn over frequency (TOF) of the FTS catalysts, which in turn leads to a better conversion of the reactants as well as an increase in the FTS rate (Eq. (6.5)) [Martinez and Prieto, 2007].

$$R_{conv.CO} = [\%CO\ conv. \times CO\ flow\ (ml/min) \times molar\ volume\ (1\ atm, 25^oC)\ (\mu\ mole/\ ml)] / g\ cat \quad (6.5)$$

Improvement of the uniformity of the catalyst particles leads to a better stability of the products and the FTS activity. These results reveal that FT activity of the catalysts is strongly dependent on the size distribution of the cobalt cluster.

Figure 6.11 also presents the effect of catalyst preparation route on the water gas shift reaction. Water gas shift reaction rate is equal to the formation rate of carbon dioxide (R_{FCO2}) and can be defined by:

$$R_{WGS} = R_{FCO2} = g\,CO_2 \text{ produced/gcat./min} \quad (6.6)$$

The WGS rate (Eq. (6.6)) is higher for the $MECo_c$ than for the $IWCo_d$ catalyst. The increase in the CO_2 formation rate can be attributed to the increase in water partial pressure, due to an increase in FTS reaction rate [Tavasoli et al., 2005]. Moreover, Hayashi et al., found that Fe catalysts prepared by microemulsion technique have superior selectivity and activity for C_{2+} oxygenate, which can be attributed to the existence of the stable oxides species (FeO) during the reaction [Hayashi et al., 2002]. According to TPR results, the $MECo_c$ reduction peak attributed to CoO reduction is obtained at 465 ^oC versus 452 ^oC for the $IWCo_d$ catalyst, indicating that after the catalyst reduction more CoO species remain on the $MECo_c$ catalyst, thus resulting in easier CO_2 formation.

6.5 Conclusions

This research has been carried out using inert carbon nanotubes (CNT)-supported cobalt catalysts to compare the effects of microemulsion technique for catalyst preparation with that of the incipient wetness impregnation method. Cobalt nanoparticles produced at relatively high loadings of 10 wt% with the microemulsion technique show a narrow particle size distribution. It was also found that FT activity and selectivity of the catalysts are dependent upon the size distribution of the cobalt cluster. According to TEM analysis, small Co particles (2–6 nm) are mostly confined inside the CNTs where influence of its electron deficiency in the inside surface has changed the commonly expected results. Thus, CNTs as a catalyst carrier-support with Co nanoparticles maintained high reducibility of Co which will not normally occur with small particles supported on oxidic catalysts. The proposed microemulsion technique also increased the CO conversion by 15% compared to those prepared by incipient wetness impregnation. This new catalyst preparation method may offer an attractive alternative for nanoparticles

synthesis by reverse microemulsion and for fundamental catalytic studies especially such for structure-sensitive FT catalysis.

6.6 References

Bechara, R., D.Balloy and D.Vanhove, "Catalytic properties of Co/Al_2O_3 system for hydrocarbon synthesis," Applied Catalysis A: General **207**, 343-353 (2001).

Bezemer, G. L., J.H. Bitter, H.P.C.E Kuipers, H. Oosterbeek, J.E Holewijn, X. Xu, X., F. Kaptejin, A. Jos Van Dillen and K.P de Jong, "Cobalt Particle size Effects in the Fischer-Tropsch Reaction studied with Carbon Nanofiber Supported Catalysts," Journal of American Chemical Society **128**, 3956-3964 (2006 a)

Bezemer, G.L., P.B. Radstake, V.Koot, A.J. van Dillen, J.W. Geus, K.P. de Jong, "Preparation of Fischer–Tropsch cobalt catalysts supported on carbon nanofibers and silica using homogeneous deposition-precipitation," Journal of Catalysis **237,** 291-302 (2006 b).

Bezemer, G.L., A.V. Laak, A. J. V. Dillen and K.P. Jong, "Cobalt Supported on Carbon Nanofibers - A Promising Novel Fischer-Tropsch Catalyst," Studies in Surface Science and Catalysis **147**, 259-264 (2004).

Chen, W., Z. Fan, X. Pan, X. Bao, "Effect of Confinement in Carbon Nanotubes on the Activity of Fischer-Tropsch Iron Catalyst," Journal of American Chemical Society **130**, 9414-9419 (2008).

Dauscher, A., R. Touroude, G. Maire, J. Kizling, M. Boutonnet-Kizling, "Influence of the Preparation Mode on Metal-Support Interactions in Pt/TiO_2 Catalysts," Journal of Catalysis **143**, 155-165 (1993).

Dry, M.E., "High quality diesel via the Fisher-Tropsch process: A review," Journal of chemical technology and biotechnology **77**, 43-50 (2001).

Eriksson, S. U. Nylen, S.Rojas and M.Boutonnet, "Preparation of catalysts from microemulsion and their applications in heterogeneous catalysis," Applied Catalysis A: General **265**, 207-219 (2004).

Ernst, B., S.Libs, P.Chaumette, A. Kiennermann, "Preparation and characterization of Fischer–Tropsch active Co/SiO_2 catalysts," Applied Catalysis A: General **186**, 145-168 (1999)

Hanaoka, T., W-Y. Kim, M. Kishida, H. Nagata, K. Wakabayashi, "Enhancement of CO Hydrogenation Activity of Rh/SiO_2 with Low Rhodium Content," Chemistry Letters **17**, 645-646 (1997).

Hayashi, H., L.Z. Chen, T. Tago, M. Kishida, K. Wakabayashi, "Catalytic properties of Fe/SiO_2 catalysts prepared using microemulsion for CO hydrogenation," Applied Catalysis A: General **231**, 81-89 (2002).

Huffaman, G.P N., Shah, J.Zhao, F.E.Huggins, T.E.Hoost, S.Halvorsen and J.G.Goudwin, "In-situ XAFS investigation of K-promoted Co catalysts," Journal of Catalysis **151**, 17-25 (1994).

Jacobs,G., T.K Das, Y. Zhang, J. Li, G. Racoillet and B.H. Davis, "Fischer–Tropsch synthesis: support, loading, and promoter effects on the reducibility of cobalt catalysts," Applied Catalysis A:General **233**, 263-281 (2002).

Kim, W-Y., T Haoka, M. Kishiba and K. Wakabayshi, "Hydrogenation of carbon monoxide over zirconia-supported palladium catalysts prepared using water-in-oil microemulsion," Applied Catalysis A: General **155**, 283-289 (1997).

Li, J., G.Jacobs, T.Das, B.H.Davis, "Fischer-Tropsch synthesis: effect of water on the catalytic properties of the ruthenium promoted Co/TiO2 catalyst," Applied Catalysis A: General **233**, 255-262 (2002).

Lin, H.-Y., Y-W.Chen, "The mechanism of reduction of cobalt by hydrogen," Materials Chemistry and Physic **85**, 171-175 (2004).

Madon, R.J., E.Iglesia, "The Importance of Olefin Readsorption and H_2/CO Reactant Ratio for Hydrocarbon Chain Growth on Ruthenium Catalysts," Journal of Catalysis **139**, 576-590 (1993).

Martinez, A., C. Lopez, F. Marquez, I.Diaz, "Fischer–Tropsch synthesis of hydrocarbons over mesoporous Co/SBA-15 catalysts: the influence of metal loading, cobalt precursor, and promoters," Journal of Catalysis **220**, 486-499 (2003).

Martinez, A., G.Prieto, "Breaking the dispersion-reducibility dependence in oxide-supported cobalt nanoparticles," Journal of Catalysis **245**, 470-476 (2007).

Ojeda, M., S.Rojas, M.Boutonnet, F.J.Perez-Alonso, F. Javier Garcia-Garcia and J.L.G Fierro, "Synthesis of Rh nano-particles by the microemulsion technology: Particle size effect on the CO+H_2 reaction," Applied Catalysis A: General **274**, 33-41 (2004).

Saib, A.M., M. Clayeys, E. van Steen, "Silica supported cobalt Fischer–Tropsch catalysts: effect of pore diameter of support," Catalysis Today **71**, 395-402 (2002)

Tago, T., T.Hanaoka, P.Dhupatemiya, H.Hayashi, M.Kishida, K.Wakabayashi, "Effects of Rh content on catalytic behavior in CO hydrogenation with Rh–silica catalysts prepared using microemulsion," Catalysis Letter **64**, 27-31 (2000).

Tavasoli, A., Y. Mortazavi, A. Khodadadi and K. Sadagiani, "Effects of different loadings of Ru and Re on physico-chemical properties and performance of 15% Co/Al_2O_3 FTS catalysts," Iranian Journal of Chemistry and Chemical Engineering **35**, 9-15 (2005).

Tavasoli, A., R.M. Abbaslou, M. Trépanier and A.K.Dalai, "Fischer-Tropsch synthesis over cobalt supported on carbon nanotubes in a slurry reactor," Applied Catalysis A: Genreal **345**, 134-142 (2008 a)

Tavasoli, A., K.Sadaghiani and K. Khorashe, A.A. Seifkordi, A.A. Rohani and A. Nakhaeipour, "Cobalt supported on carbon nanotubes: a promising novel Fischer-Tropsch synthesis catalyst," Fuel Processing Technology **89**, 491-498 (2008 b).

Trépanier, M., A. Tavasoli, A.K. Dalai and N. Abatzoglou, " Fischer-Tropsch synthesis over carbon nanotubes supported cobalt catalysts in a fixed bed reactor: Influence of acid treatment," Fuel Processing Technology **90**, 367-374 (2009 a).

Trépanier, M., A. Tavasoli, A.K. Dalai, and N. Abatzoglou, "Co, Ru and K loadings effects on the activity and selectivity of carbons nanotubes supported cobalt catalyst in FTS," Applied Catalysis A.General **353,** 193-202 (2009 b).

Chapter 7: Phenomenological kinetics study on CNT-supported RuKCo FTS catalyst in a fixed bed reactor

A similar version of this chapter has been submitted in The Canadian Journal of Chemical Engineering.

Trépanier, M., C. A.Dorval Dion, A.K. Dalai., N. Abatzoglou, Intrinsic Kinetics of Fischer-Tropsch Synthesis CNT-supported RuKCo Catalyst in a Fixed Bed Reactor, The Canadian Journal of Chemical Engineering (submitted).

The work discussed in this chapter was also included in paper presentation at the following conference:

Trépanier, M. C. A. Dorval Dion, A.K. Dalai, N. Abatzoglou, (August 2010) Intrinsic Kinetics of Fischer-Tropsch Synthesis with a CNT-supported RuKCo Catalyst in Fixed-Bed Reactor, 3rd International IUPAC Conference on Green Chemistry, Ottawa, Canada.

Contribution of Ph.D Candidate

The laboratory experiments, data analysis and results interpretation for the promoted catalysts study was performed by Mariane Trépanier and Christopher A. Dorval Dion. Drs.Dalai and Abatzoglou provided editorial assistance, the main idea of the research project and financial support. The submitted manuscript was written and presented by Mariane Trépanier.

Contribution of this manuscript to Overall Study

This chapter is the final step of the Ph.D research project. The ultimate goal of a research project in catalysis work is to develop a model that defines the kinetic of the catalyst and that it can be related to a large variety of operating conditions. The previous chapters identified Ru.5K.0016 (Co15) as the optimized catalyst in this Ph.D research

project. This final chapter shows the kinetic model development for the Ru.5K.0016 (Co15) catalyst. The kinetic modeling was used to identify the activation energy of the reaction and the kinetics parameters. This part of the research allows determining the best fitted kinetic model for the novel Co/CNT catalyst.

7.1 Abstract

The rate of syngas (H_2/CO) consumption over a RuKCo/CNT Fischer-Tropsch synthesis (FTS) catalyst was measured in a fixed bed micro-reactor at 210-225 °C, 2-3.5 MPa, H_2/CO feed molar ratios of 1-2.5 and gas hourly space velocity (GHSV) range of 2700-3600 h^{-1}. The data have been used to model the kinetics of the FTS reactions within the range of the studied conditions. One empirical power law model and four semi-empirical kinetic models based on Langmuir-Hinshelwood-type equation have been evaluated. The best fitting was obtained with the equation: $-r_{H_2+CO} = \frac{18.5\times10^{-5} P_{H_2}^{0.39}}{(1+7.2\times10^{-2} P_{CO}^{0.72} P_{H_2}^{0.1})^2}$ similar to that proposed by Brötz et al. The estimated activation energy (E=80-85 kJ/mol) is lower than that is reported in the literature. These results are related to the unique physical and chemical properties of carbon nanotube supports that decrease the activation energy of the catalyst.

7.2 Introduction

Extensive studies on FTS catalysts showed that cobalt outperforms other catalysts in terms of economical viability, low water gas shift reaction (WGS), and FTS products selectivity (high quality middle-distillate and diesel fuels) [Bechara et al., 2001; Dry et al., 1981; Iglesia, 1997; Jacobs et al., 2002; Oukaci et al., 1999]. Previous study demonstrated that the unique structural properties of CNTs as support increases the reducibility of the catalyst, lowers the sintering of the cobalt particles, and increases the FTS products selectivity [Tavasoli et al., 2008; Tavasoli et al., 2009; Trépanier et al., 2009a; Trépanier et al., 2009b]. Moreover, ruthenium (Ru) as a promoter for the cobalt catalyst increases the FTS rate by increasing the dispersion of cobalt clusters and decreasing the reduction temperature of the cobalt oxides [Iglesia et al., 1993a; Tavasoli

et al., 2005; Trépanier et al., 2009b]. K, as a promoter, also increases the chain growth probability (α) [Huffman et al., 1994; Trépanier et al., 2009b].

Several studies have investigated the kinetic of FTS on cobalt catalyst [Brötz, 1949; Iglesia et al., 1993b; Sarup and Wojciechowski, 1989; Yates and Satterfield, 1991; Zennaro et al., 2000]. Yates and Satterfield, Sarup and Wojciechowski, Iglesia et al., studied the kinetics of relevant cobalt catalyst supported on Al_2O_3, SiO_2 and Kiselgurh showing reaction orders for H_2 and CO rates in the range of 0.5 to 2 and -1.0 to 0.65, respectively. The activation energies for these studies cover a range of 98-103 kJ/mol [Brötz, 1949; Iglesia et al., 1993b; Sarup and Wojciechowski, 1989; Yates and Satterfield, 1991]. However, the activation energy of the Co/TiO_2 catalyst studied by Zennaro et al. was estimated at 83.4 kJ/mol [Zennaro et al., 2000]. No kinetic data are available in the literature on CNT-supported and promoted cobalt catalysts.

Ribeiro et al. have clearly established that catalyst characterization and statistical validation of the results are the guidelines for conducting and reporting activity/kinetic data [Ribeiro et al., 1997]. Moreover, effects of support, promoters, heat-mass transfer, and catalyst deactivation on measured kinetic should also be part of the kinetic study [Anderson, 1956; Ribeiro et al., 1997; Zennaro et al., 2000]. Assuring the absence of pore diffusion, mass transfer, and heat transfer limitations increases the reliability of the studied kinetic model [Anderson, 1956; Fogler, 2002; Ribeiro et al., 1997; Zennaro et al., 2000].

The objectives of this work were to (1) obtain statistically significant kinetic data for the Ru.5K.0016(Co15)/CNT catalyst under representative reaction conditions in the absence of heat and mass transport limitation, and deactivation; (2) prove the statistical significance of the data and, (3) develop a kinetic model of the rate of synthesis gas consumption ($CO + H_2$) on the cobalt catalyst in the absence of appreciable WGS activity.

7.3 Experimental

7.3.1 Catalyst preparation

Prior to catalyst preparation, the Mknano-MWCNT (>95 %) support was treated with 30 wt. % HNO_3 at 100 ^oC overnight, washed with distilled water, and dried at 120^oC for

6 h. The Ru.5K.0016(Co 15)/CNT catalyst was prepared using the co-incipient wetness impregnation of cobalt nitrate (Co $(NO_3)_2.6H_2O$ 99.0 %, Merck), potassium nitrate (KNO_3), and ruthenium (III) nitrosylnitrate up to 15, 0.0016 and 0.5 wt. %, respectively. After the impregnation step, the catalyst was dried at 120 ^oC and calcined at 400 ^oC under argon flow for 3 h and slowly exposed to an oxygen atmosphere during the cooling step.

The cobalt (15 wt. %) and ruthenium (0.5 wt. %) loading of the calcined catalysts were verified by an Inductively Coupled Plasma Atomic Emission Spectroscopy (ICP-AES) system.

7.3.2 Catalyst characterization

The treated CNTs and catalysts were characterized by Transmission Electron Microscopy (TEM). Sample specimens for TEM studies were prepared by ultrasonic dispersion of the catalysts in methanol. The suspensions were dropped onto a carbon-coated copper grid. TEM investigations were carried out using a Hitachi H-7500 (120kV).

A Perkin Elmer TG/DTA Thermogravimetric differential thermal analyzer was used to measure weight changes of the sample when heated under a flow of argon (flow rate of 40 ml/min) at a constant heating rate of 10 °C/min.

The surface area, pore volume, and average pore radius of the catalysts were measured by an ASAP-2000 system from Micromeritics. The samples were degassed at 200 ^oC for 2 h under 50 mTorr vacuum and their BET area, pore volume, and average pore radius were determined.

XRD measurements of the calcined catalysts were conducted with a Philips PW1840 X-ray diffractometer with monochromatized Cu/K_α radiation. Using the Scherer equation, the average size of the Co_3O_4 crystallites in the calcined catalysts was estimated from the line broadening of a Co_3O_4 peak at 2θ of 36.8^o.

Temperature programmed reduction (TPR) spectra of the calcined catalysts were recorded using a CHEMBET-3000, equipped with a thermal conductivity detector. To remove traces of water, the catalyst samples were first purged in a flow of Ar at 150 ^oC, and then cooled to 40 ^oC. The TPR of 0.1 g of each sample was performed using 9.5 %

hydrogen in an argon gas mixture with a flow rate of 40 cm^3/min. The samples were heated from 40 to 600 ^oC with a heating rate of 10 ^oC /min.

7.3.3 FTS rate measurements

The experiments were performed in a fixed bed micro reactor using 1 g of catalyst powder (400-500 μ) diluted with 2.5 g of 90 Mesh SiC to eliminate the temperature gradient. Catalyst activation was conducted first *in-situ* under pure hydrogen at a flow rate of 3600 h^{-1} and a temperature of 380 ^oC for 20 h. During the experiment, the liquid products were continuously removed from the reactor and passed through two traps, one maintained at 100 ^oC (hot trap) and the other at 0 ^oC (cold trap). The contents of both hot and cold traps were removed after every run. The catalyst was also replaced after each run. The hydrocarbon and water fractions were separated and analyzed by Varian 3400 GC liquid analyzer. The uncondensed vapor stream was depressurized to atmospheric pressure through a back pressure regulator. The composition of the outlet gas stream was determined using an on-line GC-2014 Shimadzu gas chromatograph. Table 7.1 shows the experimental plan.

Table 7. 1: Experimental plan

Experiment [ε]	T (°C)	P (MPa)	H_2/CO	GHSV (g_{cat}^{-1} h^{-1})
1A	220	2.5	2	3600
2A	220	2.5	2	3300
3A	220	2.5	2	3000
4A	220	2.5	2	2700
1B	210	2	2	3600
2B	215	2	2	3600
3B	220	2	2	3600
4B	225	2	2	3600
1C	220	2.5	2.5	3600
2C	220	2.5	2	3600
3C	220	2.5	1.5	3600
4C	220	2.5	1	3600
1D	210	2	1	2700
2D	210	2.5	1.5	3000
3D	210	3	2	3300
4D	210	3.5	2.5	3600
Re[γ]	210	2	1	2700
5D	215	2	1.5	3300
6D	215	2.5	1	3600
7D	215	3	2.5	2700
8D	215	3.5	2	3000
Re[γ]	215	2	1.5	3300
9D	220	3	1	3000
10D	220	3.5	1.5	2700
11D	220	2	2	3600
12D	220	2.5	2.5	3300
Re[γ]	220	3	1	3000
13D	225	2	2.5	3000
14D	225	2.5	2	2700
15D	225	3	1.5	3600
16D	225	3.5	1	3300
Re[γ]	225	2	2.5	3000

[ε] Series A runs were conducted on a fresh catalyst at different flow rate (external mass transfer limitation study). Series B runs were conducted on a fresh catalyst at different temperatures. Series C runs were conducted on a fresh catalyst at different H_2/CO ratios. Series D runs conducted on a fresh catalyst at different H_2/CO ratios were conducted with fresh catalyst and the activity of the catalyst was verified with replicates.

[γ] Re is the replicate experimental point

Runs A show the preliminary experiments that have been done to evaluate the mass transfer limitation that may disguise the rate measurement. The catalyst was initially operated under FT synthesis conditions shown by runs B and C, where the temperature and the H_2/CO ratio varied, respectively for a period of 24 h to ensure that operating conditions achieved their normal FTS products selectivity and activity. Runs D show the FTS test conditions used to measure the kinetic rate. The measurements were made after each run reached a steady-state reaction (12 h).

7.3.4 Evaluation of mass transfer limitation

Prior to the kinetic study, influence of pore diffusion and mass transfer limitation were evaluated. The Weisz-Prater criterion (C_{WP}) was used to evaluate the influence of pore diffusion limitation of the catalysts and estimated to be 0.0016 (bulk diffusivity of CO/H_2 of 2.79 x 10^{-3} cm^2/s and of effective diffusivity of 9.3 x 10^{-2} cm^2/s), confirming the negligible effect of pore diffusion resistance on the reaction rate (with $C_{wp} < 1$) for catalyst powder in size of 500 μ (eq.7.1) [Fogler, 2002].

$$C_{wp} = \frac{-r_{A(obs)} * \rho_c * R^2}{D_e * C_{AS}} \leq 1 \qquad (7.1)$$

$-r_A = -r_{CO+H2}$ = reaction rate per unit mass of catalyst
ρ_c = catalyst density
R = catalyst particle radius
C_{AS} =surface concentration of reactant (CO)
D_e =Effective diffusivity

Mass transfer also occurs between the bulk fluid and the external surface of the catalyst. This external diffusion resistance affect the overall rate of reaction if the rate is of the same order of magnitude with the other steps [Fogler, 2002]. To evaluate the role of external diffusion the influence of gas velocity has been studied. Figure 7.1 shows that for a gas velocity range between 2700 and 3600 GHSV h^{-1}, the product selectivity remains the same.

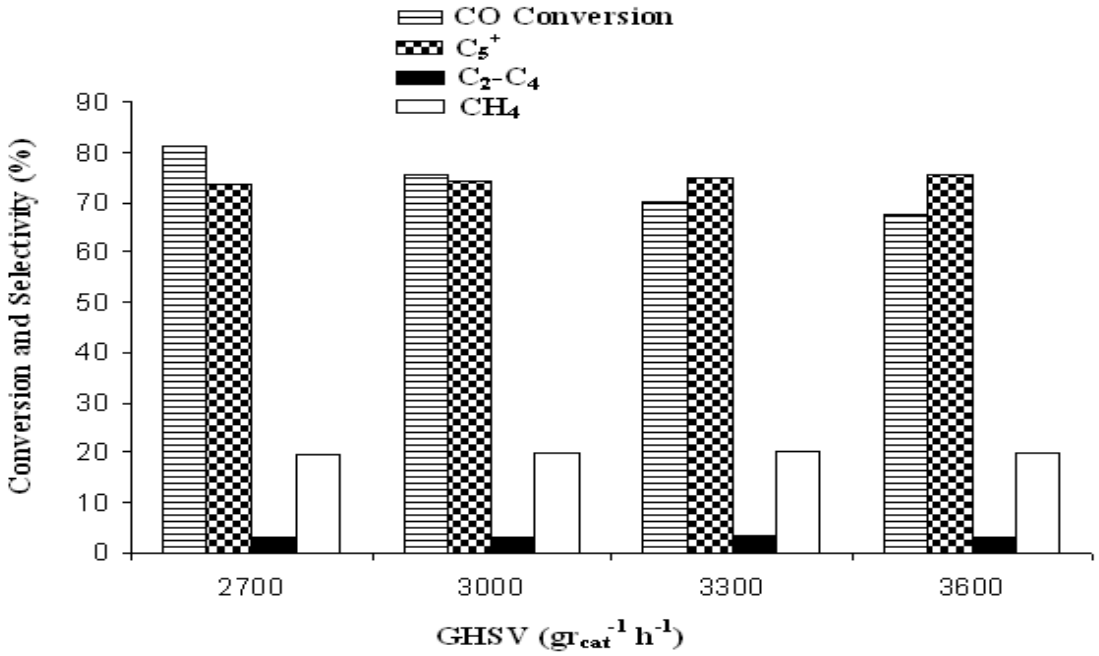

Figure 7. 1: Variation of CO conversion, C_5^+ selectivity and methane selectivity at different GHSV over 15Co0.5Ru0.0016K/CNT catalyst (T=220°C, P=2 MPa, H_2/CO=2)

.

Thus, the results indicate that within this GHSV range there is a low risk of external mass transfer limitation. In mass transfer-dominated reactions, the concentration of the reactant will decrease resulting in a reduction of formation rate of the desired products [Fogler, 2002]. Study of the influence of the Knudsen diffusivity by using the mean free path (λ) correlation is another tool to determine the effect of external mass transfer on the reaction rate. External mass transfer resistance will predominate when Knudsen diffusivity is lower than the bulk diffusivity [Smith, 1981]. Knudsen diffusion occurs when the mean free path of the gas molecule is near the diameter of the catalyst pore (D) or if the Knudsen number ($K_n = \lambda/D$) is > 10 [Fogler, 2002; Michiel, 2001]. Considering that CNT are mesoporous material, a pore diameter of 20 nm has been used for comparision. The mean free path equation follows [Perry and Green, 1997]:

$$\lambda = \frac{K_B T}{\sqrt{2}\pi\sigma^2 P} \tag{7.2}$$

where K_B is the Boltzman constant (~ 1.38 x 10^{-23} jK^{-1}), T is the reaction temperature in kelvin (503 K), σ is the gas molecule diameter (CO = 0.39 x 10^{-9} m) and P is the

reaction pressure (20 atm) [Perry et al, 1997]. According to these parameters, the mean free path evaluated for the CO gas is $\lambda = 5.1 \times 10^{-9}$ m. Thus, the Knudsen number (λ/D) is egual to 0.25 which proposed that mass transfer is direct by a transition mode between the bulk and the Knudsen diffusivity. The $K_n < 10$ indicates that there is no significant external mass transfer limitation cause by Knudsen diffusion at the catalyst surface. However, according to these results, only assumption of negligible mass transfer limitation at the catalyst surface can be consider. Farther analyses are necessary to ensure no mass transfer limitation.

7.4 Results and Discussions

7.4.1 Catalyst characterization results

The TEM images of the catalyst revealed that the particles are well dispersed inside the tubes and also adhering on the external perimeter of the tube walls (Figure 7.2).

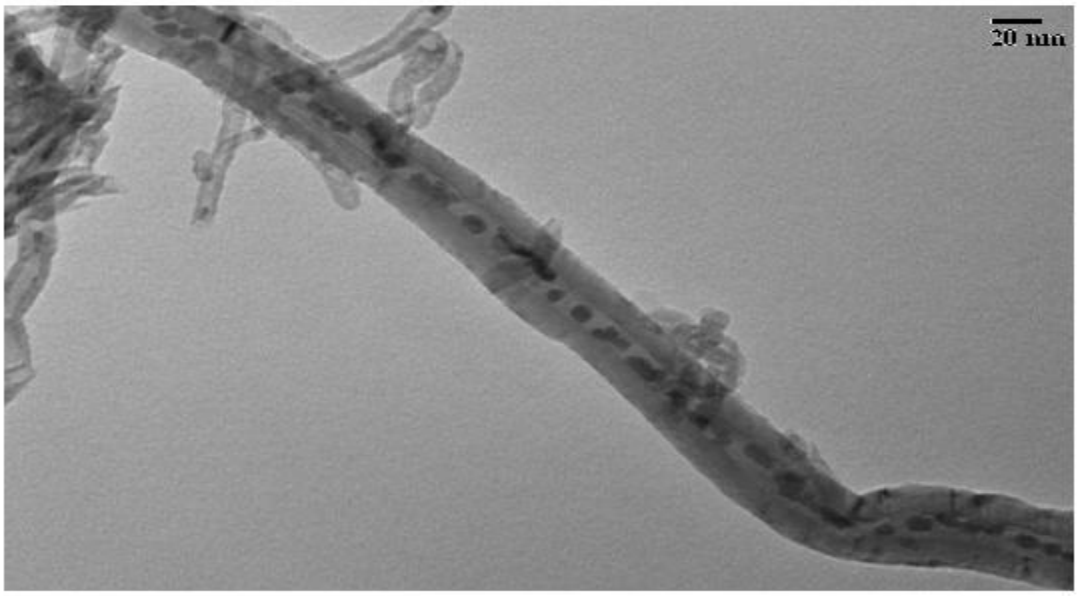

Figure 7. 2: TEM image of the Ru.5K.0016(Co15)

As reported in our previous work, the particles inside the tubes were fairly uniform and in size range of 3-9 nm in accordance with the average inner diameter of the CNTs, whereas those on the outer surface have grown to about 8-15 nm. The CNT channels restricted the growth of the particles inside the tubes [Trépanier et al., 2009a; Trépanier et al 2009b; Trépanier et al., 2010].

Results of surface area measurements pore volume and percentage dispersion are shown in Table 7.2.

Table 7. 2: BET surface area, porosity and XRD data

Catalysts	BET ($m^2/g \pm 11.2$)	Pore volume (cm^3/g ±0.003)	Average pore radius (±0.07nm)	XRD (d_{Co3O4}) nm
Co15	170	0.5	5.7	9.6
Ru.5K.0016(Co15)	178	0.6	5.6	9.5

Due to low amounts of K and Ru, the BET area, pore volume and % dispersion of the studied catalysts are close to that reported for the unpromoted Co15 catalyst in our previous work [Trépanier et al., 2009b]. The surface area of the Ru.5K.0016(Co15) catalyst is 178 m^2/g, the pore volume is 0.6 cm^3/g and the average pore radius is 5.6 nm.

X-ray diffraction patterns of the support and calcined catalysts are shown in Figure 7.3.

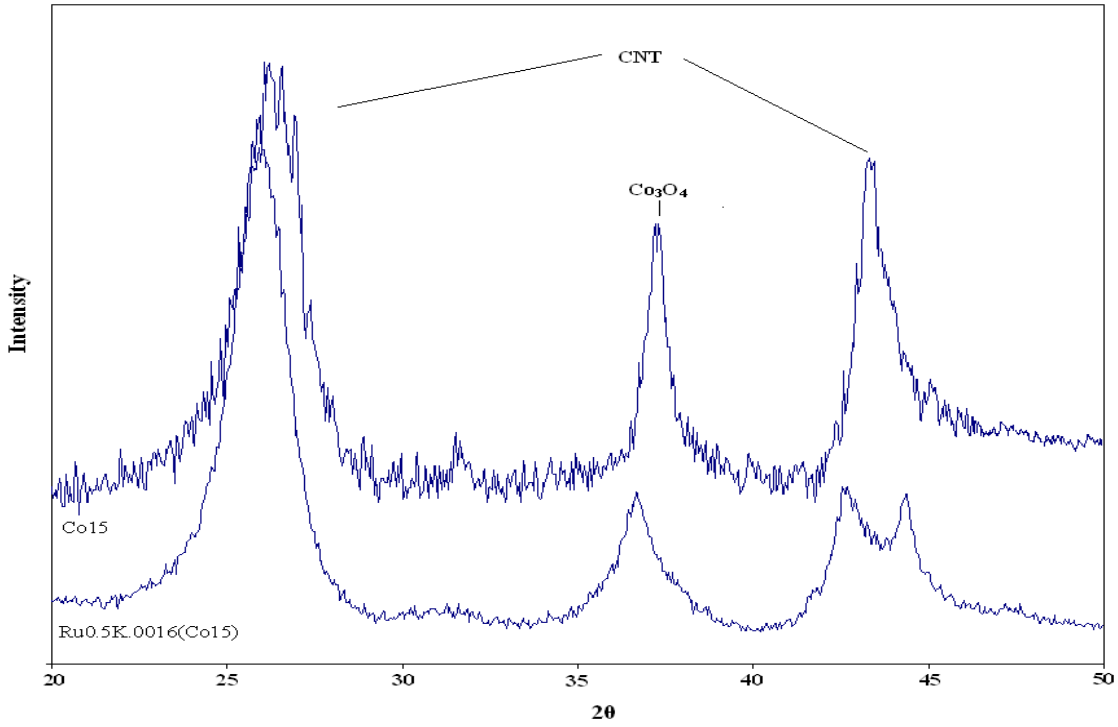

Figure 7. 3: XRD spectra for pure Co15 and Ru.5K.0016(Co15).

In the XRD spectrum of the support CNT and all the catalysts, peaks at 25 and 43° correspond to carbon nanotubes, while the other peaks are related to different crystal

planes of Co_3O_4. The peak at 36.8° is the most intense peak of Co_3O_4 in the XRD spectrum. The Ru.5K.0016(Co15)/CNT catalyst is compared with the unpromoted Co15 catalyst from our previous work. As reported, due to low amount of Ru and K promoters in the XRD spectrum no peak was observed, indicating diffraction lines of Ru and K oxides [Trépanier et al., 2009b]. Table 7.2 also shows the average Co_3O_4 particle size of the catalysts calculated from XRD spectrum and Scherer equation at 2θ of 36.8° [Bechara et al., 2001]. Table 7.2 compares the average particle size of Ru.5K.0016K(Co15) catalyst with Co15 catalyst which are, 9.5 and 9.6 nm, respectively. These results indicate that the addition of Ru and K to the Co15 catalyst slightly influences the average particle size.

The activation of the catalysts in hydrogen atmosphere was studied by temperature programmed reduction (TPR) experiments. Figure 7.4 shows the TPR spectra of the calcined Ru.5K.0016K(Co15) catalyst compared to Co15, Ru0.5(Co15) and K.0016(Co15) catalysts from our previous work [Trépanier et al., 2009a].

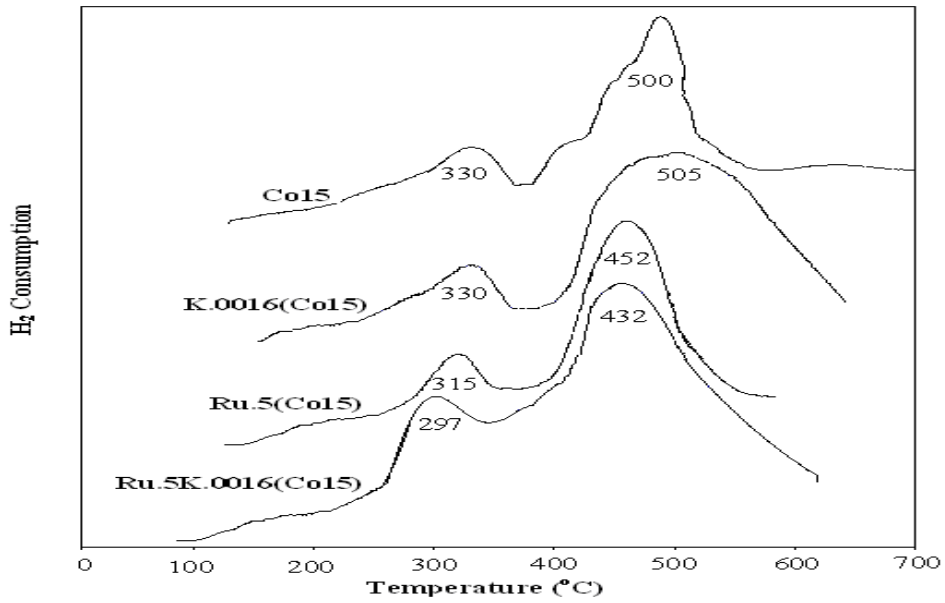

Figure 7. 4: TPR profiles of calcined Co15, K.0016(Co15), Ru.5(Co15) and Ru.5K00.16(Co15)

The first peak of the TPR profile is typically assigned to the reduction of Co_3O_4 to CoO, although a fraction of the peak likely comprises the reduction of the larger, bulk-like CoO

species to Co^o [Tavasoli et al., 2009]. The second peak around 450-500^{o}C is mainly assigned to the second step reduction, which is due to the reduction of CoO to Co^o. This peak also includes the reduction of cobalt species that interact with support [Tavasoli et al., 2009]. The Ru promoter shifts both TPR peaks to a lower temperature, while the K promoter has not significant influence on the reduction behavior of the catalyst. However, Figure 7.4 shows that mixing Ru and K promoters on Co15 catalyst increases the reducibility of the catalyst by decreasing the first peak temperature from 330 to 297 ^{o}C and the second peak temperature from 500 to 432 ^{o}C. Das et al. [Das et al., 2003] have shown that the reduction of ruthenium oxide occurs at temperatures lower than that of cobalt. Ru enhances the spillover of hydrogen on the catalyst surface. In our previous work, the addition of potassium on Co15 catalyst decreased its reducibility [Trépanier et al., 2009b]. It seems that mixing K with Ru promoters inhibits the effect of potassium on the reducibility of the catalysts.

7.4.2 FTS catalyst activity and selectivity

A set of experiments (Runs B and C, Table 1) was performed to evaluate the Ru.5K.0016(Co15)/CNT catalysts in terms of its FTS selectivity and activity. Table 7.3 shows the % CO conversion, CO_2, CH_4, C_2-C_4 and C_{5+} selectivity at different pressures and temperatures during the first 24 h.

Table 7. 3: Performance of Ru.5K.0016(15Co)/CNT catalysts for FTS in a Fixed Bed reactor after 24h.

T (^{o}C)	P (MPa)	CO conversion (%)	CO_2	CH_4	C_2-C_4	C_{5+}	FTS rate	α^a
210	2	65.5	5.3	13.4	3.7	80.1	0.29	0.93
220	2	67.5	6.3	18.5	3.8	70	0.34	0.90
220	2.5	69.5	4.3	14.4	3.3	85.2	0.32	0.92
225	2	88.2	6.3	16.7	3.03	74.5	0.33	0.83

$H_2/CO = 2$, GHSV = 3600 $g_{cat}^{-1}h^{-1}$

[a] Anderson-Schulz-Flory plot for hydrocarbons with 5-22 carbons atoms

Increasing the temperature, increases the %CO conversion and the light hydrocarbons (CH_4 and C_2-C_4) selectivity, whereas C_{5+} decreases. As reported in other study, at high temperature, olefins are preferentially hydrogenated and chain propagation is suppressed, which explains the increase of methane selectivity [Dry et al., 1981; Jacobs et al., 2002]. Our previous studies also show that %CO conversion strongly depends on the reaction temperature [Tavasoli et al., 2008; Trépanier et al., 2009a]. Indeed, increasing the FTS reaction temperature increases the mobility of hydrogen on the catalyst surface which leads to higher % CO conversion. These results are similar to what is normally observed for the Co-Ru FTS catalysts [Sari et al., 2009; Tavasoli et al., 2005; Trépanier et al., 2009b]. Table 7.3 shows the influence of pressure and temperature on the FTS turnover rate ($g_{HC}/gcat^{-1}h^{-1}$) and the chain growth probability (α) for hydrocarbons with 5-22 carbon atoms. Increasing the temperature from 210 to 225 ^{o}C increases the FTS rate from 0.29 to 0.33 while decreasing the α from 0.93 to 0.83. However, increasing the pressure increases the α from 0.90 to 0.92. Increasing the total pressure increases the rate of propagation which is consistent with the decreased selectivity of methane. The chain growth probability (α) is high compared to similar studies on Co-based catalysts [Sari et al., 2009; Trépanier et al., 2009b; Zennaro et al., 2000]. Thus, it seems that the addition of Ru and a small amount of K onto the catalyst have improved the Anderson-Schulz-Flory distribution for hydrocarbons with 5-22 carbon atoms. The addition of K to the Co/CNT FTS catalyst increases significantly the α-olefin selectivity [Trépanier et al., 2009b]. Potassium increases significantly the CO chemisorption to the catalyst which restricted the H_2 mobility by blocking the low-coordination edge and corner sites for dissociative adsorption of hydrogen [Trépanier et al., 2009b]. The increase in CO adsorption rates as well as the reduction of hydrogen adsorption rates could qualitatively explain the decrease in hydrogenation of α-alkenes to alkanes and thus results the increased of chain growth probability. The addition of Ru to the Co/CNT FTS catalyst decreases the methane formation and increases the C_{5+} selectivity. The Ru promoter enhances the reduction of cobalt and increases the number of active sites available for the FTS reaction [Das et al., 2003; Trépanier et al., 2009ab Zennaro et al., 2000].

Figure 7.5 shows the hydrocarbons distribution under different H_2/CO ratios.

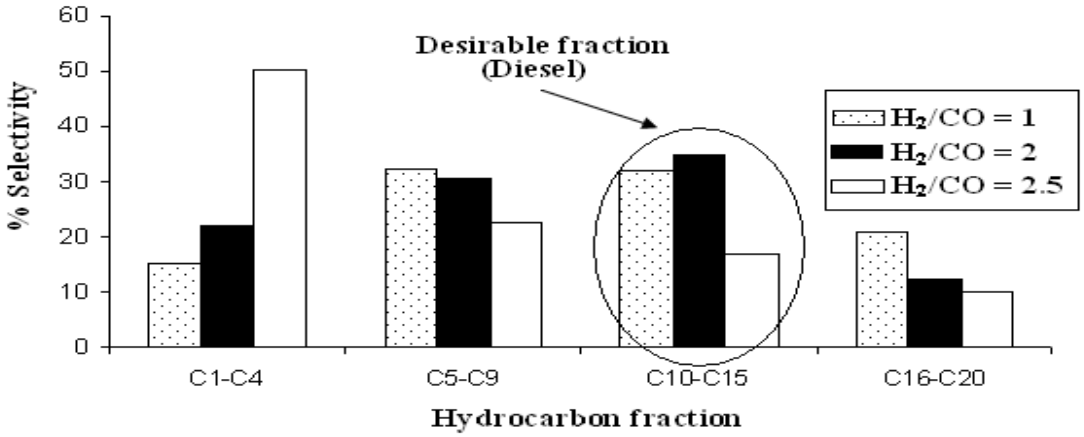

Figure 7. 5: Effect of the H_2/CO ratio on the hydrocarbon products distribution over Ru.5K.0016K(Co15)/CNT (P=2 MPa, T=220°C, GHSV=3600 h^{-1})

The results show that a low H_2/CO ratio (1) leads to higher hydrocarbons (C_{10}^{+} > 75 %) and lower light hydrocarbons (C_1-C_9 < 25 %). On the opposite, a high H_2/CO ratio (of 2) leads to lower hydrocarbons (C_1-C_9 > 70%) and lower heavy ones (C_{10+} < 30%). The desirable product distribution for FTS synthesis seems to be ideal at a ratio of H_2/CO =2 according to Figure 7.5. These observations have already been reported by many studies regarding the cobalt-FTS catalyst [Tavasoli et al., 2007a; Trépanier et al., 2009a]. Figure 7.5 also indicates that light hydrocarbons increased with increasing partial pressure of H_2. High partial pressure of H_2 leads to increase in the hydrogen species to the catalyst surface, which accelerates its combination with carbon species and chain growth initiation. Consequently, formation of light hydrocarbons is preferred at high hydrogen partial pressure. On the other hand, decreasing the H_2/CO ratio will increase the partial pressure of CO on the gas phase, resulting in an increase in the amount of CO adsorbed at the surface. The increase of dissociative adsorption of the CO on the catalyst surface will increase the chain growth probability and decrease the termination reaction of the paraffin [Trépanier et al., 2009a].

7.5 Kinetic Model

7.5.1 Development of kinetic model

The Taguchi experimental design method was used to make the experimental plan. This statistical design method minimizes the overall variance of the estimated parameters and decreases the amount of needed experiments without restricting prohibitively the confidence region for the estimated parameters [Neter and Wasserman, 1974]. The experimental design plan shown in Table 7.1 (runs D) evaluated the nonlinear nature of the kinetic model of the Fischer-Tropsch synthesis. The kinetic study included a total of 19 sets of experimental data with variation of pressure (2-3.5 MPa), temperature (210-225^{o}C), gas velocity (2700-3600 GHSV h^{-1}), and H_2/CO ratio (1-2.5).

The synthesis gas conversion rate depends on partial pressure of the feed constituents and temperature. The models shown in Table 7.4 were developed by Sarup and Woijciechowski, Iglesia et al., and Anderson et al.

Table 7. 4: Kinetic models tested for 0.5Ru0.0016K(15Co)/CNT

Model	Study	Rate equation
1	Power law	$-r_{H_2+CO} = aP_{H_2}^{\alpha} P_{CO}^{\beta}$
2	Iglesia et al.	$-r_{H_2+CO} = \frac{aP_{H_2}^{\alpha} P_{CO}^{\beta}}{1+bP_{CO}^{\beta}}$
3	Sarup & Wojciechowski	$-r_{H_2+CO} = \frac{aP_{H_2}^{\alpha} P_{CO}^{\beta}}{(1+bP_{CO}^{\beta})^2}$
4	Anderson adapted to this study	$-r_{H_2+CO} = \frac{aP_{H_2}^{\alpha} P_{CO}^{\beta}}{(1+bP_{CO}^{\beta}P_{H_2}^{\alpha})^2}$
5	Sarup & Wojciechowski	$-r_{H_2+CO} = \frac{aP_{H_2}^{\alpha} P_{CO}^{\beta}}{(1+bP_{CO}^{\nu}P_{H_2}^{o})^2}$
6	This Study	$-r_{H_2+CO} = \frac{aP_{H_2}^{\alpha}}{(1+bP_{CO}^{\beta})^2}$
7	This Study	$-r_{H_2+CO} = \frac{aP_{H_2}^{\alpha}}{(1+bP_{CO}^{\beta}P_{H_2}^{\alpha})^2}$

The power law equation ($-r_{H_2+CO} = aP_{H_2}^{\alpha} P_{CO}^{\beta}$) is widely recognized to predict rate over a narrow range of reaction conditions, while Langmuir-Hinshelwood (LH) correlations are for a wider range of conditions. It is still unclear which of the rate expression numbers proposed in Table 7.4 for synthesis gas conversion provides the best representation of available data. Variations of these LH rate equations and the power law are related to the hydrogen and carbon monoxide type of adsorption on the catalyst surface and the reaction conditions. Previous research shows that H_2 and CO adsorb dissociatively on cobalt catalyst [Sarup and Wojciechowski, 1989; Yates and Satterfield, 1991]. Moreover, observation shows that CO is adsorbed more strongly than H_2 [Sarup and Wojciechowski, 1989]. In Table 7.4, two models (6, 7) have been adapted to the present study after observation of the experimentals results and kinetics model developed by Brötz [Brötz, 1949]. In these developed models, *a* is a kinetic constant and *b* represents the adsorption constant. Both of these parameters are temperature dependent and evaluated according to the Arrhenius equations [Sarup and Wojciechowski, 1989; Tavasoli et al., 2007; Yates and Satterfield, 1991]:

$$a = a_0 \exp(-E / RT) \tag{7.3}$$

$$b = b_0 \exp(\Delta H / RT) \tag{7.4}$$

where E and ΔH are the apparent activation energy and the heat of reaction, respectively. The α and β exponents represent the reaction orders. Exponent of the total denominator terms give information on the reactant surface reaction behavior (monomolecular or bimolecular). The υ and o exponent on the denominator partial pressure describe the dependence of surface coverage by the reactants (depending on the rate controlling step).

The chemical reaction of the synthesis of hydrocarbons from CO and H_2 is generally accepted onto this form:

$$n\mathrm{CO} + 2n\,\mathrm{H_2} \longrightarrow -(\mathrm{CH_2})_n- + n\mathrm{H_2O} \tag{7.5}$$

The development of kinetic models has to consider the rate limiting step of the reaction mechanism. Sarup and Wojciechowski proposed that dissociation of CO adsorption can be the rate limiting step of the FTS reaction [Sarup and Wojciechowski, 1989]. However, Rautavuoma and van der Bann found kinetic evidences for hydrogenation of surface carbon as the rate limiting step [Rautavuoma et al., 1981].

If we assume that carbon monoxide is strongly adsorbed compared to H_2 and is fully dissociated, the power law expression will show negative exponents for carbon monoxide and positive ones for hydrogen [Sarup and Wojciechowski, 1989]. Moreover, when coverage of the active sites dissociated CO is high, P_{CO} will dominate the denominator [Sarup and Wojciechowski, 1989]. Overall, the choice of the appropriate model to define the syngas consumption is part of the experimental evidence available to judge the applicability of a given model.

7.5.2 Evaluation of the kinetic model

The data were fitted to models of Table 7.4 using a nonlinear optimization least squares (R^2) fitting routine to obtain the kinetic parameter constant. The Microsoft's Excel solver (Generalized reduced gradient algorithm) approach was used; it gives comparable results with other studies [Anderson, 1956; Brötz, 1949; Iglesia et al., 1993b; Sarup and Wojciechowski, 1989; Zennaro et al., 2000]. The discrimination between the rival models (Table 7.4) is based on the statistical analysis and the physical meaning of the final equation rate. The goodness of fit of the experimental data and the 7 different models are shown on Figure 7.6.

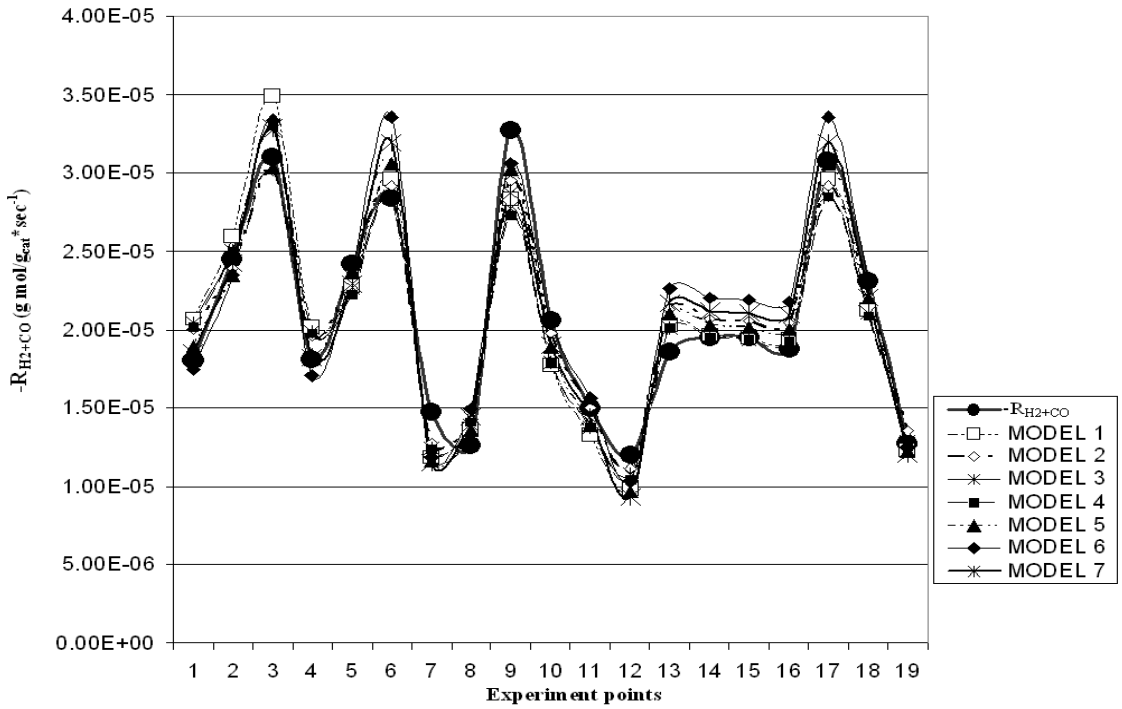

Figure 7. 6: Comparison of calculated and experimental rate for disappearance of CO and H_2

The Mean Absolute Relative Residuals (MARR) and the Residuals Sum of Square (RSS) indicate the correlation between the calculated and experimental values. The significance of kinetics models have been evaluated with the $f_{0.05}$-test which represents a statistical significance of 95 % of the overall regression. If the f_{model}-value is greater than $f_{0.05}$, the model cannot be rejected. The definition of each statistical indicator is listed:

(1) *f*-test:

MSR/MSE

MSE = (SSE/n-k-1) = Mean square of regression

MSR = SSR/k = Mean square of error

SSE = Sum of residuals square for error

SSR= Sum of square for regression

(2) MARR:

$\sum_{i=1}^{n} \frac{|f-h|}{n \cdot f}$ Where h is the expected value (model) and f is the observed value.

(3) RSS:

$\sum_{i=1}^{n} (f-h)^2$ Where h is the expected value (model) and f is the observed value

7.5.3 Kinetic Results

The kinetic parameters of the seven models are shown in Table 7.5.

Table 7. 5: Calculated kinetic parameters for each tested models.

Model	a_0 x 10^5	b_0 x 10^2	E (kJ/mol)	ΔH (kJ/mol)	α	β	υ	o
1	4.24	-	80.1	-	0.46	-1.14	-	-
2	5.44	2.1	83.5	-76.8	0.45	-1.8	-	-
3	4.59	0.00025	85.6	-98.3	0.5	-1.28	-	-
4	4.33	0.00015	75.6	-98.3	0.46	-1.02	-	-
5	5.11	1.43	81.1	-98.7	0.46	-0.91	0.18	0.35
6	7.37	7.63	85.1	-80.1	0.39	0.86	-	-
7	18.5	7.2	82.4	-71.4	0.39	0.72	-	0.1

The modeling results provide satisfactory goodness of fit, as shown in Figure 7.6. For all the studied kinetic models, the value of the apparent activation energy fits within the narrow range of 80-85 kJ/mol, which is lower than the usual activation energy reported in the other studies (98-104 kJ/mol) [Anderson, 1956; Brötz , 1949; Iglesia et al., 1993b; Ribeiro et al., 1997; Sarup and Wojciechowski, 1989; Zennaro et al., 2000]. Previous works have shown that carbon nanotubes have unique physical and chemical properties

(compared to other commonly used FTS supports) that change the expected FTS-catalyst surface reactions [Tavasoli et al., 2008; Tavasoli et al., 2009; Trépanier et al., 2009a; Trépanier et al., 2009b]. As reported in many studies, different surface reaction mechanisms and rate determination steps lead to various forms of kinetic equations and kinetic parameters [Anderson, 1956; Brötz, 1949; Iglesia et al., 1993b; Fogler, 2002; Ribeiro et al., 1997; Sarup and Wojciechowski, 1989; Zennaro et al., 2000]. CNT as a Co-catalyst support lowers the reducibility of the catalyst and increase the FTS activity [Tavasoli et al., 2008; Tavasoli et al., 2009; Trépanier et al., 2009a; Trépanier et al., 2009b]. Moreover, Ru as promoter enhances furthermore the activity of the Co/CNT catalyst [Trépanier et al., 2009b]. The improvement is namely proven by the lower activation energy. The activation energy value higher than 80 kJ/mol shows that the process has no pore diffusion limitation [Sarup and Wojciechowski, 1989], and confirms the validity of the experimental methods and parameter estimation techniques. Figure 7.7 shows the Arrhenius correlation between the kinetic constant and the temperature that have been used to evaluate the activation energy (E) of the studied model.

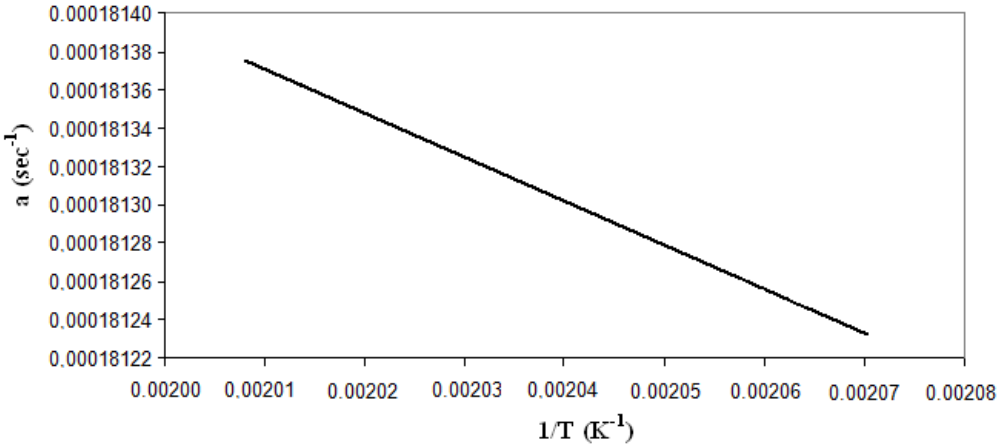

Figure 7. 7: Arrhenius activation energy plot for model 7.

The kinetic parameter (a) has been evaluated with experimental data and model 7 for a temperature range from 210 to 225 ^{o}C. The following equation has been used to determine the activation energy [Fogler, 2002]:

$$E = \frac{-(2.3 \times R \times Log\left(\frac{a_2}{a_1}\right)}{\frac{1}{T_2} - \frac{1}{T_1}} = 82.4kJ \quad (7.6)$$

The power law kinetic parameters suggested that carbon monoxide is strongly adsorbed compared to H_2 and is fully dissociated according to the negative exponent (-1.14) for carbon monoxide and the positive one for hydrogen (0.46) [Sarup and Wojciechowski, 1989]. Models 2, 3, and 4 show negative adsorption coefficients for the partial pressure of CO, which represents a physically unreasonable situation [Sarup and Wojciechowski, 1989]. Model 4 is similar to model 5, but show a positive adsorption coefficient. Models 5, 6, and 7 show bimolecular reactions at the catalyst surface, which correspond well with the dissociative adsorption mechanism developed by Sarup and Wojciechowski [Sarup and Wojciechowski, 1989].

$$H_2 + 2S \rightarrow 2HS \quad (H_2 \text{ dissociative adsorption}) \quad (7.7)$$

$$CO + 2S \rightarrow CS + OS \text{ (CO dissociative adsorption)} \quad (7.8)$$

Models 6 and 7, show a zero order for CO thus suggesting a strong dissociative adsorption of CO at the catalyst surface. The most plausible explanation is that the addition of K as a promoter enhances the CO chemisorption at the catalyst surface [Huffman et al., 1994; Trépanier et al., 2009b]. Moreover, the addition of Ru increases the FTS rate due to the increased hydrogen mobility on the catalyst surface. Therefore, CO dissociated adsorption seems to be the limiting rate step of reaction and that the reaction rate is directly depending upon hydrogen partial. Visconti et al., and Iglesia have also observed that the dissociative adsorption of CO at the catalyst surface was the limiting reaction step for the FTS using a Co/Al_2O_3 [Iglesia, 1997; Visconti et al., 2007].

The statistical analysis for each developed model and constant are shown on Table 7.6.

Table 7. 6: Statistical analysis for the studied model.

Model	R^2	MARR[a] %	RSS[b] (10^{10})	*f*-Test[c]
1	0.901	8.83	8.38	168
2	0.941	6.70	6.16	241
3	0.913	7.31	6.75	169
4	0.902	7.67	6.76	149
5	0.944	6.92	7.85	300
6	0.900	9.43	9.45	157
7	0.913	8.0	8.65	183

[a] Mean absolute relative residuals
[b] Residual some of squares
[c] $f_{0.05,17} = 4.45$

The statistical indicators show that each model is statistically adequate, the significance of kinetics models (*f*-test) shows that models 2, 5, and 7 have the highest significance. Among them, model 5, has the highest R^2 value. . Figure 7.8 compares the experimental and predicted synthesis gas conversion rates of models 1, 2, 5, and 7.

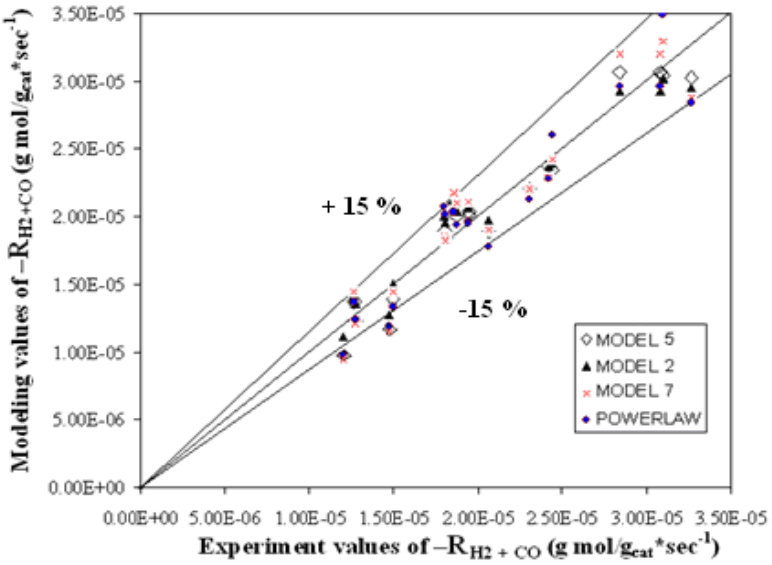

Figure 7. 8: Parity graph of experimental and modeling rates for disappearance of synthesis gas.

Since the data are statistically best fitted by model 5 but they are physically better explained by model 7, model 7 (eqn.7.9) has been preferred. Model 7 evaluate a wide range of P_{CO} and P_{H2} at different operating conditions of synthesis with Ru.5K.0016(Co15)/CNT catalyst.

$$-r_{H_2+CO} = \frac{18.5\times10^{-5} P_{H_2}^{0.39}}{(1+7.2\times10^{-2} P_{CO}^{0.72} P_{H_2}^{0.1})^2}$$

(7.9)

Figure 7.9 confirms model 7 predictions that increasing the partial pressure of H_2 will increase the rate of reaction (α positive).

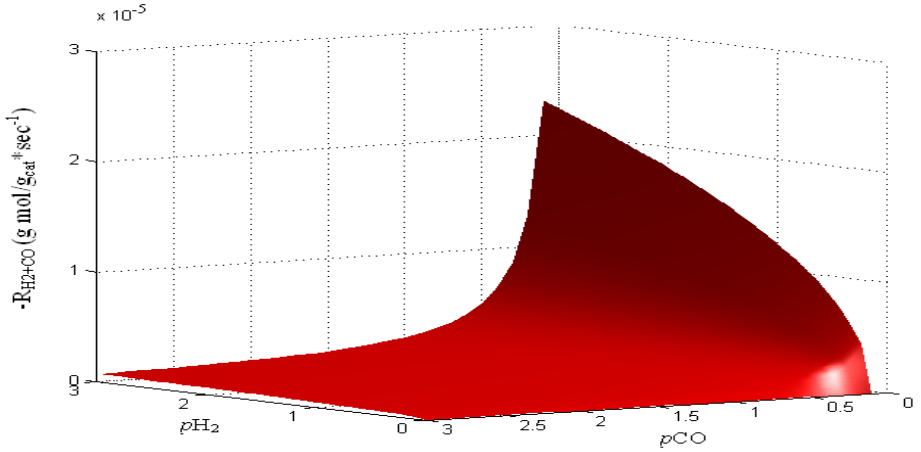

Figure 7. 9: Model 7 prediction showing the influence of H_2/CO ratio on the rate of consumption of synthesis gas.

Figure 7.10 also predicts the influence of temperature.

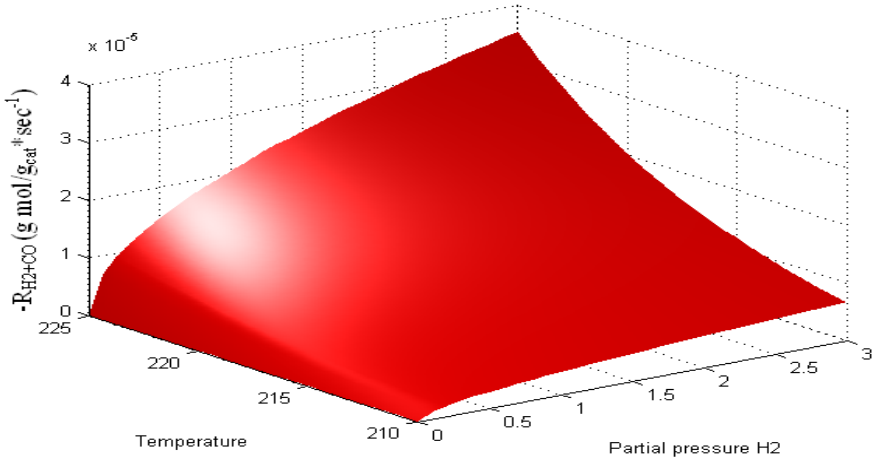

Figure 7. 10: Model 7 prediction showing the influence of temperature and partial pressure of H_2 on the rate of consumption of synthesis gas.

Thus, increasing the temperature increases the value of the rate constant resulting increased rate of reaction. These predictions are also discussed in the catalyst activity section of this manuscript and confirm the theoretical validity of the model.

7.6 Conclusions

The objectives of this work were to obtain a statistically representative kinetic model for the Ru.5K.0016(Co15)/CNT catalyst that enlighten the catalyst surface reaction phenomenons during the synthesis gas (CO + H_2) consumption. The kinetic parameters obtained by the kinetic models are in good agreement with those obtained in the previous study of Co-based FTS catalyst. The activation energy values evaluated for the studied models are between 80 to 85 kJ/mol. According to the kinetic model developed, the CO is strongly adsorbed dissociatively at the catalyst surface and the reaction rate is significantly influenced by the partial pressure of H_2. The data of this study are fitted fairly well by a simple power law expression, but they are best fitted by the Sarup and Woijciechowski model: $-r_{H_2+CO} = \frac{aP_{H_2}^{0.46}P_{CO}^{-0.91}}{(1+bP_{CO}^{0.18}P_{H_2}^{0.35})^2}$. However, in terms of physical understanding of the catalyst surface reactions, the best kinetic to describe the Ru.5K.0016(Co15)/CNT FTS catalyst is $-r_{H_2+CO} = \frac{18.5\times10^{-5}P_{H_2}^{0.39}}{(1+7.2\times10^{-2}P_{CO}^{0.72}P_{H_2}^{0.1})^2}$.

7.7 References

Anderson. R.B., "Experimental method in Catalytic Research," in: "Catalysis vol 4," P.H. Emmet, Eds., Reinhold, New York (1956), Chap.1-2 and 3.

Bechara, R., D.Balloy and D.Vanhove, "Catalytic properties of Co/Al_2O_3 system for hydrocarbon synthesis," Applied Catalysis A: General **207**, 343-353 (2001).

Das, T. K., G.Jacobs, P.M. Patterson, W.A. Conner, J.Li, B.H. Davis, "Fischer-tropsch synthesis characterization and catalytic properties of rhenium promoted cobalt alumina catalysts," Fuel **82**, 805-815 (2003).

Dry, M.E., "The Fischer-Tropsch Synthesis,"in "Catalysis, Science and Technology Vol.1,"J.R. Anderson and M.Boudart, Eds., Springer, Berlin (1981), p.159-255.

Folger, H. S, "Elements of Chemical Reaction Engineering 3th ed," in " Physical and Chemical Engineering Sciences," Upper Saddle River, Eds., New Jersey (2002), pp.69, 690, 706.

Hazewhkel, M., " Encyclopedia of Mathematic," Verlog Berlin, Eds., Springer, Hedeilberg, New York (2001).

Huffaman, G.P N., Shah, J.Zhao, F.E.Huggins, T.E.Hoost, S.Halvorsen and J.G.Goudwin, "In-situ XAFS investigation of K-promoted Co catalysts," Journal of Catalysis **151**, 17-25 (1994).

Iglesia, E., "Design, synthesis, and use of cobalt-based Fischer-Tropsch synthesis catalysts," Applied Catalysis A: General **161**, 59-78 (1997).

Iglesia, E., S.L.Soled, R.A. Fiatto, A. Grayson, "Bimetallic Synergy in Cobalt Ruthenium Fischer-Tropsch Synthesis Catalysts," Journal of Catalysis **143**, 345-368 (1993a).

Iglesia, E., S.C. Reyes, S.L. Soled, "Computer-Aided Design of Catalysts," in "E.R. Becker,"C,J.Pereira, Eds., Dekker, New-York (1993b).

Jacobs,G., T.K Das, Y. Zhang, J. Li, G. Racoillet and B.H. Davis, "Fischer–Tropsch synthesis: support, loading, and promoter effects on the reducibility of cobalt catalysts," Applied Catalysis A:General **233**, 263-281 (2002).

Neter, J. and W. Wasserman, "Applied Linear Statistical Models," R.DIrwin, Eds., Homewood, Illinois (1974), pp.117-121

Oukaci,R., J.G.Goodwin Jr. and A. H. Singleton, "Effect of Titanium Doping on the Activity of Alumina-Supported Cobalt-Based Fischer-Tropsch Catalysts," Applied Catalysis A: General **186**, 129-144 (1999).

Perry, R.H., D.W. Green, "Perry's Chemical Engineer's Handbook (7^{th} Edition), Mc Graw-Hill (1997).

Rautavuoma, A.O.I and H.S. van der Bann, " Kinetics and Mechanism of the Fischer-Tropsch Hydrocarbon Synthesis on a Cobalt on Alumina Catalyst," Applied Catalysis **1**, 247-272 (1981).

Ribeiro, F.H., A.E. Schach von Wittenau, C.H. Bartholomew and G.A. Samorjai, "Reproducibility of Turnover Rates in Heterogeneous Metal Catalysis: Compilation of Data and Guidelines for Data Analysis," Catalysis Review Science Engineering **39**, 49-76 (1997).

Sari,A., Y.Zamani and S.A.Taheri, "Intrinsic Kinetics of Fischer-Tropsch reactions over an industrial Co-Ru/Al_2O_3 catalyst in slurry phase reactor," Fuel Processing Technology **90**, 1305-1313 (2009).

Sarup,B., and B.W. Wojciechowski,"Studies of the Fischer-Tropsch Synthesis on a cobalt catalyst II. Kinetics of carbon monoxide conversion to methane and higher hydrocarbon," The Canadian Journal of Chemical Engineering **74**, 62-74 (1989).

Smith, J.M., "Chemical Engineering Kinetics," McGraw-Hill, Inc., US (1981), p.450-517

Tavasoli, A., Y. Mortazavi, A. Khodadadi and K. Sadagiani, "Effects of different loadings of Ru and Re on physico-chemical properties and performance of 15% Co/Al_2O_3 FTS catalysts," Iranian Journal of Chemistry and Chemical Engineering **35**, 9-15 (2005).

Tavasoli, A., A.M. Rashidi, K. S. Zadeh, A. Karimi, A.A. Kodadadi, Y. Mortazavi, "Carbon nanotubes supported cobalt catalyst for converting synthesis gas into hydrocarbons," EP patent 1782885 A1 (2007).

Tavasoli, A., R.M. Abbaslou, M. Trépanier and A.K.Dalai, "Fischer-Tropsch synthesis over cobalt supported on carbon nanotubes in a slurry reactor," Applied Catalysis A: Genreal **345**, 134-142 (2008)

Tavasoli, A., M. Trépanier, R.M. Malek Abbaslou, K. A. Dalai and N. Abatzoglou, "Fischer–Tropsch synthesis on mono- and bimetallic Co and Fe catalysts supported on carbon nanotubes," Fuel.Proc.Tech **90**, 1486-1494 (2009).

Trépanier, M., A. Tavasoli, A.K. Dalai and N. Abatzoglou, " Fischer-Tropsch synthesis over carbon nanotubes supported cobalt catalysts in a fixed bed reactor: Influence of acid treatment," Fuel Processing Technology **90**, 367-374 (2009 a).

Trépanier, M., A. Tavasoli, A.K. Dalai, and N. Abatzoglou, "Co, Ru and K loadings effects on the activity and selectivity of carbons nanotubes supported cobalt catalyst in FTS," Applied Catalysis A.General **353,** 193-202 (2009 b).

Trépanier, M., A.K. Dalai, N. Abatzoglou, "Synthesis of CNT-supported cobalt nanopartciles catalysts using a Microemulsion technique: Role of nanoparticle size on reducibility, activity and selectivity in Fischer-Trospch reactions,"Applied Catalysis A: General **374**, (2010) 79-86.

Visconti, C.G., E. Tranconi, L. Lietti, R. Zennaro, P. Forzatti, "Development of a complete kinetic model for the Fishcer-Tropsch Synthesis over Co/Al_2O_3 catalyst,"Chemical Engineering Science **62**, 5338-5343 (2007).

Yates, I.C and C. N. Satterfield, "Intrinsic Kinetics of the Fischer-Tropsch Synhtesis on a Cobalt Catalyst," Energy & Fuels **5**, 168-173 (1991).

Zennaro,R., M.Tagliabue and C.H. Bartholomew, "Kinetics of Fischer-Tropsch synthesis on titania-supported cobalt," Catalysis Today **58**, 309-319 (2000).

Chapter 8: Summary

8.1 Overall Ph. D Project Discussion and Conclusions

This Ph. D project involves the engineering of a novel Co/CNT FTS catalyst. This involved many aspects of the catalyst development including the screening of the catalyst, support functionalization, catalyst lifetime study, metal loadings and promoters optimization, catalyst preparation technique, catalyst structure properties study and kinetic model development of the catalyst.

This Ph. D project reached objectives by developing a novel cobalt catalyst supported on carbon nanotubes that is suitable for Fischer-Tropsch synthesis process in a Fixed Bed Reactor. To optimize this catalyst it is important to primarily functionalize the CNT support with acid treatment. The support functionalization was studied by using acid treatment on carbon nanotubes at 25 and 100 ^{o}C. The HNO_3 acid treatment at 100^{o}C shows the best results. This step was needed in order to open the caps, break the carbon nanotubes, add defects and acid functional groups at the surface of the CNT support and more important, for allowing the cobalt particles to be deposited inside the CNT, and benefiting from the inner surface electron-deficiency interaction. Thus, most of the metal particles were homogeneously distributed inside the tubes and the rest on the outer surface of the CNTs. The deposition of cobalt particles inside the CNT pores improves the catalytic behaviour of the Co/CNT catalyst. Thus, the confinement of the cobalt particles inside the CNT results in high catalyst reducibility, high selectivity for C_{5+} and high FTS activity. This particular characteristic of the CNT makes this new catalyst carrier really attractive for catalytic reactions. The support functionalization also increases the BET surface area and the reducibility of the catalyst metals. The FTS activity and % CO conversion of 10Co/CNT increases by 36 and 114 % with 30 % HNO_3 acid at 25 and 100 ^{o}C treatment, respectively. The acidic functional group increases the absorption of hydrogen on catalyst surface. Also, breaking the tubes leads to shorter tubes as well as lower internal mass transfer limitation for reactants and desorption of products.

The evaluation of the Co/CNT catalyst at different operating conditions shows that the products distribution follows a distinct shift to lower molecular weight hydrocarbons at high temperature (230^{o}C). The C_{5+} selectivity and the O/P ratio also decreased. High temperature increases the hydrogen mobility which enhances the termination to paraffins against chain growth. Decreasing the H_2/CO ratio from 2 to 1 increased the amount of CO adsorbed on catalyst surface which increases the chain growth probability. The optimized operating conditions studied for this novel catalyst in a Fixed Bed Reactor are a temperature of 220 ^{o}C, a H_2/CO ratio of 2 and a pressure of 2 MPa.

A lifetime study has been performed to evaluate the stability of the Co/CNT catalyst. Cobalt catalysts supported on CNTs have shown two different types of deactivation mechanisms: cobalt oxidation and sintering. The main irreversible deactivation causes are the cobalt particle sintering that is shown by a reverse exponential law. The confinement of cobalt particles inside the CNT has decreased the sintering phenomenon of the particle as compared to the particle located on the outer layers. The interior electron-deficient of the CNT leads to particular interaction of the interior nanotubes surface with the metal particles, which inhibits the sintering rates of the cobalt oxides. The physical encapsulation of the metal particles inside the pores also sems ro reduce the metal site sintering. The results of this deactivation study reveal that to enhance the lifetime of the catalyst, the metal particle should be distributed inside the CNT. Moreover, confinement of reaction intermediates inside the channels increases the contact time with active metal sites, resulting in the production of heavier hydrocarbons.

Due to high cost of cobalt, it is important to determine the appropriate loading of cobalt to maximize the availability of active cobalt sites for participation in the reaction. Thus, the improvement of Co/CNT catalysts with different loadings of cobalt, ruthenium and potassium were also studied. Increasing the amount of Co from 15 to 30 wt. % decreases the reduction temperature from 500 to 485 ^{o}C and decreases dispersion. Moreover, increasing the cobalt loadings up to 30 wt. %, increases the FTS activity and the heavier hydrocarbons molecules selectivity and decreases the methane selectivity. The catalyst loaded with 15 wt. % of cobalt shows a fairly good % CO conversion (50 %) and high selectivity for FTS products. In order to minimize the amount of cobalt and

optimize the performance of the catalyst, ruthenium and potassium promoters have been added to the Co15 catalyst. Ru promoter enhances the reducibility, increases the dispersion and decreases the average cobalt cluster sizes. Potassium shifts the reduction temperatures to higher temperatures. Ru.5(Co15) increases the FTS rate of Co15 catalyst by a factor of 1.4 while addition of 0.0066 wt. % K decreases the FTS rate by a factor of 7.5. Addition of 0.5 wt. % ruthenium and 0.0016 wt. % potassium on the Co15 catalyst shows the greatest FTS product selectivity and activity. Ruthenium enriched the surface of the cobalt catalyst and potassium increases the selectivity for α-olefins. Both promoters enhanced the selectivity towards higher molecular weight hydrocarbons.

The Fe/Co bimetallic catalysts on CNTs support have also been studied. Bimetallic catalysts containing cobalt and a small amount of iron have different catalytic characteristics than catalysts containing only Fe or Co metals. The structural data obtained by XRD and EDX techniques pointed the formation of Co-Fe alloys on the catalyst surface. The Co-Fe alloys formation appears to be one of the causes of this differentiation in catalytic behaviour. FTS reaction rate and percentage CO conversion increased remarkably with addition of 0.5 wt. % of iron to cobalt catalyst with a highest CO conversion of 56 %. Increasing the amount of iron up to 4 wt. % to cobalt catalyst decreases the reducibility, the metal dispersion and the % CO conversion. The ratio of Fe to Co plays an important role in controlling the metal dispersion and degree of reduction in the bimetallic systems. The addition of iron to cobalt catalyst increased the undesired WGS reaction rate and increased the selectivity towards methane. Thus, Fe enriched surface decreased the chain growth by α-olefins readsorption and secondary reactions. A particular result with the bimetallic catalyst is the selectivity towards alcohol. Addition of 4 wt. % of iron increased the alcohol selectivity from 2.3 (cobalt monometallic catalyst) to 26.3 wt. % . The Co-Fe alloys appear to be responsible for the rather high selectivity toward alcohol formation. The high alcohol selectivity of Fe10/CNT catalyst can be attributed to the difficult dissociation of CO on the iron clusters. Thus, the behavior of bimetallic catalysts regarding selectivity toward alcohol can be attributed to the presence of Co-Fe alloys which decreases the CO dissociative adsorption. The relative proportion ROH/HC is also highly dependent on the presence of Co-Fe alloys. Bimetallic Co-Fe

catalysts with an iron wt. % higher than 0.5 wt. % are less effective than cobalt mono-metallic catalyst in terms of FTS process and are recommended for alcohol synthesis.

The previous studies have revealed that FTS process is influenced by catalyst structure properties. Microemulsion has been used as a new nanocatalyst preparation technique to have a better understanding of the particle size effect in FT catalysis using a novel Co/CNT catalyst. The cobalt nanoparticles produced show a narrow particle size distribution. As expected, FT activity and selectivity of the catalysts are dependent upon the size distribution of the cobalt cluster. The small Co particles (2-6nm) are mostly confined inside the CNTs where influence of its electron deficiency in the inside surface has changed the commonly expected results. CNTs as a catalyst carrier for Co nanoparticles maintained high reducibility of Co which will not normally occur with nanoparticle supported on oxidic catalysts support. The proposed microemulsion technique also increased the CO conversion by 15 % compared to those prepared by incipient wetness impregnation. Uniformity of the catalyst particles leads to a better stability of the products and the FTS activity. This new catalyst preparation method may offer an attractive alternative for nanoparticle synthesis by reverse microemulsion and for fundamental catalytic studies especially such for structure-sensitive FT catalysis.

Finally, this study has been completed by developing a statistically representative kinetic model for the optimized Ru.5K.0016(Co15) catalyst. The experimental data of the study fit fairly well with a simple Langmuir-Hinshelwood power law expression ($-r_{H_2+CO} = aP_{H_2}^{0.46}P_{CO}^{-1.14}$), but in order to have a better representative kinetic model for a large range of operating conditions, the best evaluated model to describe this new catalyst is $-r_{H_2+CO} = \frac{aP_{H_2}^{0.39}}{(1+bP_{CO}^{0.72}P_{H_2}^{0.1})^2}$. The model suggested that the CO strongly adsorbs dissociatively at the catalyst surface and the reaction rate is significantly influenced by the partial pressure of H_2. This model has been statistically evaluated by the sum of square (R^2), the mean absolute relative residuals (MARR) and the residuals sum of square (RSS) to ensure the best fitted model.

To conclude, the originality of this Ph.D research project relies on the development of a cobalt nanocatalyst that improved the products selectivity in FTS, decreased the sintering extent which is the most important deactivation cause in this type

of catalysis and allowed a high reducibility of nanoparticles (5 nm <). Nanocatalyst reduction is usually problematic in the cause of oxidic supports such as Al_2O_3, TiO_2 and SiO_2. CNTs as cobalt FTS catalyst support has increased the reducibility of nanoparticles and allowed for mass transfer with no significant external or internal diffusion limitation. Moreover, a kinetic model for cobalt promoted catalysis supported on CNT has been developed. This new catalyst has also been characterized extensively and it has been shown that it possesses the required features as a FTS catalyst.

8.2 Achievement of Research Objectives

All the research objectives listed in Chapter 1 (items in section 1.3) have been achieved over the course of the Ph.D. project. The thesis chapters in which the thesis objectives are achieved are included below in brackets after each numbered listing for reference.

i. The development of a novel cobalt FTS catalyst supported on carbon nanotubes was achieved using a micro Fixed Bed Reactor. The catalysts have been evaluated at different operating process parameters. (Chapter 2)

ii. In order to determine the optimum support for this novel Co/CNT catalyst, the CNT support has been functionalized with acid treatment. The best acid treatment and operating conditions for Co/CNT catalyst in a micro FBR have been studied. (Chapter 2)

iii. As part of the catalyst study, the stability and lifetime of the Co/CNT catalyst have been determined. The deactivation causes were found to be the cobalt oxidation and the particles sintering. The deactivation mechanism developed shows that the CO conversion decreases linearly during the cobalt oxidation and start to decrease exponentialy when particles' sintering occurs. (Chapter 3)

iii. With the catalyst evaluation completed, the improvement of this novel catalyst has been performed by increasing the cobalt loading on catalyst support and by adding promoters. Ruthenium and potassium have both properties to improve the efficiency of the Co/CNT. The bimetallic Co/Fe catalyst has also been studied showing a high selectivity for alcohol products. (Chapters 4 and 5)

iv. In order to have a better understanding of the catalyst surface reactions, a new nano-catalyst preparation technique has been developed to evaluate the influence of cobalt nanoparticle sizes on the activity and selectivity of the catalyst. The microemulsion was used to develop uniform nanoparticle at different sizes. (Chapter 6)

v. Finally, to have a complete study of this novel Co/CNT catalyst, a kinetic model was developed for the optimized catalyst evaluated in Chapter 4 (Ru.5K.0016(Co15)/CNT). The model was developed under intrinsic conditions (no internal or external transfer limitation) and the kinetic parameters were representative of the experimental data.

8.3 Project Recommendations

In order to continue to develop this new Co/CNT FTS catalyst, recommendations for the continuation are given bellow:

(1) Evaluation of the Co/CNT catalyst under industrial realistic syngas composition (CO, H_2, N_2, H_2S, H_2O and CO_2):

This new Co/CNT catalyst has been evaluated under ideal process operating conditions in order to have a clear idea of his catalytic behavior. However, the time available was limited for the experimental trials under realistic industrial conditions. The syngas that has been used for this research project is composed of pure hydrogen and pure carbon monoxide. According to literature, the real composition of the syngas after biomass gasification is estimated as: 17-22 v/v.% of CO, 10-15 v/v.% of CO_2, 16-20 v/v.% of H_2 and 50-55 v/v.% of N_2 [Rajvanshi, 1986]. It would be of interest to study the influence of the syngas composition onto the catalyst performance (activity and selectivity). Moreover, poisoning of the catalyst by undesirable compounds such as water and H_2S causes the catalyst deactivation [Jacobs et al., 2004]. Further study can then be performed regarding the influence of water addition on the catalyst lifetime. Water can also be used to increase the amount of hydrogen available in the feed stock according to

the WGS reaction mechanism [Jacobs et al., 2004]. Thus, it would also be of interest to evaluate the proper amount of water necessary to enhance the hydrogen production and thus increase the H_2/CO ratio for realistic industrial conditions.

(2) Evaluation of the promoted Co/CNT catalyst in a slurry reactor.

As reported in Chapter 1, this research project involves the use of a FBR instead of a slurry reactor to evaluate the performance of the novel Co/CNT catalyst. The slurry reactor is commonly used in the industry and at laboratory scale [De Klerk, 2009b; Fogler, 2002]. It leads to homogeneous mixing of the feed stock and low pressure drop. Chapter 1 also indicates that slurry reactor is limited by mass transfer from the bulk liquid to the catalyst surface and this influences the final results [Fogler, 2002]. Thus, it would be of interest to evaluate the activity and selectivity of this novel catalyst using a slurry reactor and compare the results with the one obtained in this Ph. D research project.

(3) Further optimization on RuKCo/CNT

As reported in Chapter 4, the optimized catalyst was determined after evaluating the effects of Ru and K addition onto Co/CNT catalyst. It would be of interest to evaluate also the influence of positioning the particles inside or outside the CNT with this promoted catalyst and see if there is any influence on the hydrocarbon liquids distribution.

(4) Catalyst characterization

This Ph.D research project has shown that confinement of cobalt particle inside the CNT influences the catalytic behavior of the Co/CNT catalyst. However, the special electron interactions between the inner wall of the carbon nanotubes and the cobalt particle have not been specifically identified. It would be of interest to use EXAFS characterization to improve the knowledge regarding this particular phenomenon. Moreover, in Chapter 6, the microemulsion catalyst preparation method has been used to evaluate the influence of particle size on FTS reactions. The FTS as a structure sensitive reaction is influenced by the cobalt structure on the catalyst surface. Thus it would be of

interest to do X-ray Absorption Near Edge Structure (XANES), Extended X-Ray Absorption Fine Structure (EXAFS) and X-ray photoelectron spectroscopic (XPS) studies to evaluate the influence of each Co^{o}, CoO, Co_3O_4 structure on the FTS mechanism. Moreover, *insitu* characterization of the catalyst will also be of interest to have a better understanding of the catalyst behavior during the FT reactions. This research project has only characterized the catalyst before of after the FTS reactions.

Appendix A: Sample calculation for ASF distribution

The chain growth probability of the FTS process is determined by the Anderson-Schultz-Florey (ASF) model. The ASF chain growth mechanism, mathematically described as: $Wn/n = (1 - \alpha)^2 \alpha^{n-1}$ [Anderson, 1956]. Where n is the number of carbon in the product, Wn is the weight fraction of hydrocarbons (olefins + paraffins) and α is the ASF chain growth probability.

For the K.0066(Co15) catalyst hydrocarbons distribution:

Table A-1: Hydrocarbons distribution for K.0066(Co15) catalysts obtained with a Varian 3400 GC liquid chromatograph.

n	Wn (%)
5	0.28
6	1.9
7	16.2
8	14.3
9	13.3
10	12.4
11	13.3
12	11.9
13	6.6
14	4.28
15	1.9
16	0.95
17	0.95
18	0.95
19	0.28
20	0.28
21	0.095

The chain growth probability can be evaluated using a semi-logarithmic plot of weight product contents (Wn) versus carbon number (n). The slope of the line reflecting the chain growth probability (α) [Anderson, 1956; Claeys and Van Steen, 2002; Ma et al., 1999]

Figure A-1 shows the carbon number as a function of Ln(Wn/n):

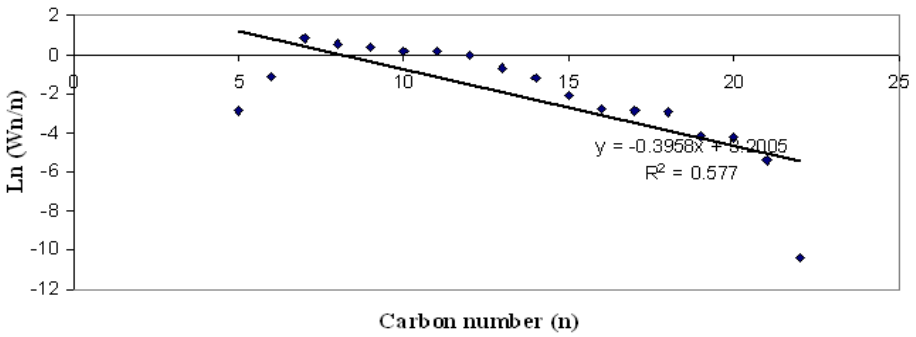

Figure A-1: ASF distribution

Thus, the resultant chain growth probability for K.0066(Co15) catalyst is:

$\alpha = e^{(-0.3958)} = 1.48$ (Eq. A-1)

Appendix B: Sample calculation of Weisz-Prater criterion (C_{WP})

The Weisz-Prater criterion is use to determine if internal diffusion is limiting the reaction [Folger, 2002]. This criterion can be evaluated with the following equation:

$$C_{WP} = \frac{-r'_{A(Obs)}\rho R^2}{D_e C_{AS}} \qquad \text{(Eq.B-1)}$$

Where, r_A' is the reaction rate per unit mass of catalyst observed during the reaction, ρ is the catalyst density, R is the catalyst particle radius, D_e is the effective diffusivity and C_{AS} is the reactant A concentration at the surface of the catalyst. If $C_{WP} << 1$, there is no internal diffusion limitation if $C_{WP} >> 1$, internal diffusion limits the reaction [Fogler, 2002].

The equation to evaluate the effective diffusivity of binary gas mixtures (Eq.B-2) have been developed by Satterfield in 1970 and Lennard-Jones:

$$D_{12} = \frac{0.001858 T_a^{3/2}[(M_1 + M_2)/(M_1 M_2)]^{1/2}}{p\sigma_{12}^2 \Omega_D} \qquad \text{(Eq.B-2)}$$

Where T_a is the temperature (K) of the reaction, M_i is the molecular weight of species, p is the pressure (atm), Ω_D is the collision integral and σ is the Boltzman constant [Satterfield, 1970].

The effective diffusivity for a binary gas mixtures of CO and H_2 at 220°C and at a pressure of 20 atm is calculated as follows:

1) According to Table 1.3 of [Satterfield , 1970] the Boltzman constant for CO and H_2 are:

$\sigma_{CO} = 3.69\ A^o$
$\sigma_{H2} = 2.827\ A^o$

$$\sigma_{12} = \frac{\sigma_1 + \sigma_2}{2} = \frac{3.69 + 2.82}{2} = 3.25 A^o \qquad \text{(Eq.B-3)}$$

From Table 1.1 of [Satterfield , 1970], $p\sigma_{12}^2 = 0.651\,cm^2/sec*atm$

2) The collision integral (Ω_D) is a function of : kT_a/ε_{12}, where ε_i/k are obtained on Table 1.3 of [Satterfield , 1970]:

$$\frac{\varepsilon_1}{k} = 91.7$$

$$\frac{\varepsilon_2}{k} = 59.7$$

$$\frac{\varepsilon_{12}}{kT_a} = \left(\frac{\varepsilon_1}{k}\right)^{0.5}\left(\frac{\varepsilon_2}{k}\right)^{0.5}\left(\frac{1}{T_a}\right) = (91.7)^{0.5}(59.7)^{0.5}\left(\frac{1}{493}\right) = 0.15 \qquad \text{(Eq.B-4)}$$

$$\frac{kT_a}{\varepsilon_{12}} = \frac{1}{0.15} = 6.66$$

From Table 1.2 of [Satterfield, 1970] for a value of $kT_a/\varepsilon_{12} = 6.66$, $\Omega_D = 0.8124$

3) The molecular weight of CO = 28g/mol and the molecular weight of H_2 =2g/mol

Therefore, D_{12} can be calculated as follows:

$$D_{12} = \frac{0.00185(493)^{3/2}[(28+2)/(28\times 2)]^{1/2}}{0.651\times 0.8124} = 0.279 \text{ cm}^2/\text{s}$$

The effective diffusivity D_e now becomes:

$$D_e = D_{12}\frac{\theta}{\tau} \qquad \text{(Eq.B-5)}$$

Where θ is the porosity of catalyst and τ is the tortuosity factor.

Without any other information on the catalyst pellet, a good estimation value for θ is 0.5 and the tortuosity of CNT is usually considered between 1 and 2.

$$D_e = 0.279\times\frac{0.5}{1.5} = 9.3\times 10^{-2} \text{ cm}^2/\text{s}$$

<u>If the diameter of the pellet is 500μm</u>:

$$R = (500\mu m \times \frac{1\times 10^{-4} cm}{1\mu m})/2 = 0.025 cm$$

The intial C_{AS} = 4.24 x 10^{-5}gmol/ml

ρ = 1.33 g/ cm^3 for CNT

$-r_{A(Obs)}$ = 8.06 x 10^{-6} gmol/gcat*s

The C_{WP} is calculated using equation C-1:

$$C_{WP} = \frac{0.00000806 \times 1.33 \times (0.025)^2}{0.093 \times (0.0000425)} = 0.00169$$

C_{WP} is << 1. There is no internal diffusion limitation

Appendix C: Sample calculation of the Sherrer Equation

The shapes of the peaks, in X-Ray diffraction, contain additional and often valuable information. The shape, particularly the width, of the peak is a measure of the amplitude of thermal oscillations of the atoms at their regular lattice. The Sherrer Equation has been developed to evaluate the crystal particle size related to the width of a diffraction peak.

The Sherrer equation is defined as follows:

$$d = (k \times \lambda)/(\beta Cos\theta) \qquad \text{Eq.(C-1)}$$

Where d is the crystallite size in nm, k is the Sherrer constant, λ is the wavelength of radiation and β is the integral breath of peak (in radians 2 θ) located at angle θ.

There are many factors that determine the width β of a diffraction peak. These include:

1. instrumental factors
2. the presence of defects to the perfect lattice
3. differences in strain in different grains
4. the size of the crystallites

The constant k is typically close to unity and ranges from 0.8-1.39.

To calculate the crystal size of Co_3O_4 on the surface of the catalyst:

1) Defined β as shown in Figure C-1

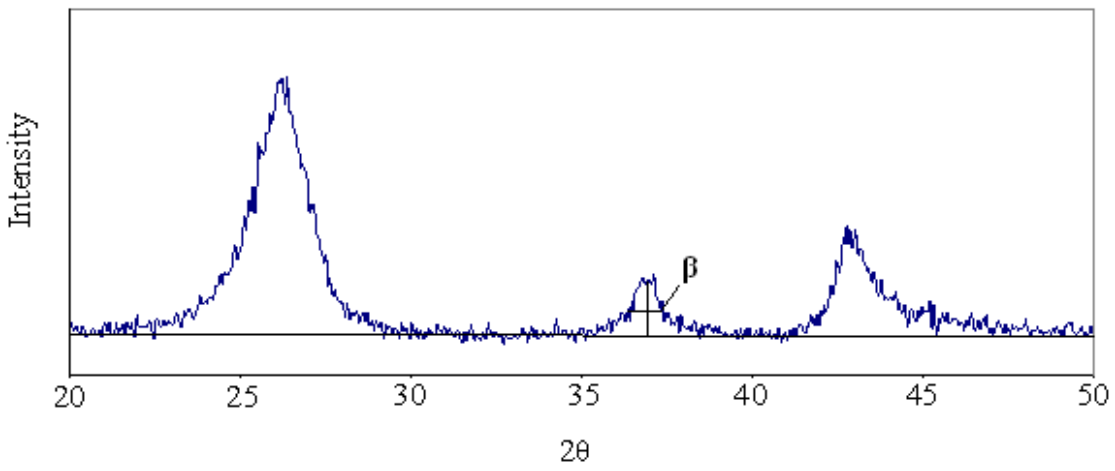

Figure C-1: XRD spectra of Co/CNT catalyst showing the measurement of the integral breath (β) of peak in 2θ = 36.8 (Co_3O_4).

2) Calculated the crystallite size (*d*) with the Sherrer Equation:

k =0.9
$\lambda = 0.154$
$\beta = 37.45\ (2\theta) - 36.65\ (2\theta) = 0.8$
Radian of $\beta = 0.8 * 2\pi/360^{o} = 0.0139$
$2\theta = 36.8^{o}$
$\text{Cos}\ (\theta) = \text{Cos}\ (36.8/2) = 0.8$

$$d = (k \times \lambda)/(\beta Cos\theta)$$

$$d = (0.9 \times 0.154)/(0.8 \times 0.0139) = 12.46\,\text{nm}$$

Appendix D: Mass balance

Mass balance on C and O (24 h)

3600 GHSV/h, H_2/CO =2, P = 2 MPa T= 220 °C

Percentage of total mass loss for the FTS process = 6.6 %

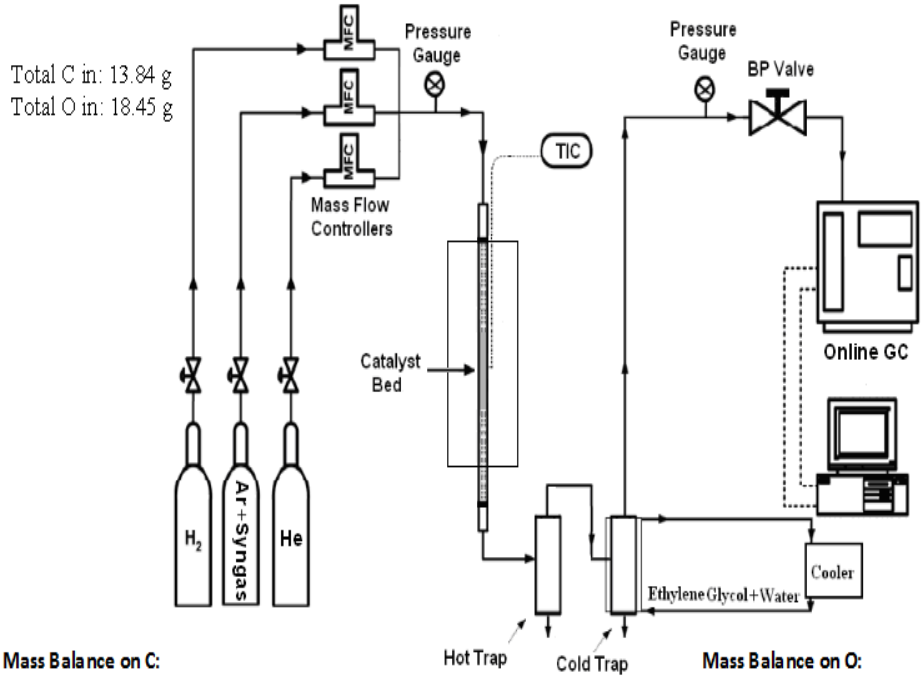

Mass Balance on C:

Total CO consumed: 8.16 g of C/day

CO out: 5.67 g of C

CO_2 : 0.45 g of C

CH_4 : 1.528 g of C

C_2H_6 : 0.147 g of C

C_3H_8 : 0.31 g of C

C_5H_{12} : 1.15 g of C

Liquid Hydrocarbon : 1.53 g of C

Wax : 2.48 g of C

Total C out from FTS products : 7.96 g of C/day

Lost of carbon : 0.207g/day

% Lost of carbon: 2.45 %

Mass Balance on O:

Total CO consumed: 10.89 g of O/day

CO out: 7.56 g of O

H_2O : 7.73 g of O

CO_2 : 1.21 g of O

*Negligible alcohol formation

Total O out from FTS products: 8.94 g of O / day

Lost of oxygen: 1.91 g / day

% Lost of oxygen : 17.5 %